The Role of XBP1s in the Unfolded Protein Response and *N*-Linked Glycosylation

by

Kenny Chen

B.S. Chemistry
University of California, Los Angeles, 2014

SUBMITTED TO THE DEPARTMENT OF CHEMISTRY
IN PARTIAL FULFILLMENT OF THE REQUIREMENTS FOR THE DEGREE OF

DOCTOR OF PHILOSOPHY IN CHEMISTRY
AT THE
MASSACHUSETTS INSTITUTE OF TECHNOLOGY

September 2020

Signature of Author: _____
Department of Chemistry
May 27, 2020

Certified by: _____
Matthew D. Shoulders
Associate Professor of Chemistry
Thesis Supervisor

Accepted by: _____
Robert W. Field
Haslam and Dewey Professor of Chemistry
Chair, Departmental Committee on Graduate Students

This doctoral thesis has been examined by a committee of the

Department of Chemistry as follows:

_____

Laura L. Kiessling
Novartis Professor of Chemistry
Thesis Committee Chair

_____

Matthew D. Shoulders
Associate Professor of Chemistry
Thesis Supervisor

_____

Barbara Imperiali
Class of 1922 Professor of Chemistry and Biology
Thesis Committee Member

The Role of XBP1s in the Unfolded Protein Response and *N*-Linked Glycosylation

by

Kenny Chen

Submitted to the Department of Chemistry
on June 10, 2020 in Partial Fulfillment of the
Requirements for the Degree of Doctor of Philosophy
in Chemistry

Abstract

The secretory pathway processes approximately one-third of the cellular proteome, modifying proteins with diverse chemical structures such as carbohydrates. These modifications can help guide protein folding and expand the functional diversity of the proteome, ultimately influencing intracellular signaling and extracellular interactions. The endoplasmic reticulum (ER) is the site of protein folding along the secretory pathway, featuring a suite of chaperones to assist protein folding and quality control factors for degrading misfolded proteins. Co- and post-translational modifications such as *N*-glycosylation take place in the ER, and glycoproteins are further processed in the Golgi to yield a vast array of *N*-glycan structures.

During both normal physiology and disease, cells encounter environments that can result in proteotoxic stress. The proteostasis network safeguards against protein misfolding stress through the upregulation of chaperones and quality control factors. The unfolded protein response (UPR) regulates the ER's proteostasis network through the activity of transcription factors that remodel the expression of proteostasis regulators. Prior studies in our lab have established a role for the UPR's XBP1s transcription factor in *N*-glycan maturation, demonstrating that XBP1s bridges ER stress with the molecular architecture of *N*-glycans. However, these studies were limited to analyzing ectopically expressed model proteins. This thesis examines the role of XBP1s in regulating the structural distribution of *N*-glycans in endogenous systems, and explores the mechanisms by which XBP1s activation is regulated.

We employed stress-independent activation of XBP1s and glycomic analyses by lectin microarrays and mass spectrometry to show that XBP1s drives significant changes in sialylation and bisecting GlcNAc in HEK293 cells, and in high-mannose, branched, and core fucosylated *N*-glycans in HeLa cells. We also inhibited formation of XBP1s in breast cancer cells displaying constitutively high levels of XBP1s to show that glycosylation features associated with malignancy are modestly affected when XBP1s formation is blocked. Lastly, we demonstrated that pharmacological activation of the IRE1-XBP1s signaling axis cannot be sustained despite loss of co-chaperones negatively regulating IRE1. Our results demonstrate that XBP1s is a significant regulator of both the UPR and *N*-glycosylation, and they emphasize the importance of studying the regulation of IRE1-XBP1s signaling for understanding disease targets.

Thesis Supervisor: Matthew D. Shoulders
Title: Associate Professor of Chemistry

Acknowledgements

Graduate school has been everything I thought it would be: adventure, many late nights (some all-nighters), friendships forged out of a shared experience. I have only achieved what I have with the support of my family, friends, and mentors. My advisor, Matt, has supported me when I didn't know I needed it. Anna, my classmate since Day 1, and I share countless jokes. Jimin, Kathryn, and Marie held me accountable on our morning runs when it was below freezing. Everyone in the Shoulders Lab has felt like family. Support, scientific or personal, built the foundation that kept me excited to keeping learning during graduate school. I acknowledge, in no particular order,

Family

My Thesis Advisor
Matthew D. Shoulders

My Thesis Committee Members (current and retired)
Laura L. Kiessling
Barbara Imperiali
Alexander M. Klibanov

Shoulders Lab
Anna Ponomarenko
Jimin Yoon
Kathryn Yammine
Christopher E. R. Richardson
Madeline Y. Wong
Chichi Li
Seo-yeon Kim
Emmanuel E. Nekongo
Duc Doan
Gina Choi
Rebecca M. Sebastian
Louis J. Papa, III
Azade S. Hosseini
Samuel J. Hendel
Andrew S. DiChiara
Agata A. Bikovtseva
Camden Holm
Betty Lou McClanahan

Collaborators Across the US and Around the World

Past Mentors
Eric Zheng, Vertex Pharmaceuticals
Poh-Choo Pang, Imperial College London
Olga Aprelikova, National Institutes of Health
Jeffrey E. Green, National Institutes of Health
Michael D. Chambers, University of California, Los Angeles
Albert J. Courey, University of California, Los Angeles
Vincent Stepanik, California Institute of Technology
Angelike Stathopoulos, California Institute of Technology

Neighbors at the Warehouse
Claudia and David Darmofal
Marie Shi Feng
Brenden A. Butters

The Chemistry Education Office
Jennifer Weisman

The Department of Chemistry EHS Committee

Old Friends
Tai-Lun Ng
Wilson Wong
Rebecca Fong
Hanna Kim
Edmund Fong

Dedication

妈妈 爸爸 姐姐 和所有我愛的人
Mom, Dad, Sister & Loved Ones

手紙 ～拝啓 十五の君へ～

My 15-Year-Old Self

Table of Contents

Table of Figures

Chapter 1

Chapter 2

Chapter 3

Chapter 4

Table of Abbreviations

Abbreviation	Explanation
1-DMM	1-Deoxymannojirimycin (Mannosidase I Inhibitor)
3’ DGE	3’ Digital Gene Expression RNA-Seq
4μ8C	4-Methyl Umbelliferone 8-Carbaldehyde (IRE1 Inhibitor)
aa	Amino Acid
AAL	*Aleuria aurantia* Lectin (Fucose Binder)
AATD	Alpha-1 Antitrypsin Deficiency
AAVS1	Adeno-Associated Virus Integration Site 1
AOL	*Aspergillus oryzae* Lectin (Fucose Binder)
APP	Amyloid Precursor Protein
ATCC	American Type Culture Collection
ATF2	Activating Transcription Factor 2
ATF4	Activating Transcription Factor 4
ATF6	Activating Transcription Factor 6
ATF6f	Activating Transcription Factor 6, Cytosolic Fragment
ATG	Start Codon; Methionine Translation Initiation Codon
BiP	Binding-Immunoglobulin Protein (Hsp70 Family Chaperone)
BMP2	Bone Morphogenetic Protein 2
Calsepa	*Calystegia sepium* Lectin (Oligomannose Binder)
CD2	Cluster of Differentiation 2 (Cell Adhesion Molecule)
CDS	Coding Sequence
CFTR	Cystic Fibrosis Transmembrane Conductance Regulator
CHAPS	3-[(3-Cholamidopropyl)dimethylammonio]-1-propanesulfonate (Detergent)
ChIP	Chromatin Immunoprecipitation

CHO	Chinese Hamster Ovary Cell Line
CHOP	C/EBP Homologous Protein (Transcription Factor)
CRISPR	Clustered Regularly Interspaced Short Palindromic Repeats
DAX	DHFR.ATF6 and Tet-Inducible XBP1s
diCBM40	Divalent Carbohydrate-Binding Module (NanI from *Clostridium perfringens*; α2,6- and α2,3-Sialic Acid Binder)
DMEM	Dulbecco's Modified Eagle Medium
DMSO	Dimethyl Sulfoxide
Dox	Doxycycline
DTT	Dithiothreitol
EDTA	Ethylenediaminetetraacetic Acid (Metal Ion Chelator)
EGFR	Epidermal Growth Factor Receptor
EGTA	Ethylene Glycol-bis(β-aminoethyl ether)-*N*,*N*,*N′*,*N′*-tetraacetic Acid (Metal Ion Chelator)
eIF2	Eukaryotic Initiation Factor 2
EMT	Epithelial–Mesenchymal Transition
ER	Endoplasmic Reticulum
ERAD	Endoplasmic Reticulum-Associated Protein Degradation
ERdj4	Endoplasmic Reticulum DNA J Domain-Containing Protein 4 (Hsp40 Family Co-Chaperone)
ERSE	Endoplasmic Reticulum Stress Response Element
Ex	Exon
FBS	Fetal Bovine Serum
FDR	False Discovery Rate
GC-MS	Gas Chromatography Mass Spectrometry
gDNA	Genomic DNA
GEP	Granulin-Epithelin Precursor
GlcNAc	*N*-Acetylglucosamine

Glycogene	Glycosylation-Related Gene
GNA	*Galanthus nivalis* Agglutinin Lectin (Oligomannose Binder)
GNL	*Galanthus nivalis* Lectin (Oligomannose Binder)
GO	Gene Ontology
Grp94	Glucose-Regulated Protein, 94 kDa (Hsp90 Family Chaperone)
GSEA	Gene Set Enrichment Analysis
HBP	Hexosamine Biosynthetic Pathway
HCC1937	Human Triple-Negative Breast Cancer Cell Line (Named after the Hamon Cancer Center)
HEK293	Human Embryonic Kidney 293 Cell Line
HeLa	Human Cervical Epithelial Cancer Cell Line (named after Henrietta Lacks)
HHL	*Hippeastrum hybrid* Lectin (High-Mannose Binder)
HIF1α	Hypoxia Inducible Factor 1 Subunit Alpha
HNF1α	Hepatocyte Nuclear Factor 1-Alpha (Transcription Factor)
HPD motif	Histidine-Proline-Aspartate Motif in the ERdj4 J Domain
Hs 578T	Human Triple-Negative Breast Cancer Cell Line (Named after *Homo sapiens* No. 578, Tumor)
HSF1	Heat Shock Transcription Factor 1
Hsp	Heat Shock Protein (Class of Molecular Chaperones)
HYOU1	Hypoxia Up-Regulated 1 (Hsp70 Family Chaperone)
IPA	Small Molecule IRE1/PERK Activator
IRE1	Inositol-Requiring Enzyme 1
L1CAM	L1 Cell Adhesion Molecule
LacdiNAc	*N*,*N'*-Diacetyllactosamine
LacNAc	*N*-Acetyllactosamine
LcH	*Lens culinaris* Agglutinin Lectin (Core Fucose Binder)
m/z	Mass-to-Charge Ratio

MALDI-TOF MS	Matrix Assisted Laser Desorption Ionization Time of Flight Mass Spectrometry
Man5	Oligomannose *N*-Linked Oligosaccharide with 5 Mannosyl Residues
Man7	Oligomannose *N*-Linked Oligosaccharide with 7 Mannosyl Residues
Man9	Oligomannose *N*-Linked Oligosaccharide with 9 Mannosyl Residues
MCF7	Human Luminal Breast Cancer Cell Line (named after the Michigan Cancer Foundation)
MDA-MB-231	Human Triple-Negative Breast Cancer Cell Line (named after the MD Anderson Cancer Center, Metastatic Breast)
MDSC	Myeloid Derived Suppressor Cell
MES	2-(*N*-Morpholino)ethanesulfonic Acid (Buffer)
miRNA	microRNA
MOPS	3-(*N*-Morpholino)propanesulfonic Acid (Buffer)
MS	Mass Spectrometry
MS/MS	Tandem Mass Spectrometry
MW	Molecular Weight
NES	Normalized Enrichment Score
NeuAc	*N*-Acetylneuraminic Acid (Sialic Acid)
NF-κB	Nuclear Factor Kappa-Light-Chain-Enhancer of Activated B Cells
NK	Natural Killer Cells (Large Granular Lymphocytes)
NPA	*Narcissus pseudonarcissus* Lectin (Oligomannose Binder)
NTC	No Template Control
PAIN	Pan-Assay Interference Compound
PBS	Phosphate-Buffered Saline
PBS-T	Phosphate-Buffered Saline with Tween 20 Detergent
PCR	Polymerase Chain Reaction
PD-1	Programmed Cell Death 1 (Inhibitory Checkpoint Molecule)
PD-L1	Programmed Cell Death 1 Ligand 1 (PD-1 Ligand)

PERK	Protein Kinase R-like Endoplasmic Reticulum Kinase
PHA-E	*Phaseolus vulgaris* Erythroagglutinin Lectin (Bisecting GlcNAc Binder)
PHA-L	*Phaseolus vulgaris* Leucoagglutinin Lectin (β1,6-Branching GlcNAc Binder)
PMAA	Partially Methylated Alditol Acetate
Proteostasis	Protein Homeostasis
PSA	*Pisum sativum* Agglutinin Lectin (Core Fucose Binder)
PSL-I	*Polyporus squamosus* Lectin I (α2,6-Sialic Acid Binder)
qRT-PCR	Quantitative Real-Time Polymerase Chain Reaction
rCVN	Recombinant Cyanovirin Lectin (from *Nostoc ellipsosporum*; High-Mannose Binder)
rGRFT	Recombinant *Griffithsia sp.* Lectin (High-Mannose Binder)
RIPA	Radioimmunoprecipitation Assay Buffer
rSVN	Recombinant Scytovirin Lectin (from *Scytonema varium*; High-Mannose Binder)
SDS	Sodium Dodecyl Sulfate (Detergent)
SDS-PAGE	Sodium Dodecyl Sulfate Polyacrylamide Gel Electrophoresis
Sec63	Protein Translocation Regulator; Part of the ER Translocon Complex
sgDNAJB9	Single Guide RNA Targeting *DNAJB9*
sgRNA	Single Guide RNA
SNA-I	*Sambucus nigra* Lectin (α2,6-Sialic Acid Binder)
T-47D	Human Luminal Breast Cancer Cell Line
TAG	Termination Codon (Stop Codon)
TBS	Tris-Buffered Saline
TBS-T	Tris-Buffered Saline with Tween 20 Detergent
Tg	Thapsigargin (Sarco/Endoplasmic Reticulum Ca^{2+} ATPase Inhibitor)
TJA-I	*Trichosanthes japonica* Agglutinin I Lectin (α2,6-Sialic Acid Binder)
TJA-II	*Trichosanthes japonica* Agglutinin II Lectin (Fucose Binder)

TNBC	Triple-Negative Breast Cancer
TRAIL	Tumor Necrosis Factor (TNF)-Related Apoptosis-Inducing Ligand
Tris	Tris(hydroxymethyl)aminomethane (Buffer)
UDA	*Urtica dioica* Agglutinin Lectin (Oligomannose Binder)
UDP-GlcNAc	Uridine Diphosphate *N*-Acetylglucosamine
UPR	Unfolded Protein Response
WT	Wild Type
XBP1	X-Box Binding Protein 1
XBP1s	Spliced X-Box Binding Protein 1
XBP1u	Unspliced X-Box Binding Protein 1
ZR-75-1	Human Luminal Breast Cancer Cell Line

Chapter 1

Crosstalk between the Unfolded Protein Response and *N*-Linked Glycosylation

Summary

Protein homeostasis (proteostasis) is orchestrated by numerous players, including chaperone proteins that enhance folding, quality control factors that facilitate degradation, and enzymes that install post-translational modifications that affect protein stability and function. Proteostasis is tightly regulated in the cell, and proteostatic dysfunction is associated with many diseases such as neurodegeneration and cancer. Proteostasis influences, and is influenced by, a multitude of cellular pathways including glycosylation, but the crosstalk between pathways is not yet well-understood. Glycosylation, one of the most common post-translational modifications, presents several challenges to its study, including template-free biosynthesis, structurally similar building blocks, and highly branched structures. Glycosylation is regulated at multiple levels, and emerging evidence shows that upstream transcription factors may control the final molecular architecture of sugars used to modify proteins. There are data demonstrating that proteostasis and glycosylation are linked, but relatively little mechanistic work has been performed to probe the underlying biology. Notably, dysregulation of both proteostasis and glycosylation contributes to the development of cancer. In this chapter, we discuss the crosstalk between proteostasis and glycosylation, focusing on their roles in diseases such as cancer.

Introduction to Protein Folding and Disease

Cells dynamically synthesize, fold, and degrade proteins with assistance from the proteostasis network (**Figure 1.1**).[1-2] The vast majority of proteins adopt defined three-dimensional structures to exert their biological functions.[3] Even proteins with intrinsically disordered regions must be maintained in functional states and often still must fold to function in their roles as molecular switches,[4-5] regulatory hubs for protein–protein interaction networks,[6-8] and components of membrane-less organelles.[9-10] Protein misfolding is known to cause a number of diseases, such as cystic fibrosis.[11-12] Additionally, diseases associated with amyloid aggregates, such as Alzheimer's and Parkinson's, have been linked to the decline in proteostasis that accompanies aging.[13-14] Furthermore, cancers often feature dysregulated proteostasis and upregulation of cytoprotective elements that enhance cancer cell survival in conditions that would otherwise cause protein misfolding injury and oxidative stress. The importance of proteostasis in cancer is highlighted by the overexpression of the BiP Hsp70 chaperone, which plays a central role in the unfolded protein response (UPR),[15] in many types of cancers,[16-20] as well as overexpression of numerous other chaperones.[21-27]

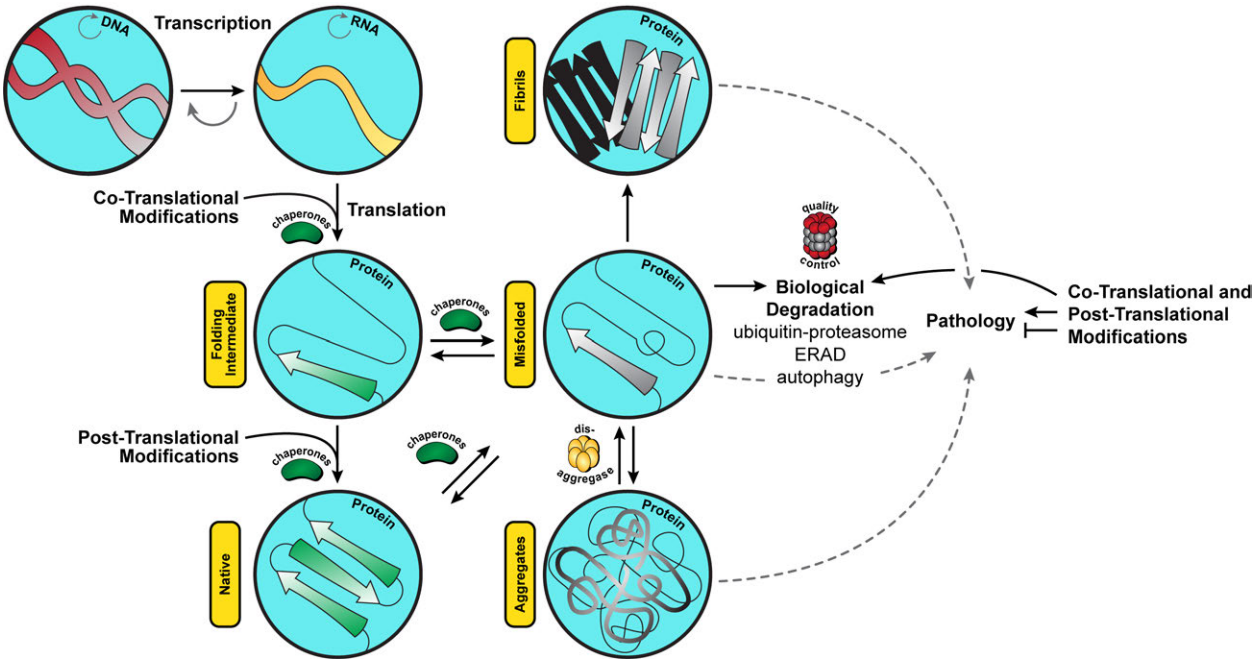

Figure 1.1: Protein homeostasis is a dynamic process. During and after translation, proteins can undergo folding to adopt defined three-dimensional structures. Misfolded proteins lack function and can also lead to the formation of amyloid fibrils and amorphous aggregates, which have been associated with pathology. Steps between folding intermediates, native states, and misfolded states are mediated by players such as chaperone proteins and protein disulfide isomerases. Cells feature mechanisms for quality control of misfolded proteins such as the ubiquitin-proteasome system (UPS), ER–associated degradation (ERAD), and autophagy. Co-translational and post-translational modifications can impart new biological activity or enhanced stability to proteins, but can also contribute to pathology. Post-translational modifications are also used to facilitate protein degradation, as in the case for ERAD and the UPS. Disease can occur when there is proteostasis imbalance.

Active research on proteostasis has led to breakthrough therapies, including small molecules to treat the underlying cause of cystic fibrosis, correcting and potentiating misfolded and non-functional forms of the CFTR chloride ion channel.[28-29] On the other hand, clinical trials for antibodies targeting downstream consequences of failed proteostasis, such as amyloid-β oligomers and fibrils in Alzheimer's disease, have failed to achieve cognitive benefit.[30-31] These clinical setbacks with Alzheimer's disease are just a few examples of our limited understanding of diseases associated with proteostasis, but do suggest the need to correct proteostasis in cells, before irreversible protein aggregation has occurred. Proteostasis modulators for cancer treatment include the blockbuster drug bortezomib, a proteasome inhibitor approved for multiple myeloma.[32] However, resistance to bortezomib treatment can result from alterations in cellular metabolism and glycosylation.[33-34]

Here, we introduce the proteostasis network, post-translational modifications with focus on *N*-linked glycosylation, and the hallmarks of cancer. Furthermore, we provide the conceptual framework for crosstalk between the endoplasmic reticulum's (ER's) unfolded protein response and *N*-glycosylation using cancer as an exemplar biological context.

The Proteostasis Network

Cellular proteostasis is regulated by many elements, and different subcellular compartments are controlled by distinct regulators. Within the cytosol, protein folding capacity is maintained by a number of chaperone systems, including ribosome-associated chaperones, the heat shock factor 1 (HSF1)-regulated Hsp40/70/90 systems, and the TRiC/CCT chaperonins.[35]

Among the proteostasis networks of a eukaryotic cell, that of the secretory pathway is of particular interest, as roughly one-third of the proteome passes through the ER and Golgi for processing and maturation in these specialized subcellular compartments.[36] The secretory pathway begins with translocation of nascent polypeptides into the ER membrane, followed by further processing in the Golgi, and finally export to cellular membranes, the lysosome, or the extracellular milieu. The proteostasis network in the ER is regulated by the unfolded protein response, which safeguards the ER from protein misfolding stress.[15] In cases of unresolved ER stress, the UPR commits cells to apoptosis via signaling through Bcl-2 family members, TRAIL receptors, death receptors, and activation of caspases.[37-41]

The UPR is comprised of the three ER transmembrane sensor proteins IRE1, ATF6, and PERK, each of which signals to its downstream transcriptional effector XBP1s, cleaved ATF6 (ATF6f), and ATF4, respectively, through distinct mechanisms (**Figure 1.2**).[15] Each of the three branches of the UPR induces expression of certain genes and biological responses with some overlap,[42-47] including but not limited to genes encoding chaperone proteins, quality control factors including components of the ubiquitin-proteasome system, and genes involved in metabolism and glycosylation.[48-49]

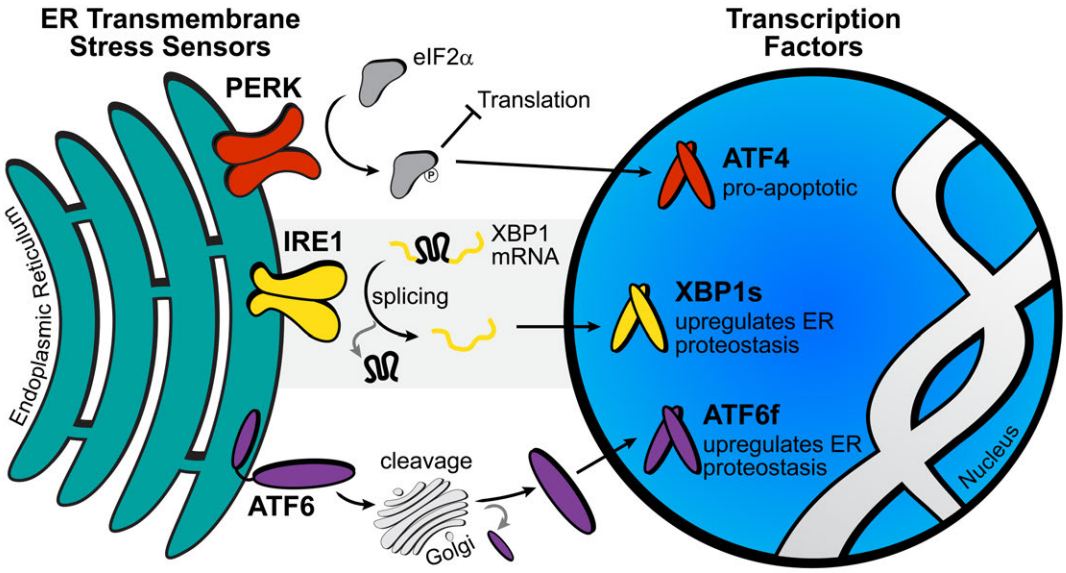

Figure 1.2: The unfolded protein response safeguards ER proteostasis through three distinct pathways. PERK, IRE1, and ATF6 are ER transmembrane sensor proteins that signal to their respective transcription factors ATF4, XBP1s, and ATF6f. PERK activation can also lead to blocking protein translation. Each pathway involves a distinct mechanism, including phosphorylation of eIF2α (PERK-ATF4), splicing of *XBP1* mRNA (IRE1-XBP1s), and cleavage of ATF6. The XBP1s and ATF6f transcription factors upregulate the ER proteostasis network via induced expression of genes for proteins involved in protein folding, such as chaperones, to mitigate ER stress. Unresolved stress can lead to apoptosis via the ATF4 transcription factor.

The mitochondrion coordinates its own unfolded protein response[50] that induces expression of mitochondrial chaperones and proteases, with consequences seen in immunity, metabolism, cell survival, and aging.[51-52] Interestingly, cytosolic proteostasis has been linked to protein import into mitochondria,[53] and the ER makes extensive contact sites with mitochondria,[54-56] hinting at the possibility of crosstalk between the cytosolic, ER, and mitochondrial proteostasis networks.[57-59]

Due to the widespread influence of dysregulated proteostasis in biology and disease, it is unsurprising that the proteostasis network is a drug target for many diseases beyond the aforementioned cystic fibrosis and neurodegenerative disorders. For example, there is great interest in targeting the proteostasis network for treating the lysosomal storage disorders Gaucher disease and Tay-Sachs disease,[60] and liver diseases caused by aggregates of alpha-1 antitrypsin (AATD).[61] Furthermore, chaperones are often necessary for folding metastable oncogenes such as v-Src[62-64] and other cancer-related client proteins.[65] ER proteostasis in particular is a cancer target, with inhibitors for the Grp94 Hsp90 chaperone in development.[66]

Chemical Tools to Control the Unfolded Protein Response

Professional secretory cells, such as B cells and pancreatic β-cells, rely on upregulation of the unfolded protein response (**Figure 1.2**) in accordance with their roles in secreting antibodies and insulin,

respectively. Additionally, normal physiology including embryogenesis and development require robust proteostasis and dependence on protein folding capacity. Furthermore, ER proteostasis plays important roles in disease,[67] especially in a variety cancers.[68-70] In order to fully understand the functions of the UPR in biology and disease, stress-independent methods of activation are required beyond those that induce the global UPR.

Classic tools used to induce ER stress include the compounds thapsigargin, tunicamycin, and Brefeldin A.[71] Such compounds activate global ER stress by blocking calcium ion import into the ER (thapsigargin), blocking protein *N*-glycosylation (tunicamycin), or blocking protein transport from the ER to the Golgi (Brefeldin A). These ER stressors can lead to massive protein misfolding, thus activating all three branches of the UPR. Applications of such compounds have led to dissection of the effects of ER stress on autophagy and other aspects of biology,[72] but their global consequences for cell health make branch-specific effects difficult to analyze. Moreover, ER stressors are not viable therapeutic drugs for UPR modulation, as they are highly cytotoxic.

Chemical genetic methods have been developed to modulate ER proteostasis without global UPR induction,[42, 44] allowing elucidation of branch-specific biology. Screening methods for small molecule, pharmacologic control of ATF6 have identified compounds that selectively activate ATF6.[73-74] Molecules that activate IRE1 have largely proven to be quite cytotoxic or pleiotropic,[75] and lacking in sustained potency.[76-78] The search for potent, selective activators of IRE1 is ongoing, with promising first-in-class compounds recently identified from high-throughput screening.[79] Pharmacologic control of ATF6 and IRE1 have shown promising effects in conferring protection from heart damage following myocardial ischemia/reperfusion *in vivo*, and in reducing secretion of toxic amyloid precursor protein (APP) in cellular models, respectively.[73, 79] Extensive overviews of tools and methods to control the UPR and cellular proteostasis have been reported elsewhere[80-81] and will not be further discussed in this chapter.

Post-Translational Modifications

Owing to compartmentalization of the ER and Golgi, secretory pathway proteins are presented unique environments for protein maturation, including glycosylation by a suite of enzymes (i.e., glycosyltransferases and glycosidases) and disulfide bond formation by protein disulfide isomerases. Such co- and post-translational modifications can impart enhanced stability and functional diversity. For example, proteins undergoing glycosylation are covalently modified with sugars to yield linear or branched sugar structures called glycans (**Figure 1.3**). Glycans attached to proteins (or to other glycoconjugates such as lipids) help comprise the layer of sugars on the cell surface called the glycocalyx. The glycocalyx contributes to cell–cell recognition and cell–matrix interactions.[82] Glycans also affect the function of proteins, influencing downstream biology (further discussed in the following section).

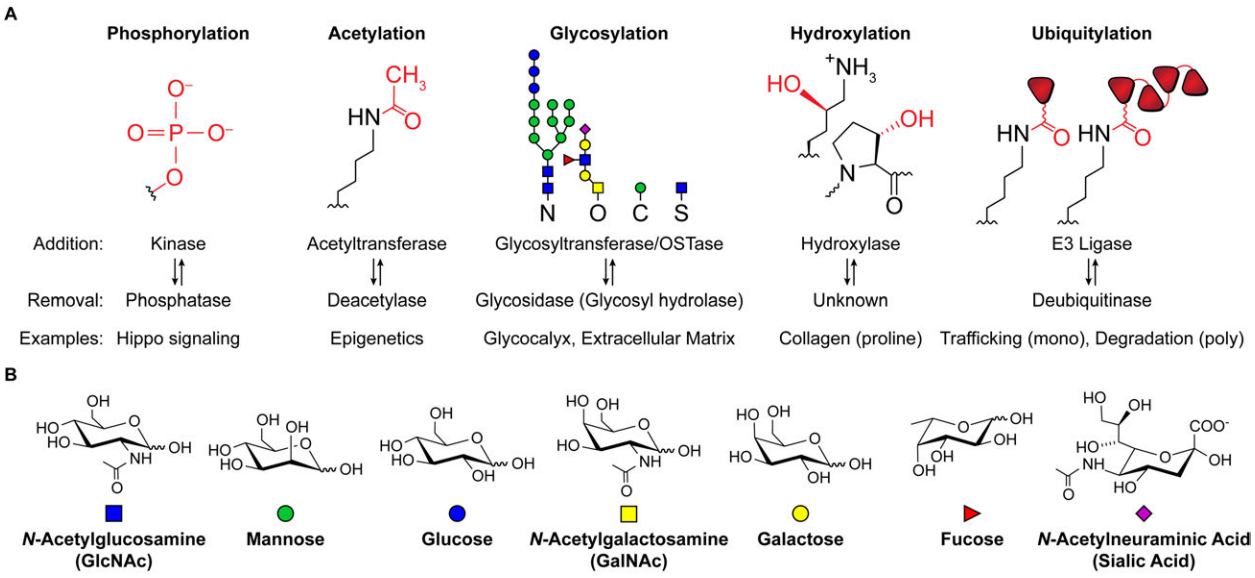

Figure 1.3: Post-translational modifications are chemical groups attached to proteins via covalent linkages. ***A***: Such modifications are diverse and only a small selection is presented here. Some modifications such as phosphorylation, acetylation, and hydroxylation use small chemical moieties (shown in red), but their effects on protein conformation and function can be profound. Others, such as glycosylation and ubiquitylation, use larger chemical groups (sugars and proteins, respectively) to build linear or branched structures. These modifications are installed or removed by specific enzymes. Examples of the roles of post-translational modifications are highlighted. ***B***: Chemical structures of common monosaccharide building blocks used in protein glycosylation. Several are structural isomers, such as the hexose sugars (mannose, glucose, and galactose) and the HexNAc sugars (GlcNAc and GalNAc).

Proteins can also be modified with ubiquitin, a small regulatory protein that can direct other proteins for proteasomal degradation when polyubiquitinated (i.e. modified with a chain of ubiquitin molecules) (**Figure 1.3*A***). Ubiquitin-mediated protein degradation takes place as a quality control mechanism for misfolded proteins (**Figure 1.1**), such as those in the ER destined for ER–associated degradation (ERAD).[83] In contrast to polyubiquitylation, monoubiquitylation of proteins does not target proteins for degradation, but instead can affect protein localization and endocytic trafficking.[84] Additional post-translational modifications include phosphorylation, acetylation, and hydroxylation (**Figure 1.3*A***),[85] which can confer additional levels of regulation and dramatically alter the structure and function of proteins, acting as molecular switches or rheostats for tuning activity. The entire repertoire of post-translational modifications is too grand to be described in detail here. We will focus on *N*-linked glycosylation in particular for its emerging connections to the unfolded protein response.

N-Linked Glycosylation

Unlike macromolecules such as nucleic acids (DNA and RNA) or proteins, glycans are synthesized without templates, instead relying on the biosynthesis of nucleotide-activated monosaccharides as building

blocks,[86-87] their associated transporters,[88] and enzymes that mediate the addition and removal of monosaccharides.[89] Structural isomers of monosaccharides are often the building blocks of glycans (**Figure 1.3*B***), making discrimination of these sugars based on molecular weight alone challenging.[90] Researchers have developed chemical tools and methods to study glycosylation, utilizing bioorthogonal chemistry, metabolic and chemoenzymatic engineering, array-based technologies, and mass spectrometry.[91-96]

Several forms of glycosylation occur in cells, including *O*-linked glycosylation, *C*-linked mannosylation, *S*-linked glycosylation, glypiation (glycosylphosphatidylinositol anchor attachment), and phosphoglycosylation. *N*-Linked glycosylation of asparagine is, however, the most common.[97] Again, we focus on *N*-linked glycosylation here owing to its emerging connections to ER proteostasis and the UPR. *N*-Glycosylation features step-wise synthesis of a precursor oligosaccharide, *en bloc* transfer of the precursor, followed by further step-wise processing (**Figure 1.4*A***),[98] with the potential to create highly branched structures. *N*-Glycosylation is evolutionary conserved[99] and has wide-ranging effects in health and disease.[100] All kingdoms of life feature *N*-glycosylation, but may utilize specialized building blocks depending on the organism.[101] Initial studies had suggested that over half of the proteome is *N*-glycosylated,[102] but more recent analyses suggest one-fifth as the upper limit.[97]

N-Glycans can adopt various structures that influence protein function (**Figure 1.4*B***). They contribute to the formation of distinct proteoforms[103] with glycan-dependent functions in immunity, development and beyond.[104-105] For example *N*-glycans can influence the threshold of immune activation. Specifically, a deficiency in MGAT5, a β1,6-branching GlcNAc transferase, lowers the activation threshold of T cells and increases the incidence of autoimmunity by enhancing T cell receptor clustering that results from altered *N*-acetyllactosamine levels and galectin binding.[106] *N*-Glycans have also been reported to affect viral escape from the immune system. The HIV gp120 envelope glycoprotein is heavily glycosylated with high-mannose glycans, which protect it from proteolytic processing required for antigen presentation and cytotoxic T cell priming.[107] Additionally, the *N*-glycans on gp120 help form the protective glycan shield that allows HIV to evade neutralizing antibodies.[108] Other *N*-glycan epitopes that modulate immune function include core fucose, which was shown to be required for T cell activation.[109] The core fucose epitope is further required during development, evidenced by the poor survival of mice lacking Fut8, the fucosyltransferase enzyme responsible for initiating core fucosylation, due to growth and respiratory defects.[110-111] These examples provide just a snapshot of the many roles of *N*-glycans in biology and disease.

Therapeutic antibodies are often engineered to display desired *N*-glycan modifications, which can function as structural rheostats and thus modulated accordingly. For example, a monoclonal antibody against EGFR was chemoenzymatically engineered to display desired sialylated and non-fucosylated (afucosylated) glycans, optimizing binding affinity and enhancing cytotoxic activity against human skin

cancer cells.[112] Afucosylated glycans have emerged as prominent determinants of enhanced antibody-dependent cell cytotoxicity[113-115] and are often desirable for antibodies used as anti-cancer therapeutics.

N-Glycans in Protein Quality Control

Early in the secretory pathway, *N*-glycans mediate protein folding and quality control by allowing access to the lectin-based protein chaperones calnexin and calreticulin in the ER,[116] as well as to their partner proteins in folding, oxidation, and glycan trimming.[117-118] Glycoproteins with the specific glycan structure

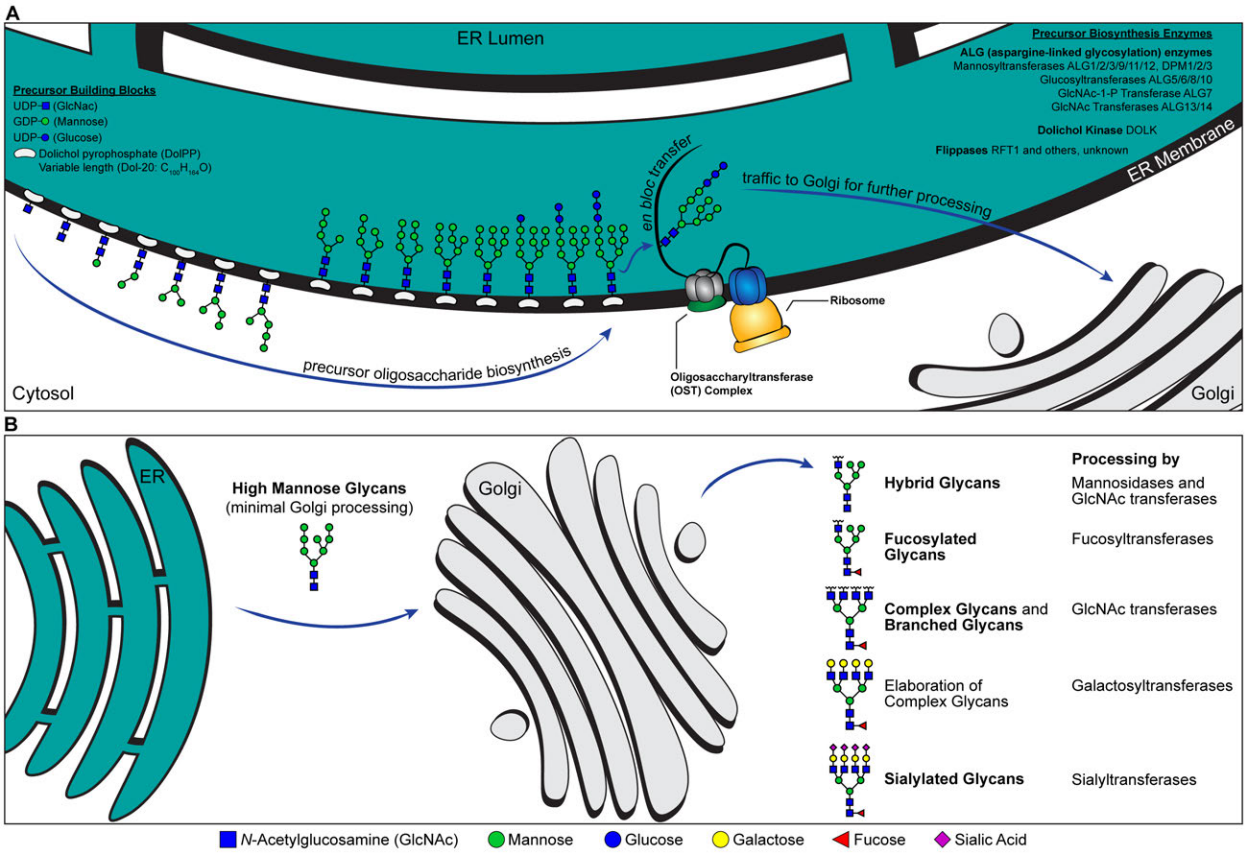

Figure 1.4: Protein *N*-linked glycosylation is a co- and post-translational modification that installs glycans onto asparagine side chains of proteins. ***A***: A 14-residue precursor oligosaccharide is first synthesized in a step-wise fashion while attached to a dolichol pyrophosphate molecule on the ER membrane. Monosaccharide substrates in the form of nucleotide sugars are each added to the growing sugar chain by their respective transferase enzymes, and the biosynthesis of the precursor requires the action of flippase enzymes after attachment of the seventh monosaccharide. After the 14-residue precursor is biosynthesized, it is added to a nascent glycoprotein by the oligosaccharyltransferase complex as the polypeptide translocates from the ribosome to the ER. After installation of the precursor, initial trimming occurs in the ER and the nascent glycoprotein is trafficked to the Golgi for further processing. ***B***: Glycosylation enzymes in the Golgi process the *N*-glycan with sequential removal and addition of monosaccharides by specific enzymes, ultimately yielding a vast array of potential glycan structures, including hybrid glycans, complex glycans, core fucosylated glycans, and sialylated glycans. The specific identity of the glycan has important and varied effects on cellular communication and the function of proteins. Emerging evidence shows that certain transcription factors may coordinately remodel the expression of enzymes to yield specific glycan structures.

of $Glc_1Man_9GlcNAc_2$ (Glc, glucose; Man, mannose; GlcNAc, *N*-acetylglucosamine) cycle through calnexin/calreticulin binding until the terminal glucose is trimmed from the structure, thereby preventing re-entry into the folding cycle. Proper folding and re-entry into the cycle is monitored by the UGGT glucosyltransferase enzyme that can re-install the terminal glucose for another cycle of folding. Additionally, glycans serve as signals for ER–associated degradation whereby glycoproteins that fail to properly fold are processed by the EDEM mannosidase enzymes, retrotranslocated to the cytosol with the help of lectin receptors, and tagged for ubiquitin-mediated proteasomal degradation.[83]

Deciphering Regulation of Glycosylation

Our current understanding of how glycosylation is regulated is quite poor. Hundreds of genes are involved in *N*-glycosylation, and how the cell regulates all of these players in a coordinated fashion is not well-understood, though the roles of transcription factors and miRNA in regulating glycosylation are emerging. Evidence of transcription factors controlling glycosylation-related gene (glycogene) expression is in general lacking, with information available for only about two dozen glycogene–transcription factor interactions.[119] Examples of transcription factors controlling glycogene expression include the HNF1α and ATF2 transcription factors, which can regulate the expression of fucosyltransferase and fucose biosynthesis genes.[120-122]

Regulation of gene expression by miRNA can also control the expression of individual glycogenes.[123] A recent analysis of sequencing reads from the human genome and experimental validation suggested that 2,300 true human mature miRNAs exist, half of which were annotated in the miRBase database at the time of publication.[124] Currently 80 glycogenes are known to be regulated by miRNAs[123] but because accurate miRNA prediction algorithms are currently lacking, most studies have focused on individual miRNAs. Looking forward, the development of focused CRISPR-Cas9 libraries targeting human miRNAs[125] could make high-throughput screens for miRNA–glycosylation biology more feasible.

A Novel Connection: XBP1s and Glycosylation

Previous studies had shown that XBP1s can activate the hexosamine biosynthetic pathway (HBP), a glucose metabolic pathway that generates the UDP-GlcNAc metabolite used for protein glycosylation, but it was unknown whether XBP1s influences either the extent of protein *N*-glycosylation or the final structure of glycans decorating proteins.[87, 126] Our lab discovered that XBP1s activation can remodel the expression of glycosylation enzymes.[127] As one of the major regulators of the unfolded protein response, XBP1s plays instrumental roles in controlling the expression of chaperone proteins and quality control factors, but it was surprising to discover that XBP1s can also coordinate the expression of multiple glycogenes that influence glycan structures.

Using stress-independent activation of XBP1s and glycomic profiling by mass spectrometry, our group went on to show that XBP1s alters the structural distribution of *N*-glycans installed on a secreted glycoprotein domain derived from the CD2 adhesion protein, shifting from majority oligomannose *N*-glycans to predominantly hybrid *N*-glycans.[127] XBP1s activation also influenced terminal *N*-glycan epitopes such as LacdiNAc (*N*,*N*'-diacetyllactosamine) and fucosylated LacdiNAc. Pulse-chase studies demonstrated that synthesis and trafficking of the model protein were not affected, thus the observed *N*-glycan changes were due to alterations in *N*-glycan maturation, likely mediated by shifts in glycogene expression. We demonstrated that the effects of XBP1s in shifting glycoform distributions were generalizable to the secreted collagen-α1(I) C-propeptide domain.[127] These findings suggest that intracellular stress signaling, and XBP1s in particular, can coordinately regulate the molecular architecture of *N*-glycans. However, the CD2 and collagen protein domains used in these initial studies[127] were ectopically expressed and, in the case of CD2 involved a domain that is not normally glycosylated, rendering the biological relevance of XBP1s-dependent remodeling of glycosylation uncertain at the time. Nonetheless, these studies demonstrated that XBP1s bridges ER proteostasis with *N*-glycan maturation, which has potential to influence disease progression. Both ER stress and glycosylation contribute to the development of cancer[128-130] and resistance to cancer therapies,[131-136] suggesting a potential role for crosstalk between ER stress and glycosylation.

The Hallmarks of Cancers

Cancers are heterogeneous diseases distributed across the body,[137-139] and are the second leading cause of death (after heart disease) in the United States.[140] There are over 100 types of cancer,[141] among which the most common are colorectal, lung, breast, and prostate cancer.[140] Despite this heterogeneity, all cancers feature uncontrolled cell division and a dysregulation of normal tissue homeostasis that can lead to metastasis, or the spread to distant body parts. Cancer cells grow continuously and overcome biological safeguards such as apoptosis and senescence, while feedback mechanisms such as cell cycle checkpoints are broken. Metastatic cancer can lead to organ damage, and weakened immune systems associated with cancer treatments lead to higher risk of complications such as infections and sepsis.[142]

The Hallmarks of Cancer describe eight biological alterations that enable transformation of healthy cells into malignant cells.[141, 143] These principles include (1) sustaining proliferative signaling, (2) evading growth suppressors, (3) resisting cell death, (4) enabling replicative immortality, (5) inducing angiogenesis, (6) activating invasion and metastasis, (7) reprogramming of energy metabolism, and (8) evading immune destruction (**Figure 1.5*A***). These hallmarks encompass the effects of oncogenes such as Ras, PI3K, and EGFR;[103, 144-147] inactivation of tumor suppressors such as Rb, p53, and Hippo;[148-150] upregulation of anti-

apoptotic factors;[151] expression of telomerase;[152] induction of angiogenesis in hypoxic conditions;[153-154] EMT transition states;[155] metabolic rewiring and oncometabolites;[156-157] and immunoediting.[158]

Defining the Hallmarks of Cancer provides a framework to study the disease and to identify potential therapeutic targets. These hallmarks have been updated over time,[143] reflecting progress in our understanding of cancer. As cancer research advances, we may expect to add to the list of cancer hallmarks (**Figure 1.5*B***).[129, 159-162]

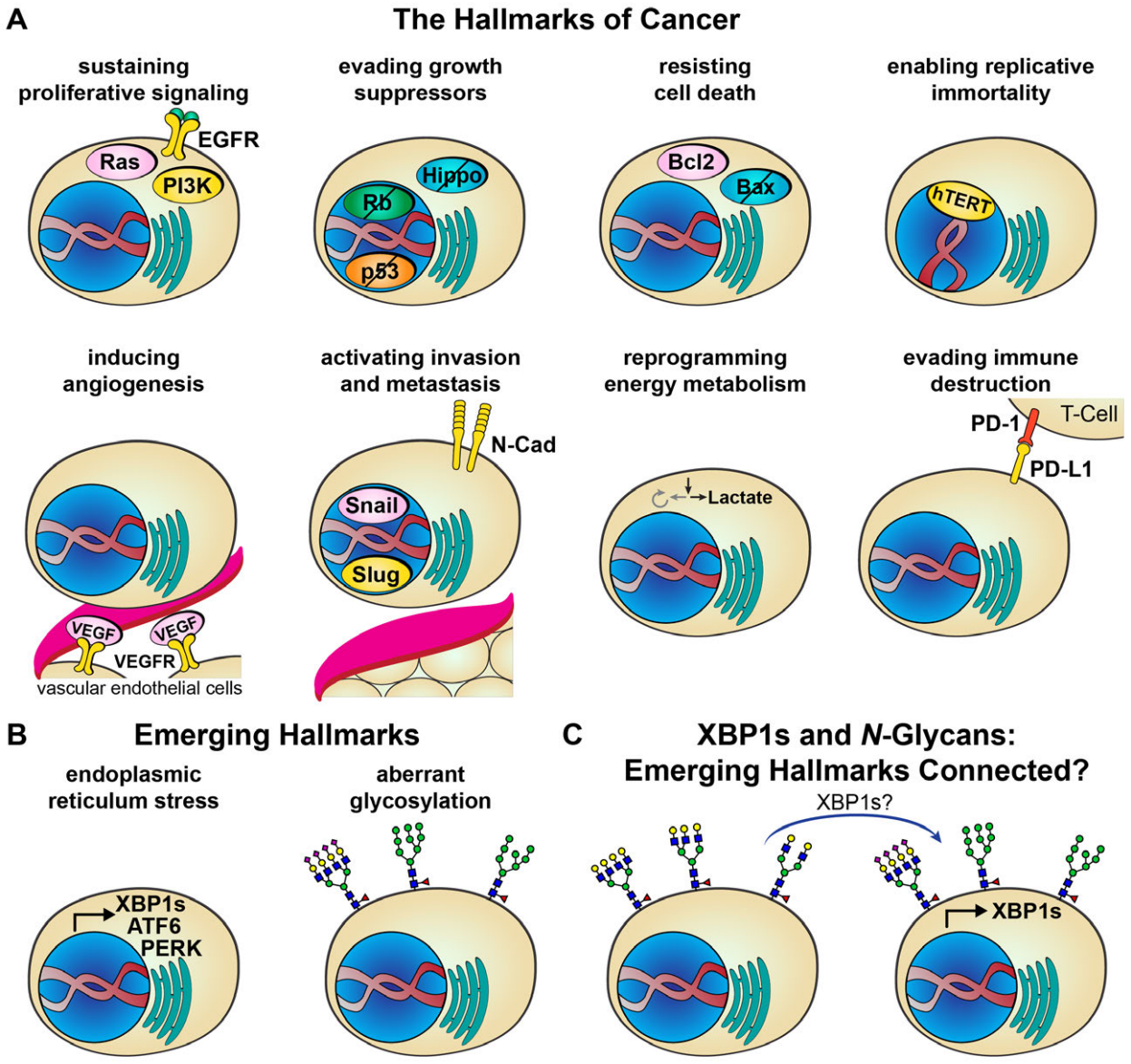

Figure 1.5: Emerging cancer hallmarks and new connections. ***A***: The Hallmarks of Cancer describe eight alterations in healthy cells that enable transformation into malignant cells. ***B***: Many biological processes have been proposed as emerging cancer hallmarks, including ER stress and glycosylation. ***C***: Work in our lab has suggested that XBP1s may be a master regulator of both ER stress and protein glycosylation, potentially linking two emerging cancer hallmarks.

Connection between Emerging Hallmarks of Cancer: ER Stress and Glycosylation

Emerging hallmarks of cancer include DNA replication stress,[159] ER stress,[129] glycosylation,[160-161] and circadian regulation.[162] Tumors undergo significant stress conditions, including nutrient deprivation and hypoxia, which affect metabolism, glycosylation, protein synthesis,[163-164] and can impede the cell's protein folding capacity, leading to ER stress.[165-166] Additionally, ER stress responses can negatively regulate anti-tumor immunity.[167-169] XBP1s activity inhibits the capacity of dendritic cells to support T cell function, and the UPR transcription factor CHOP regulates the activity of immune-suppressive myeloid-derived suppressor cells (MDSCs). Inducing ER stress in mice with thapsigargin enhances tumor growth by increasing the immunosuppressive capacity of MDSCs. These observations suggest that targeting ER stress might be an effective strategy to enhance existing cancer immunotherapies.

Another attractive target for cancer therapy is glycosylation,[170] given that the surface of every cell is covered with a layer of sugars (i.e., the glycocalyx) that can modulate various biological processes, and that glycosylation is often dysregulated in cancer, leading to tumor-associated carbohydrate antigens that can serve as biomarkers.[171-172] For example, the sugars on the cancer cell surface are often transformed to display more sialic acid, mannose, or fucose residues. Since cancer cells often feature upregulation of proteostasis factors such as XBP1s, it is possible that the transcriptional remodeling of glycogenes resulting from XBP1s activation[127] may also induce changes in glycan structure that contribute to malignancy. Thus, XBP1s may bridge ER stress and glycosylation as connected cancer hallmarks (**Figure 1.5*C***).

Conclusions

The UPR and glycosylation each modulate biological processes that contribute to a multitude of diseases. Our current understanding of the interplay between the UPR and glycosylation is nascent, but such a conceptual framework will help illuminate future studies. Protein glycosylation is regulated at many levels, including by transcription factors, but our overall understanding of which transcription factor–glycogene pairs exist and contribute to biology is incomplete, with mechanistic work available for only about 15 glycogenes.[119] In the following chapters, we combine stress-independent activation of XBP1s in cells with glycomic analyses to profile glycosylation changes on endogenous proteins (**Chapter 2**). We then describe the results of direct, pharmacological inhibition of IRE1 to prevent formation of endogenous XBP1s in breast cancer cells, and report on the associated glycomic changes (**Chapter 3**). Lastly, we explore the negative feedback loop regulating IRE1 activity as a mechanism that prevents sustained pharmacological IRE1 activation (**Chapter 4**). Our results demonstrate that XBP1s is a significant player in regulating glycosylation, with varying effects across cell types. In addition, our findings on IRE1 regulation emphasize the importance of continued research to identify regulators of the IRE1-XBP1s signaling axis for target discovery.

References

[1] Balchin, D.; Hayer-Hartl, M.; Hartl, F. U., In vivo aspects of protein folding and quality control. *Science* **2016,** *353* (6294), aac4354.

[2] Balch, W. E.; Morimoto, R. I.; Dillin, A.; Kelly, J. W., Adapting proteostasis for disease intervention. *Science* **2008,** *319* (5865), 916-9.

[3] Dill, K. A.; MacCallum, J. L., The protein-folding problem, 50 years on. *Science* **2012,** *338* (6110), 1042-6.

[4] Choi, U. B.; Sanabria, H.; Smirnova, T.; Bowen, M. E.; Weninger, K. R., Spontaneous Switching among Conformational Ensembles in Intrinsically Disordered Proteins. *Biomolecules* **2019,** *9* (3).

[5] Marceau, A. H.; Brison, C. M.; Nerli, S.; Arsenault, H. E.; McShan, A. C.; Chen, E.; Lee, H. W.; Benanti, J. A.; Sgourakis, N. G.; Rubin, S. M., An order-to-disorder structural switch activates the FoxM1 transcription factor. *Elife* **2019,** *8*.

[6] Haynes, C.; Oldfield, C. J.; Ji, F.; Klitgord, N.; Cusick, M. E.; Radivojac, P.; Uversky, V. N.; Vidal, M.; Iakoucheva, L. M., Intrinsic disorder is a common feature of hub proteins from four eukaryotic interactomes. *PLoS Comput Biol* **2006,** *2* (8), e100.

[7] Kwong, P. N.; Chambers, M.; Vashisht, A. A.; Turki-Judeh, W.; Yau, T. Y.; Wohlschlegel, J. A.; Courey, A. J., The Central Region of the Drosophila Co-repressor Groucho as a Regulatory Hub. *J Biol Chem* **2015,** *290* (50), 30119-30.

[8] Berlow, R. B.; Dyson, H. J.; Wright, P. E., Expanding the Paradigm: Intrinsically Disordered Proteins and Allosteric Regulation. *J Mol Biol* **2018,** *430* (16), 2309-2320.

[9] Saito, M.; Hess, D.; Eglinger, J.; Fritsch, A. W.; Kreysing, M.; Weinert, B. T.; Choudhary, C.; Matthias, P., Acetylation of intrinsically disordered regions regulates phase separation. *Nat Chem Biol* **2019,** *15* (1), 51-61.

[10] Uversky, V. N., Intrinsically disordered proteins in overcrowded milieu: Membrane-less organelles, phase separation, and intrinsic disorder. *Curr Opin Struct Biol* **2017,** *44*, 18-30.

[11] Chiti, F.; Dobson, C. M., Protein Misfolding, Amyloid Formation, and Human Disease: A Summary of Progress Over the Last Decade. *Annu Rev Biochem* **2017,** *86*, 27-68.

[12] Hartl, F. U., Protein Misfolding Diseases. *Annu Rev Biochem* **2017,** *86*, 21-26.

[13] Hipp, M. S.; Kasturi, P.; Hartl, F. U., The proteostasis network and its decline in ageing. *Nat Rev Mol Cell Biol* **2019,** *20* (7), 421-435.

[14] Santra, M.; Dill, K. A.; de Graff, A. M. R., Proteostasis collapse is a driver of cell aging and death. *Proc Natl Acad Sci U S A* **2019,** *116* (44), 22173-22178.

[15] Wong, M. Y.; DiChiara, A. S.; Suen, P. H.; Chen, K.; Doan, N. D.; Shoulders, M. D., Adapting Secretory Proteostasis and Function Through the Unfolded Protein Response. *Curr Top Microbiol Immunol* **2018,** *414*, 1-25.

[16] Lee, H. K.; Xiang, C.; Cazacu, S.; Finniss, S.; Kazimirsky, G.; Lemke, N.; Lehman, N. L.; Rempel, S. A.; Mikkelsen, T.; Brodie, C., GRP78 is overexpressed in glioblastomas and regulates glioma cell growth and apoptosis. *Neuro Oncol* **2008,** *10* (3), 236-43.

[17] Gifford, J. B.; Huang, W.; Zeleniak, A. E.; Hindoyan, A.; Wu, H.; Donahue, T. R.; Hill, R., Expression of GRP78, Master Regulator of the Unfolded Protein Response, Increases Chemoresistance in Pancreatic Ductal Adenocarcinoma. *Mol Cancer Ther* **2016,** *15* (5), 1043-52.

[18] Niu, Z.; Wang, M.; Zhou, L.; Yao, L.; Liao, Q.; Zhao, Y., Elevated GRP78 expression is associated with poor prognosis in patients with pancreatic cancer. *Sci Rep* **2015,** *5*, 16067.

[19] Fernandez, P. M.; Tabbara, S. O.; Jacobs, L. K.; Manning, F. C.; Tsangaris, T. N.; Schwartz, A. M.; Kennedy, K. A.; Patierno, S. R., Overexpression of the glucose-regulated stress gene GRP78 in malignant but not benign human breast lesions. *Breast Cancer Res Treat* **2000,** *59* (1), 15-26.

[20] Pyrko, P.; Schonthal, A. H.; Hofman, F. M.; Chen, T. C.; Lee, A. S., The unfolded protein response regulator GRP78/BiP as a novel target for increasing chemosensitivity in malignant gliomas. *Cancer Res* **2007,** *67* (20), 9809-16.

[21] Wang, Q.; He, Z.; Zhang, J.; Wang, Y.; Wang, T.; Tong, S.; Wang, L.; Wang, S.; Chen, Y., Overexpression of endoplasmic reticulum molecular chaperone GRP94 and GRP78 in human lung cancer tissues and its significance. *Cancer Detect Prev* **2005,** *29* (6), 544-51.

[22] Chen, X.; Ding, Y.; Liu, C. G.; Mikhail, S.; Yang, C. S., Overexpression of glucose-regulated protein 94 (Grp94) in esophageal adenocarcinomas of a rat surgical model and humans. *Carcinogenesis* **2002,** *23* (1), 123-30.

[23] Santana-Codina, N.; Muixi, L.; Foj, R.; Sanz-Pamplona, R.; Badia-Villanueva, M.; Abramowicz, A.; Marce-Grau, A.; Cosialls, A. M.; Gil, J.; Archila, I.; Pedrosa, L.; Gonzalez, J.; Aldecoa, I.; Sierra, A., GRP94 promotes brain metastasis by engaging pro-survival autophagy. *Neuro Oncol* **2019**.

[24] Ghosh, S.; Shinogle, H. E.; Galeva, N. A.; Dobrowsky, R. T.; Blagg, B. S., Endoplasmic Reticulum-resident Heat Shock Protein 90 (HSP90) Isoform Glucose-regulated Protein 94 (GRP94) Regulates Cell Polarity and Cancer Cell Migration by Affecting Intracellular Transport. *J Biol Chem* **2016,** *291* (16), 8309-23.

[25] Sheng, W.; Chen, C.; Dong, M.; Zhou, J.; Liu, Q.; Dong, Q.; Li, F., Overexpression of calreticulin contributes to the development and progression of pancreatic cancer. *J Cell Physiol* **2014,** *229* (7), 887-97.

[26] Stojadinovic, A.; Hooke, J. A.; Shriver, C. D.; Nissan, A.; Kovatich, A. J.; Kao, T. C.; Ponniah, S.; Peoples, G. E.; Moroni, M., HYOU1/Orp150 expression in breast cancer. *Med Sci Monit* **2007,** *13* (11), Br231-239.

[27] Zhou, Y.; Liao, Q.; Li, X.; Wang, H.; Wei, F.; Chen, J.; Yang, J.; Zeng, Z.; Guo, X.; Chen, P.; Zhang, W.; Tang, K.; Li, X.; Xiong, W.; Li, G., HYOU1, Regulated by LPLUNC1, Is Up-Regulated in Nasopharyngeal Carcinoma and Associated with Poor Prognosis. *J Cancer* **2016,** *7* (4), 367-76.

[28] Middleton, P. G.; Mall, M. A.; Drevinek, P.; Lands, L. C.; McKone, E. F.; Polineni, D.; Ramsey, B. W.; Taylor-Cousar, J. L.; Tullis, E.; Vermeulen, F.; Marigowda, G.; McKee, C. M.; Moskowitz, S. M.; Nair, N.; Savage, J.; Simard, C.; Tian, S.; Waltz, D.; Xuan, F.; Rowe, S. M.; Jain, R., Elexacaftor-Tezacaftor-Ivacaftor for Cystic Fibrosis with a Single Phe508del Allele. *N Engl J Med* **2019,** *381* (19), 1809-1819.

[29] Heijerman, H. G. M.; McKone, E. F.; Downey, D. G.; Van Braeckel, E.; Rowe, S. M.; Tullis, E.; Mall, M. A.; Welter, J. J.; Ramsey, B. W.; McKee, C. M.; Marigowda, G.; Moskowitz, S. M.; Waltz, D.; Sosnay, P. R.; Simard, C.; Ahluwalia, N.; Xuan, F.; Zhang, Y.; Taylor-Cousar, J. L.; McCoy, K. S., Efficacy and safety of the elexacaftor plus tezacaftor plus ivacaftor combination regimen in people with cystic fibrosis homozygous for the F508del mutation: a double-blind, randomised, phase 3 trial. *Lancet* **2019,** *394* (10212), 1940-1948.

[30] Selkoe, D. J., Alzheimer disease and aducanumab: adjusting our approach. *Nat Rev Neurol* **2019,** *15* (7), 365-366.

[31] Howard, R.; Liu, K. Y., Questions EMERGE as Biogen claims aducanumab turnaround. *Nat Rev Neurol* **2020,** *16* (2), 63-64.

[32] Besse, A.; Besse, L.; Kraus, M.; Mendez-Lopez, M.; Bader, J.; Xin, B. T.; de Bruin, G.; Maurits, E.; Overkleeft, H. S.; Driessen, C., Proteasome Inhibition in Multiple Myeloma: Head-to-Head Comparison of Currently Available Proteasome Inhibitors. *Cell Chem Biol* **2019,** *26* (3), 340-351.e3.

[33] Tibullo, D.; Giallongo, C.; Romano, A.; Vicario, N.; Barbato, A.; Puglisi, F.; Parenti, R.; Amorini, A. M.; Wissam Saab, M.; Tavazzi, B.; Mangione, R.; Brundo, M. V.; Lazzarino, G.; Palumbo, G. A.; Volti, G. L.; Raimondo, F. D.; Lazzarino, G., Mitochondrial Functions, Energy Metabolism and Protein Glycosylation are Interconnected Processes Mediating Resistance to Bortezomib in Multiple Myeloma Cells. *Biomolecules* **2020,** *10* (5).

[34] Luanpitpong, S.; Chanthra, N.; Janan, M.; Poohadsuan, J.; Samart, P.; Y, U. P.; Rojanasakul, Y.; Issaragrisil, S., Inhibition of O-GlcNAcase Sensitizes Apoptosis and Reverses Bortezomib Resistance in Mantle Cell Lymphoma through Modification of Truncated Bid. *Mol Cancer Ther* **2018,** *17* (2), 484-496.

[35] Vabulas, R. M.; Raychaudhuri, S.; Hayer-Hartl, M.; Hartl, F. U., Protein folding in the cytoplasm and the heat shock response. *Cold Spring Harb Perspect Biol* **2010,** *2* (12), a004390.

[36] Braakman, I.; Bulleid, N. J., Protein folding and modification in the mammalian endoplasmic reticulum. *Annu Rev Biochem* **2011,** *80*, 71-99.

[37] Chang, T. K.; Lawrence, D. A.; Lu, M.; Tan, J.; Harnoss, J. M.; Marsters, S. A.; Liu, P.; Sandoval, W.; Martin, S. E.; Ashkenazi, A., Coordination between Two Branches of the Unfolded Protein Response Determines Apoptotic Cell Fate. *Mol Cell* **2018,** *71* (4), 629-636.e5.

[38] Panganiban, R. A.; Park, H. R.; Sun, M.; Shumyatcher, M.; Himes, B. E.; Lu, Q., Genome-wide CRISPR screen identifies suppressors of endoplasmic reticulum stress-induced apoptosis. *Proc Natl Acad Sci U S A* **2019,** *116* (27), 13384-13393.

[39] Llambi, F.; Wang, Y. M.; Victor, B.; Yang, M.; Schneider, D. M.; Gingras, S.; Parsons, M. J.; Zheng, J. H.; Brown, S. A.; Pelletier, S.; Moldoveanu, T.; Chen, T.; Green, D. R., BOK Is a Non-canonical BCL-2 Family Effector of Apoptosis Regulated by ER-Associated Degradation. *Cell* **2016,** *165* (2), 421-33.

[40] Glab, J. A.; Doerflinger, M.; Nedeva, C.; Jose, I.; Mbogo, G. W.; Paton, J. C.; Paton, A. W.; Kueh, A. J.; Herold, M. J.; Huang, D. C.; Segal, D.; Brumatti, G.; Puthalakath, H., DR5 and caspase-8 are dispensable in ER stress-induced apoptosis. *Cell Death Differ* **2017,** *24* (5), 944-950.

[41] Lam, M.; Marsters, S. A.; Ashkenazi, A.; Walter, P., Misfolded proteins bind and activate death receptor 5 to trigger apoptosis during unresolved endoplasmic reticulum stress. *Elife* **2020,** *9*.

[42] Shoulders, M. D.; Ryno, L. M.; Genereux, J. C.; Moresco, J. J.; Tu, P. G.; Wu, C.; Yates, J. R., 3rd; Su, A. I.; Kelly, J. W.; Wiseman, R. L., Stress-independent activation of XBP1s and/or ATF6 reveals three functionally diverse ER proteostasis environments. *Cell Rep* **2013,** *3* (4), 1279-92.

[43] Okada, T.; Yoshida, H.; Akazawa, R.; Negishi, M.; Mori, K., Distinct roles of activating transcription factor 6 (ATF6) and double-stranded RNA-activated protein kinase-like endoplasmic reticulum kinase (PERK) in transcription during the mammalian unfolded protein response. *Biochem J* **2002,** *366* (Pt 2), 585-94.

[44] Lee, A. H.; Iwakoshi, N. N.; Glimcher, L. H., XBP-1 regulates a subset of endoplasmic reticulum resident chaperone genes in the unfolded protein response. *Mol Cell Biol* **2003,** *23* (21), 7448-59.

[45] Yamamoto, K.; Sato, T.; Matsui, T.; Sato, M.; Okada, T.; Yoshida, H.; Harada, A.; Mori, K., Transcriptional induction of mammalian ER quality control proteins is mediated by single or combined action of ATF6alpha and XBP1. *Dev Cell* **2007,** *13* (3), 365-76.

[46] Bommiasamy, H.; Back, S. H.; Fagone, P.; Lee, K.; Meshinchi, S.; Vink, E.; Sriburi, R.; Frank, M.; Jackowski, S.; Kaufman, R. J.; Brewer, J. W., ATF6alpha induces XBP1-independent expansion of the endoplasmic reticulum. *J Cell Sci* **2009,** *122* (Pt 10), 1626-36.

[47] Lin, J. H.; Li, H.; Zhang, Y.; Ron, D.; Walter, P., Divergent effects of PERK and IRE1 signaling on cell viability. *PLoS One* **2009,** *4* (1), e4170.

[48] Acosta-Alvear, D.; Zhou, Y.; Blais, A.; Tsikitis, M.; Lents, N. H.; Arias, C.; Lennon, C. J.; Kluger, Y.; Dynlacht, B. D., XBP1 controls diverse cell type- and condition-specific transcriptional regulatory networks. *Mol Cell* **2007,** *27* (1), 53-66.

[49] Wong, M. Y.; Chen, K.; Antonopoulos, A.; Kasper, B. T.; Dewal, M. B.; Taylor, R. J.; Whittaker, C. A.; Hein, P. P.; Dell, A.; Genereux, J. C.; Haslam, S. M.; Mahal, L. K.; Shoulders, M. D., XBP1s activation can globally remodel N-glycan structure distribution patterns. *Proc Natl Acad Sci U S A* **2018,** *115* (43), E10089-E10098.

[50] Melber, A.; Haynes, C. M., UPR(mt) regulation and output: a stress response mediated by mitochondrial-nuclear communication. *Cell Res* **2018,** *28* (3), 281-295.

[51] Wang, S.; Gao, K.; Liu, Y., UPR(mt) coordinates immunity to maintain mitochondrial homeostasis and animal fitness. *Mitochondrion* **2018,** *41*, 9-13.

[52] Moehle, E. A.; Shen, K.; Dillin, A., Mitochondrial proteostasis in the context of cellular and organismal health and aging. *J Biol Chem* **2019,** *294* (14), 5396-5407.

[53] Ruan, L.; Zhou, C.; Jin, E.; Kucharavy, A.; Zhang, Y.; Wen, Z.; Florens, L.; Li, R., Cytosolic proteostasis through importing of misfolded proteins into mitochondria. *Nature* **2017,** *543* (7645), 443-446.

[54] Hamasaki, M.; Furuta, N.; Matsuda, A.; Nezu, A.; Yamamoto, A.; Fujita, N.; Oomori, H.; Noda, T.; Haraguchi, T.; Hiraoka, Y.; Amano, A.; Yoshimori, T., Autophagosomes form at ER-mitochondria contact sites. *Nature* **2013,** *495* (7441), 389-93.

[55] Lee, K. S.; Huh, S.; Lee, S.; Wu, Z.; Kim, A. K.; Kang, H. Y.; Lu, B., Altered ER-mitochondria contact impacts mitochondria calcium homeostasis and contributes to neurodegeneration in vivo in disease models. *Proc Natl Acad Sci U S A* **2018,** *115* (38), E8844-e8853.

[56] Friedman, J. R.; Lackner, L. L.; West, M.; DiBenedetto, J. R.; Nunnari, J.; Voeltz, G. K., ER tubules mark sites of mitochondrial division. *Science* **2011,** *334* (6054), 358-62.

[57] Peric, M.; Bou Dib, P.; Dennerlein, S.; Musa, M.; Rudan, M.; Lovric, A.; Nikolic, A.; Saric, A.; Sobocanec, S.; Macak, Z.; Raimundo, N.; Krisko, A., Crosstalk between cellular compartments protects against proteotoxicity and extends lifespan. *Sci Rep* **2016,** *6*, 28751.

[58] Arrieta, A.; Blackwood, E. A.; Stauffer, W. T.; Glembotski, C. C., Integrating ER and Mitochondrial Proteostasis in the Healthy and Diseased Heart. *Front Cardiovasc Med* **2019,** *6*, 193.

[59] Labbadia, J.; Brielmann, R. M.; Neto, M. F.; Lin, Y. F.; Haynes, C. M.; Morimoto, R. I., Mitochondrial Stress Restores the Heat Shock Response and Prevents Proteostasis Collapse during Aging. *Cell Rep* **2017,** *21* (6), 1481-1494.

[60] Wang, F.; Song, W.; Brancati, G.; Segatori, L., Inhibition of endoplasmic reticulum-associated degradation rescues native folding in loss of function protein misfolding diseases. *J Biol Chem* **2011,** *286* (50), 43454-64.

[61] Smith, S. E.; Granell, S.; Salcedo-Sicilia, L.; Baldini, G.; Egea, G.; Teckman, J. H.; Baldini, G., Activating transcription factor 6 limits intracellular accumulation of mutant alpha(1)-antitrypsin Z and mitochondrial damage in hepatoma cells. *J Biol Chem* **2011,** *286* (48), 41563-77.

[62] Xu, Y.; Lindquist, S., Heat-shock protein hsp90 governs the activity of pp60v-src kinase. *Proc Natl Acad Sci U S A* **1993,** *90* (15), 7074-8.

[63] Whitesell, L.; Mimnaugh, E. G.; De Costa, B.; Myers, C. E.; Neckers, L. M., Inhibition of heat shock protein HSP90-pp60v-src heteroprotein complex formation by benzoquinone ansamycins: essential role for stress proteins in oncogenic transformation. *Proc Natl Acad Sci U S A* **1994,** *91* (18), 8324-8.

[64] Boczek, E. E.; Reefschlager, L. G.; Dehling, M.; Struller, T. J.; Hausler, E.; Seidl, A.; Kaila, V. R.; Buchner, J., Conformational processing of oncogenic v-Src kinase by the molecular chaperone Hsp90. *Proc Natl Acad Sci U S A* **2015,** *112* (25), E3189-98.

[65] Whitesell, L.; Lindquist, S. L., HSP90 and the chaperoning of cancer. *Nat Rev Cancer* **2005,** *5* (10), 761-72.

[66] Crowley, V. M.; Huard, D. J. E.; Lieberman, R. L.; Blagg, B. S. J., Second Generation Grp94-Selective Inhibitors Provide Opportunities for the Inhibition of Metastatic Cancer. *Chemistry* **2017,** *23* (62), 15775-15782.

[67] Oakes, S. A.; Papa, F. R., The role of endoplasmic reticulum stress in human pathology. *Annu Rev Pathol* **2015,** *10*, 173-94.

[68] Chen, X.; Iliopoulos, D.; Zhang, Q.; Tang, Q.; Greenblatt, M. B.; Hatziapostolou, M.; Lim, E.; Tam, W. L.; Ni, M.; Chen, Y.; Mai, J.; Shen, H.; Hu, D. Z.; Adoro, S.; Hu, B.; Song, M.; Tan, C.; Landis, M. D.; Ferrari, M.; Shin, S. J.; Brown, M.; Chang, J. C.; Liu, X. S.; Glimcher, L. H., XBP1 promotes triple-negative breast cancer by controlling the HIF1alpha pathway. *Nature* **2014,** *508* (7494), 103-107.

[69] Saito, S.; Furuno, A.; Sakurai, J.; Sakamoto, A.; Park, H. R.; Shin-Ya, K.; Tsuruo, T.; Tomida, A., Chemical genomics identifies the unfolded protein response as a target for selective cancer cell killing during glucose deprivation. *Cancer Res* **2009,** *69* (10), 4225-34.

[70] Mimura, N.; Fulciniti, M.; Gorgun, G.; Tai, Y. T.; Cirstea, D.; Santo, L.; Hu, Y.; Fabre, C.; Minami, J.; Ohguchi, H.; Kiziltepe, T.; Ikeda, H.; Kawano, Y.; French, M.; Blumenthal, M.; Tam, V.; Kertesz, N. L.; Malyankar, U. M.; Hokenson, M.; Pham, T.; Zeng, Q.; Patterson, J. B.; Richardson, P. G.; Munshi, N. C.; Anderson, K. C., Blockade of XBP1 splicing by inhibition of IRE1alpha is a promising therapeutic option in multiple myeloma. *Blood* **2012,** *119* (24), 5772-81.

[71] Oslowski, C. M.; Urano, F., Measuring ER stress and the unfolded protein response using mammalian tissue culture system. *Methods Enzymol* **2011,** *490*, 71-92.

[72] Ding, W. X.; Ni, H. M.; Gao, W.; Hou, Y. F.; Melan, M. A.; Chen, X.; Stolz, D. B.; Shao, Z. M.; Yin, X. M., Differential effects of endoplasmic reticulum stress-induced autophagy on cell survival. *J Biol Chem* **2007,** *282* (7), 4702-10.

[73] Blackwood, E. A.; Azizi, K.; Thuerauf, D. J.; Paxman, R. J.; Plate, L.; Kelly, J. W.; Wiseman, R. L.; Glembotski, C. C., Pharmacologic ATF6 activation confers global protection in widespread disease models by reprograming cellular proteostasis. *Nat Commun* **2019,** *10* (1), 187.

[74] Paxman, R.; Plate, L.; Blackwood, E. A.; Glembotski, C.; Powers, E. T.; Wiseman, R. L.; Kelly, J. W., Pharmacologic ATF6 activating compounds are metabolically activated to selectively modify endoplasmic reticulum proteins. *Elife* **2018,** *7*.

[75] Mendez, A. S.; Alfaro, J.; Morales-Soto, M. A.; Dar, A. C.; McCullagh, E.; Gotthardt, K.; Li, H.; Acosta-Alvear, D.; Sidrauski, C.; Korennykh, A. V.; Bernales, S.; Shokat, K. M.; Walter, P., Endoplasmic reticulum stress-independent activation of unfolded protein response kinases by a small molecule ATP-mimic. *Elife* **2015,** *4*.

[76] Wang, L.; Perera, B. G.; Hari, S. B.; Bhhatarai, B.; Backes, B. J.; Seeliger, M. A.; Schurer, S. C.; Oakes, S. A.; Papa, F. R.; Maly, D. J., Divergent allosteric control of the IRE1alpha endoribonuclease using kinase inhibitors. *Nat Chem Biol* **2012,** *8* (12), 982-9.

[77] Korennykh, A. V.; Egea, P. F.; Korostelev, A. A.; Finer-Moore, J.; Zhang, C.; Shokat, K. M.; Stroud, R. M.; Walter, P., The unfolded protein response signals through high-order assembly of Ire1. *Nature* **2009,** *457* (7230), 687-93.

[78] Cole, K. S.; Grandjean, J. M. D.; Chen, K.; Witt, C. H.; O'Day, J.; Shoulders, M. D.; Wiseman, R. L.; Weerapana, E., Characterization of an A-Site Selective Protein Disulfide Isomerase A1 Inhibitor. *Biochemistry* **2018,** *57* (13), 2035-2043.

[79] Grandjean, J. M. D.; Madhavan, A.; Cech, L.; Seguinot, B. O.; Paxman, R. J.; Smith, E.; Scampavia, L.; Powers, E. T.; Cooley, C. B.; Plate, L.; Spicer, T. P.; Kelly, J. W.; Wiseman, R. L., Pharmacologic IRE1/XBP1s Activation Confers Targeted Endoplasmic Reticulum Proteostasis Reprogramming. *Nature Chemical Biology* **2020,** *in press*.

[80] Sebastian, R. M.; Shoulders, M. D., Chemical Biology Framework to Illuminate Proteostasis. *Annu Rev Biochem* **2020**.

[81] Hetz, C.; Axten, J. M.; Patterson, J. B., Pharmacological targeting of the unfolded protein response for disease intervention. *Nat Chem Biol* **2019,** *15* (8), 764-775.

[82] Tarbell, J. M.; Cancel, L. M., The glycocalyx and its significance in human medicine. *J Intern Med* **2016,** *280* (1), 97-113.

[83] Needham, P. G.; Guerriero, C. J.; Brodsky, J. L., Chaperoning Endoplasmic Reticulum-Associated Degradation (ERAD) and Protein Conformational Diseases. *Cold Spring Harb Perspect Biol* **2019,** *11* (8).

[84] Komander, D.; Rape, M., The ubiquitin code. *Annu Rev Biochem* **2012,** *81*, 203-29.

[85] Walsh, C. T.; Garneau-Tsodikova, S.; Gatto, G. J., Jr., Protein posttranslational modifications: the chemistry of proteome diversifications. *Angew Chem Int Ed Engl* **2005,** *44* (45), 7342-72.

[86] Oikari, S.; Makkonen, K.; Deen, A. J.; Tyni, I.; Karna, R.; Tammi, R. H.; Tammi, M. I., Hexosamine biosynthesis in keratinocytes: roles of GFAT and GNPDA enzymes in the maintenance of UDP-GlcNAc content and hyaluronan synthesis. *Glycobiology* **2016,** *26* (7), 710-22.

[87] Denzel, M. S.; Storm, N. J.; Gutschmidt, A.; Baddi, R.; Hinze, Y.; Jarosch, E.; Sommer, T.; Hoppe, T.; Antebi, A., Hexosamine pathway metabolites enhance protein quality control and prolong life. *Cell* **2014,** *156* (6), 1167-1178.

[88] Maszczak-Seneczko, D.; Sosicka, P.; Olczak, T.; Jakimowicz, P.; Majkowski, M.; Olczak, M., UDP-N-acetylglucosamine transporter (SLC35A3) regulates biosynthesis of highly branched N-glycans and keratan sulfate. *J Biol Chem* **2013,** *288* (30), 21850-60.

[89] Moremen, K. W.; Haltiwanger, R. S., Emerging structural insights into glycosyltransferase-mediated synthesis of glycans. *Nat Chem Biol* **2019,** *15* (9), 853-864.

[90] De Leoz, M. L. A.; Duewer, D. L.; Fung, A.; Liu, L.; Yau, H. K.; Potter, O.; Staples, G. O.; Furuki, K.; Frenkel, R.; Hu, Y.; Sosic, Z.; Zhang, P.; Altmann, F.; Gru Nwald-Grube, C.; Shao, C.; Zaia, J.; Evers, W.; Pengelley, S.; Suckau, D.; Wiechmann, A.; Resemann, A.; Jabs, W.; Beck, A.; Froehlich, J. W.; Huang, C.; Li, Y.; Liu, Y.; Sun, S.; Wang, Y.; Seo, Y.; An, H. J.; Reichardt, N. C.; Ruiz, J. E.; Archer-Hartmann, S.; Azadi, P.; Bell, L.; Lakos, Z.; An, Y.; Cipollo, J. F.; Pucic-Bakovic, M.; Stambuk, J.; Lauc, G.; Li, X.; Wang, P. G.; Bock, A.; Hennig, R.; Rapp, E.; Creskey, M.; Cyr, T. D.; Nakano, M.; Sugiyama, T.; Leung, P. A.; Link-Lenczowski, P.; Jaworek, J.; Yang, S.; Zhang, H.; Kelly, T.; Klapoetke, S.; Cao, R.; Kim, J. Y.; Lee, H. K.; Lee, J. Y.; Yoo, J. S.; Kim, S. R.; Suh, S. K.; de Haan, N.; Falck, D.; Lageveen-Kammeijer, G. S. M.; Wuhrer, M.; Emery, R. J.; Kozak, R. P.; Liew, L. P.; Royle, L.; Urbanowicz, P. A.; Packer, N. H.; Song, X.; Everest-Dass, A.; Lattova, E.; Cajic, S.; Alagesan, K.; Kolarich, D.; Kasali, T.; Lindo, V.; Chen, Y.; Goswami, K.; Gau, B.; Amunugama, R.; Jones, R.; Stroop, C. J. M.; Kato, K.; Yagi, H.; Kondo, S.; Yuen, C. T.; Harazono, A.; Shi, X.; Magnelli, P. E.; Kasper, B. T.; Mahal, L.; Harvey, D. J.; O'Flaherty, R.; Rudd, P. M.; Saldova, R.; Hecht, E. S.; Muddiman, D. C.; Kang, J.; Bhoskar, P.; Menard, D.; Saati, A.; Merle, C.; Mast, S.; Tep, S.; Truong, J.; Nishikaze, T.; Sekiya, S.; Shafer, A.; Funaoka, S.; Toyoda, M.; de Vreugd, P.; Caron, C.; Pradhan, P.; Tan, N. C.; Mechref, Y.; Patil, S.; Rohrer, J. S.; Chakrabarti, R.; Dadke, D.; Lahori, M.; Zou, C.; Cairo, C.; Reiz, B.; Whittal, R. M.; Lebrilla, C. B.; Wu, L.; Guttman, A.; Szigeti, M.; Kremkow, B. G.; Lee, K. H.; Sihlbom, C.; Adamczyk, B.; Jin, C.; Karlsson, N. G.; Ornros, J.; Larson, G.; Nilsson, J.; Meyer, B.; Wiegandt, A.; Komatsu, E.; Perreault, H.; Bodnar, E. D.; Said, N.; Francois, Y. N.; Leize-Wagner, E.; Maier, S.; Zeck, A.; Heck, A. J. R.; Yang, Y.; Haselberg, R.; Yu, Y. Q.; Alley, W.; Leone, J. W.; Yuan, H.; Stein, S. E., NIST Interlaboratory Study on Glycosylation Analysis of Monoclonal Antibodies: Comparison of Results from Diverse Analytical Methods. *Mol Cell Proteomics* **2020,** *19* (1), 11-30.

[91] Palaniappan, K. K.; Bertozzi, C. R., Chemical Glycoproteomics. *Chem Rev* **2016,** *116* (23), 14277-14306.

[92] Griffin, M. E.; Hsieh-Wilson, L. C., Glycan Engineering for Cell and Developmental Biology. *Cell Chem Biol* **2016,** *23* (1), 108-121.

[93] Lopez Aguilar, A.; Briard, J. G.; Yang, L.; Ovryn, B.; Macauley, M. S.; Wu, P., Tools for Studying Glycans: Recent Advances in Chemoenzymatic Glycan Labeling. *ACS Chem Biol* **2017,** *12* (3), 611-621.

[94] Geissner, A.; Reinhardt, A.; Rademacher, C.; Johannssen, T.; Monteiro, J.; Lepenies, B.; Thepaut, M.; Fieschi, F.; Mrazkova, J.; Wimmerova, M.; Schuhmacher, F.; Gotze, S.; Grunstein, D.; Guo, X.; Hahm, H. S.; Kandasamy, J.; Leonori, D.; Martin, C. E.; Parameswarappa, S. G.; Pasari, S.; Schlegel, M. K.; Tanaka, H.; Xiao, G.; Yang, Y.; Pereira, C. L.; Anish, C.; Seeberger, P. H., Microbe-focused glycan array screening platform. *Proc Natl Acad Sci U S A* **2019,** *116* (6), 1958-1967.

[95] Pilobello, K. T.; Slawek, D. E.; Mahal, L. K., A ratiometric lectin microarray approach to analysis of the dynamic mammalian glycome. *Proc Natl Acad Sci U S A* **2007,** *104* (28), 11534-9.

[96] Haslam, S. M.; North, S. J.; Dell, A., Mass spectrometric analysis of N- and O-glycosylation of tissues and cells. *Curr Opin Struct Biol* **2006,** *16* (5), 584-91.

[97] Khoury, G. A.; Baliban, R. C.; Floudas, C. A., Proteome-wide post-translational modification statistics: frequency analysis and curation of the swiss-prot database. *Sci Rep* **2011,** *1*.

[98] Kornfeld, R.; Kornfeld, S., Assembly of asparagine-linked oligosaccharides. *Annu Rev Biochem* **1985,** *54*, 631-64.

[99] Park, C.; Zhang, J., Genome-wide evolutionary conservation of N-glycosylation sites. *Mol Biol Evol* **2011,** *28* (8), 2351-7.

[100] Lauc, G.; Pezer, M.; Rudan, I.; Campbell, H., Mechanisms of disease: The human N-glycome. *Biochim Biophys Acta* **2016,** *1860* (8), 1574-82.

[101] Eichler, J.; Imperiali, B., Biogenesis of Asparagine-Linked Glycoproteins Across Domains of Life-Similarities and Differences. *ACS Chem Biol* **2018,** *13* (4), 833-837.

[102] Apweiler, R.; Hermjakob, H.; Sharon, N., On the frequency of protein glycosylation, as deduced from analysis of the SWISS-PROT database. *Biochim Biophys Acta* **1999,** *1473* (1), 4-8.

[103] Aebersold, R.; Agar, J. N.; Amster, I. J.; Baker, M. S.; Bertozzi, C. R.; Boja, E. S.; Costello, C. E.; Cravatt, B. F.; Fenselau, C.; Garcia, B. A.; Ge, Y.; Gunawardena, J.; Hendrickson, R. C.; Hergenrother, P. J.; Huber, C. G.; Ivanov, A. R.; Jensen, O. N.; Jewett, M. C.; Kelleher, N. L.; Kiessling, L. L.; Krogan, N. J.; Larsen, M. R.; Loo, J. A.; Ogorzalek Loo, R. R.; Lundberg, E.; MacCoss, M. J.; Mallick, P.; Mootha, V. K.; Mrksich, M.; Muir, T. W.; Patrie, S. M.; Pesavento, J. J.; Pitteri, S. J.; Rodriguez, H.; Saghatelian, A.; Sandoval, W.; Schluter, H.; Sechi, S.; Slavoff, S. A.; Smith, L. M.; Snyder, M. P.; Thomas, P. M.; Uhlen, M.; Van Eyk, J. E.; Vidal, M.; Walt, D. R.; White, F. M.; Williams, E. R.; Wohlschlager, T.; Wysocki, V. H.; Yates, N. A.; Young, N. L.; Zhang, B., How many human proteoforms are there? *Nat Chem Biol* **2018,** *14* (3), 206-214.

[104] Varki, A., Biological roles of glycans. *Glycobiology* **2017,** *27* (1), 3-49.

[105] Wolfert, M. A.; Boons, G. J., Adaptive immune activation: glycosylation does matter. *Nat Chem Biol* **2013,** *9* (12), 776-84.

[106] Demetriou, M.; Granovsky, M.; Quaggin, S.; Dennis, J. W., Negative regulation of T-cell activation and autoimmunity by Mgat5 N-glycosylation. *Nature* **2001,** *409* (6821), 733-9.

[107] Li, H.; Xu, C. F.; Blais, S.; Wan, Q.; Zhang, H. T.; Landry, S. J.; Hioe, C. E., Proximal glycans outside of the epitopes regulate the presentation of HIV-1 envelope gp120 helper epitopes. *J Immunol* **2009,** *182* (10), 6369-78.

[108] Zhou, T.; Doria-Rose, N. A.; Cheng, C.; Stewart-Jones, G. B. E.; Chuang, G. Y.; Chambers, M.; Druz, A.; Geng, H.; McKee, K.; Kwon, Y. D.; O'Dell, S.; Sastry, M.; Schmidt, S. D.; Xu, K.; Chen, L.; Chen, R. E.; Louder, M. K.; Pancera, M.; Wanninger, T. G.; Zhang, B.; Zheng, A.; Farney, S. K.; Foulds, K. E.; Georgiev, I. S.; Joyce, M. G.; Lemmin, T.; Narpala, S.; Rawi, R.; Soto, C.; Todd, J. P.; Shen, C. H.; Tsybovsky, Y.; Yang, Y.; Zhao, P.; Haynes, B. F.; Stamatatos, L.; Tiemeyer, M.; Wells, L.; Scorpio, D. G.; Shapiro, L.; McDermott, A. B.; Mascola, J. R.; Kwong, P. D., Quantification of the Impact of the HIV-1-Glycan Shield on Antibody Elicitation. *Cell Rep* **2017,** *19* (4), 719-732.

[109] Liang, W.; Mao, S.; Sun, S.; Li, M.; Li, Z.; Yu, R.; Ma, T.; Gu, J.; Zhang, J.; Taniguchi, N.; Li, W., Core Fucosylation of the T Cell Receptor Is Required for T Cell Activation. *Front Immunol* **2018,** *9*, 78.

[110] Wang, X.; Inoue, S.; Gu, J.; Miyoshi, E.; Noda, K.; Li, W.; Mizuno-Horikawa, Y.; Nakano, M.; Asahi, M.; Takahashi, M.; Uozumi, N.; Ihara, S.; Lee, S. H.; Ikeda, Y.; Yamaguchi, Y.; Aze, Y.; Tomiyama, Y.; Fujii, J.; Suzuki, K.; Kondo, A.; Shapiro, S. D.; Lopez-Otin, C.; Kuwaki, T.; Okabe, M.; Honke, K.; Taniguchi, N., Dysregulation of TGF-beta1 receptor activation leads to abnormal lung development and emphysema-like phenotype in core fucose-deficient mice. *Proc Natl Acad Sci U S A* **2005,** *102* (44), 15791-6.

[111] Wang, X.; Gu, J.; Miyoshi, E.; Honke, K.; Taniguchi, N., Phenotype changes of Fut8 knockout mouse: core fucosylation is crucial for the function of growth factor receptor(s). *Methods Enzymol* **2006,** *417*, 11-22.

[112] Giddens, J. P.; Lomino, J. V.; DiLillo, D. J.; Ravetch, J. V.; Wang, L. X., Site-selective chemoenzymatic glycoengineering of Fab and Fc glycans of a therapeutic antibody. *Proc Natl Acad Sci U S A* **2018,** *115* (47), 12023-12027.

[113] Ishii, T.; Ishida, T.; Utsunomiya, A.; Inagaki, A.; Yano, H.; Komatsu, H.; Iida, S.; Imada, K.; Uchiyama, T.; Akinaga, S.; Shitara, K.; Ueda, R., Defucosylated humanized anti-CCR4 monoclonal antibody KW-0761 as a novel immunotherapeutic agent for adult T-cell leukemia/lymphoma. *Clin Cancer Res* **2010,** *16* (5), 1520-31.

[114] Pereira, N. A.; Chan, K. F.; Lin, P. C.; Song, Z., The "less-is-more" in therapeutic antibodies: Afucosylated anti-cancer antibodies with enhanced antibody-dependent cellular cytotoxicity. *MAbs* **2018,** *10* (5), 693-711.

[115] Yamane-Ohnuki, N.; Satoh, M., Production of therapeutic antibodies with controlled fucosylation. *MAbs* **2009,** *1* (3), 230-6.

[116] Xu, C.; Ng, D. T., Glycosylation-directed quality control of protein folding. *Nat Rev Mol Cell Biol* **2015,** *16* (12), 742-52.

[117] Kozlov, G.; Munoz-Escobar, J.; Castro, K.; Gehring, K., Mapping the ER Interactome: The P Domains of Calnexin and Calreticulin as Plurivalent Adapters for Foldases and Chaperones. *Structure* **2017,** *25* (9), 1415-1422.e3.

[118] Kiuchi, T.; Izumi, M.; Mukogawa, Y.; Shimada, A.; Okamoto, R.; Seko, A.; Sakono, M.; Takeda, Y.; Ito, Y.; Kajihara, Y., Monitoring of Glycoprotein Quality Control System with a Series of Chemically Synthesized Homogeneous Native and Misfolded Glycoproteins. *J Am Chem Soc* **2018,** *140* (50), 17499-17507.

[119] Neelamegham, S.; Mahal, L. K., Multi-level regulation of cellular glycosylation: from genes to transcript to enzyme to structure. *Curr Opin Struct Biol* **2016,** *40*, 145-152.

[120] Lauc, G.; Essafi, A.; Huffman, J. E.; Hayward, C.; Knezevic, A.; Kattla, J. J.; Polasek, O.; Gornik, O.; Vitart, V.; Abrahams, J. L.; Pucic, M.; Novokmet, M.; Redzic, I.; Campbell, S.; Wild, S. H.; Borovecki, F.; Wang, W.; Kolcic, I.; Zgaga, L.; Gyllensten, U.; Wilson, J. F.; Wright, A. F.; Hastie, N. D.; Campbell, H.; Rudd, P. M.; Rudan, I., Genomics meets glycomics-the first GWAS study of human N-Glycome identifies HNF1alpha as a master regulator of plasma protein fucosylation. *PLoS Genet* **2010,** *6* (12), e1001256.

[121] Zoldos, V.; Horvat, T.; Novokmet, M.; Cuenin, C.; Muzinic, A.; Pucic, M.; Huffman, J. E.; Gornik, O.; Polasek, O.; Campbell, H.; Hayward, C.; Wright, A. F.; Rudan, I.; Owen, K.; McCarthy, M. I.; Herceg, Z.; Lauc, G., Epigenetic silencing of HNF1A associates with changes in the composition of the human plasma N-glycome. *Epigenetics* **2012,** *7* (2), 164-72.

[122] Lau, E.; Feng, Y.; Claps, G.; Fukuda, M. N.; Perlina, A.; Donn, D.; Jilaveanu, L.; Kluger, H.; Freeze, H. H.; Ronai, Z. A., The transcription factor ATF2 promotes melanoma metastasis by suppressing protein fucosylation. *Sci Signal* **2015,** *8* (406), ra124.

[123] Thu, C. T.; Mahal, L. K., Sweet Control: MicroRNA Regulation of the Glycome. *Biochemistry* **2019**.

[124] Alles, J.; Fehlmann, T.; Fischer, U.; Backes, C.; Galata, V.; Minet, M.; Hart, M.; Abu-Halima, M.; Grasser, F. A.; Lenhof, H. P.; Keller, A.; Meese, E., An estimate of the total number of true human miRNAs. *Nucleic Acids Res* **2019,** *47* (7), 3353-3364.

[125] Kurata, J. S.; Lin, R. J., MicroRNA-focused CRISPR-Cas9 library screen reveals fitness-associated miRNAs. *Rna* **2018,** *24* (7), 966-981.

[126] Wang, Z. V.; Deng, Y.; Gao, N.; Pedrozo, Z.; Li, D. L.; Morales, C. R.; Criollo, A.; Luo, X.; Tan, W.; Jiang, N.; Lehrman, M. A.; Rothermel, B. A.; Lee, A. H.; Lavandero, S.; Mammen, P. P. A.; Ferdous, A.; Gillette, T. G.; Scherer, P. E.; Hill, J. A., Spliced X-box binding protein 1 couples the unfolded protein response to hexosamine biosynthetic pathway. *Cell* **2014,** *156* (6), 1179-1192.

[127] Dewal, M. B.; DiChiara, A. S.; Antonopoulos, A.; Taylor, R. J.; Harmon, C. J.; Haslam, S. M.; Dell, A.; Shoulders, M. D., XBP1s Links the Unfolded Protein Response to the Molecular Architecture of Mature N-Glycans. *Chem Biol* **2015,** *22* (10), 1301-12.

[128] Peixoto, A.; Relvas-Santos, M.; Azevedo, R.; Santos, L. L.; Ferreira, J. A., Protein Glycosylation and Tumor Microenvironment Alterations Driving Cancer Hallmarks. *Front Oncol* **2019,** *9*, 380.

[129] Urra, H.; Dufey, E.; Avril, T.; Chevet, E.; Hetz, C., Endoplasmic Reticulum Stress and the Hallmarks of Cancer. *Trends Cancer* **2016,** *2* (5), 252-262.

[130] Papaioannou, A.; Chevet, E., Driving Cancer Tumorigenesis and Metastasis Through UPR Signaling. *Curr Top Microbiol Immunol* **2018,** *414*, 159-192.

[131] Terai, H.; Kitajima, S.; Potter, D. S.; Matsui, Y.; Quiceno, L. G.; Chen, T.; Kim, T. J.; Rusan, M.; Thai, T. C.; Piccioni, F.; Donovan, K. A.; Kwiatkowski, N.; Hinohara, K.; Wei, G.; Gray, N. S.; Fischer, E. S.; Wong, K. K.; Shimamura, T.; Letai, A.; Hammerman, P. S.; Barbie, D. A., ER Stress Signaling Promotes the Survival of Cancer "Persister Cells" Tolerant to EGFR Tyrosine Kinase Inhibitors. *Cancer Res* **2018,** *78* (4), 1044-1057.

[132] Rodvold, J. J.; Chiu, K. T.; Hiramatsu, N.; Nussbacher, J. K.; Galimberti, V.; Mahadevan, N. R.; Willert, K.; Lin, J. H.; Zanetti, M., Intercellular transmission of the unfolded protein response promotes survival and drug resistance in cancer cells. *Sci Signal* **2017,** *10* (482).

[133] Cerezo, M.; Lehraiki, A.; Millet, A.; Rouaud, F.; Plaisant, M.; Jaune, E.; Botton, T.; Ronco, C.; Abbe, P.; Amdouni, H.; Passeron, T.; Hofman, V.; Mograbi, B.; Dabert-Gay, A. S.; Debayle, D.; Alcor, D.; Rabhi, N.; Annicotte, J. S.; Heliot, L.; Gonzalez-Pisfil, M.; Robert, C.; Morera, S.; Vigouroux, A.; Gual, P.; Ali, M. M. U.; Bertolotto, C.; Hofman, P.; Ballotti, R.; Benhida, R.; Rocchi, S., Compounds Triggering ER Stress Exert Anti-Melanoma Effects and Overcome BRAF Inhibitor Resistance. *Cancer Cell* **2016,** *29* (6), 805-819.

[134] Wu, J.; Chen, S.; Liu, H.; Zhang, Z.; Ni, Z.; Chen, J.; Yang, Z.; Nie, Y.; Fan, D., Tunicamycin specifically aggravates ER stress and overcomes chemoresistance in multidrug-resistant gastric cancer cells by inhibiting N-glycosylation. *J Exp Clin Cancer Res* **2018,** *37* (1), 272.

[135] Zhao, R.; Qin, W.; Qin, R.; Han, J.; Li, C.; Wang, Y.; Xu, C., Lectin array and glycogene expression analyses of ovarian cancer cell line A2780 and its cisplatin-resistant derivate cell line A2780-cp. *Clin Proteomics* **2017,** *14*, 20.

[136] Zhang, Z.; Zhao, Y.; Jiang, L.; Miao, X.; Zhou, H.; Jia, L., Glycomic alterations are associated with multidrug resistance in human leukemia. *Int J Biochem Cell Biol* **2012,** *44* (8), 1244-53.

[137] Zhu, L.; Finkelstein, D.; Gao, C.; Shi, L.; Wang, Y.; Lopez-Terrada, D.; Wang, K.; Utley, S.; Pounds, S.; Neale, G.; Ellison, D.; Onar-Thomas, A.; Gilbertson, R. J., Multi-organ Mapping of Cancer Risk. *Cell* **2016,** *166* (5), 1132-1146.e7.

[138] Lawrence, M. S.; Stojanov, P.; Polak, P.; Kryukov, G. V.; Cibulskis, K.; Sivachenko, A.; Carter, S. L.; Stewart, C.; Mermel, C. H.; Roberts, S. A.; Kiezun, A.; Hammerman, P. S.; McKenna, A.; Drier, Y.; Zou, L.; Ramos, A. H.; Pugh, T. J.; Stransky, N.; Helman, E.; Kim, J.; Sougnez, C.; Ambrogio, L.; Nickerson, E.; Shefler, E.; Cortes, M. L.; Auclair, D.; Saksena, G.; Voet, D.; Noble,

M.; DiCara, D.; Lin, P.; Lichtenstein, L.; Heiman, D. I.; Fennell, T.; Imielinski, M.; Hernandez, B.; Hodis, E.; Baca, S.; Dulak, A. M.; Lohr, J.; Landau, D. A.; Wu, C. J.; Melendez-Zajgla, J.; Hidalgo-Miranda, A.; Koren, A.; McCarroll, S. A.; Mora, J.; Crompton, B.; Onofrio, R.; Parkin, M.; Winckler, W.; Ardlie, K.; Gabriel, S. B.; Roberts, C. W. M.; Biegel, J. A.; Stegmaier, K.; Bass, A. J.; Garraway, L. A.; Meyerson, M.; Golub, T. R.; Gordenin, D. A.; Sunyaev, S.; Lander, E. S.; Getz, G., Mutational heterogeneity in cancer and the search for new cancer-associated genes. *Nature* **2013,** *499* (7457), 214-218.

[139] Hoadley, K. A.; Yau, C.; Hinoue, T.; Wolf, D. M.; Lazar, A. J.; Drill, E.; Shen, R.; Taylor, A. M.; Cherniack, A. D.; Thorsson, V.; Akbani, R.; Bowlby, R.; Wong, C. K.; Wiznerowicz, M.; Sanchez-Vega, F.; Robertson, A. G.; Schneider, B. G.; Lawrence, M. S.; Noushmehr, H.; Malta, T. M.; Stuart, J. M.; Benz, C. C.; Laird, P. W., Cell-of-Origin Patterns Dominate the Molecular Classification of 10,000 Tumors from 33 Types of Cancer. *Cell* **2018,** *173* (2), 291-304.e6.

[140] Siegel, R. L.; Miller, K. D.; Jemal, A., Cancer statistics, 2020. *CA Cancer J Clin* **2020,** *70* (1), 7-30.

[141] Hanahan, D.; Weinberg, R. A., The hallmarks of cancer. *Cell* **2000,** *100* (1), 57-70.

[142] Zaorsky, N. G.; Churilla, T. M.; Egleston, B. L.; Fisher, S. G.; Ridge, J. A.; Horwitz, E. M.; Meyer, J. E., Causes of death among cancer patients. *Ann Oncol* **2017,** *28* (2), 400-407.

[143] Hanahan, D.; Weinberg, R. A., Hallmarks of cancer: the next generation. *Cell* **2011,** *144* (5), 646-74.

[144] Fruman, D. A.; Chiu, H.; Hopkins, B. D.; Bagrodia, S.; Cantley, L. C.; Abraham, R. T., The PI3K Pathway in Human Disease. *Cell* **2017,** *170* (4), 605-635.

[145] Wang, Z., ErbB Receptors and Cancer. *Methods Mol Biol* **2017,** *1652*, 3-35.

[146] Zhu, Z.; Aref, A. R.; Cohoon, T. J.; Barbie, T. U.; Imamura, Y.; Yang, S.; Moody, S. E.; Shen, R. R.; Schinzel, A. C.; Thai, T. C.; Reibel, J. B.; Tamayo, P.; Godfrey, J. T.; Qian, Z. R.; Page, A. N.; Maciag, K.; Chan, E. M.; Silkworth, W.; Labowsky, M. T.; Rozhansky, L.; Mesirov, J. P.; Gillanders, W. E.; Ogino, S.; Hacohen, N.; Gaudet, S.; Eck, M. J.; Engelman, J. A.; Corcoran, R. B.; Wong, K. K.; Hahn, W. C.; Barbie, D. A., Inhibition of KRAS-driven tumorigenicity by interruption of an autocrine cytokine circuit. *Cancer Discov* **2014,** *4* (4), 452-65.

[147] Young, C. D.; Zimmerman, L. J.; Hoshino, D.; Formisano, L.; Hanker, A. B.; Gatza, M. L.; Morrison, M. M.; Moore, P. D.; Whitwell, C. A.; Dave, B.; Stricker, T.; Bhola, N. E.; Silva, G. O.; Patel, P.; Brantley-Sieders, D. M.; Levin, M.; Horiates, M.; Palma, N. A.; Wang, K.; Stephens, P. J.; Perou, C. M.; Weaver, A. M.; O'Shaughnessy, J. A.; Chang, J. C.; Park, B. H.; Liebler, D. C.; Cook, R. S.; Arteaga, C. L., Activating PIK3CA Mutations Induce an Epidermal Growth Factor Receptor (EGFR)/Extracellular Signal-regulated Kinase (ERK) Paracrine Signaling Axis in Basal-like Breast Cancer. *Mol Cell Proteomics* **2015,** *14* (7), 1959-76.

[148] Thangavel, C.; Boopathi, E.; Liu, Y.; Haber, A.; Ertel, A.; Bhardwaj, A.; Addya, S.; Williams, N.; Ciment, S. J.; Cotzia, P.; Dean, J. L.; Snook, A.; McNair, C.; Price, M.; Hernandez, J. R.; Zhao, S. G.; Birbe, R.; McCarthy, J. B.; Turley, E. A.; Pienta, K. J.; Feng, F. Y.; Dicker, A. P.; Knudsen, K. E.; Den, R. B., RB Loss Promotes Prostate Cancer Metastasis. *Cancer Res* **2017,** *77* (4), 982-995.

[149] Donehower, L. A.; Soussi, T.; Korkut, A.; Liu, Y.; Schultz, A.; Cardenas, M.; Li, X.; Babur, O.; Hsu, T. K.; Lichtarge, O.; Weinstein, J. N.; Akbani, R.; Wheeler, D. A., Integrated Analysis of TP53 Gene and Pathway Alterations in The Cancer Genome Atlas. *Cell Rep* **2019,** *28* (5), 1370-1384.e5.

[150] Sohn, B. H.; Shim, J. J.; Kim, S. B.; Jang, K. Y.; Kim, S. M.; Kim, J. H.; Hwang, J. E.; Jang, H. J.; Lee, H. S.; Kim, S. C.; Jeong, W.; Kim, S. S.; Park, E. S.; Heo, J.; Kim, Y. J.; Kim, D. G.; Leem, S. H.; Kaseb, A.; Hassan, M. M.; Cha, M.; Chu, I. S.; Johnson, R. L.; Park, Y. Y.; Lee, J. S.,

Inactivation of Hippo Pathway Is Significantly Associated with Poor Prognosis in Hepatocellular Carcinoma. *Clin Cancer Res* **2016,** *22* (5), 1256-64.

[151] Adams, J. M.; Cory, S., The BCL-2 arbiters of apoptosis and their growing role as cancer targets. *Cell Death Differ* **2018,** *25* (1), 27-36.

[152] Shay, J. W., Role of Telomeres and Telomerase in Aging and Cancer. *Cancer Discov* **2016,** *6* (6), 584-93.

[153] Quintero-Fabian, S.; Arreola, R.; Becerril-Villanueva, E.; Torres-Romero, J. C.; Arana-Argaez, V.; Lara-Riegos, J.; Ramirez-Camacho, M. A.; Alvarez-Sanchez, M. E., Role of Matrix Metalloproteinases in Angiogenesis and Cancer. *Front Oncol* **2019,** *9*, 1370.

[154] Bhandari, V.; Li, C. H.; Bristow, R. G.; Boutros, P. C., Divergent mutational processes distinguish hypoxic and normoxic tumours. *Nat Commun* **2020,** *11* (1), 737.

[155] Pastushenko, I.; Blanpain, C., EMT Transition States during Tumor Progression and Metastasis. *Trends Cell Biol* **2019,** *29* (3), 212-226.

[156] Dang, L.; White, D. W.; Gross, S.; Bennett, B. D.; Bittinger, M. A.; Driggers, E. M.; Fantin, V. R.; Jang, H. G.; Jin, S.; Keenan, M. C.; Marks, K. M.; Prins, R. M.; Ward, P. S.; Yen, K. E.; Liau, L. M.; Rabinowitz, J. D.; Cantley, L. C.; Thompson, C. B.; Vander Heiden, M. G.; Su, S. M., Cancer-associated IDH1 mutations produce 2-hydroxyglutarate. *Nature* **2009,** *462* (7274), 739-44.

[157] Losman, J. A.; Looper, R. E.; Koivunen, P.; Lee, S.; Schneider, R. K.; McMahon, C.; Cowley, G. S.; Root, D. E.; Ebert, B. L.; Kaelin, W. G., Jr., (R)-2-hydroxyglutarate is sufficient to promote leukemogenesis and its effects are reversible. *Science* **2013,** *339* (6127), 1621-5.

[158] O'Donnell, J. S.; Teng, M. W. L.; Smyth, M. J., Cancer immunoediting and resistance to T cell-based immunotherapy. *Nat Rev Clin Oncol* **2019,** *16* (3), 151-167.

[159] Macheret, M.; Halazonetis, T. D., DNA replication stress as a hallmark of cancer. *Annu Rev Pathol* **2015,** *10*, 425-48.

[160] Vajaria, B. N.; Patel, P. S., Glycosylation: a hallmark of cancer? *Glycoconj J* **2017,** *34* (2), 147-156.

[161] Munkley, J.; Elliott, D. J., Hallmarks of glycosylation in cancer. *Oncotarget* **2016,** *7* (23), 35478-89.

[162] El-Athman, R.; Relogio, A., Escaping Circadian Regulation: An Emerging Hallmark of Cancer? *Cell Syst* **2018,** *6* (3), 266-267.

[163] Sun, L.; Song, L.; Wan, Q.; Wu, G.; Li, X.; Wang, Y.; Wang, J.; Liu, Z.; Zhong, X.; He, X.; Shen, S.; Pan, X.; Li, A.; Wang, Y.; Gao, P.; Tang, H.; Zhang, H., cMyc-mediated activation of serine biosynthesis pathway is critical for cancer progression under nutrient deprivation conditions. *Cell Res* **2015,** *25* (4), 429-44.

[164] Gameiro, P. A.; Struhl, K., Nutrient Deprivation Elicits a Transcriptional and Translational Inflammatory Response Coupled to Decreased Protein Synthesis. *Cell Rep* **2018,** *24* (6), 1415-1424.

[165] Balsa, E.; Soustek, M. S.; Thomas, A.; Cogliati, S.; Garcia-Poyatos, C.; Martin-Garcia, E.; Jedrychowski, M.; Gygi, S. P.; Enriquez, J. A.; Puigserver, P., ER and Nutrient Stress Promote Assembly of Respiratory Chain Supercomplexes through the PERK-eIF2alpha Axis. *Mol Cell* **2019,** *74* (5), 877-890.e6.

[166] Iurlaro, R.; Puschel, F.; Leon-Annicchiarico, C. L.; O'Connor, H.; Martin, S. J.; Palou-Gramon, D.; Lucendo, E.; Munoz-Pinedo, C., Glucose Deprivation Induces ATF4-Mediated Apoptosis through TRAIL Death Receptors. *Mol Cell Biol* **2017,** *37* (10).

[167] Cubillos-Ruiz, J. R.; Silberman, P. C.; Rutkowski, M. R.; Chopra, S.; Perales-Puchalt, A.; Song, M.; Zhang, S.; Bettigole, S. E.; Gupta, D.; Holcomb, K.; Ellenson, L. H.; Caputo, T.; Lee, A. H.; Conejo-Garcia, J. R.; Glimcher, L. H., ER Stress Sensor XBP1 Controls Anti-tumor Immunity by Disrupting Dendritic Cell Homeostasis. *Cell* **2015,** *161* (7), 1527-38.

[168] Lee, B. R.; Chang, S. Y.; Hong, E. H.; Kwon, B. E.; Kim, H. M.; Kim, Y. J.; Lee, J.; Cho, H. J.; Cheon, J. H.; Ko, H. J., Elevated endoplasmic reticulum stress reinforced immunosuppression in the tumor microenvironment via myeloid-derived suppressor cells. *Oncotarget* **2014,** *5* (23), 12331-45.

[169] Thevenot, P. T.; Sierra, R. A.; Raber, P. L.; Al-Khami, A. A.; Trillo-Tinoco, J.; Zarreii, P.; Ochoa, A. C.; Cui, Y.; Del Valle, L.; Rodriguez, P. C., The stress-response sensor chop regulates the function and accumulation of myeloid-derived suppressor cells in tumors. *Immunity* **2014,** *41* (3), 389-401.

[170] Padler-Karavani, V., Aiming at the sweet side of cancer: aberrant glycosylation as possible target for personalized-medicine. *Cancer Lett* **2014,** *352* (1), 102-12.

[171] Hakomori, S., Tumor-associated carbohydrate antigens. *Annu Rev Immunol* **1984,** *2*, 103-26.

[172] Pearce, O. M. T., Cancer glycan epitopes: biosynthesis, structure and function. *Glycobiology* **2018,** *28* (9), 670-696.

Chapter 2

XBP1s Activation Can Globally Remodel *N*-Glycan Structure Distribution Patterns

Summary

Classically, the unfolded protein response (UPR) safeguards secretory pathway proteostasis. The most ancient arm of the UPR, the IRE1-activated spliced X-box binding protein 1 (XBP1s)-mediated response, has roles in secretory pathway maturation beyond resolving proteostatic stress. Understanding the consequences of XBP1s activation for cellular processes is critical for elucidating mechanistic connections between XBP1s and development, immunity, and disease. Here, we show that a key functional output of XBP1s activation is a cell type-dependent shift in the distribution of *N*-glycan structures on endogenous membrane and secreted proteomes. For example, XBP1s activity decreased levels of sialylation and bisecting GlcNAc in the HEK293 membrane proteome and secretome, while substantially increasing the population of oligomannose *N*-glycans only in the secretome. In HeLa cell membranes, stress-independent XBP1s activation increased the population of high-mannose and tetraantennary *N*-glycans, and also enhanced core fucosylation. mRNA profiling experiments suggest that XBP1s-mediated remodeling of the *N*-glycome is, at least in part, a consequence of coordinated transcriptional resculpting of *N*-glycan maturation pathways by XBP1s. The discovery of XBP1s-induced *N*-glycan structural remodeling on a glycome-wide scale suggests that XBP1s can act as a master regulator of *N*-glycan maturation. Moreover, because the sugars on cell-surface proteins or on proteins secreted from an XBP1s-activated cell can be molecularly distinct from those of an unactivated cell, these findings reveal a potential new mechanism for translating intracellular stress signaling into altered interactions with the extracellular environment.

Reproduced (adapted) with permission from *Proceedings of the National Academy of Sciences U S A* under the *PNAS* license: Wong MY, Chen K, Antonopoulos A, Kasper BT, Dewal MB, Taylor RJ, Whittaker CA, Hein PP, Dell A, Genereux JC, Haslam SM, Mahal LK, and Shoulders MD. *Proc Natl Acad Sci USA*. **2018**, 115 (43), E10089–E10098.

Author List (Author Contributions on the following page)

Madeline Y. Wong*, Kenny Chen*, Aristotelis Antonopoulos*, Brian T. Kasper*, Mahender B. Dewal, Rebecca J. Taylor, Charles A. Whittaker, Pyae P. Hein, Anne Dell, Joseph C. Genereux, Stuart M. Haslam[1], Lara K. Mahal[1], and Matthew D. Shoulders[1].

*M.Y.W., K.C., A.A., and B.T.K. contributed equally to this work.

[1]Co-corresponding authors.

Author Contributions

M.Y.W., K.C., M.B.D., A.D., S.M.H., L.K.M., and M.D.S. designed experiments; M.Y.W., K.C., A.A., B.T.K., M.B.D., R.J.T., P.P.H., and J.C.G. performed research; M.Y.W., K.C., A.A., B.T.K., C.A.W., A.D., J.C.G., S.M.H., L.K.M., and M.D.S. analyzed data; and M.Y.W., K.C., A.A., B.T.K., C.A.W., A.D., J.C.G., S.M.H., L.K.M., and M.D.S. wrote the paper.

Introduction

The unfolded protein response (UPR) is classically responsible for maintaining proteostasis in the secretory pathway.[1] In the metazoan UPR, three transmembrane proteins (IRE1, PERK, and ATF6) act to detect protein misfolding stress in the endoplasmic reticulum (ER). Once stress is detected, activation of each sensor results in the production of a distinctive transcription factor—spliced X-box binding protein 1 (XBP1s), ATF4, or ATF6(1–373), respectively.[2] The targets of these transcription factors include a suite of ER chaperones and quality control factors that can resolve proteostatic challenges caused by physiologic and environmental changes. The central role of the UPR in maintaining secretory proteostasis has catalyzed extensive efforts to delineate relevant mechanisms of induction,[3] define cellular effects of UPR activation, and create tools to modulate individual UPR arms.[4-6]

The IRE1-XBP1s pathway is the most ancient UPR arm.[2] Recent work continues to define essential functions for the XBP1s transcription factor, in particular, that are distinctive from proteostasis maintenance. For example, XBP1s is critical for development, immune response, memory formation, and cell-nonautonomous ER stress signaling.[7-10] Moreover, chronic up-regulation of the XBP1s transcription factor is a pathologic hallmark of numerous malignancies.[11] Consistent with its diverse regulatory functions, the IRE1-XBP1s arm can be activated independent of PERK-ATF4 and ATF6 in response to assorted stimuli.[1] Attaining mechanistic understanding of these diverse processes requires first comprehensively defining the molecular consequences of XBP1s induction.

The majority of proteins traversing the secretory pathway are co- or post-translationally *N*-glycosylated.[12] A 14-residue oligosaccharide with the structure $Glc_3Man_9GlcNAc_2$ (Glc, glucose; Man, mannose; GlcNAc, *N*-acetylglucosamine) is installed on Asn residues within specific amino acid sequons. XBP1s may modulate the extent to which *N*-linked glycans are installed by the cell,[13] thereby potentially assisting *N*-glycoprotein trafficking and directly enhancing proteostasis by providing improved access to the ER's lectin-based chaperone and quality control machineries. Downstream of *N*-glycan installation, the immature sugar is processed in both the ER and the Golgi to yield the vast array of high- and oligomannose, hybrid, and complex *N*-glycan structures presented on secreted and cell-surface proteins.[14] The molecular architecture of this *N*-glycome is dynamic, with consequences for both normal and pathologic processes, including cell motility and adhesion, cell–cell interactions, and immune system function.[15-17] However, our understanding of how intracellular signaling pathways coordinately define *N*-glycan maturation and thereby regulate these processes remains incomplete.

We previously reported that stress-independent activation of XBP1s can significantly modify the structural distribution of *N*-glycans installed at the single *N*-glycosylation site of a soluble, secreted glycoprotein domain derived from the CD2 adhesion protein.[18] The observed changes were specifically caused by XBP1s-mediated alterations in *N*-glycan maturation, not by modified CD2 protein synthesis or

trafficking. These findings hint at the possibility that XBP1s may regulate the molecular architecture of the endogenous *N*-glycome in a coordinated manner. However, the CD2 protein domain used in our prior studies was an ectopically expressed, soluble, and glycosylation-naïve protein variant,[18] rendering the biological relevance of the observed XBP1s-dependent remodeling of *N*-glycan maturation uncertain.

Here, we ask (*i*) whether induction of the transcription factor XBP1s results in altered *N*-glycan structures on endogenous proteins, and (*ii*) whether such remodeling is sufficiently significant to be observed in a glycome-wide experiment, not just on individual, purified glycoproteins. We find that stress-independent XBP1s activation can substantially alter the composition of the *N*-glycome in a cell type- and proteome-dependent manner. The resulting changes in the distribution of *N*-glycan structures indicate that XBP1s-activated cell membranes, and proteins secreted from XBP1s-activated cells, are often distinguishable at the molecular level from those of cells with basal levels of UPR signaling. These observations suggest a new mechanism to translate intracellular stress signaling to the extracellular milieu, a phenomenon with important implications for our emerging understanding of how the UPR shapes higher-order biological activities (e.g., organismal development and immune response) beyond just the maintenance of ER proteostasis.

Results

Experimental Platform and Workflow to Scrutinize Effects of XBP1s on the N-Glycome

Our objective here was to test the hypotheses that XBP1s-mediated remodeling of *N*-glycan structures (*i*) occurs on endogenous glycoproteins and (*ii*) is sufficiently significant to be observed in experiments surveying the glycome. Application of a traditional ER stress inducer such as thapsigargin (Tg) does cause XBP1s activation, and is therefore one possible experimental approach. However, the pleiotropic consequences of ER stressors, including extensive ER protein misfolding and high cytotoxicity, limit the reliability and interpretation of the resulting data. Selective induction of XBP1s using chemical genetics is an alternative strategy that we and others have employed to elucidate consequences of XBP1s activity.[4, 19] This strategy results in XBP1s induction in the absence of global UPR activation by ER stress. Such selective and chronic XBP1s activation is observed in numerous relevant settings, including development, the immune response, and cancer.[7-8, 11]

In this work, we employed two cell lines engineered for ER stress-independent induction of XBP1s transcriptional activity. In both cell lines, XBP1s was placed under control of the tetracycline repressor, providing doxycycline (dox)-regulated expression of XBP1s. The first stable cell line we used, termed HEK^{XBP1s}, was derived from the human embryonic kidney cell line and was reported previously.[4] The second cell line, developed for this study, was a stable HeLa cell line (derived from the cervical epithelial line) termed $HeLa^{XBP1s}$. In both HEK^{XBP1s} (Supporting Figure S.1*A*) and $HeLa^{XBP1s}$ (Supporting Figure S.1*B*)

cells, treatment with dox up-regulated mRNA expression for the established XBP1s target genes *ERDJ4* and *SEC24D* to levels similar to those induced by treatment with the classic ER stressor Tg. In both cases, XBP1s activation occurred independent of global UPR induction, as well-known transcripts induced by the PERK-ATF4 arm of the UPR were not up-regulated (e.g., *CHOP* and *GADD34*; Supporting Figure S.1 *A* and *B*).

In previous work, we characterized the consequences of sustained XBP1s activation for the transcriptome and proteome of HEK^{XBP1s} cells.[4] As the HeLa^{XBP1s} cell line was newly developed, we sequenced mRNA from vehicle-, dox-, or Tg-treated HeLa^{XBP1s} cells in biological triplicate. Hierarchical clustering of differentially expressed coding genes showed that XBP1s activation preferentially clustered with vehicle-treated rather than Tg-treated samples, indicating that the transcriptional consequences of chronic XBP1s activation were significantly muted relative to treatment with an ER stressor (Supporting Figure S.1*C*). As expected (Supporting Figure S.1*D*), and in line with our previous observations for HEK^{XBP1s} cells,[4] gene set enrichment analysis revealed specific gene sets enriched in the XBP1s-activated lines alone (e.g., the unfolded protein binding gene set), others that were enriched in both XBP1s-activated and Tg-treated cells (e.g., the response to ER stress gene set), and a third group of gene sets enriched only in Tg-treated cells (e.g., the intrinsic apoptotic signaling in response to the ER stress gene set) (see *Appendix 1*, Dataset S.1 *A–D* for full results). HEK^{XBP1s} and HeLa^{XBP1s} cells thus provide two distinct cell types in which we can induce sustained XBP1s activity over the time period required for an intracellular signal like XBP1s-mediated transcription to propagate to the mature *N*-glycoproteome.

With appropriate cell lines in hand, we devised an experimental workflow to test for effects of XBP1s activation on *N*-glycan maturation. As illustrated in **Figure 2.1*A***, we treated HEK^{XBP1s} cells in complete media with vehicle (control), dox (to activate XBP1s), or Tg (to induce ER stress and the global UPR), followed by isolation of the membrane fraction by ultracentrifugation. Alternatively, we treated HEK^{XBP1s} cells identically in a serum-free media formulation (FreeStyle media) such that we could harvest and concentrate the secreted proteome for downstream glycomic analyses while minimizing contamination from serum glycoproteins. We used FreeStyle media instead of serum-free Dulbecco's modified Eagle's medium (DMEM) because we have observed that serum-free DMEM causes significant cell stress over longer treatments such as the 24 h used here. Grp78 was detected in the FreeStyle media only upon XBP1s activation (Supporting Figure S.2), suggesting that the presence of any ER proteins in the XBP1s-activated secretome is a consequence of UPR activity, as has previously been observed by others.[20] For HeLa^{XBP1s} cells, we carried out an identical workflow but isolated only the membrane fraction, as in our observation HeLa cells are less secretory than HEK cells.

After isolating membrane and secreted protein fractions, we next carried out two types of glycomic experiments on the samples: (*i*) lectin microarray analysis, which enabled us to directly compare relative

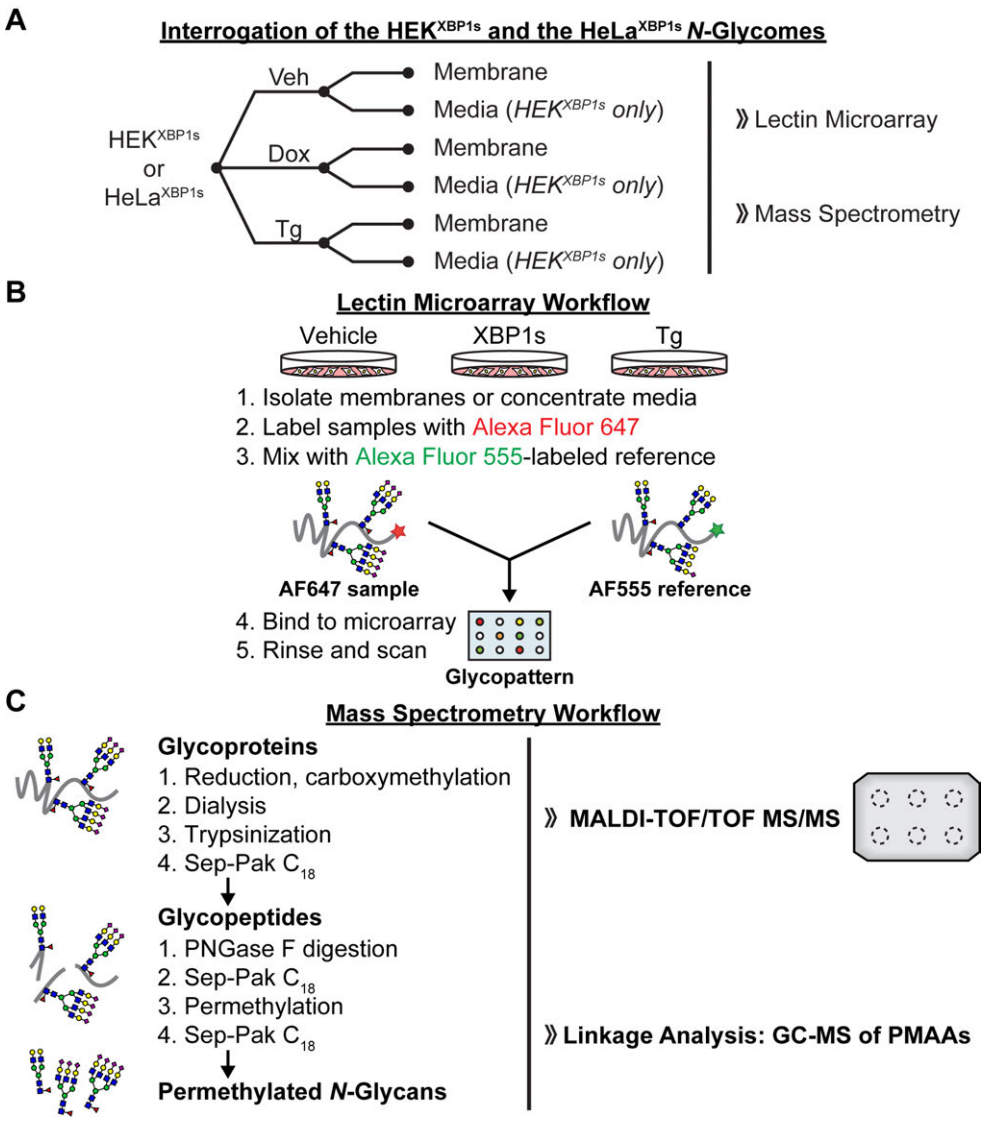

Figure 2.1: Experimental workflows for glycomic analyses. (***A***) Experimental workflow for glycoproteome extraction and analysis. (***B***) Glycan analysis by lectin microarrays. (***C***) MS analysis of *N*-glycomes.

levels of glycan motifs/substructures,[21] and (*ii*) mass spectrometry, which provided a more detailed analysis of glycan structures. We used dual-color lectin microarrays (**Figure 2.1*B***) on biological triplicates to gain insight into potential glycome remodeling owing to XBP1s activation and/or Tg treatment. We measured the relative binding of fluorescently labeled glycoproteome samples and an orthogonally labeled common reference to immobilized lectins on our microarray. The lectin microarrays we employed were composed of ~90 unique lectins with diverse sugar-binding specificities (see *Appendix 1*, Dataset S.2 for a complete list). Samples were labeled with Alexa Fluor 647 or 555, mixed with an equal amount of an orthogonally labeled common reference sample (a mix of all replicates for all conditions), and incubated with the microarray. The resulting data leverage the known glycan-binding preferences of lectins to gain insight into

changes in the levels of glycan substructures, providing a systems-level perspective on differences in glycan epitopes via relative quantitation of the glycan epitopes/substructures recognized by a particular lectin across sample conditions.[21]

We also used MALDI-TOF MS and TOF/TOF MS/MS (**Figure 2.1*C***) to obtain a molecular-level view of *N*-glycome composition in our samples. We performed GC-MS linkage analyses in parallel, yielding further detail by characterizing specific sugar linkages. All MS analyses were performed in a minimum of biological duplicate. These MS techniques provide detailed structural information to validate and enhance the lectin microarray findings. Notably, while MS can pinpoint shifts in the overall composition of the glycome within a sample (i.e., what percentage of overall glycans in a given sample have sialic acid), the methods used here do not provide direct comparison of a specific glycan's absolute abundance between two samples (e.g., how much sialic acid is expressed in sample 1 vs. sample 2). Thus, percentage changes from MS represent shifts in the profile whereas percentage changes from the lectin microarray represent changes in the overall levels of an epitope. By combining the ability of lectin microarrays to provide collective expression changes for glycan motifs (regardless of parent glycan backbone) with the capacity of MS to supply detailed structural analysis of individual glycans, we were able to evaluate at high resolution whether and to what extent XBP1s modulates glycome architecture. Results from these complementary analyses are presented below.

XBP1s Remodels the HEK^{XBP1s} Cell-Membrane N-Glycome

We began by assaying the *N*-glycome of HEK^{XBP1s} cell membranes upon XBP1s activation or Tg treatment, following the workflow in **Figure 2.1*A***. Lectin microarray analysis of selective XBP1s activation in HEK^{XBP1s} membranes (*Appendix 1*, Dataset S.3*A*) revealed a significant decrease in α2,6-sialylation (**Figure 2.2*A*** and Supporting Figure S.3*A*, *Left*). The α2,6-sialic acid-specific lectins SNA-I, TJA-I, and PSL-I showed an average 29% decrease in binding relative to the vehicle-treated control. Our engineered recombinant lectin diCBM40, which binds both α2,3- and α2,6-linked sialic acids with similar affinity,[22] showed a 35% loss in binding, further supporting a decrease in α2,6-sialylation. XBP1s activation also decreased bisecting *N*-glycans, as indicated by decreasing PHA-E signal (**Figure 2.2*A*** and Supporting Figure S.3*A*, *Left*).

Fully consistent with the lectin microarray analyses, MALDI-TOF MS analysis confirmed that XBP1s activation of HEK^{XBP1s} cells resulted in reduced sialylation of cell-membrane *N*-glycans and provided additional detail to the specific epitopes affected. Specifically, in XBP1s-activated cells, the relative abundance of ions at *m/z* 3054 and 3415 (green peaks in **Figure 2.2*B***, *Top* versus **Figure 2.2*B***, *Middle*)—corresponding to triantennary *N*-glycans with one or two NeuAc (*N*-acetylneuraminic acid) residues, respectively—decreased substantially (e.g., ~84% for *m/z* 3054) with respect to the relative

abundance of the ion at *m/z* 2693, an undecorated triantennary *N*-glycan. Similar results were observed for tetraantennary *N*-glycans in XBP1s-activated cells (red peaks in **Figure 2.2*B***, *Top* versus **Figure 2.2*B***, *Middle*). Specifically, the relative abundance of ions at *m/z* 3503, 3864, and 4226, which correspond to singly, doubly, and triply sialylated structures, decreased substantially (e.g., ∼85% for *m/z* 3503) upon XBP1s activation compared with the relative abundance of the undecorated tetraantennary *N*-glycan at *m/z* 3142. Similar but less intense reductions in sialylation were also observed for higher-mass *N*-glycans (Supporting Figure S.3*B*). For example, in XBP1s-activated cells, the ions at *m/z* 5124 and 5485—corresponding mainly to tetraantennary *N*-glycans with two additional LacNAc (*N*-acetyllactosamine) repeats and three or four NeuAc residues—decreased by ∼22 and ∼44%, respectively, compared with the relative abundance of the ion at *m/z* 4763, which only has two NeuAc residues (Supporting Figure S.3*B*, *Top* versus Supporting Figure S.3*B*, *Middle*). Lower-mass biantennary glycans also displayed an ∼80% decrease in sialylation (Supporting Figure S.3*C*, *Left* versus Supporting Figure S.3*C*, *Middle*).

We also performed GC-MS analysis (Supporting Table S.1) to add linkage details to our findings from the MALDI-TOF MS, and to further evaluate our lectin microarray findings. The detection of 6-linked galactose showed that a portion of NeuAc residues were α2,6-linked. The abundance of these α2,6-linked NeuAc residues substantially decreased in XBP1s-activated HEK^{XBP1s} cells (23.6% in vehicle samples versus 4.0% in XBP1s-activated samples), in concordance with the lectin microarray data that specifically indicated reduced α2,6-sialylation (**Figure 2.2*A***). We also identified 3,4,6-linked mannose by GC-MS, verifying the presence of minor amounts of bisecting *N*-glycans in HEK^{XBP1s} cell membranes. The abundance of these epitopes also decreased upon XBP1s activation in HEK^{XBP1s} cells (Supporting Table S.1), again in agreement with the observation of decreased bisecting *N*-glycans by lectin microarrays (**Figure 2*A***).

Collectively, these data reveal that XBP1s activation in HEK^{XBP1s} cells substantially remodeled the composition of the membrane *N*-glycome, as summarized in **Figure 2*C*** and Supporting Table S.2. Moreover, XBP1s-induced changes in the *N*-glycome were consistently detected both via lectin microarrays and MS. In particular, we observed a strong reduction in sialylation, specifically α2,6-sialylation, as well as a reduction in bisecting *N*-glycans.

Next, to ask whether induction of ER protein misfolding, and therefore all UPR pathways, has related effects on *N*-glycome composition, we performed the same analyses on membrane *N*-glycans from Tg-treated HEK^{XBP1s} cells. We found that the overall glycomic profile closely mirrored that of selective XBP1s activation in that we observed reduced sialylation and a reduction in bisecting GlcNAc (*Appendix 1*, Dataset S.3*A*). However, the magnitude of the changes was less substantial. SNA-I and diCBM40 still showed statistically significant decreases in binding (19 and 40%, respectively; **Figure 2.2*A*** and Supporting Figure S.3*A*, *Right*). In contrast, while other α2,6-sialic acid-binding lectins (e.g., PSL and TJA-I) also

Figure 2.2: Analysis of the HEK^{XBP1s} membrane glycoproteome. Full caption on the following page.

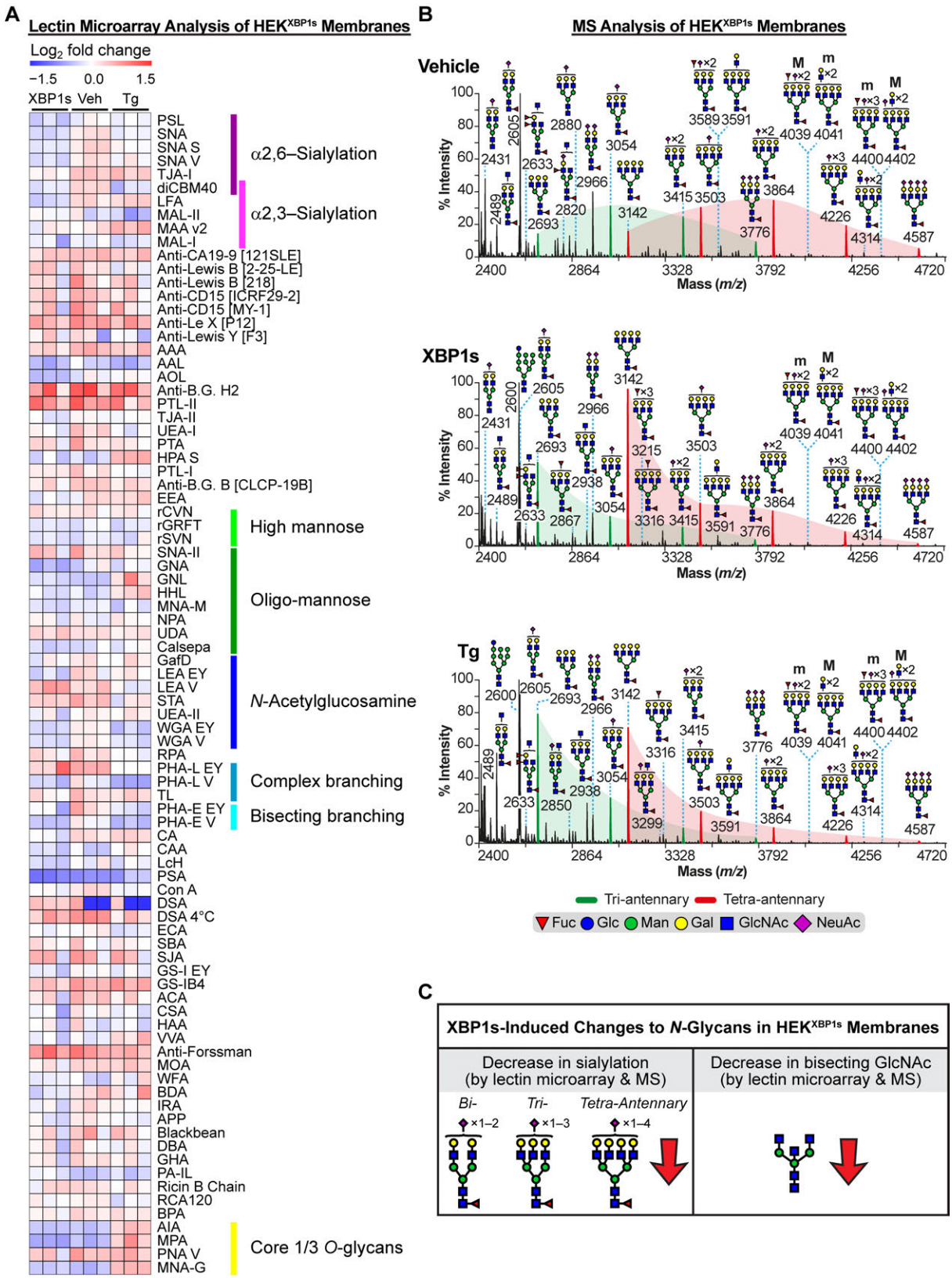

Figure 2.2: Analysis of the HEK^{XBP1s} membrane glycoproteome. (***A***) Heatmap of lectin microarray data generated from HEK^{XBP1s} membrane glycoproteomes. Full lectin names, print concentration, and sources are listed in *Appendix 1*, Dataset S.2*A*. Color intensity represents normalized $\log_2$ ratio data relative to a pooled sample reference. Each column represents one biological replicate of the indicated sample. Select lectin groups with shared binding specificities are annotated (*Right*). See also Supporting Figure S.3*A* and *Appendix 1*, Dataset S.3*A*. (***B***) Partial MALDI-TOF mass spectra from the HEK^{XBP1s} membrane proteome. Green and red peaks correspond to tri- and tetraantennary *N*-glycans with various levels of sialylation. Green- and red-shaded areas highlight the distribution shift of sialylation toward fewer NeuAcs on tri- and tetraantennary *N*-glycans. Structures above a bracket were not unequivocally defined. "M" and "m" designations indicate major and minor abundances, respectively. Putative structures are based on composition, tandem MS, and knowledge of biosynthetic pathways. All molecular ions are $[M+Na]^+$. High-mass spectra are presented in Supporting Figure S.3*B*, with GC-MS data in Supporting Table S.1. (***C***) Summary of XBP1s-induced changes to the HEK^{XBP1s} membrane *N*-glycome (see also Supporting Tables S.2 and S.3).

displayed reduced overall binding, they did not meet the statistical cutoff. A reduction in sialylation was also observed in the MALDI-TOF MS data, evident both in the relative abundance of sialylated to undecorated triantennary *N*-glycans (green peaks in **Figure 2.2*B***, *Top* versus **Figure 2.2*B***, *Bottom*) and the relative abundance of sialylated to undecorated tetraantennary *N*-glycans (red peaks in **Figure 2.2*B***, *Top* versus **Figure 2.2*B***, *Bottom*). Sialylation of biantennary *N*-glycans also decreased substantially upon Tg treatment (Supporting Figure S.3*C*, *Left* versus Supporting Figure S.3*C*, *Right*). GC-MS linkage analysis (Supporting Table S.1) confirmed a decrease in α2,6-linked NeuAcs, evidenced by a shift in the relative abundance of 6-linked galactose from 23.6% on vehicle-treated HEK^{XBP1s} cells to 4.1% on Tg-treated cells. Like XBP1s, activation of global ER stress by Tg also caused a loss of bisecting GlcNAc, observed by reduced PHA-E binding in lectin microarrays (**Figure 2.2*A*** and Supporting Figure S.3*A*, *Right*) and by a decrease in 3,4,6-mannose by GC-MS analysis (Supporting Table S.1). Notably, a gain in core 1/3 O-glycans was also observed upon Tg treatment, evidenced by increased binding to the lectins AIA, MPA, and MNA-G (**Figure 2.2*A*** and Supporting Figure S.3*A*, *Right*). Detailed *O*-glycan analysis was not performed using MALDI-TOF MS here, but this last result suggests that further investigation may reveal interesting ER stress-mediated changes to *O*-linked glycoforms, in addition to *N*-linked glycoforms. The Tg-mediated alterations in the HEK^{XBP1s} membrane glycome are summarized in Supporting Table S.3.

XBP1s Remodels HeLa^{XBP1s} Membrane N-Glycoproteomes in a Cell Type-Dependent Manner

We next asked whether activation of the XBP1s transcription factor has broader consequences for *N*-glycome composition across cell types. In particular, because cells derived from different tissues often have very different baseline *N*-glycome profiles,[23-24] we were interested in the consequences of XBP1s activation in distinctive cellular contexts. To address this question, we employed our HeLa^{XBP1s} cells following the workflow in **Figure 2.1*A***. We first confirmed that the baseline glycome profiles of HEK^{XBP1s} versus HeLa^{XBP1s} cells were different. By lectin microarray analysis, HEK^{XBP1s} and HeLa^{XBP1s} cells

displayed strikingly different levels of oligomannose *N*-glycans (Man_7 to Man_5) and sialylation epitopes (Supporting Figure S.4). Additionally, we found using MALDI-TOF/TOF MS/MS that, whereas high-mass poly-LacNAc *N*-glycans in HEK^{XBP1s} membranes consisted of linear LacNAc repeats (Supporting Figure S.3*D*), in $HeLa^{XBP1s}$ cell membranes the high-mass *N*-glycans consisted of I-branched poly-LacNAc repeats (Supporting Figure S.5 *A* and *B*). GC-MS linkage analysis confirmed the presence of 3,6-linked galactose in $HeLa^{XBP1s}$ cells, in concordance with the presence of I-branched LacNAcs (Supporting Table S.1).

Coincident with these quite distinctive baseline *N*-glycome profiles, lectin microarray analysis revealed a unique shift in the membrane glycomic profile upon XBP1s activation in $HeLa^{XBP1s}$ cells (**Figure 2.3*A***, Supporting Figure S.5*C* and *Appendix 1*, Dataset S.3*B*) relative to that observed in HEK^{XBP1s} cells. XBP1s-activated $HeLa^{XBP1s}$ membranes exhibited increased levels of less processed *N*-linked glycans relative to vehicle-treated controls, based on increased signal from several high- (Man_9 to Man_7) and oligomannose-binding lectins (rGRFT, HHL, NPA, GNL, and Calsepa).[25] Additionally, XBP1s activation resulted in increased core fucosylation (PSA and LcH) and β1,6-GlcNAc branching (PHA-L, which binds tri- and tetraantennary glycans). No shift in sialylation was observed.

MALDI-TOF MS analysis was fully consistent with these observations. Similar to the microarray data, no significant changes in sialylation were observed. For example, the ratio of ions at *m/z* 3054, 3415, and 3776 (corresponding to triantennary *N*-glycans with one to three NeuAc residues, respectively) over the ion at *m/z* 2693 (corresponding to nonsialylated triantennary *N*-glycan) did not shift upon XBP1s activation (comparing the intensity of the green peaks within the green-shaded areas in **Figure 2.3*B***, *Top* versus **Figure 2.3*B***, *Middle*). Similarly, no change was observed in sialylation of the tetraantennary *N*-glycans (comparing the intensity of the red peaks within the red-shaded areas in **Figure 2.3*B***, *Top* versus **Figure 2.3*B***, *Middle*). Instead, consistent with the lectin microarrays, the most striking consequence of XBP1s activation for the $HeLa^{XBP1s}$ membrane glycome was a 97% increase in the relative abundance of tetra- versus triantennary *N*-glycans (intensity of all of the red versus all of the green peaks in **Figure 2.3*B***, *Top* versus **Figure 2.3*B***, *Middle*). GC-MS linkage analysis further confirmed the MALDI-TOF MS and microarray data, demonstrating (*i*) an increase in tetraantennary *N*-glycans revealed by increased 2,4- and 2,6-linked mannose in the partially permethylated alditol acetates (Supporting Table S.1) and (*ii*) an increase in core fucosylation revealed by increased levels of 4,6-linked GlcNAc (Supporting Table S.1).

As performed here, MALDI-TOF MS does not permit quantitation of relative high- and oligomannose levels between two samples, and so we were unable to further validate that particular finding from the lectin microarray using the MS data. Moreover, the experimental strategy of cell-membrane isolation by ultracentrifugation can be problematic when assessing changes in levels of less processed *N*-glycans on membrane proteins, as all cell membranes are isolated in the ultracentrifugation step. Therefore, to further evaluate the increase in high-mannose levels observed via lectin microarrays upon XBP1s

Figure 2.3: Analysis of the HeLa^{XBP1s} membrane glycoproteome. Full caption on the following page.

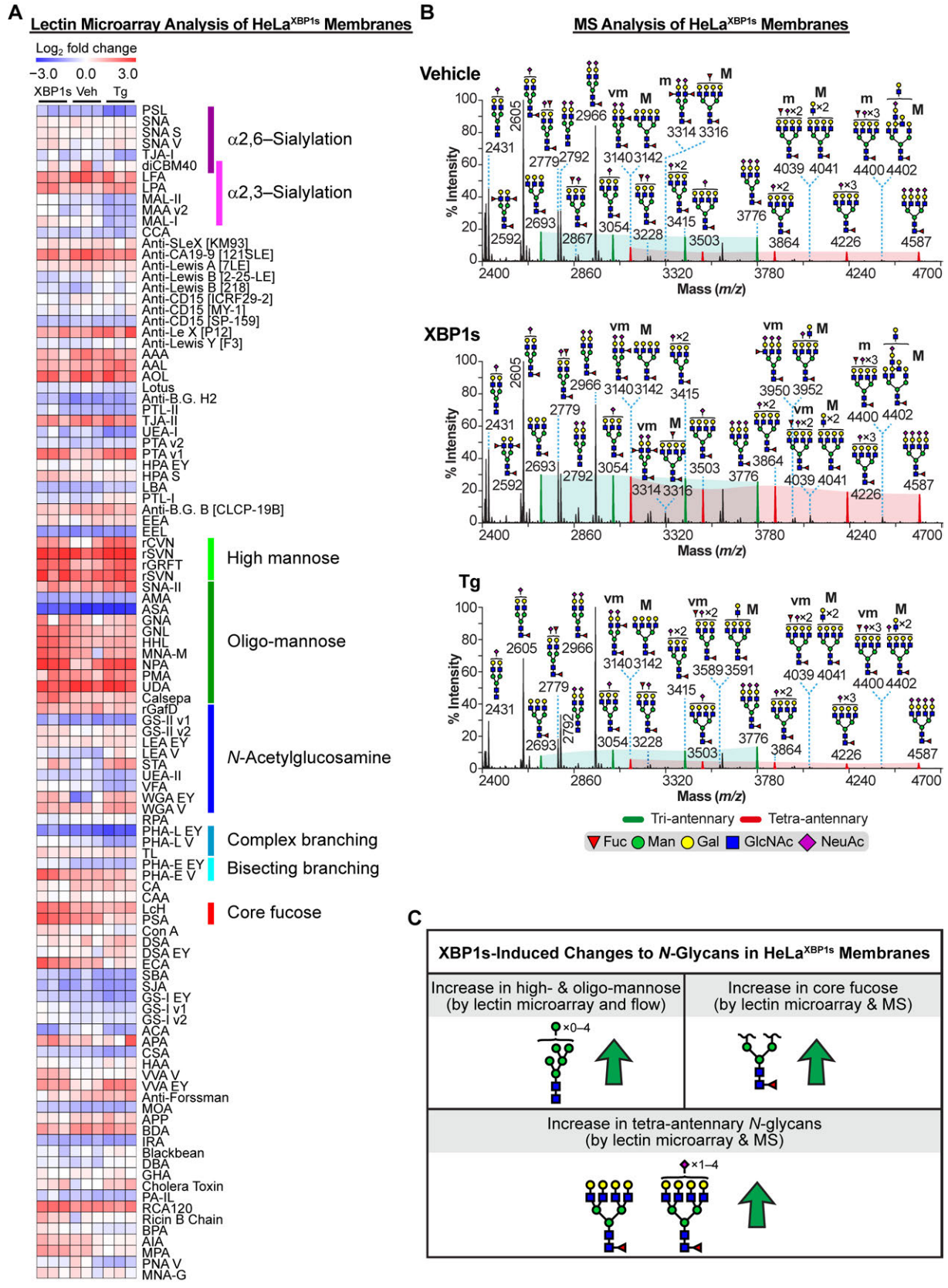

Figure 2.3: Analysis of the HeLa^{XBP1s} membrane glycoproteome. (***A***) Heatmap of lectin microarray data generated from HeLa^{XBP1s} membrane glycoproteomes. Full lectin names, print concentration, and sources are listed in *Appendix 1*, Dataset S.2*B*. Color intensity represents normalized $\log_2$ ratio data relative to a pooled sample reference. Each column represents one biological replicate of the indicated sample. Select lectin groups with shared binding specificities are annotated (*Right*). See also Supporting Figure S.5*C* and *Appendix 1*, Dataset S.3*B*. (***B***) Partial MALDI-TOF mass spectra from the HeLa^{XBP1s} membrane proteome. Green and red peaks correspond to tri- and tetraantennary *N*-glycans with various levels of sialylation. Green- and red-shaded areas highlight the increased abundance of tetraantennary *N*-glycans. The designation "vm" indicates very minor species; see **Figure 2.2*B*** legend for description of other annotations. High-mass spectra and selected MS/MS fragmentations are presented in Supporting Figure S5 *A* and *B*, with GC-MS data in Supporting Table S.1. (***C***) Summary of XBP1s-induced changes to the HeLa^{XBP1s} membrane *N*-glycome (see also Supporting Tables S.2 and S.3).

activation (**Figure 2.3*A***), we turned to a lectin-based flow cytometry approach.[26] We incubated live HeLa^{XBP1s} cells, treated with dox or vehicle as above, with biotinylated HHL, a lectin that preferentially binds high-mannose *N*-glycans.[27] We then stained cells with Cy5-streptavidin to enable quantitative fluorescence detection of high-mannose *N*-glycans. XBP1s-activated HeLa^{XBP1s} cells displayed a modest but significant increase in HHL signal compared with vehicle-treated control cells (Supporting Figure S.6*A*, *Left* and *Middle*). We confirmed that HHL was detecting bona fide high-mannose *N*-glycans by showing that (*i*) inhibiting lectin binding with methyl α-D-mannopyranoside reduced the signal (Supporting Figure S.6*A*, *Right*) and (*ii*) the mannosidase I inhibitor 1-deoxymannojirimycin[28] increased HHL binding without causing a loss of cell viability (Supporting Figure S.6 *B*–*D*).

Collectively, these data reveal that XBP1s activation in HeLa^{XBP1s} cells substantially remodels the HeLa membrane *N*-glycome, as summarized in **Figure 2.3*C*** and Supporting Table S.2. In particular, we observed strong increases in both core fucosylation and the abundance of tetraantennary *N*-glycans via both lectin microarray and MALDI-TOF MS analyses. In addition, the combination of lectin microarrays and lectin flow cytometry experiments revealed that XBP1s activation increased levels of high- and oligomannose *N*-glycans on the HeLa^{XBP1s} cell surface.

Stress-induced, global UPR activation via Tg treatment of HeLa^{XBP1s} cells also caused increases in high-mannose levels (**Figure 2.3*A*** and Supporting Figure S.5*C*, *Right*; see also *Appendix 1*, Dataset S.3*B*), demonstrated by significantly increased binding of the α1,2-mannose–specific antiviral lectins rSVN and rCVN, in addition to rGRFT. However, Tg treatment also induced a loss of β1,6-branched *N*-glycans based on decreased signal from PHA-L, revealing a distinct difference from the XBP1s-induced signal (**Figure 2.3*A*** and Supporting Figure S.5*C*, *Right*). Again, no changes in sialylation were observed. These observations were fully confirmed by our MALDI-TOF MS analysis, in which Tg-treated cells did not display increased tetraantennary *N*-glycans relative to vehicle-treated cells (red versus green shading in **Figure 2.3*B***, *Top* versus **Figure 2.3*B***, *Bottom*). Instead, as anticipated from the lectin microarray work (**Figure 2.3*A***), a decrease in 2,4- and 2,6-linked mannose was observed by GC-MS, the latter being

consistent with a loss of β1,6-branched *N*-glycans (Supporting Table S.1). The Tg-mediated alterations in the HeLa^{XBP1s} membrane glycome are summarized in Supporting Table S.3.

In summary, the ability of XBP1s (or even stress-induced UPR activation) to globally remodel the *N*-glycome extends beyond just a single cell type. The molecular nature of the resulting changes in *N*-glycan distribution patterns is cell type-dependent, likely owing at least in part to differences in baseline *N*-glycome composition. The magnitude of the effects can be quite substantial.

XBP1s Remodels the N-Glycan Composition of the HEK^{XBP1s} Secretome

The observation that XBP1s activation alters the structure distribution pattern of *N*-glycans on cell surfaces in a cell type-dependent manner suggests that cell–cell interactions, cell adhesion, and receptor signaling could all be modified by XBP1s. Beyond cell membranes, a large portion of the *N*-glycoproteome is composed of soluble, secreted proteins. Alterations in the *N*-glycans on secreted proteins could provide a mechanism for long-distance transmission of cell stress signals, or engender other important phenotypes. Therefore, we next asked whether XBP1s-mediated remodeling extends to the secreted *N*-glycome.

The secretome from XBP1s-activated HEK^{XBP1s} cells displayed substantial *N*-glycome remodeling when analyzed by lectin microarrays (**Figure 2.4*A***, Supporting Figure S.7, *Left*, and *Appendix 1*, Dataset S.3*C*). A decrease in both β1,6 *N*-glycan branching (PHA-L) and bisecting GlcNAc (PHA-E) was observed, similar to our findings for the HEK^{XBP1s} membrane *N*-glycome. A modest (27%) but not statistically significant decrease in binding to α2,6-sialylation epitopes based on the lectins SNA-I and diCMB40 was also observed. These results were confirmed by our MALDI-TOF MS and GC-MS analyses (see below). We also observed a significant increase in binding to oligomannose-targeting lectins (HHL, UDA, NPA, Calsepa, and GNA).

MALDI-TOF MS analysis (**Figure 2.4*B***) revealed that *N*-glycans isolated from the secretome of HEK^{XBP1}s cells featured abundant core fucosylated bi- (purple peaks; *m/z* 2244, 2605, and 2966), tetra- (red peaks; *m/z* 3142, 3503, 3864, 4226, and 4587), and, to a lesser extent, triantennary (green peaks; *m/z* 2693, 3054, 3415, and 3776) *N*-glycans. Upon XBP1s activation, the tri- and tetraantennary, but not the biantennary, *N*-glycans exhibited reduced sialylation (**Figure 2.4*B***, *Top* versus **Figure 2.4*B***, *Middle*). For example, the relative abundance of molecular ions at *m/z* 3503, 3864, 4226, and 4587 compared with *m/z* 3142 was reduced from vehicle-treated levels in the XBP1s-activated secretome (red peaks in **Figure 2.4*B***, *Top* versus **Figure 2.4*B***, *Middle*). GC-MS analysis confirmed a small reduction in α2,6-sialylation overall (Supporting Table S.1; 6-linked galactose: vehicle 98.9% versus XBP1s 63.8%), consistent with our lectin microarray analysis. The decreases in bisected *N*-glycans and β1,6-branching observed by microarray were also confirmed by our GC-MS data (Supporting Table S.1; 3,4,6-linked mannose: vehicle 4.7% versus XBP1s 2.3%; 2,6-linked mannose: vehicle 105.8% versus XBP1s 71.1%).

Figure 2.4: Analysis of the HEK^{XBP1s} secreted glycoproteome. Full caption on the following page.

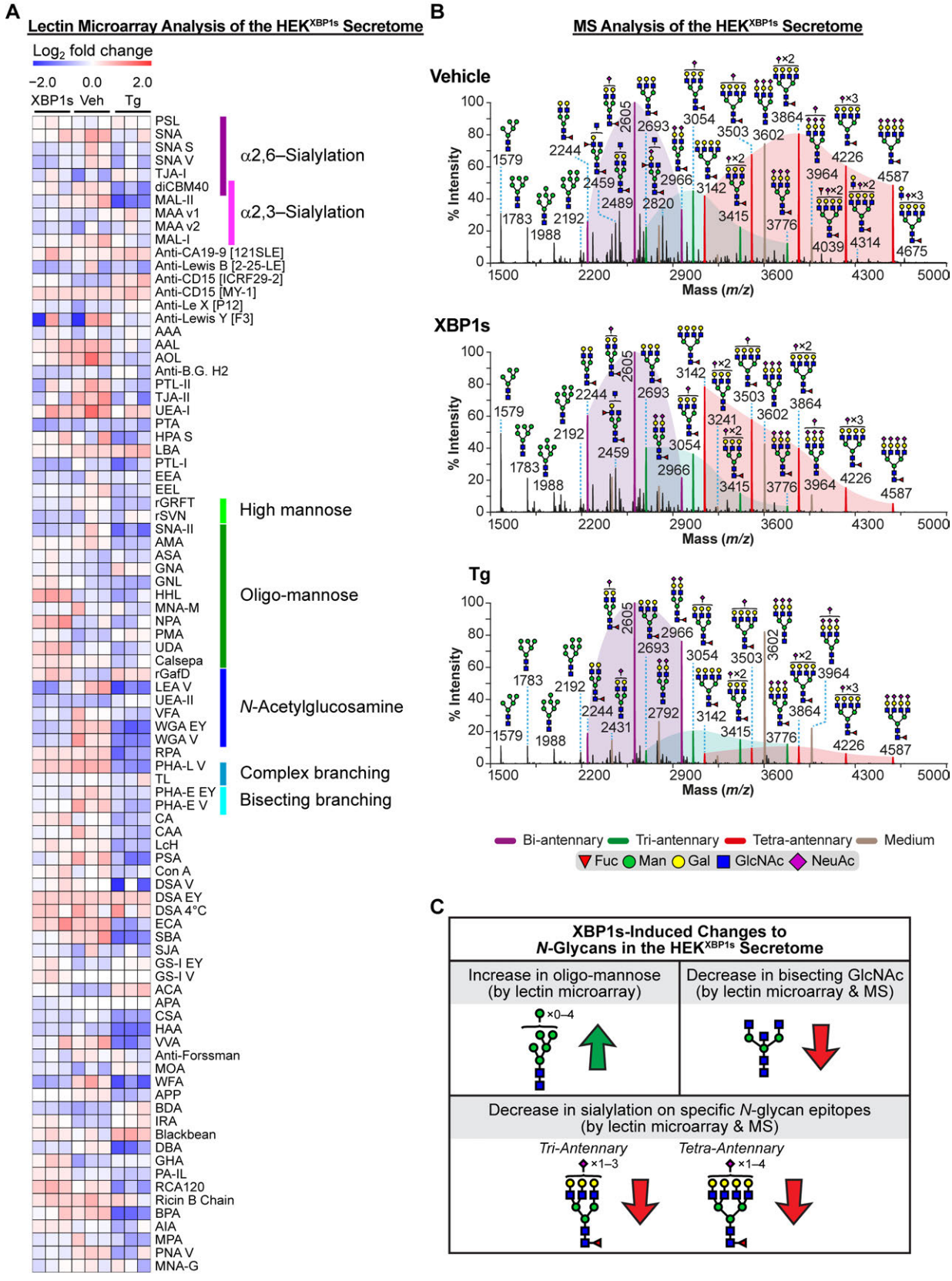

Figure 2.4: Analysis of the HEK^{XBP1s} secreted glycoproteome. (***A***) Heatmap of lectin microarray data generated from HEK^{XBP1s} secreted glycoproteomes. Full lectin names, print concentration, and sources are listed in *Appendix 1*, Dataset S.2*A*. Color intensity represents normalized $\log_2$ ratio data relative to a pooled sample reference. Each column represents one biological replicate of the indicated sample. Select lectin groups with shared binding specificities are annotated (*Right*). See also Supporting Figure S.7 and *Appendix 1*, Dataset S.3C. (***B***) Partial MALDI-TOF mass spectra from the HEK^{XBP1s} secretome. Purple, green, and red peaks correspond to bi, tri-, and tetraantennary *N*-glycans with various levels of sialylation. Purple-, green-, and red-shaded areas highlight the distribution shift of sialylation on the corresponding bi-, tri-, and tetraantennary *N*-glycans. Noncore fucosylated structures corresponded to residual FBS-derived *N*-glycans that we characterized previously (brown peaks; *m/z* 2792, 3602, and 3964).[31] These FBS-derived *N*-glycans were observed consistently in all samples and were excluded from the analyses as previously described.[32] GC-MS data are presented in Supporting Table S.1. See **Figure 2.2*B*** legend for description of other annotations. (***C***) Summary of XBP1s-induced changes to the HEK^{XBP1s} secreted *N*-glycome (see also Supporting Tables S.2 and S.3).

Collectively, these data reveal that XBP1s activation in HEK^{XBP1s} cells substantially remodels the composition of the secreted *N*-glycome, as summarized in **Figure 2.4*C*** and Supporting Table S.2. Lectin microarray analyses revealed an increase in oligomannose levels. Both lectin microarray and MALDI-TOF MS analyses demonstrated a decrease in bisecting *N*-glycans. MALDI-TOF MS showed a loss of sialylation on specific *N*-glycan epitopes (for tri- and tetraantennary but not biantennary *N*-glycans), suggesting possible protein-specific effects influencing loss of sialylation. While the reduction in bisecting *N*-glycans and a loss of sialylation are both consistent with our observations for the HEK^{XBP1s} membrane *N*-glycomes (**Figure 2.2*C***), the increase in oligomannose levels is limited to the secretome. This observation highlights the importance of separately evaluating membrane and secreted *N*-glycans in glycomic experiments, as we have also noted in prior work.[29-30]

We also analyzed the consequences of stress-induced, global UPR activation via Tg treatment on the composition of the secreted *N*-glycome in HEK^{XBP1s} cells. The secreted *N*-glycome of Tg-treated HEK^{XBP1s} cells was similar to that of XBP1s-activated cells in that reduced levels of β1,6 *N*-glycan branching (decreased binding to PHA-L) and bisecting GlcNAc (decreased binding to PHA-E) were observed (**Figure 2.4*A*** and Supporting Figure S.7, *Right*; see also *Appendix 1*, Dataset S.3*C*). MALDI-TOF MS and GC-MS analyses (**Figure 2.4*B***, *Top* versus **Figure 2.4*B***, *Bottom* and Supporting Table S.1) confirmed the decreases in levels of tri- and tetraantennary *N*-glycans (β1,6 *N*-glycan branching shown by changes in 2,4-linked mannose and 2,6-linked mannose levels). There was no impact on overall α2,6-sialylation, although a decrease in α2,3-sialylation was observed via reduced binding to MAL-I, MAL-II, and diCBM40 (**Figure 2.4*A***). In contrast to the secretome of XBP1s-activated cells, Tg treatment did not induce an increase in oligomannose levels. These Tg-mediated alterations in the HEK^{XBP1s} secreted glycoproteome are summarized in Supporting Table S.3.

XBP1s Does Not Significantly Alter the Proteomic Composition of the HEK^{XBP1s} Secretome

We questioned whether XBP1s-driven changes in the *N*-glycan architecture of the HEK^{XBP1s} secretome could be attributed to changes in the composition of the proteome caused by XBP1s activation. To assess this hypothesis, we induced XBP1s by dox treatment for 24 h and then collected conditioned, serum-free DMEM after a 6-h incubation of vehicle-treated or dox-treated cells in biological triplicate. We used serum-free DMEM, not FreeStyle media optimized for HEK cell growth, because FreeStyle media contain various proprietary peptides that interfere with MS analysis. The use of serum-free DMEM limited us to a 6-h incubation instead of the longer incubation used in our glycomic experiments, to avoid extensive autophagy induction and cell toxicity. We precipitated total protein from the collected media, followed by denaturing, reducing, alkylating, and trypsinizing peptides. The digested samples were then labeled with isobaric mass tags to permit quantitative assessment of proteome composition and identify any XBP1s-mediated changes. Using this approach, we were able to quantify 700 secreted proteins across all samples (*Appendix 1*, Dataset S.4). Using significance thresholds of unadjusted p value ≤ 0.05 and fold change ≥ 1.5, we found that levels of only 16 of these 700 proteins were changed by XBP1s activation [we further note that no proteins qualified using a false discovery rate (FDR) threshold of 10% by Benjamini–Hochberg analysis]. Of those 16 proteins, only 9 are annotated in UniProtKB as being *N*-glycosylated. These data led us to conclude that the observed changes in the secreted glycome are unlikely to be driven by changes in the composition of the secreted proteome. Instead, we hypothesized that altered biosynthesis of *N*-glycans is the controlling factor.

Selective XBP1s Induction Remodels the Glycogene Transcriptome

Control mechanisms of *N*-glycan biosynthesis are not well-understood. One possible way in which induction of XBP1s could lead to an altered glycome is via enhanced flux through the secretory pathway that overwhelms the *N*-glycan maturation machinery and causes uncoordinated changes in structure distribution patterns. However, global changes in protein secretion that might suggest the Golgi *N*-glycan maturation pathway is overwhelmed upon XBP1s activation have not been detected (see *Appendix 1*, Dataset S.4 and work by Wiseman and coworkers[4]). Moreover, while the changes in oligomannose levels in HeLa^{XBP1s} membranes and HEK^{XBP1s} secretomes could possibly be linked to increased flux overwhelming the *N*-glycan maturation pathway, it seems unlikely that many of the other changes observed (e.g., increases in core fucosylation, alterations in *N*-glycan branching, and changes in specific types of sialylation) could be explained by this hypothesis. Thus, although we cannot completely exclude the possibility, we believe the "overwhelming flux" hypothesis is unlikely to be correct.

A second possible explanation is that XBP1s activation either directly (as it is a transcription factor), or indirectly (as it can alter the expression of other transcription factors)[4, 33-34] modifies the

expression of enzymes involved in *N*-glycan maturation and biosynthesis (known as glycogenes), leading to transcriptionally encoded changes in *N*-glycome architecture. This explanation would be consistent with prior work showing that alterations in the expression of glycogene transcripts can induce changes in the *N*-glycome.[24, 35] To evaluate this possibility, we used both previously published data for HEK^{XBP1s} cells[4] and our new RNA-sequencing (RNA-seq) data for HeLa^{XBP1s} cells to characterize the glycogene transcript-level changes induced by chronic, selective XBP1s activation in vehicle- versus dox-treated cells. In both HEK^{XBP1s} cells and HeLa^{XBP1s} cells, gene set enrichment analysis (GSEA) highlighted *N*-linked glycosylation as a highly enriched pathway under conditions of chronic, selective XBP1s activation (*Appendix 1*, Dataset S.1*C*).[4] Indeed, GO groups related to protein glycosylation are the most enriched gene sets in XBP1s-activated cells, after XBP1s- and IRE1-regulated aspects of the classical unfolded protein response. Furthermore, standard GSEA indicated strong enrichment of genes involved in biosynthesis of the lipid-linked oligosaccharide in both HEK^{XBP1s} and HeLa^{XBP1s} cells (Supporting Figure S.8 and *Appendix 1*, Dataset S.1*E*). However, our data suggest that XBP1s activation does not globally alter transcripts involved in *N*-glycan maturation, as examination of a comprehensive gene set involved in *N*-glycan trimming and elaboration showed no global enrichment in XBP1s-activated cells (Supporting Figure S.8 and *Appendix 1,* Dataset S.1*E*). This observation suggests that XBP1s regulates specific subsets of these glycogenes, consistent with the changes in levels of only specific epitopes observed in our glycomic analyses.

We next manually curated a list of 1,310 genes related to protein *N*-glycosylation from gene ontology datasets (the gene sets used and full list of *N*-glycosylation–related genes analyzed are shown in *Appendix 1*, Dataset S.5 *A* and *B*, respectively). These *N*-glycosylation–related genes included not just enzymes involved in *N*-glycan biosynthesis, trimming, and modification but also sugar transporters, monosaccharide synthases, and catabolic enzymes. We plotted the changes in expression levels of these individual glycogenes upon XBP1s activation for HEK^{XBP1s} and HeLa^{XBP1s} cells in the volcano plots in **Figure 2.5** ***A*** and ***C***, respectively. As some glycogenes are expressed at low levels,[36] we also employed a commercially available Qiagen RT2 Profiler Human Glycosylation PCR Array to analyze transcript levels of selected glycogenes. For transcripts that were detected by multiple methods, we used the qPCR array results, rationalizing that the latter is more sensitive.[37]

For HEK^{XBP1s} cells, 39 of 950 expressed glycogene transcripts were significantly altered by chronic XBP1s activation (teal in **Figure 2.5*A***; see *Appendix 1*, Dataset S.5*C* for a complete list of results). This analysis (*i*) confirms the remodeling of the glycogene transcriptome induced by XBP1s activation in HEK^{XBP1s} cells, especially for a number of glycogenes directly involved in *N*-glycan maturation, and (*ii*) is in concordance with key features of the *N*-glycome remodeling caused by XBP1s activation in both the membrane and secretome of HEK^{XBP1s} cells (**Figures 2.2*C*** and **2.4*C***, respectively).

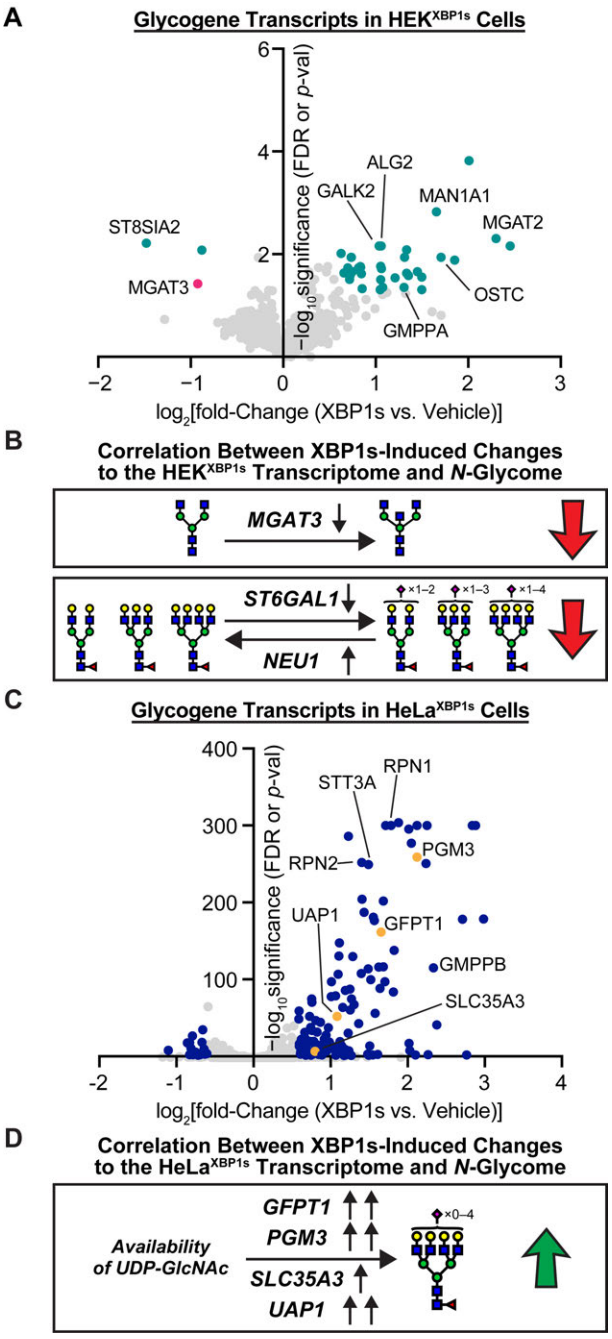

Figure 2.5: Glycogene analysis in HEK^{XBP1s} and HeLa^{XBP1s} cells. (***A***) Volcano plot showing XBP1s activation-induced changes in glycosylation-related transcripts in HEK^{XBP1s} cells. Glycogenes analyzed are listed in *Appendix 1*, Dataset S.5*B*. Data shown were obtained either from the Qiagen Human Glycosylation qPCR Array or, if a transcript of interest was not included in the qPCR array, extracted from previously published HEK^{XBP1s} microarray data.[4] Transcripts shown in teal meet significance and fold-change thresholds of FDR or *p* value ≤ 0.05 and fold change ≥ 1.5 upon XBP1s activation. Gene symbols are shown for outliers and transcripts of particular interest. (***B***) Decreased expression of *MGAT3* (shown in pink in ***A***), a GlcNAc transferase,[38] could account for the loss in bisecting GlcNAc observed on HEK^{XBP1s} secreted and membrane glycoproteins upon XBP1s activation. Decreased expression of *ST6GAL1* and increased expression of *NEU1* could account for the reduced sialylation observed for HEK^{XBP1s} secreted and membrane glycoproteins upon XBP1s activation. (***C***) Volcano plot showing XBP1s activation-induced changes in glycosylation-related transcripts in HeLa^{XBP1s} cells. Glycogenes analyzed are listed in *Appendix 1*, Dataset S.5*B*. Data shown were obtained either from the Qiagen Human Glycosylation qPCR Array or, if a transcript of interest was not included in the qPCR array, extracted from the RNA-seq data. Transcripts shown in blue meet significance and fold-change thresholds of FDR or *p* value ≤ 0.05 and fold change ≥ 1.5 upon XBP1s activation. Gene symbols are shown for outliers and transcripts of particular interest. (***D***) Increased expression of *GFPT1*, *PGM3*, *SLC35A3*, or *UAP1*, which are enzymes involved in regulating UDP-GlcNAc availability (shown in orange in ***C***), could contribute to increased tetraantennary *N*-glycans observed on HeLa^{XBP1s} membranes upon XBP1s activation.

Specifically (**Figure 2.5*B***), reduced levels of *MGAT3* (shown in pink in **Figure 2.5*A***), which encodes the enzyme responsible for introduction of bisecting GlcNAc residues,[38] correlate with the reduction in bisected *N*-glycans observed most significantly in the HEK^{XBP1}s membrane *N*-glycome (**Figure 2.2*C***), but also in the secreted *N*-glycome (**Figure 2.4*C***). Although below the threshold for significance, there was also a decrease in the transcripts of the α2,6-sialyltransferase gene *ST6GAL1* (0.69-fold for XBP1s-activated HEK^{XBP1s} versus control, $p = 0.23$) and an increase in transcript levels for the sialidase gene *NEU1* (1.4-

fold for XBP1s-activated HEK^{XBP1s} versus control, $p = 0.25$) that together may contribute to the loss of α2,6-sialylation, especially on more branched structures, that we observed (**Figure 2.5*B***).

For HeLa^{XBP1s} cells, 155 of 1,075 expressed glycogene transcripts were significantly altered by chronic XBP1s activation (blue in **Figure 2.5*C***; see *Appendix 1*, Dataset S.5*D* for a complete list of results). As was also the case in the HEK^{XBP1s} transcriptome data, this analysis is again in concordance with at least one key feature of the *N*-glycome remodeling caused by XBP1s activation in HeLa^{XBP1s} cell membranes (**Figure 2.3*C***). Specifically (**Figure 2.5*D***), XBP1s-activated HeLa^{XBP1s} cells exhibited increased expression of genes affecting nucleotide sugar availability (Supporting Figure S.9 and *Appendix 1*, Dataset S.5*D*). Among the genes significantly overexpressed, we observed plasma membrane glucose transporters, such as GLUT1 and GLUT3 (encoded by *SLC2A1* and *SLC2A3*, respectively), which could potentially increase glucose availability in the cytosol. We also identified genes in the hexosamine biosynthetic pathway required for the biosynthesis of the UDP-GlcNAc sugar donor,[39] including *PGM3* (4.35-fold increase), *UAP1* (2.12-fold increase), and the rate-limiting *GFPT1* (3.15-fold increase).[40] The increased expression of these enzymes, which collectively regulate cytosolic levels of UDP-GlcNAc (Supporting Figure S.9), was accompanied by an increase in the Golgi UDP-GlcNAc transporter *SLC35A3*, thus increasing potential UDP-GlcNAc availability for Golgi glycosyltransferases.[41] Levels of UDP-GlcNAc have been shown to affect the levels of tri- and tetraantennary *N*-glycans.[39] It is therefore likely that, even in the absence of altered *MGAT5* expression, the abundance of tetraantennary *N*-glycans observed in HeLa^{XBP1s} cells might increase with XBP1s activation owing to increased UDP-GlcNAc concentrations in the Golgi. The connection between changes in UDP-GlcNAc levels and MGAT5-dependent β1,6-branching, in the absence of protein expression changes, is well-established.[42] In further support of this hypothesis, changes in the level of functional *PGM3* have been correlated with altered *N*-glycomic profiles in human neutrophils,[43] and increased expression of *UAP1* in human prostate cancer cells has been correlated with increase abundance of UDP-GlcNAc.[44]

Collectively, these transcript-level results provide insights into the detailed mechanism of some of the XBP1s-induced changes in cellular *N*-glycome architectures. XBP1s activation results in a coordinated remodeling of the glycogene transcriptome at multiple levels, particularly for specific subsets of genes involved in *N*-glycan maturation and the availability of nucleotide sugar donors. In several cases, the alterations in glycogene transcript levels are in concordance with *N*-glycome–level changes induced by XBP1s activation. It should be noted, however, that *N*-glycosylation is regulated at many levels—not just transcriptionally, but also at the levels of translation (via microRNA), enzyme localization, and sugar metabolism/transport.[13, 24, 36, 45-47] Thus, it is to be expected that XBP1s-induced changes in the glycogene transcriptome would be unlikely to directly explain all of the *N*-glycome changes we observed.

Discussion

Previous work has revealed the paradigmatic role of XBP1s in resolving protein misfolding stress and in expanding the secretory pathway. The impact of XBP1s activation on *N*-glycan maturation for specific ectopically overexpressed secreted proteins and possibly on *N*-glycan site occupancy has also been demonstrated.[13, 18] However, it remained unclear whether or not selective XBP1s activation could alter *N*-glycan maturation on endogenous proteins. Strikingly, our data show that chronic XBP1s activation can generate changes of sufficient magnitude to be detected in glycome-wide assays that assess global carbohydrate composition in cell membranes and in the secretome.

XBP1s-mediated changes in *N*-glycome composition occur across multiple cell types. The nature of these changes displays some cell-type specificity, likely owing to the very different baseline *N*-glycome compositions of different cells. As summarized in Supporting Table S.2, upon stress-independent XBP1s activation in three different sets of samples, we observed increases in oligomannose levels in two sample sets (HEK^{XBP1s} secretomes and $HeLa^{XBP1s}$ membranes), reductions in sialylation in two sample sets (HEK^{XBP1s} membranes and HEK^{XBP1s} secretomes), decreases in bisecting GlcNAc in two sample sets (HEK^{XBP1s} membranes and HEK^{XBP1s} secretomes), and increases in core fucosylation and tetraantennary *N*-glycans in one sample set ($HeLa^{XBP1s}$ membranes). These results were consistently observed by multiple analytical methods, including lectin microarrays, MALDI-TOF MS, GC-MS, and lectin flow cytometry. We note that, in many cases, related changes were also induced by global, stress-mediated UPR activation using Tg treatment (Supporting Table S.3). However, the capacity of XBP1s activation alone to remodel the *N*-glycome indicates the key role of this transcription factor in driving *N*-glycome remodeling. ER stress is not required.

XBP1s-induced alterations in *N*-glycome architectures appear to reflect, at least in part, a coordinated response owing to remodeling of the glycogene transcriptome. In particular, changes in the expression of specific transcripts encoding enzymes directly involved in *N*-glycan maturation were induced by XBP1s activation. *N*-Glycome remodeling driven by changes in glycogene transcript levels is consistent with observations that differential expression of glycosylation-related transcripts,[24] or even individual glycogenes,[48] can give rise to cell type- and disease-specific glycosylation profiles. However, full prediction of how glycogene transcriptome changes will be reflected in secreted and cell-membrane *N*-glycome architectures remains very challenging, likely owing to the fact that multiple variables, and not just glycogene transcript levels, play a role in *N*-glycan biosynthesis.[13, 24, 36, 45-47] Thus, unsurprisingly, although some features of the XBP1s-remodeled *N*-glycome correlate with transcript-level changes in glycogene expression (**Figure 2.5** ***B*** and ***D***), a direct correlation with all features does not exist. Further studies to fully detail the intermediate steps that propagate XBP1s activation to an altered *N*-glycome are an important subject for future work.

Another interesting aspect of our data is the differential impact of XBP1s activation on membrane versus secreted glycoproteins, particularly with respect to an increase in oligomannose levels in the secretome. Secreted glycoproteins on exosomes have been shown to have a glycosylation phenotype distinct from that of the originating cell membranes.[29] Moreover, high- and oligomannose glycans are enriched in exosomes, and there are data indicating that glycosylation can act as a trafficking marker for these secreted vesicles.[49] In the body, secreted glycoproteins can impact biology at sites distant to the cell, and there are many glycan-binding proteins involved in innate immunity. Cell-nonautonomous UPR signaling has been observed in metabolic regulation, immune system activation, and tumorigenesis,[50] all processes that are also responsive to target- and/or epitope-specific glycosylation.[17, 51-52] Cumulatively, these observations raise the intriguing possibility that cells may use XBP1s-enacted changes in glycosylation in the secretome to signal for immune system functions or for cell-nonautonomous stress signaling.[8, 10]

Selective activation of the IRE1-XBP1s arm of the UPR, even in the absence of ER protein misfolding stress, is a widely observed biological phenomenon. For example, selective XBP1s activation is involved in both memory formation and circadian clock regulation.[9, 53] Similarly, selective induction of the XBP1s arm of the UPR plays a critical role in aspects of the immune response and in development.[7-8] The molecular mechanisms by which XBP1s activity influences these processes continue to be investigated. Our results indicate that a functional role for XBP1s-altered glycosylation must be considered. Beyond these phenomena, selective, chronic XBP1s activation is also commonly observed in malignancies.[11] It is noteworthy that another common feature of cancer cells is modified *N*-glycosylation.[16, 52] Our findings open the possibility of a mechanistic connection between chronic XBP1s activity in cancer and metastasis-promoting, neoplastic *N*-glycosylation patterns.

In conclusion, the capacity of XBP1s-mediated transcriptional regulation to remodel the molecular architecture of the *N*-glycome provides a potential new pathway for intracellular stress signaling to be propagated to the extracellular milieu. XBP1s-induced changes to the *N*-glycome may also hold implications for pathologic processes, such as development of neoplastic glycosylation patterns that support cancer metastasis. In ongoing work, we are using glycoproteomic strategies to identify the specific endogenous proteins whose *N*-glycans are altered by XBP1s, and characterizing the functional consequences of such *N*-glycome remodeling.

Materials and Methods

Cells and Reagents

HEK^{XBP1s} cells were cultured as previously described.[18] HeLa-TREx cells were obtained from Invitrogen and cultured in complete DMEM supplemented with 10% fetal bovine serum (FBS), as well as geneticin sulfate (G418, 500 μg/mL) to maintain the tetracycline repressor. A pLenti4.XBP1s construct, along with a linear marker for puromycin resistance, was transfected into HeLa.TREx cells using Xfect (Clontech). Stable HeLa^{XBP1s} cell lines were selected by culturing in puromycin (0.5 μg/mL). An optimized single colony was selected and characterized by Western blot and qPCR before use in these experiments.

Lectin Microarray Glycomic Analyses

Lectin microarrays were generated as previously described.[54] Briefly, they were manufactured in-house with a Nano-plotter v2.0 piezoelectric non-contact array printer (GeSiM) using a nano A-J tip. Arrays were printed on Nexterion Slide H (Schott Nexterion) under 50% relative humidity at a surface temperature of 12 °C. Commercial lectins and antibodies were purchased from Vector Labs, R&D Systems, Santa Cruz, TCI, AbCam, E.Y. Labs, or Sigma-Aldrich. The recombinant lectins rGRFT, rCVN, and rSVN were generous gifts from Dr. B. O'Keefe (NCI Frederick). For a list of all printed lectins see *Appendix 1*, Dataset S.2. We note that while the diversity of printed lectins allows for a wide range in the detection of glycan epitopes, we are unable to observe some epitopes (e.g. α2,8-linked sialic acids) on our current array.

Prior to sample hybridization, lectin microarray slides were blocked for 1 h with 50 mM ethanolamine in 50 mM sodium borate buffer (pH 8.8) followed by three washes with 0.005% PBS-T (pH 7.4). Sample protein concentration and the degree of fluorescent label incorporation was determined by measuring absorbances at 280, 555, and 650 nm per the manufacturer's instructions on a NanoDrop ND-2000c spectrophotometer (Thermo Scientific). Equal protein amounts (5 μg) of sample and contrasting labeled reference were mixed in 0.005% PBS-T (pH 7.4) for a final concentration of 67 ng/μL of protein. Slides were then loaded into a hybridization cassette (Arrayit) to isolate individual arrays (24 per slide). Samples were loaded onto individual arrays along with one array for the reference vs reference sample per slide. Samples were hybridized for 2 h at 25 °C with gentle agitation. After hybridization, samples were removed and arrays were washed 4× with 0.005% PBS-T (pH 7.4) for 10 min each. Slides were removed, submerged in ddH_2O, and spun dry. Arrays were scanned using a GenePix 4300A array scanner (PMT 550 laser power 100% for both fluorescent channels).

Background-subtracted median fluorescence intensities were extracted using GenePix Pro v7.2. Non-active lectins were defined as having an average of both channel SNRs < 3 in > 90% of the data and removed prior to further analysis. Data were median-normalized in each fluorescent channel and the $\log_2$

of the sample/reference ratio was calculated for each technical replicate for each lectin. Technical replicates were then averaged for each lectin within each array. The ratios across individual biological triplicates per lectin were compared across treatments using a two-tailed Student's *t*-test.

MALDI-TOF MS and TOF/TOF MS/MS Glycomic Analyses

All samples were treated as described previously.[55] Briefly, each sample was subjected to sonication in the presence of detergent (CHAPS), reduction in 4 M guanidine-HCl (Pierce, Cramlington, Northumberland, UK), carboxymethylation, and trypsin digestion. The digested glycoproteins were then purified by HLB plus C_{18}-Sep-Pak (Waters Corp, Hertfordshire, UK; 186000132). *N*-Glycans were released by peptide *N*-glycosidase F (E.C. 3.5.1.52; Roche Applied Science, Burgess Hill, UK) digestion. Released *N*-glycans were permethylated using the sodium hydroxide procedure and purified by classic C_{18}-Sep-Pak (Waters, WAT051910). Permethylated *N*-glycans were eluted at the 50% acetonitrile fraction. We note that polysialylated structures deriving from the activity of α2,8-sialyltransferase (ST8SIA2) enzyme were not analyzed from the above released *N*-glycans.[56]

MS and MS/MS data were acquired using a 4800 MALDI-TOF/TOF (Applied Biosystems, Darmstadt, Germany) mass spectrometer. Permethylated samples were dissolved in 10 μL of methanol and 1 μL of dissolved sample was premixed with 1 μL of matrix (10 mg/mL 3,4-diaminobenzophenone in 75% (v/v) aqueous acetonitrile), spotted onto a target plate and dried under vacuum. For the MS/MS studies the collision energy was set to 1 kV, and Ar was used as the collision gas. The 4700 Calibration standard kit, calmix (Applied Biosystems), was used as the external calibrant for the MS mode and [Glu1] fibrinopeptide B human (Sigma-Aldrich) was used as an external calibrant for the MS/MS mode.

MS and MS/MS data were processed using Data Explorer 4.9 Software (Applied Biosystems). The processed spectra were subjected to manual assignment and annotation with the aid of a glycobioinformatics tool, GlycoWorkBench.[57] The proposed assignments for the selected peaks were based on ^{12}C isotopic composition together with knowledge of the biosynthetic pathways. The proposed structures were then confirmed by data obtained from MS/MS and linkage analysis experiments.

For MALDI-TOF analysis of secretome samples, we note that even in commercial "serum-free" media, MS detects serum-derived glycoproteins.[31] In prior work we have shown that the FBS-derived glycans can be identified and removed from the analysis without impacting analysis of other glycan structures, just as we have done here.[32, 58] Thus, the presence of these peaks does not significantly impact detection of other glycan structures in the secretome.

GC-MS Glycan Linkage Analyses

Partially methylated alditol acetates (PMAAs) were prepared as previously described.[55] Linkage analyses of PMAAs were performed on a Scion 456-GC SQ instrument (Bruker) fitted with a BR-5ms fused silica capillary column (15 m × 0.25 mm i.d.; Bruker). The sample was dissolved in ~20 μL of hexanes and injected manually (4–5 μL) at a split ratio of 1/10. Injector temperature was set at 250 °C. Helium was used a carrier gas at constant flow of 1 mL/min. PMAAs were eluted with the following linear gradient oven: initially the oven temperature was set at 60 °C for 1 min, heated to 300 °C at a rate of 8 °C per min, then held at 300 °C for 1 min.

RNA Extraction and Real-Time qPCR

HEK^{XBP1s} and $HeLa^{XBP1s}$ cells were plated and treated as for lectin microarray analysis (below). After 72 h of XBP1s activation with 1 μg/mL dox (or 24 h of treatment with 0.1% DMSO or 750 nM Tg), cells were washed with PBS and RNA was extracted using the Omega E.Z.N.A. Total RNA extraction kit. cDNA was prepared from 500 ng RNA, normalized for all samples in each run, using an Applied Biosystems Reverse Transcriptase cDNA Kit in a BioRad Thermocycler. Samples were run on a Light Cycler 480 II Real Time PCR Instrument in the MIT BioMicro Center using previously described primers and data were analyzed as described previously.[4, 18] For qPCR arrays, HEK^{XBP1s} and $HeLa^{XBP1s}$ cells were treated for 48 h with 1 μg/mL dox or 0.1% DMSO prior to harvesting. RNA was then extracted using the Qiagen RNeasy kit, cDNA was prepared from equal amounts of RNA using the Qiagen RT2 First Strand Kit in a BioRad Thermocycler, and samples were loaded on an RT^2 Profiler PCR Array for Human Glycosylation (Qiagen PAHS-046Z). Analyses were performed in a Light Cycler 480 II Real Time PCR Instrument in the MIT BioMicro Center. Data from three biological replicates were analyzed using the ΔΔCt method. A list of glycogenes was manually curated from the HEK^{XBP1s} microarray[4] and $HeLa^{XBP1s}$ RNA-Seq data, and then combined with detected glycogenes from the PCR array (*Appendix 1*, Dataset S.5). Significance cut-offs used were FDR or *p*-value ≤ 0.05 and fold-change ≥ 1.5.

RNA-Seq

$HeLa^{XBP1s}$ cells were plated in biological triplicate at a density of 6×10^5 cells per well in 6-well plates and allowed to adhere overnight. Cells were then treated for 48 h with vehicle or 1 μg/mL dox, or for 24 h with 750 nM Tg. Cells were harvested and RNA was extracted using the RNeasy Plus Mini Kit (Qiagen). RNA quality was confirmed using a Fragment Analyzer (Advanced Analytical). RNA samples were then loaded on a HiSeq cartridge as a 50 base single-end run with 6 + 6 nucleotide indexes. *H. sapiens* RNA-Seq reads were aligned to hg19 with bowtie version 1.0.1[59] and expression was summarized using

rsem version 1.2.26[60] using the ensemble gencode annotation release 75. Differential expression analysis was done with deseq2 version 1.10.0[61] running under R version 3.2.3. Default options were selected for deseq2 runs, except Cooks Cutoff and Independent Filtering were both set to false during results preparation. Gene Set Enrichment Analysis[62] Java command-line version 2.3.0 beta was run in both pre-ranked and standard mode using the stat output from deseq2 to order genes. Custom gene sets and a selected subset from MSigDB version 5.2 were analyzed; these gene sets are provided in *Appendix 1*, Datasets S.1*E* and S.5*A*. Hierarchical clustering was performed with Spotfire 7.6.1, using counts of transcripts with highest expression for each gene.

Membrane Proteome Preparation

HeLa^{XBP1s} or HEK293^{XBP1s} cells were plated in 10 cm dishes at a density of 1×10^6 cells per plate and allowed to adhere overnight. The next day, XBP1s expression was induced by treatment with 1 μg/mL dox. Vehicle and Tg-treated plates received fresh media and either DMSO or 750 nM Tg for 24 h before harvesting. After 72 h of induction, cells were harvested by scraping in 1× PBS + 1 mM EDTA, sonicated to disrupt cells, and then centrifuged at 35k RPM at 4 °C for 1 h to pellet the membrane fraction. Pellets were resuspended in 100 μL PBS, homogenized with 21G and 27G needles, and protein concentrations were measured via A280 on a NanoDrop ND-1000 spectrophotometer.

Secretome Preparation from HEK^{XBP1s} Cells

Prior to plating cells, 15 cm dishes were coated with 0.05 mg/mL of poly-D-lysine hydrobromide (Sigma P6407) for 10 min at room temperature. Each dish was washed three times with PBS before seeding with 10×10^6 HEK^{XBP1s} cells in complete medium. After 24 h, media were changed to add the appropriate compounds: 1 μg/mL dox for XBP1s activation or 0.1% DMSO for control. After another 24 h, media were removed and cells were washed with PBS (containing Ca^{2+} and Mg^{2+}) three times. Cells were then incubated in Freestyle medium (Gibco) with either 1 μg/mL dox, 0.1% DMSO, or 750 nM of Tg. Conditioned media were harvested from cells after a total of 48 h with dox or DMSO, or 28 h with Tg. Medium samples were filtered through 0.2 μm PES membranes (VWR) and concentrated in 3 kDa MWCO centrifugal units (Millipore Amicon Ultra). For immunoblotting analysis of the secretome, 6×10^5 HEK^{XBP1s} cells were plated per well on poly-D-lysine coated 6-well plates and treated with dox or vehicle as described above. After 24 h, cells were washed with PBS (containing Ca^{2+} and Mg^{2+}) three times and then incubated in DMEM (+10% FBS, L-glutamine) or Freestyle media, with or without 1 μg/mL dox. Conditioned media were collected after 48 h, spun at 1.5k RPM at 4 °C for 5 min to pellet cell debris, and then run on 4/8% SDS-PAGE gels. Proteins were transferred to nitrocellulose membranes and incubated with an α-KDEL

(recognizes both Grp78 and Grp94, Enzo ADI-SPA-827) antibody. Blots were developed with the appropriate 800CW secondary antibody (LI-COR) prior to scanning on an Odyssey infrared imager (LI-COR).

Lectin Flow Cytometry

HeLa^{XBP1s} cells were treated with or without dox for 72 h, then very briefly trypsinized. Cells were washed twice with 2% FBS in PBS, and 1×10^6 cells/sample were incubated for 30 min at 4 °C with HHL-biotin (Vector Labs) at 5 μg/mL. Competitive sugars (200 mM α-methylmannoside, Sigma-Aldrich) were pre-incubated 30 min with lectins at room temperature for inhibitory controls. Cells were washed and resuspended in 20 μg/mL of Cy5-streptavidin (Thermo Fisher Scientific) for 20 min at 4 °C in the dark. Cells were resuspended in 1 mL of 2% FBS/PBS, passed through cell strainers (Falcon), and analyzed on a BD Accuri C6 flow cytometer.

CellTiter-Glo Assay

HeLa^{XBP1s} cells were cultured with or without doxycycline (1 μg/mL, 72 h) or 1-DMM (80 μg/mL, 24 h). Cells were counted and plated at 1×10^4 cells/well 24 h prior to carrying out the assay according to the manufacturer's instructions (Promega). In brief, cells were cultured in 100 μL of culture media and an equal volume of reagent was added to lyse cells for 2 min. After incubation at room temperature for 10 min, luminescence measurements were taken.

Resazurin Assay

HeLa^{XBP1s} cells were cultured with or without doxycycline (1 μg/mL, 72 h) or 1-DMM (80 μg/mL, 24 h). Cells were counted and plated at 1×10^4 cells/well 24 h prior to measurements. Resazurin was added to cells at a final concentration of 0.03 mg/mL for 60 min at 37 °C. Fluorescence readings were taken at 560 nm excitation, 590 nm emission.

Secretome Proteomics Analysis

HEK^{XBP1s} cells were treated with either vehicle or doxycycline for 16 h, washed well, and incubated in DMEM without serum for 6 h. Proteins were then precipitated from conditioned media with 10% TCA for 1.5 h at 4 °C and resolubilized using 1% aqueous Rapigest (Waters) in 100 mM HEPES pH 8.0. Proteins were reduced with 5 mM TCEP (Sigma) for 30 min at 37 °C, alkylated with 10 mM iodoacetamide (Sigma) for 30 min in the dark at room temperature, digested with 0.5 μg trypsin overnight at 37 °C and 600 rpm, labeled with appropriate isotopic TMT reagent in 40% CHC_3N for 1 h, quenched with 0.4% ammonium

bicarbonate for 1 h, pooled, evaporated, resuspended in buffer A (5% CHC_3N, 0.1% formic acid), brought to pH < 2 with formic acid, heated at 37 °C to precipitate Rapigest, and stored at -80 °C prior to LC/LC-MS/MS analysis.

Nanopure water and mass spectrometry grade solvents were used for all preparations. MudPIT loading columns were prepared by briefly dipping 250 μm inner diameter (ID) undeactivated fused silica capillaries (Agilent) in 3:1 Kasil 1624 (PQ Corp) : formamide, curing overnight at 100 °C, and trimming the frit to 1 mm. The columns were then rinsed with MeOH, loaded under pressure with 2.5 cm strong cation exchange resin (SCX Luna, 5 μm diameter, 125 Å pore size, Partisphere), and loaded with another 2.5 cm reversed phase resin (C18 Aqua, 5 μm diameter, 125 Å pore size, Phenomenex). The columns were rinsed well with methanol and buffer A prior to loading the peptide digest, and further washed with buffer A. Analytical columns were prepared by pulling 100 μm ID-fused capillaries to a 5 μm ID on a P-2000 tip puller (Sutter Instrument Co.) and loaded with 15 cm of reversed phase resin, followed by methanol rinsing and equilibration in buffer A. For LC-MS/MS, each loading column was connected to the analytical column by a zero-dead-volume union, and connected to the HPLC through a tee junction that allowed connection to the 2.5 kV ESI voltage. A flow rate of 300 nL/min was maintained through a 1:1000 split flow line from an Agilent 1200 pump. MuDPIT experiments were performed where each step corresponds to 0, 10, 20, 30, 40, 50, 60, 70, 80, 90, and 100% buffer C being run for 4 min at the beginning of each gradient of buffer B. Electrospray was performed directly from the analytical column by applying the ESI voltage at a tee (150 mm ID, Upchurch Scientific) directly downstream of a 1:1000 split flow used to reduce the flow rate to 300 nL/min through the columns. Electrospray directly from the LC column was done at 2.5 kV with an inlet capillary temperature of 275 °C.

Data-dependent acquisition of MS/MS spectra were performed with the following settings: eluted peptides were scanned from 300 to 1600 m/z with resolution 30000 and the mass spectrometer in a data dependent acquisition mode. The top ten peaks for each full scan were fragmented by HCD using a normalized collision energy of 45%, a 100 ms activation time, and a resolution of 7500. Dynamic exclusion parameters were 1 repeat count, 30 ms repeat duration, 500 exclusion list size, 120 s exclusion duration, and exclusion width between 0.51 and 1.51. Protein and peptide identification and protein quantitation were done with the Integrated Proteomics Pipeline - IP2 (Integrated Proteomics Applications, Inc., San Diego, CA. http://www.integratedproteomics.com/). Tandem mass spectra were extracted from raw files using Raw Xtractor 1.9.13 and were searched against a database containing 20245 human sequences (longest entry for the IPI database for each protein) with reversed sequences using ProLuCID. Carbamidomethylation (+57.02146 Da) of cysteine and TMT tagging of N-termini and of lysine residues (+229.1629 Da) were considered as static modifications. Peptide candidates were filtered using DTASelect2 (version 2.0.27) for a false positive (decoy) peptide ratio of ~1%. Quantitation was performed

using Census7, followed by deconvolution of isotopic impurity as reported in the lot analysis supplied by Thermo Fisher, and finally normalization of ratio values based on the mode. Redundant peptides were generally assigned to all proteins. The heavy to light ratio was quantified by Census.[63]

Appendix and Online Materials

Details on datasets referenced in this chapter can be found in *Appendix 1*.

Data Deposition

The RNA-sequencing analysis reported in this paper has been deposited in the Gene Expression Omnibus (GEO) database, https://www.ncbi.nlm.nih.gov/geo/ (accession no. GSE112589).

Acknowledgements

This work was supported by the 56th Edward Mallinckrodt Jr. Foundation Faculty Scholar Award, a Mizutani Foundation for Glycoscience Innovation Grant, an American Cancer Society–Ellison Foundation Research Scholar Award, and MIT (M.D.S.), NIH/NIAID Grant U01AI111598 (to L.K.M.), and BBSRC Grant BB/K016164/1 (to S.M.H. and A.D.). M.Y.W. was supported by a National Science Foundation Graduate Research Fellowship and a Prof. Amar G. Bose Research Grant. J.C.G. was supported by an NRSA from the NHLBI (F32-HL099245). This work was also supported in part by the NIH/NIEHS (Grant P30-ES002109) and Koch Institute Support (Core) Grant P30-CA14051 from the National Cancer Institute. The authors declare no conflict of interest.

Supporting Figures

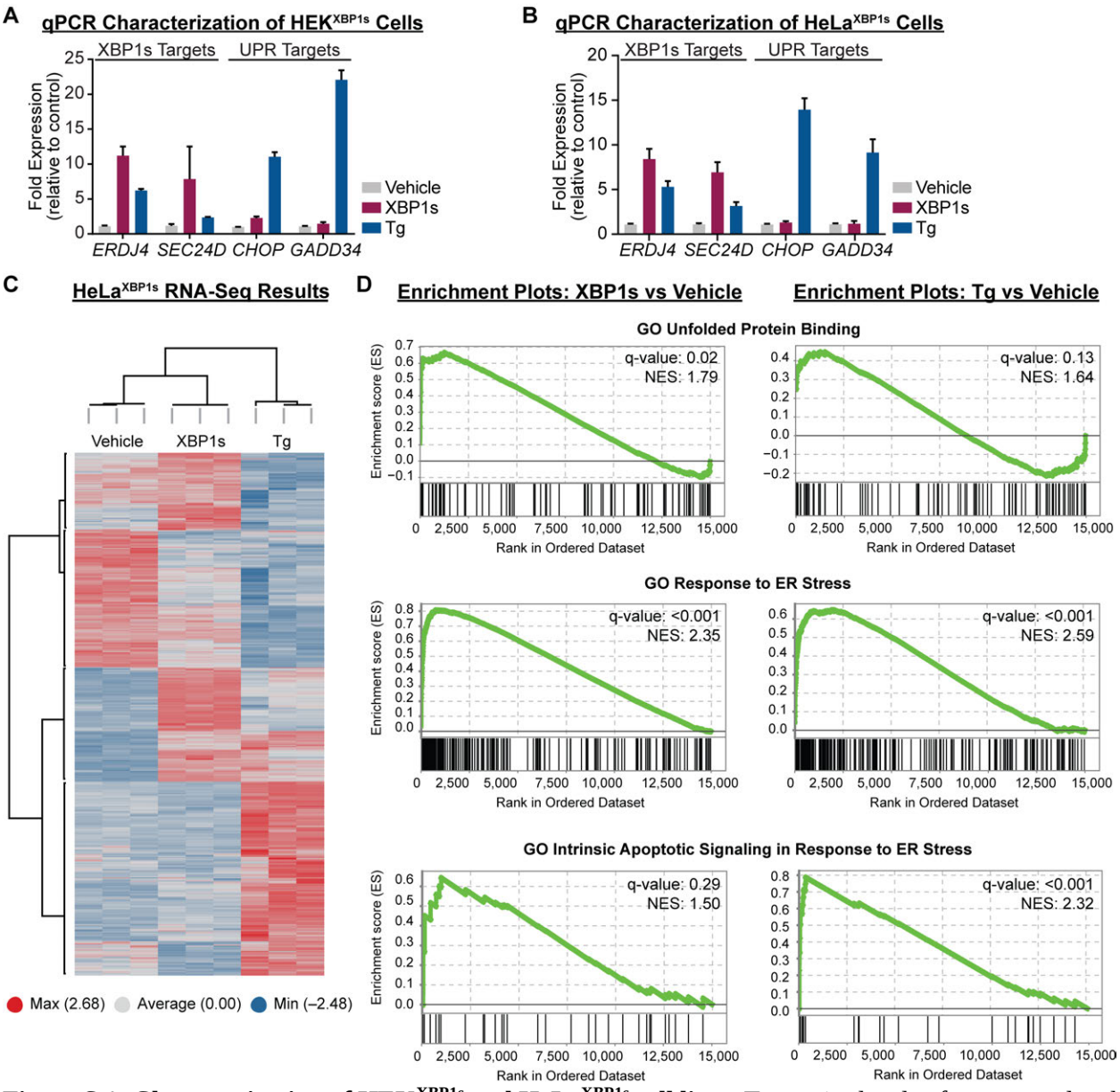

Figure S.1: Characterization of HEK^{XBP1s} and HeLa^{XBP1s} cell lines. Transcript levels of genes regulated by the IRE1-XBP1s arm (*ERDJ4* and *SEC24D*) or the PERK-ATF4 arm (*CHOP* and *GADD34*) of the UPR were measured in HEK^{XBP1s} cells (***A***) and HeLa^{XBP1s} cells (***B***) by qRT-PCR. (***C***) RNA-Seq highlights distinctive effects of stress-mediated global UPR activation versus stress-independent XBP1s activation. Hierarchical clustering of differentially expressed protein-coding genes. HeLa^{XBP1s} cells were plated at a density of 6×10^5 cells per well in 6-well plates and allowed to adhere overnight. Cells were then treated with dox (1 μg/mL, 48 h), DMSO (0.1%, 24 h), or thapsigargin (Tg; 750 nM, 24 h), total RNA was extracted with the Qiagen RNeasy Plus Mini Kit, and samples were loaded on a HiSeq cartridge. Supervised hierarchical clustering was performed using Ward's method implemented in Spotfire 7.6.1 with row-centered $\log_2$ FPKM data for genes differentially expressed in at least one of the following comparisons: Tg vs vehicle, XBP1s vs vehicle, or XBP1s vs Tg. For the hierarchical clustering, differentially expressed genes were defined as those having absolute $\log_2$ fold-change > 1 and FDR adjusted *p*-values < 0.05. (***D***) Selected GSEA enrichment plots for XBP1s versus vehicle and Tg versus vehicle showing distinct effects of XBP1s-activation versus global UPR activation with the ER stressor Tg.

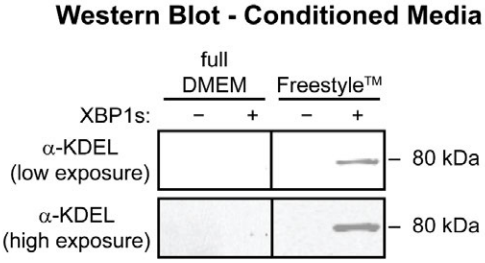

Figure S.2: Freestyle and complete DMEM media Western blot. Western blot of conditioned media from HEK^{XBP1s} cells cultured in complete DMEM or Freestyle media, shown at both low and high exposure. HEK^{XBP1s} cells were plated at a density of 6×10^5 cells per well on poly-D-lysine coated 6-well plates and allowed to adhere overnight. Cells were then treated with or without dox (1 μg/mL, 24 h), after which plates were washed three times with PBS (containing Ca^{2+} and Mg^{2+}) prior to treatment with either full DMEM (+10% FBS, L-glutamine) or Freestyle media, with or without 1 μg/mL dox. Conditioned media was collected for 48 h, spun at 1.5k RPM at 4 °C for 5 min to pellet cell debris, and then run on 4/8% SDS-PAGE polyacrylamide gels. Grp78 signal was detectable in Freestyle media samples, but only upon XBP1s activation.

Figure S.3: Analysis of the HEK^{XBP1s} membrane glycoproteome. Full caption on the following page.

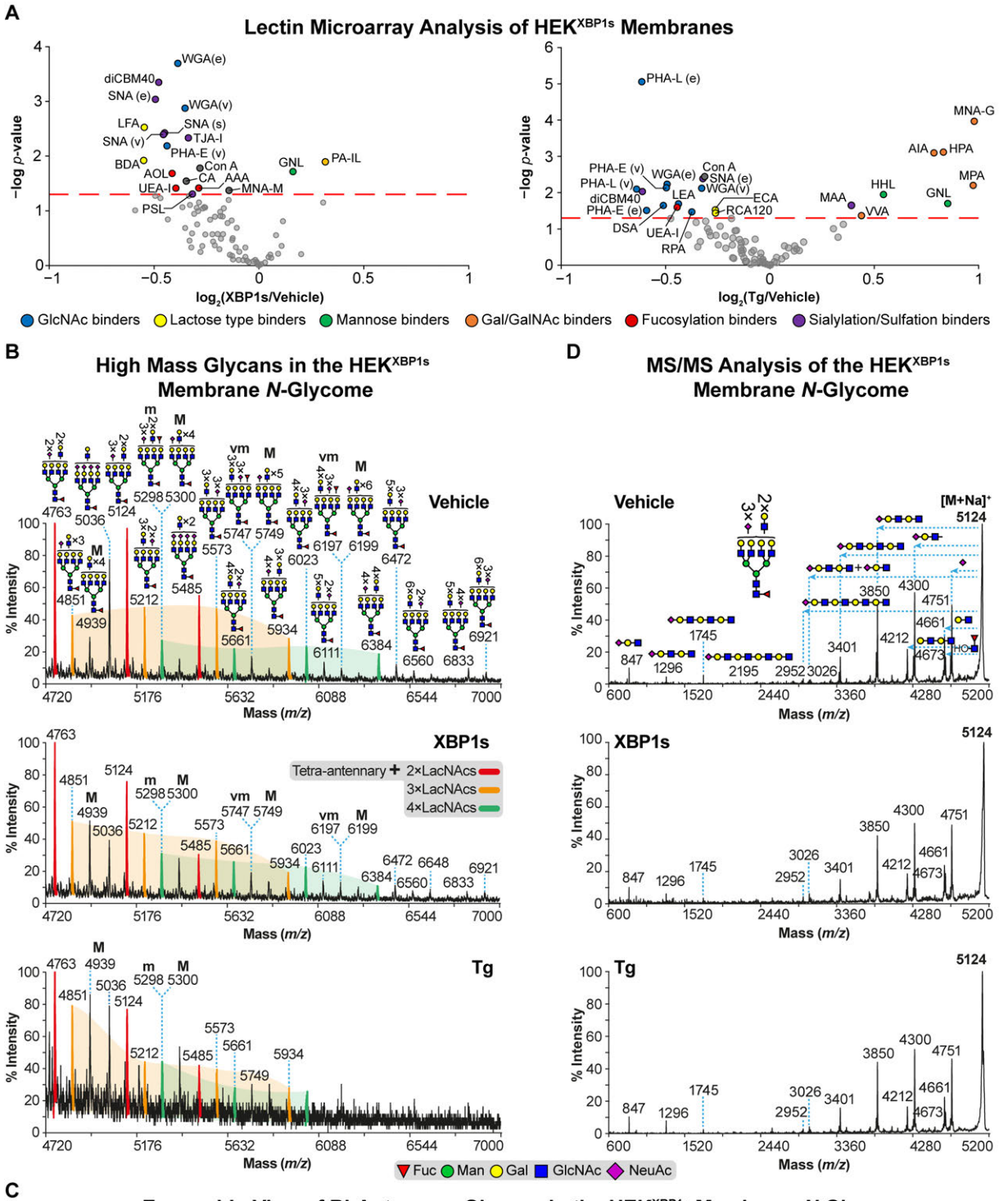

Figure S.3: Analysis of the HEK^{XBP1s} membrane glycoproteome. (***A***) Lectin microarray analysis of membrane proteomes isolated from HEK^{XBP1s} cells showed decreased sialylation and a loss of bisecting GlcNAc upon XBP1s activation (*Left*). Tg treatment (*Right*) also showed decreases in sialylation and bisecting GlcNAc, along with an increase in core 1/3 *O*-glycans. Spot colors correspond to lectin sugar specificity, as indicated; the dotted line represents a significance cutoff of p-value ≤ 0.05 across three biological replicates. (***B***) MALDI-TOF MS spectra of high mass *N*-glycans. Red, yellow and green peaks correspond to tetra-antennary *N*-glycans with 2, 3 and 4 additional LacNAc repeats, respectively, with various levels of sialylation. Yellow and green shaded areas, manually inserted, highlight the shift towards fewer NeuAc residues. Structures outside a bracket have not been unequivocally defined, and "M," "m," and "vm," designations indicate major, minor and very minor abundances, respectively. Putative structures were assigned based on glycan composition, tandem mass spectrometry data, and knowledge of biosynthetic pathways. (***C***) Zoomed-in MALDI-TOF MS spectra indicating bi-antennary *N*-glycans (red peaks) with varying levels of sialylation. Putative structures were assigned based on glycan composition, tandem mass spectrometry data, and knowledge of biosynthetic pathways. (***D***) MALDI-TOF/TOF MS/MS spectra (selected from corresponding panels in Figure S.3*B*) for vehicle, XBP1s-activated, and Tg-treated HEK^{XBP1s} membrane proteomes. Spectra depict fragments of the $[M+Na]^+$ molecular ion found at *m/z* 5124. Structures above each horizontal dashed arrow indicate loss of the designated *N*-glycan sequence from the molecular ion; vertical dashed lines indicate the corresponding fragment ion peak. All molecular and fragment ions are $[M+Na]^+$. Cartoon structures were drawn according to the Consortium for Functional Glycomics (http://www.functionalglycomics.org) guidelines. For the molecular ion at *m/z* 5124, note the fragment ions at *m/z* 4300, 3850, 3401 and 2952 that correspond to loss of sialylated-LacNAc, sialylated-$LacNAc_2$, sialylated-$LacNAc_3$ and sialylated-$LacNAc_4$ respectively. The presence of such fragment ions suggests the existence of structural isomers corresponding mainly to tetra-antennary (and to a lesser extent tri-antennary) *N*-glycans. The relative abundance of these fragment ions did not shift between vehicle-treated, XBP1s-activated and Tg-treated HEK^{XBP1s} cells, further suggesting that the ratio of structural isomers remained relatively constant.

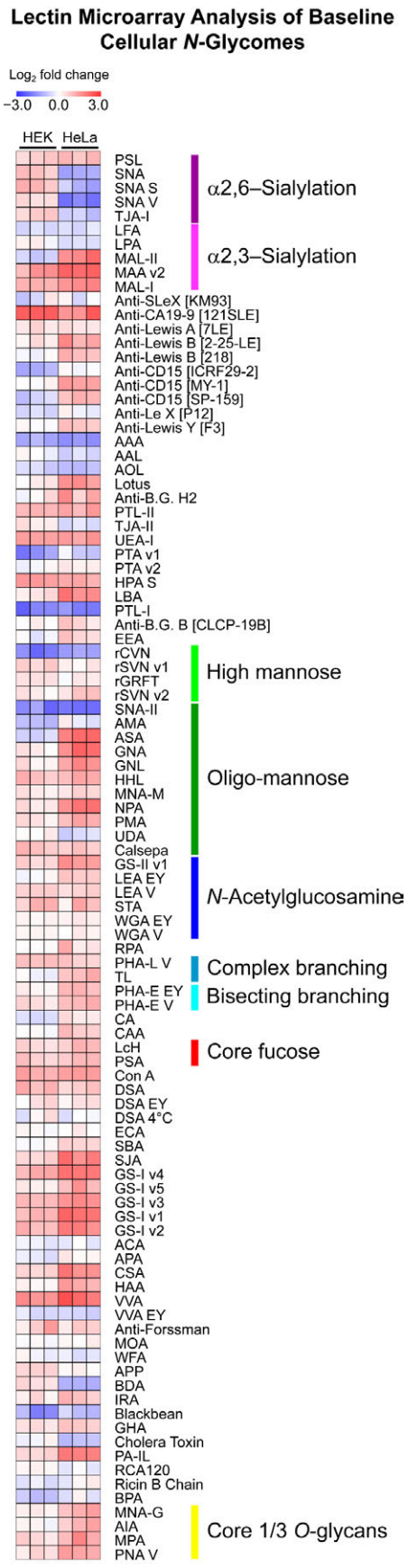

Figure S.4: Differences in baseline HEK^{XBP1s} and HeLa^{XBP1s} membrane glycoproteomes. Heat map of lectin microarray data generated from isolated HEK^{XBP1s} and HeLa^{XBP1s} membrane glycoproteomes under vehicle-treated conditions. Samples were run on the same lectin microarray slide. Color intensity represents normalized $\log_2$ ratio data relative to a pooled (in this case, multi-cell line) sample reference. Each column represents one biological replicate of the indicated sample.

Figure S.5: Analysis of the HeLa^{XBP1s} membrane *N*-glycoproteome. Full caption on the following page.

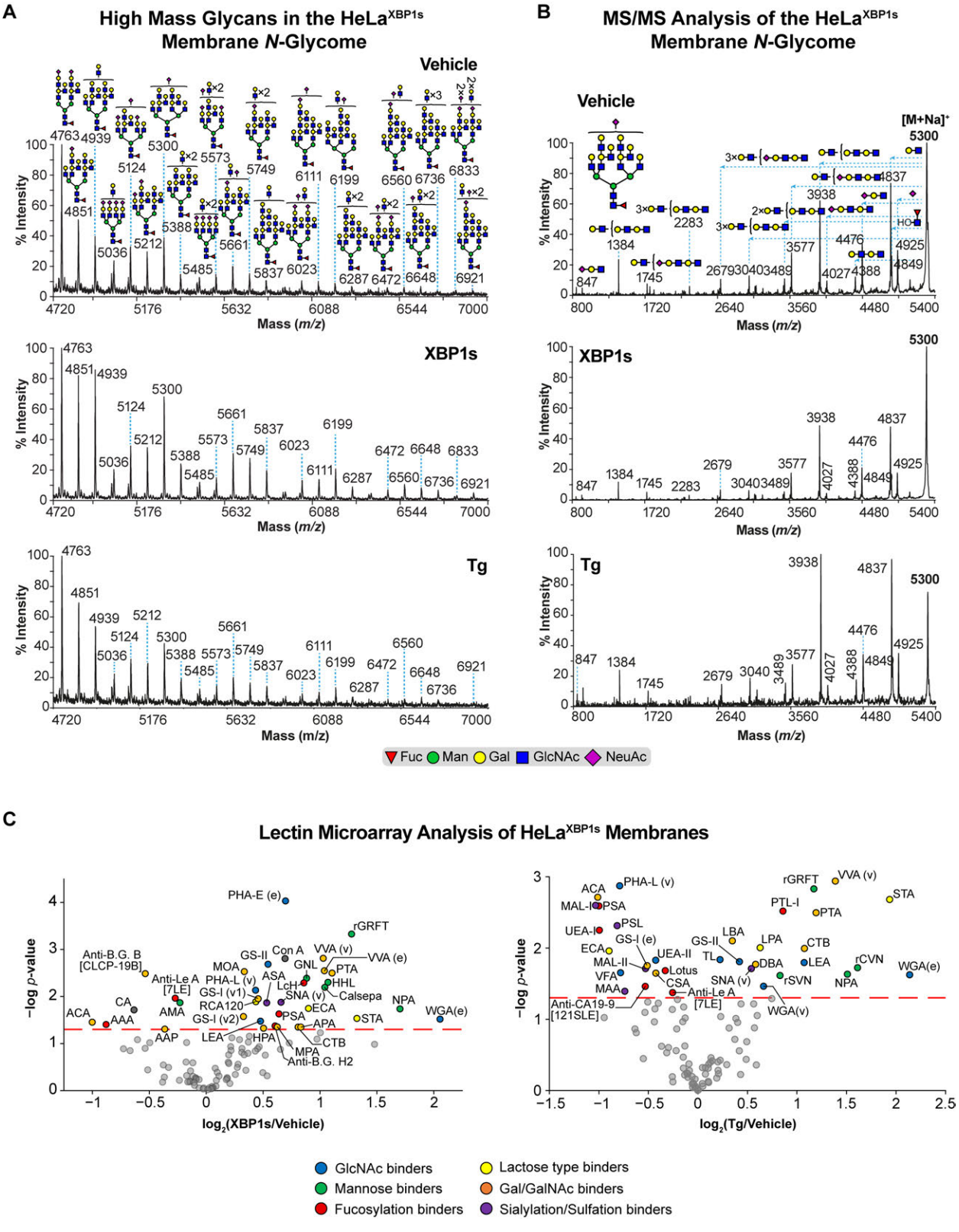

Figure S.5: Analysis of the HeLa^{XBP1s} membrane *N*-glycoproteome. (***A***) MALDI-TOF MS spectra of high mass *N*-glycans and (***B***) MALDI-TOF/TOF MS/MS spectra (selected from corresponding panels in Figure S.5*A*) for vehicle, XBP1s-activated, and Tg-treated HeLa^{XBP1s} membrane proteomes. MALDI-TOF/TOF MS/MS spectra depict fragments of the $[M+Na]^+$ molecular ion found at *m/z* 5300. (***C***) Lectin microarray analysis of membrane proteomes isolated from HeLa^{XBP1s} cells showed an increase in high-mannose *N*-glycans upon XBP1s activation (*Left*), as well as increases in core fucosylation and tetra-antennary *N*-glycans (β1,6-GlcNAc). Tg activation (*Right*) showed a similar gain of high-mannose *N*-glycans, but not increased β1,6-GlcNAc branching. Spot colors correspond to lectin sugar specificity; the dotted line represents a significance cutoff of *p*-value ≤ 0.05 across three biological replicates.

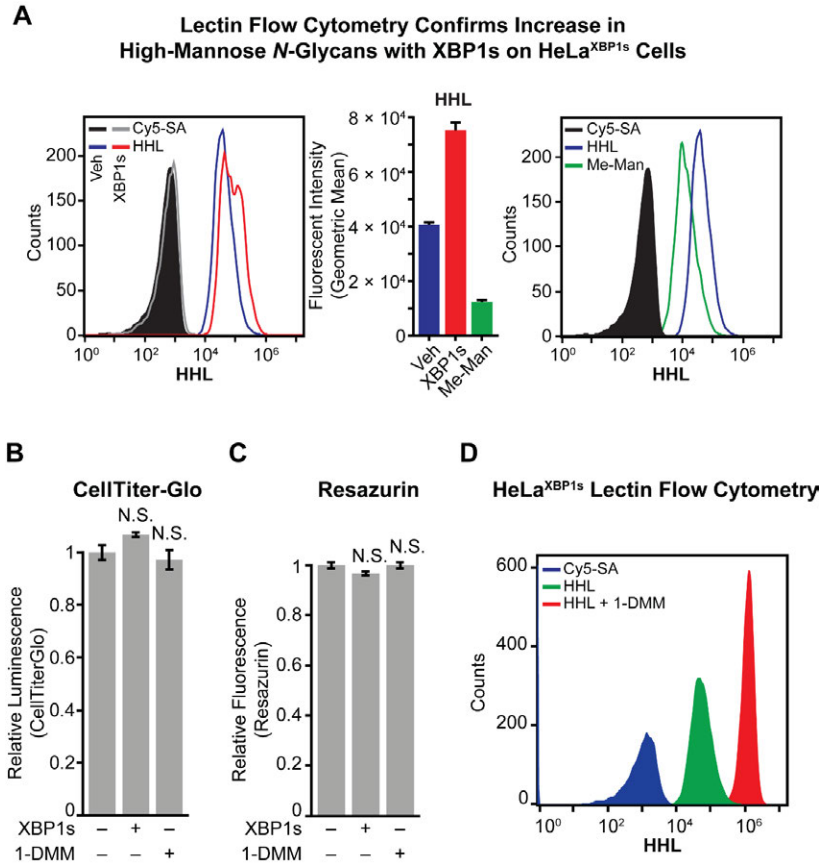

Figure S.6: Lectin flow cytometry confirms that XBP1s activation increases high-mannose *N*-glycans on HeLa^{XBP1s} cells. (***A***) Lectin flow cytometry on live HeLa^{XBP1s} cells confirmed the increase in levels of high-mannose *N*-glycans on the cell surface (*Left*, histogram; *Middle*, quantification). Inhibitory sugar controls (*Right*) were performed with methyl-mannose. Cell viability analyzed by CellTiter-Glo (***B***) or resazurin assay (***C***) was not significantly affected by treatment with dox (1 μg/mL, 72 h) or 1-deoxymannojirimycin (1-DMM, Sigma-Aldrich; 80 μg/mL, 24 h). 1×10^4 HeLa^{XBP1s} cells were seeded for each well 24 h prior to measurements. Error bars represent SEM from four replicates. (***D***) To verify that HHL recognized high-mannose glycans, HeLa^{XBP1s} cells were treated with 80 μg/mL of 1-DMM for 12 h to inhibit mannosidase-I and thus increase high-mannose *N*-glycan levels prior to analysis.

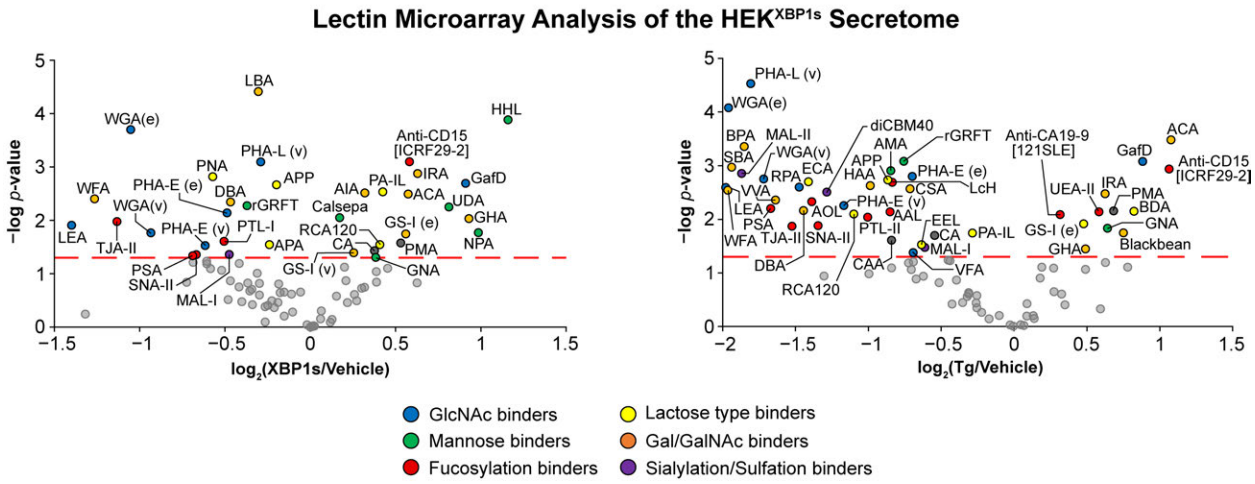

Figure S.7: Analysis of the HEK^{XBP1s} secreted glycoproteome. Lectin microarray analysis of the HEK^{XBP1s} secretome showed a decrease in bisecting GlcNAc and an increase in early processed *N*-glycans upon XBP1s activation (*Left*). Tg treatment (*Right*) showed a decrease in multi-antennary *N*-glycans with no gain in high-mannose structures. Spot colors correspond to lectin sugar specificity; the dotted line represents a significance cutoff of p-value ≤ 0.05 across three biological replicates.

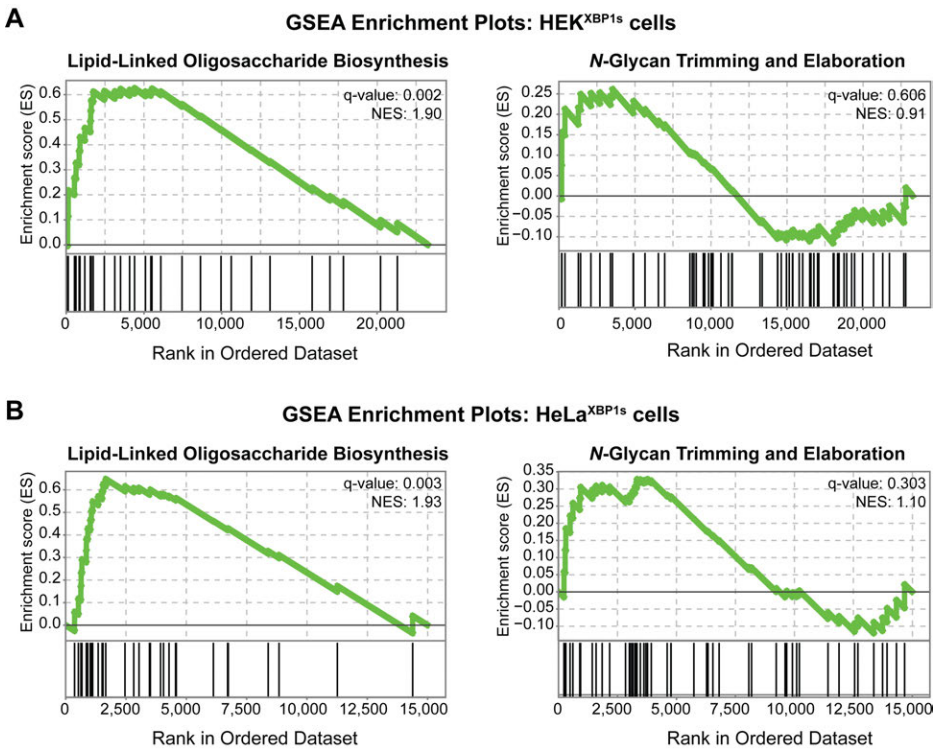

Figure S.8: XBP1s impacts expression of genes involved in lipid-linked oligosaccharide biosynthesis. (***A***) GSEA enrichment plots for HEK^{XBP1s} microarray data upon XBP1s activation using the custom gene sets listed in *Appendix 1*, Dataset S.1*E*. Standard GSEA was run using signal-to-noise ratio as a ranking metric. (***B***) Enrichment plots for HeLa^{XBP1s} RNA-Seq data upon XBP1s activation using the custom gene sets listed in *Appendix 1*, Dataset S.1*E*. Standard GSEA was run using signal-to-noise ratio as a ranking metric.

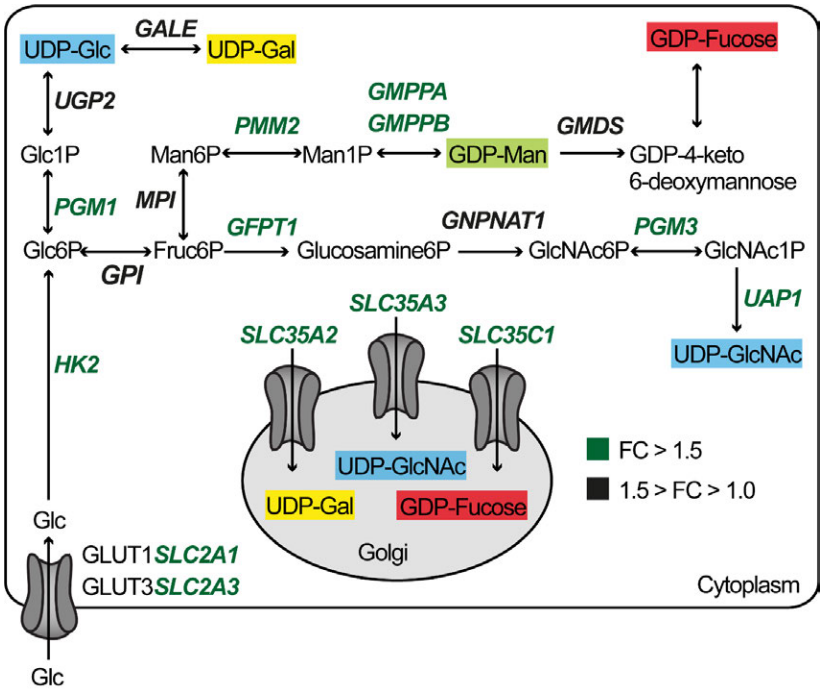

Figure S.9: XBP1s impacts expression of genes involved in nucleotide sugar donor biosynthesis. Simplified biosynthetic pathway of nucleotide sugars depicting the enzymes/transporters that are significantly upregulated upon XBP1s activation in HeLa^{XBP1s} cells. Transcripts shown in green (all with significant expression changes based on FDR or *p*-value ≤ 0.05) encode enzymes or transporters with a fold-change ≥ 1.5, while genes in black encode enzymes with fold-change between 1.0–1.5-fold. Note that *GNPDA1*, which together with *GNPDA2* catalyzes the reverse reaction of *GFPT1*, was significantly decreased (0.79-fold) in HeLa^{XBP1s} cells (*Appendix 1*, Dataset S.5*D*). Biosynthetic pathway adapted from Freeze et al.[64] and the KEGG database (*Homo sapiens* nucleotide sugar metabolism, http://www.kegg.jp).

Supporting Tables

Supporting Table S.1: GC-MS linkage analysis of partially methylated alditol acetates (PMAA) from vehicle, XBP1s-activated, and thapsigargin-treated membrane (HEK^{XBP1s} and $HeLa^{XBP1s}$) and secreted (HEK^{XBP1s}) glycoproteins.

Supporting Table S.2: Summary of observed changes to the HEK^{XBP1s} and $HeLa^{XBP1s}$ *N*-glycomes with XBP1s activation.

Supporting Table S.3: Summary of observed changes to the HEK^{XBP1s} and $HeLa^{XBP1s}$ *N*-glycomes with global UPR activation by treatment with Tg.

Supporting Table S.1: GC-MS linkage analysis of partially methylated alditol acetates (PMAA) from vehicle, XBP1s-activated, and thapsigargin-treated membrane (HEK^{XBP1s} and $HeLa^{XBP1s}$) and secreted (HEK^{XBP1s}) glycoproteins. *N*-Linked glycans were permethylated, hydrolyzed, reduced, acetylated and analyzed by GC-MS.

Quantification[a]	Identification[b]	Residue	Rt (min)	HEK membrane[c]			HeLa membrane[c]			HEK secretome[c]		
				Vehicle	XBP1s	Tg	Vehicle	XBP1s	Tg	Vehicle	XBP1s	Tg
101, 102, 115, 118, 131, 162, 175	142, 187	t-Fuc	13.88	30.1	9.6	9.2	20.6	25.9	36.5	84.8	95.5	121.5
102, 118, 129, 145, 161, 162, 205	71, 87, 113, 174	t-Man	15.32	163.9	189.7	205.4	134.4	151.8	369.8	20.2	25.3	29.4
102, 118, 129, 145, 161, 162, 205	71, 87, 113, 174	t-Gal	15.59	48.6	25.3	23.4	58.7	92.5	49.1	133.1	154.9	76.9
100, 101, 129, 130, 161, 190	71, 87, 88	2-Man	16.44	276.9	297.5	335.4	321.0	300.9	460.4	190.1	222.0	308.9
130, 190, 205	87, 88, 100, 129, 145, 161, 174, 205	2-Gal	16.71	1.2	0.3	0.7	0.0	0.7	0.0	2.9	2.3	1.0
118, 143	87, 101, 129, 174, 202, 217, 234	3-Gal	16.77	29.3	6.7	4.0	26.5	25.3	11.9	56.2	36.1	61.4
102, 118, 129, 159, 162	71, 99, 143, 173, 189, 233	6-Gal	17.24	23.6	4.0	4.1	0.0	4.1	0.0	98.9	63.8	100.1
130, 190, 233	87, 88, 172, 173	2,4-Man	17.58	13.7	6.5	7.3	8.2	16.6	5.3	36.1	25.8	25.6
100, 129, 130, 189, 190	87, 88, 99, 143, 159, 173, 174	2,6-Man	17.91	30.5	11.0	9.6	16.2	26.5	9.4	105.8	71.1	36.0
118, 129, 189, 234	74, 87, 101, 160, 174, 202, 245	3,6-Man	18.15	98.6	99.6	99.2	100.0	100.0	100.0	95.3	97.7	96.3
118, 129, 189, 234	74, 87, 101, 160, 174, 202	3,6-Gal	18.32	n.d.[d]	n.d.	n.d.	11.9	16.4	6.7	n.d.	n.d.	n.d.
118, 139	87, 97, 129, 160, 202	3,4,6-Man	18.56	1.4	0.4	0.8	n.d.	n.d.	n.d.	4.7	2.3	3.7
117, 129, 143, 145, 159, 203, 205	75, 187, 217	t-GlcNAc	18.98	2.4	1.8	4.2	1.9	2.1	0.0	4.8	2.7	1.3
117, 159, 233	75, 99, 143, 171, 203	4-GlcNAc	19.83	163.1	56.0	70.1	66.0	206.7	35.3	415.7	108.7	89.1
117, 142, 159	75, 99, 171, 231, 244	3,4-GlcNAc	20.62	1.5	0.9	0.8	1.2	2.8	10.0	5.8	5.2	2.2
117, 159	75, 99, 124, 127, 142, 143, 201, 245	4,6-GlcNAc	21.05	6.6	1.8	3.7	5.4	10.6	3.1	30.3	11.9	10.9

[a] Electron impact fragment ions used for quantification of the PMAA residues. For relative abundance, in order to minimize interference from the baseline and/or contamination, all fragment ions greater than 100 (>100) were used for the extracted ion current (XIC) chromatogram, as indicated above.

[b] Electron impact fragment ions used for identification of the PMAA residues, in addition to the ions used for quantification.

[c] Relative abundances were obtained by normalizing the integrated area peak of the extracted ion current (XIC) chromatogram of a specific residue to the summed integrated areas of the XICs of 3,6-linked mannose and 3,4,6-linked mannose.

[d] *n.d.* = not detected.

Supporting Table S.2: Summary of observed changes to the HEK^{XBP1s} and HeLa^{XBP1s} *N*-glycomes with XBP1s activation.

Observed Change with XBP1s	HEK^{XBP1s} Membrane	HEK^{XBP1s} Secretome	HeLa^{XBP1s} Membrane
Increased high-mannose		✓	✓
Decreased sialylation	✓	✓	
Decreased bisecting GlcNAc	✓	✓	
Increased core fucosylation			✓
Increased tetra-antennary glycans			✓

Supporting Table S.3: Summary of observed changes to the HEK^{XBP1s} and HeLa^{XBP1s} *N*-glycomes with global UPR activation by treatment with Tg.

Observed Change with Tg	HEK^{XBP1s} Membrane	HEK^{XBP1s} Secretome	HeLa^{XBP1s} Membrane
Increased high-mannose			✓
Decreased sialylation	✓	✓	
Decreased bisecting GlcNAc	✓	✓	
Increased core fucosylation			
Decreased branching		✓	✓
Increased core 1/3 *O*-glycans	✓		

References

[1] Wong, M. Y.; DiChiara, A. S.; Suen, P. H.; Chen, K.; Doan, N. D.; Shoulders, M. D., Adapting Secretory Proteostasis and Function Through the Unfolded Protein Response. *Curr Top Microbiol Immunol* **2018,** *414*, 1-25.

[2] Walter, P.; Ron, D., The unfolded protein response: from stress pathway to homeostatic regulation. *Science* **2011,** *334* (6059), 1081-6.

[3] Amin-Wetzel, N.; Saunders, R. A.; Kamphuis, M. J.; Rato, C.; Preissler, S.; Harding, H. P.; Ron, D., A J-Protein Co-chaperone Recruits BiP to Monomerize IRE1 and Repress the Unfolded Protein Response. *Cell* **2017,** *171* (7), 1625-1637.e13.

[4] Shoulders, M. D.; Ryno, L. M.; Genereux, J. C.; Moresco, J. J.; Tu, P. G.; Wu, C.; Yates, J. R., 3rd; Su, A. I.; Kelly, J. W.; Wiseman, R. L., Stress-independent activation of XBP1s and/or ATF6 reveals three functionally diverse ER proteostasis environments. *Cell Rep* **2013,** *3* (4), 1279-92.

[5] Mendez, A. S.; Alfaro, J.; Morales-Soto, M. A.; Dar, A. C.; McCullagh, E.; Gotthardt, K.; Li, H.; Acosta-Alvear, D.; Sidrauski, C.; Korennykh, A. V.; Bernales, S.; Shokat, K. M.; Walter, P., Endoplasmic reticulum stress-independent activation of unfolded protein response kinases by a small molecule ATP-mimic. *Elife* **2015,** *4*.

[6] Plate, L.; Cooley, C. B.; Chen, J. J.; Paxman, R. J.; Gallagher, C. M.; Madoux, F.; Genereux, J. C.; Dobbs, W.; Garza, D.; Spicer, T. P.; Scampavia, L.; Brown, S. J.; Rosen, H.; Powers, E. T.; Walter, P.; Hodder, P.; Wiseman, R. L.; Kelly, J. W., Small molecule proteostasis regulators that reprogram the ER to reduce extracellular protein aggregation. *Elife* **2016,** *5*.

[7] Martinon, F.; Chen, X.; Lee, A. H.; Glimcher, L. H., TLR activation of the transcription factor XBP1 regulates innate immune responses in macrophages. *Nat Immunol* **2010,** *11* (5), 411-8.

[8] Sun, J.; Liu, Y.; Aballay, A., Organismal regulation of XBP-1-mediated unfolded protein response during development and immune activation. *EMBO Rep* **2012,** *13* (9), 855-60.

[9] Martinez, G.; Vidal, R. L.; Mardones, P.; Serrano, F. G.; Ardiles, A. O.; Wirth, C.; Valdes, P.; Thielen, P.; Schneider, B. L.; Kerr, B.; Valdes, J. L.; Palacios, A. G.; Inestrosa, N. C.; Glimcher, L. H.; Hetz, C., Regulation of Memory Formation by the Transcription Factor XBP1. *Cell Rep* **2016,** *14* (6), 1382-1394.

[10] Taylor, R. C.; Dillin, A., XBP-1 is a cell-nonautonomous regulator of stress resistance and longevity. *Cell* **2013,** *153* (7), 1435-47.

[11] Chen, X.; Iliopoulos, D.; Zhang, Q.; Tang, Q.; Greenblatt, M. B.; Hatziapostolou, M.; Lim, E.; Tam, W. L.; Ni, M.; Chen, Y.; Mai, J.; Shen, H.; Hu, D. Z.; Adoro, S.; Hu, B.; Song, M.; Tan, C.; Landis, M. D.; Ferrari, M.; Shin, S. J.; Brown, M.; Chang, J. C.; Liu, X. S.; Glimcher, L. H., XBP1 promotes triple-negative breast cancer by controlling the HIF1alpha pathway. *Nature* **2014,** *508* (7494), 103-107.

[12] Ruiz-Canada, C.; Kelleher, D. J.; Gilmore, R., Cotranslational and posttranslational N-glycosylation of polypeptides by distinct mammalian OST isoforms. *Cell* **2009,** *136* (2), 272-83.

[13] Wang, Z. V.; Deng, Y.; Gao, N.; Pedrozo, Z.; Li, D. L.; Morales, C. R.; Criollo, A.; Luo, X.; Tan, W.; Jiang, N.; Lehrman, M. A.; Rothermel, B. A.; Lee, A. H.; Lavandero, S.; Mammen, P. P. A.; Ferdous, A.; Gillette, T. G.; Scherer, P. E.; Hill, J. A., Spliced X-box binding protein 1 couples the unfolded protein response to hexosamine biosynthetic pathway. *Cell* **2014,** *156* (6), 1179-1192.

[14] Moremen, K. W.; Tiemeyer, M.; Nairn, A. V., Vertebrate protein glycosylation: diversity, synthesis and function. *Nat Rev Mol Cell Biol* **2012,** *13* (7), 448-62.

[15] Zandberg, W. F.; Kumarasamy, J.; Pinto, B. M.; Vocadlo, D. J., Metabolic inhibition of sialyl-Lewis X biosynthesis by 5-thiofucose remodels the cell surface and impairs selectin-mediated cell adhesion. *J Biol Chem* **2012,** *287* (47), 40021-30.

[16] Stowell, S. R.; Ju, T.; Cummings, R. D., Protein glycosylation in cancer. *Annu Rev Pathol* **2015,** *10*, 473-510.

[17] Pang, P. C.; Tissot, B.; Drobnis, E. Z.; Morris, H. R.; Dell, A.; Clark, G. F., Analysis of the human seminal plasma glycome reveals the presence of immunomodulatory carbohydrate functional groups. *J Proteome Res* **2009,** *8* (11), 4906-15.

[18] Dewal, M. B.; DiChiara, A. S.; Antonopoulos, A.; Taylor, R. J.; Harmon, C. J.; Haslam, S. M.; Dell, A.; Shoulders, M. D., XBP1s Links the Unfolded Protein Response to the Molecular Architecture of Mature N-Glycans. *Chem Biol* **2015,** *22* (10), 1301-12.

[19] Lee, A. H.; Iwakoshi, N. N.; Glimcher, L. H., XBP-1 regulates a subset of endoplasmic reticulum resident chaperone genes in the unfolded protein response. *Mol Cell Biol* **2003,** *23* (21), 7448-59.

[20] Lee, A. S., Glucose-regulated proteins in cancer: molecular mechanisms and therapeutic potential. *Nat Rev Cancer* **2014,** *14* (4), 263-76.

[21] Pilobello, K. T.; Slawek, D. E.; Mahal, L. K., A ratiometric lectin microarray approach to analysis of the dynamic mammalian glycome. *Proc Natl Acad Sci U S A* **2007,** *104* (28), 11534-9.

[22] Ribeiro, J. P.; Pau, W.; Pifferi, C.; Renaudet, O.; Varrot, A.; Mahal, L. K.; Imberty, A., Characterization of a high-affinity sialic acid-specific CBM40 from Clostridium perfringens and engineering of a divalent form. *Biochem J* **2016,** *473* (14), 2109-18.

[23] Fujitani, N.; Furukawa, J.; Araki, K.; Fujioka, T.; Takegawa, Y.; Piao, J.; Nishioka, T.; Tamura, T.; Nikaido, T.; Ito, M.; Nakamura, Y.; Shinohara, Y., Total cellular glycomics allows characterizing cells and streamlining the discovery process for cellular biomarkers. *Proc Natl Acad Sci U S A* **2013,** *110* (6), 2105-10.

[24] Agrawal, P.; Kurcon, T.; Pilobello, K. T.; Rakus, J. F.; Koppolu, S.; Liu, Z.; Batista, B. S.; Eng, W. S.; Hsu, K. L.; Liang, Y.; Mahal, L. K., Mapping posttranscriptional regulation of the human glycome uncovers microRNA defining the glycocode. *Proc Natl Acad Sci U S A* **2014,** *111* (11), 4338-43.

[25] Mori, T.; O'Keefe, B. R.; Sowder, R. C., 2nd; Bringans, S.; Gardella, R.; Berg, S.; Cochran, P.; Turpin, J. A.; Buckheit, R. W., Jr.; McMahon, J. B.; Boyd, M. R., Isolation and characterization of griffithsin, a novel HIV-inactivating protein, from the red alga Griffithsia sp. *J Biol Chem* **2005,** *280* (10), 9345-53.

[26] Moriwaki, K.; Miyoshi, E., Basic procedures for lectin flow cytometry. *Methods Mol Biol* **2014,** *1200*, 147-52.

[27] Kaku, H.; Van Damme, E. J.; Peumans, W. J.; Goldstein, I. J., Carbohydrate-binding specificity of the daffodil (Narcissus pseudonarcissus) and amaryllis (Hippeastrum hybr.) bulb lectins. *Arch Biochem Biophys* **1990,** *279* (2), 298-304.

[28] Mendoza, L.; Olaso, E.; Anasagasti, M. J.; Fuentes, A. M.; Vidal-Vanaclocha, F., Mannose receptor-mediated endothelial cell activation contributes to B16 melanoma cell adhesion and metastasis in liver. *J Cell Physiol* **1998,** *174* (3), 322-30.

[29] Batista, B. S.; Eng, W. S.; Pilobello, K. T.; Hendricks-Munoz, K. D.; Mahal, L. K., Identification of a conserved glycan signature for microvesicles. *J Proteome Res* **2011,** *10* (10), 4624-33.

[30] Morrison, C. J.; Easton, R. L.; Morris, H. R.; McMaster, W. R.; Piret, J. M.; Dell, A., Modification of a recombinant GPI-anchored metalloproteinase for secretion alters the protein glycosylation. *Biotechnol Bioeng* **2000,** *68* (4), 407-21.

[31] Monk, C. R.; Sutton-Smith, M.; Dell, A.; Garden, O. A., Preparation of CD25(+) and CD25(-) CD4(+) T cells for glycomic analysis--a cautionary tale of serum glycoprotein sequestration. *Glycobiology* **2006,** *16* (6), 11g-13g.

[32] Chen, Q.; Muller, J. S.; Pang, P. C.; Laval, S. H.; Haslam, S. M.; Lochmuller, H.; Dell, A., Global N-linked Glycosylation is Not Significantly Impaired in Myoblasts in Congenital Myasthenic Syndromes Caused by Defective Glutamine-Fructose-6-Phosphate Transaminase 1 (GFPT1). *Biomolecules* **2015,** *5* (4), 2758-81.

[33] Acosta-Alvear, D.; Zhou, Y.; Blais, A.; Tsikitis, M.; Lents, N. H.; Arias, C.; Lennon, C. J.; Kluger, Y.; Dynlacht, B. D., XBP1 controls diverse cell type- and condition-specific transcriptional regulatory networks. *Mol Cell* **2007,** *27* (1), 53-66.

[34] Dong, L.; Jiang, C. C.; Thorne, R. F.; Croft, A.; Yang, F.; Liu, H.; de Bock, C. E.; Hersey, P.; Zhang, X. D., Ets-1 mediates upregulation of Mcl-1 downstream of XBP-1 in human melanoma cells upon ER stress. *Oncogene* **2011,** *30* (34), 3716-26.

[35] Chen, H. L.; Li, C. F.; Grigorian, A.; Tian, W.; Demetriou, M., T cell receptor signaling co-regulates multiple Golgi genes to enhance N-glycan branching. *J Biol Chem* **2009,** *284* (47), 32454-61.

[36] Nairn, A. V.; York, W. S.; Harris, K.; Hall, E. M.; Pierce, J. M.; Moremen, K. W., Regulation of glycan structures in animal tissues: transcript profiling of glycan-related genes. *J Biol Chem* **2008,** *283* (25), 17298-313.

[37] Comelli, E. M.; Head, S. R.; Gilmartin, T.; Whisenant, T.; Haslam, S. M.; North, S. J.; Wong, N. K.; Kudo, T.; Narimatsu, H.; Esko, J. D.; Drickamer, K.; Dell, A.; Paulson, J. C., A focused microarray approach to functional glycomics: transcriptional regulation of the glycome. *Glycobiology* **2006,** *16* (2), 117-31.

[38] Narasimhan, S., Control of glycoprotein synthesis. UDP-GlcNAc:glycopeptide beta 4-N-acetylglucosaminyltransferase III, an enzyme in hen oviduct which adds GlcNAc in beta 1-4 linkage to the beta-linked mannose of the trimannosyl core of N-glycosyl oligosaccharides. *J Biol Chem* **1982,** *257* (17), 10235-42.

[39] Dennis, J. W.; Nabi, I. R.; Demetriou, M., Metabolism, cell surface organization, and disease. *Cell* **2009,** *139* (7), 1229-41.

[40] Broschat, K. O.; Gorka, C.; Page, J. D.; Martin-Berger, C. L.; Davies, M. S.; Huang Hc, H. C.; Gulve, E. A.; Salsgiver, W. J.; Kasten, T. P., Kinetic characterization of human glutamine-fructose-6-phosphate amidotransferase I: potent feedback inhibition by glucosamine 6-phosphate. *J Biol Chem* **2002,** *277* (17), 14764-70.

[41] Maszczak-Seneczko, D.; Sosicka, P.; Olczak, T.; Jakimowicz, P.; Majkowski, M.; Olczak, M., UDP-N-acetylglucosamine transporter (SLC35A3) regulates biosynthesis of highly branched N-glycans and keratan sulfate. *J Biol Chem* **2013,** *288* (30), 21850-60.

[42] Lau, K. S.; Partridge, E. A.; Grigorian, A.; Silvescu, C. I.; Reinhold, V. N.; Demetriou, M.; Dennis, J. W., Complex N-glycan number and degree of branching cooperate to regulate cell proliferation and differentiation. *Cell* **2007,** *129* (1), 123-34.

[43] Sassi, A.; Lazaroski, S.; Wu, G.; Haslam, S. M.; Fliegauf, M.; Mellouli, F.; Patiroglu, T.; Unal, E.; Ozdemir, M. A.; Jouhadi, Z.; Khadir, K.; Ben-Khemis, L.; Ben-Ali, M.; Ben-Mustapha, I.; Borchani, L.; Pfeifer, D.; Jakob, T.; Khemiri, M.; Asplund, A. C.; Gustafsson, M. O.; Lundin, K. E.; Falk-Sorqvist, E.; Moens, L. N.; Gungor, H. E.; Engelhardt, K. R.; Dziadzio, M.; Stauss, H.; Fleckenstein, B.; Meier, R.; Prayitno, K.; Maul-Pavicic, A.; Schaffer, S.; Rakhmanov, M.; Henneke, P.; Kraus, H.; Eibel, H.; Kolsch, U.; Nadifi, S.; Nilsson, M.; Bejaoui, M.; Schaffer, A. A.; Smith, C. I.; Dell, A.; Barbouche, M. R.; Grimbacher, B., Hypomorphic homozygous mutations in phosphoglucomutase 3 (PGM3) impair immunity and increase serum IgE levels. *J Allergy Clin Immunol* **2014,** *133* (5), 1410-9, 1419.e1-13.

[44] Itkonen, H. M.; Engedal, N.; Babaie, E.; Luhr, M.; Guldvik, I. J.; Minner, S.; Hohloch, J.; Tsourlakis, M. C.; Schlomm, T.; Mills, I. G., UAP1 is overexpressed in prostate cancer and is protective against inhibitors of N-linked glycosylation. *Oncogene* **2015,** *34* (28), 3744-50.

[45] Denzel, M. S.; Storm, N. J.; Gutschmidt, A.; Baddi, R.; Hinze, Y.; Jarosch, E.; Sommer, T.; Hoppe, T.; Antebi, A., Hexosamine pathway metabolites enhance protein quality control and prolong life. *Cell* **2014,** *156* (6), 1167-1178.

[46] Neelamegham, S.; Mahal, L. K., Multi-level regulation of cellular glycosylation: from genes to transcript to enzyme to structure. *Curr Opin Struct Biol* **2016,** *40*, 145-152.

[47] Nairn, A. V.; Aoki, K.; dela Rosa, M.; Porterfield, M.; Lim, J. M.; Kulik, M.; Pierce, J. M.; Wells, L.; Dalton, S.; Tiemeyer, M.; Moremen, K. W., Regulation of glycan structures in murine embryonic stem cells: combined transcript profiling of glycan-related genes and glycan structural analysis. *J Biol Chem* **2012,** *287* (45), 37835-56.

[48] Ohtsubo, K.; Chen, M. Z.; Olefsky, J. M.; Marth, J. D., Pathway to diabetes through attenuation of pancreatic beta cell glycosylation and glucose transport. *Nat Med* **2011,** *17* (9), 1067-75.

[49] Liang, Y.; Eng, W. S.; Colquhoun, D. R.; Dinglasan, R. R.; Graham, D. R.; Mahal, L. K., Complex N-linked glycans serve as a determinant for exosome/microvesicle cargo recruitment. *J Biol Chem* **2014,** *289* (47), 32526-37.

[50] Imanikia, S.; Sheng, M.; Taylor, R. C., Cell Non-autonomous UPR(ER) Signaling. *Curr Top Microbiol Immunol* **2018,** *414*, 27-43.

[51] Wellen, K. E.; Lu, C.; Mancuso, A.; Lemons, J. M.; Ryczko, M.; Dennis, J. W.; Rabinowitz, J. D.; Coller, H. A.; Thompson, C. B., The hexosamine biosynthetic pathway couples growth factor-induced glutamine uptake to glucose metabolism. *Genes Dev* **2010,** *24* (24), 2784-99.

[52] Gaziel-Sovran, A.; Segura, M. F.; Di Micco, R.; Collins, M. K.; Hanniford, D.; Vega-Saenz de Miera, E.; Rakus, J. F.; Dankert, J. F.; Shang, S.; Kerbel, R. S.; Bhardwaj, N.; Shao, Y.; Darvishian, F.; Zavadil, J.; Erlebacher, A.; Mahal, L. K.; Osman, I.; Hernando, E., miR-30b/30d regulation of GalNAc transferases enhances invasion and immunosuppression during metastasis. *Cancer Cell* **2011,** *20* (1), 104-18.

[53] Zhu, B.; Zhang, Q.; Pan, Y.; Mace, E. M.; York, B.; Antoulas, A. C.; Dacso, C. C.; O'Malley, B. W., A Cell-Autonomous Mammalian 12 hr Clock Coordinates Metabolic and Stress Rhythms. *Cell Metab* **2017,** *25* (6), 1305-1319.e9.

[54] Pilobello, K. T.; Agrawal, P.; Rouse, R.; Mahal, L. K., Advances in lectin microarray technology: optimized protocols for piezoelectric print conditions. *Curr Protoc Chem Biol* **2013,** *5* (1), 1-23.

[55] Jang-Lee, J.; North, S. J.; Sutton-Smith, M.; Goldberg, D.; Panico, M.; Morris, H.; Haslam, S.; Dell, A., Glycomic profiling of cells and tissues by mass spectrometry: fingerprinting and sequencing methodologies. *Methods Enzymol* **2006,** *415*, 59-86.

[56] Chen, C.; Constantinou, A.; Chester, K. A.; Vyas, B.; Canis, K.; Haslam, S. M.; Dell, A.; Epenetos, A. A.; Deonarain, M. P., Glycoengineering approach to half-life extension of recombinant biotherapeutics. *Bioconjug Chem* **2012,** *23* (8), 1524-33.

[57] Ceroni, A.; Maass, K.; Geyer, H.; Geyer, R.; Dell, A.; Haslam, S. M., GlycoWorkbench: a tool for the computer-assisted annotation of mass spectra of glycans. *J Proteome Res* **2008,** *7* (4), 1650-9.

[58] Rillahan, C. D.; Antonopoulos, A.; Lefort, C. T.; Sonon, R.; Azadi, P.; Ley, K.; Dell, A.; Haslam, S. M.; Paulson, J. C., Global metabolic inhibitors of sialyl- and fucosyltransferases remodel the glycome. *Nat Chem Biol* **2012,** *8* (7), 661-8.

[59] Langmead, B.; Trapnell, C.; Pop, M.; Salzberg, S. L., Ultrafast and memory-efficient alignment of short DNA sequences to the human genome. *Genome Biol* **2009,** *10* (3), R25.

[60] Li, B.; Dewey, C. N., RSEM: accurate transcript quantification from RNA-Seq data with or without a reference genome. *BMC Bioinformatics* **2011,** *12*, 323.

[61] Love, M. I.; Huber, W.; Anders, S., Moderated estimation of fold change and dispersion for RNA-seq data with DESeq2. *Genome Biol* **2014,** *15* (12), 550.

[62] Subramanian, A.; Tamayo, P.; Mootha, V. K.; Mukherjee, S.; Ebert, B. L.; Gillette, M. A.; Paulovich, A.; Pomeroy, S. L.; Golub, T. R.; Lander, E. S.; Mesirov, J. P., Gene set enrichment analysis: a knowledge-based approach for interpreting genome-wide expression profiles. *Proc Natl Acad Sci U S A* **2005,** *102* (43), 15545-50.

[63] Park, S. K.; Venable, J. D.; Xu, T.; Yates, J. R., 3rd, A quantitative analysis software tool for mass spectrometry-based proteomics. *Nat Methods* **2008,** *5* (4), 319-22.

[64] Freeze, H. H.; Elbein, A. D., Glycosylation Precursors. In *Essentials of Glycobiology*, 3 ed.; Varki, A.; Cummings, R. D.; Esko, J. D.; Stanley, P.; Hart, G. W.; Aebi, M.; Darvill, A. G.; Kinoshita, T.; Packer, N. H.; Prestegard, J. H.; Schnaar, R. L.; Seeberger, P. H., Eds. Cold Spring Harbor Laboratory Press: Cold Spring Harbor (NY), 2017.

Chapter 3

IRE1 Inhibition Leads to Modest Effects on the Triple-Negative Breast Cancer Glycome

Summary

Upregulation of the unfolded protein response is a common feature of cancer cells. Pro-survival pathways within the unfolded protein response, and the XBP1s transcription factor in particular, have been shown to promote breast cancer progression through a variety of mechanisms, including enhancing proteostasis and forming XBP1s–HIF1α or XBP1s–Myc transcriptional complexes. Aberrant glycosylation, such as hypersialylation, has also been implicated in breast cancer tumorigenesis. We aimed to determine whether XBP1s mechanistically links endoplasmic reticulum proteostasis and glycosylation phenotypes associated with triple-negative breast cancer. Here, we inhibited formation of endogenous XBP1s in breast cancer cell lines by direct inhibition of the IRE1 endoribonuclease responsible for generating the active, spliced variant of *XBP1*. Furthermore, we analyzed the glycomic profile of triple-negative breast cancer cell lines and compared them to luminal (non–triple-negative) breast cancer cell lines. We found that certain glycosylation features were shared among the triple-negative breast cancer cell lines, and that IRE1 inhibition can lead to modest, cell line-dependent changes to the glycome.

Author List

Kenny Chen, Shuhui Chen, Aristotelis Antonopoulos, Vincent L. Butty, Anne Dell, Stuart M. Haslam, Lara K. Mahal, and Matthew D. Shoulders.

Author Contributions

K.C., S.C., A.A., A.D., S.M.H., L.K.M., and M.D.S. designed experiments; K.C., S.C., and A.A. performed research; K.C., S.C., A.A., V.L.B., A.D., S.M.H., L.K.M., and M.D.S. analyzed data; and K.C., V.L.B., and M.D.S. wrote the paper.

Introduction

Cancers are heterogeneous diseases resulting from the multistep process of malignant transformation, in which cells accumulate mutations[1-4] that engender the development of tumorigenic features collectively referred to as the Hallmarks of Cancer.[5-6] While several of the described hallmarks, including evading growth suppressors and resisting cell death, are long-recognized, reprogramming energy metabolism and escaping immune destruction are more recent additions to the collection of hallmarks.[6] Consistent with our continually expanding knowledge of cancer, additional features have been proposed as emerging hallmarks of cancer, including endoplasmic reticulum (ER) stress, DNA replication stress, protein glycosylation, and circadian regulation.[7-12]

Breast cancer is one of the leading types of cancer,[13] with the triple-negative breast cancer (TNBC) subtype being particularly difficult to treat due to the lack of the estrogen and progesterone receptors and the absence of HER2 (also referred to as Neu/ErbB-2), a member of the epidermal growth factor receptor (EGFR) family. About 10% of all breast cancer cases in the United States are classified as TNBC.[14] While treatment advances for other breast cancer subtypes have led to therapies such as the blockbuster monoclonal antibody trastuzumab (Herceptin) targeting HER2, less than 20% of invasive breast cancers are positive for HER2. Thus, existing cancer treatments are limited to certain patient populations. TNBC patients receive poorer prognoses, and advances in treating TNBC have lagged behind those of other subtypes due to difficulty in developing targeted therapies.[15] With advances in immuno-oncology, efforts have turned to immune checkpoint inhibition for treating TNBC, and have resulted in the first FDA approval of immunotherapy for any type of breast cancer in 2019. The monoclonal antibody atezolizumab (Tecentriq) was approved to target PD-L1 in advanced TNBC, used in combination with the microtubule inhibitor paclitaxel.[16-17] However, the combination of atezolizumab and paclitaxel was reported to have at best a 10.3% complete response rate in patients.[17] A better understanding of breast cancer and its molecular signatures is needed to develop more effective therapies.

Advances in genomics have led to the mapping of all known breast cancer susceptibility regions and identification of genetic variants likely to be causal targets,[18] revealing target genes overrepresented in DNA integrity and immune system pathways, including TRAIL signaling and NF-κB signaling as novel pathways. Predicted target genes also include known cancer drivers and transcription factors, including *FGFR2*, *GATA3*, *MAP3K1*, *MYC*, and *XBP1*.[18-19] The spliced variant of the XBP1 transcription factor (henceforth denoted as XBP1s) has been shown to promote TNBC by assembling transcriptional complexes with HIF1α to regulate expression of hypoxia target genes, and with Myc to enhance XBP1s transcriptional activity to resolve proteotoxic stress.[20-21] Furthermore, XBP1s signaling was shown to contribute to the angiogenic switch in TNBC through HIF1α and by remodeling the tumor microenvironment, including the composition of pericytes, cancer-associated fibroblasts, and myeloid-derived suppressor cells.[20, 22] These

studies suggest that TNBC reliance on XBP1s may be a promising vulnerability to exploit in combination with anti-angiogenic therapies. XBP1s is also involved in the progression of several other cancers, including multiple myeloma, prostate cancer, and colon cancer.[23-25]

The dependence on XBP1s in various cancers is unsurprising given its prominent role in the unfolded protein response (UPR)[26] and in a myriad of diverse biological processes regulating cellular and organism homeostasis, including immunity and pain, memory formation, circadian regulation, and even food perception.[27-35] As a key player in the UPR, XBP1s can upregulate the expression of chaperone proteins to mitigate ER stress induced by accumulation of misfolded proteins, thus acting in a pro-survival manner. The rapid cell division and protein synthesis mandated by cancer cells would suggest that co-opting the UPR is one mechanism cancers use for survival, a hypothesis consistent with the finding that the UPR is upregulated in many cancers.[36] The various roles of XBP1s in biology have led to great interest in understanding the molecular mechanisms underlying the effects of XBP1s in disease.

We previously showed that, in addition to upregulating the expression of chaperone proteins, XBP1s is also capable of remodeling the expression of glycosylation-related genes (glycogenes), such as *MGAT3* which encodes a GlcNAc transferase, and for mediating shifts in *N*-glycosylation patterns when profiled in HEK293 and HeLa cells (**Chapter 2**).[37] Glycosylation is one of the most common post-translational modifications, and it modulates numerous biological processes including immunity and tumorigenesis by modifying the activity and function of proteins with sugars.[10, 38] Many aspects of biology are regulated by both XBP1s and glycosylation, leading to our hypothesis that perhaps ER proteostasis and protein glycosylation are linked in cancer, and that XBP1s sits at a critical node that regulates responses to ER stress and aberrant glycosylation patterns in cancer (**Figure 3.1*A***). In prior work, we employed stress-independent activation of XBP1s using engineered cell lines with tetracycline-inducible expression of XBP1s to show that XBP1s plays a role in *N*-glycan structural remodeling.[37, 39-40] In this current study, we sought to ask whether we could detect changes to the breast cancer glycome by inhibiting formation of endogenous XBP1s. Because TNBC cells were previously shown to feature heightened expression of XBP1s compared to luminal (non–triple-negative) breast cancer cell lines,[20] we were motivated to investigate whether constitutive expression of XBP1s in TNBCs could be responsible for malignant glycosylation signatures associated with TNBC.

We hypothesized that small molecule-mediated inhibition of IRE1 in TNBC cells featuring constitutive XBP1s activation could alter the expression of glycosylation signatures associated with malignancy. We blocked XBP1s formation by treating cells with 4μ8C,[41] an inhibitor of the IRE1 endoribonuclease that sits upstream of XBP1s and is responsible for splicing *XBP1* mRNA to generate the active, spliced variant (**Figure 3.1 *A*** and ***B***).[42-44] In addition to 4μ8C, other IRE1 inhibitors include compounds that allosterically inhibit the IRE1 RNase domain.[45] However, because these compounds

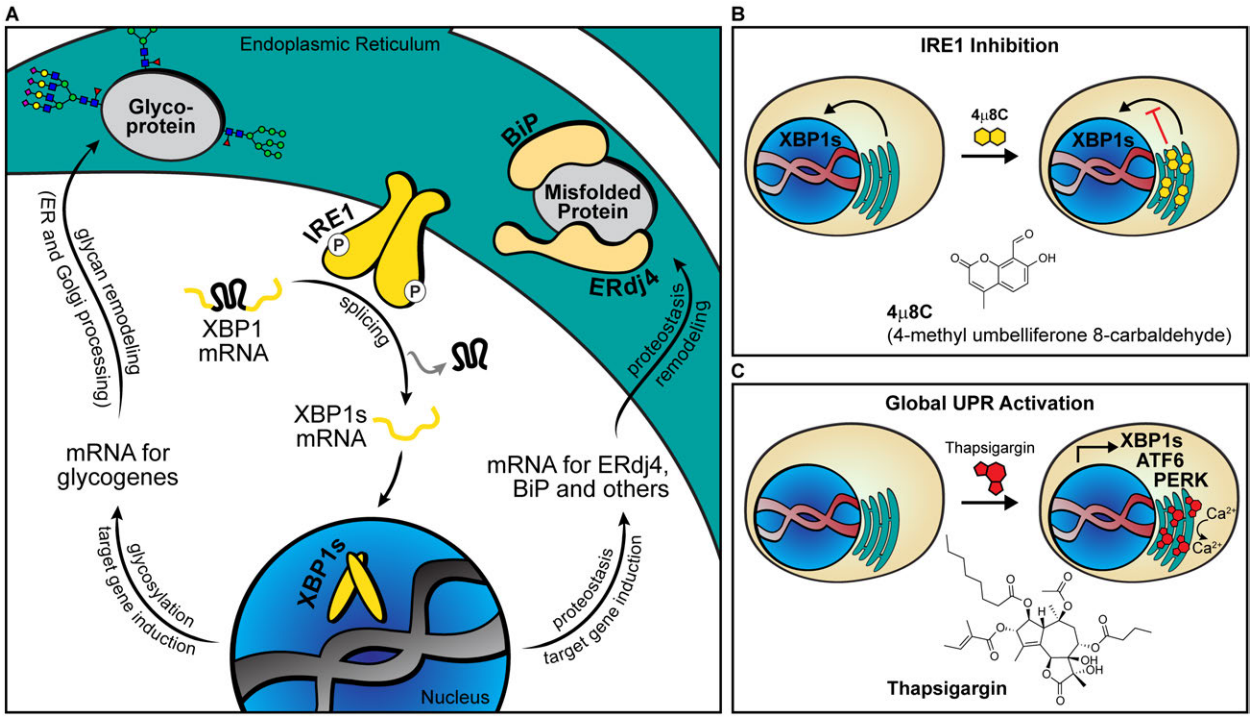

Figure 3.1: XBP1s bridges the unfolded protein response and glycosylation. ***A***: The RNase domain of IRE1 removes a 26-nucleotide intron from *XBP1* mRNA, leading to formation of the active transcription factor XBP1s. XBP1s upregulates proteostasis regulators such as the BiP Hsp70 chaperone and the ERdj4 Hsp40 co-chaperone. Additionally, XBP1s can remodel glycogene expression and alter the glycans displayed on proteins. Thus, we propose that XBP1s is a critical node bridging ER stress responses and aberrant glycosylation features in cancer. ***B***: Pharmacologic inhibition of IRE1 by the small molecule 4μ8C prevents *XBP1* splicing. ***C***: ER stress and activation of the three branches of the UPR (IRE1-XBP1s, ATF6, and PERK-ATF4) can be induced by the Ca^{2+} ATPase inhibitor thapsigargin.

allosterically modulate IRE1, it is possible that inhibition is only partial. Moreover, these compounds can exhibit off-target inhibition of the receptor tyrosine kinase c-KIT at concentrations that overlap with IRE1 inhibition.[46] 4μ8C is one of the most well-characterized and utilized IRE1 inhibitors,[27, 41, 47-55] and although it features an aldehyde moiety that could lead to potential off-target activity, the inhibitor was shown to be particularly selective for IRE1 due to its reactivity towards a lysine in the RNase domain, forming a particularly stable Schiff base that is protected due to solvent inaccessibility of the resulting imine bond.[41] We treated cells with 4μ8C and employed a combination of lectin microarrays and mass spectrometry to profile the breast cancer glycome.[56-57] We observed that across 6 breast cancer cell lines (3 TNBC and 3 non-TNBC), TNBC cells exhibited less fucosylation, more α2,3 sialylation, and more bisected *N*-glycans. Furthermore, IRE1 inhibition led to modest, cell line-dependent changes in fucosylation and sialylation phenotypes.

Results

TNBC Cells Exhibit Heightened XBP1 Splicing

We decided to take advantage of differential *XBP1* splicing across breast cancer subtypes to test whether blocking endogenous XBP1s formation is sufficient to drive changes in glycosylation. Prior work has shown that TNBC cell lines exhibit increased levels of *XBP1* splicing compared to luminal, non-TNBC cell lines, and that XBP1s is responsible for driving tumorigenicity by cooperating with HIF1α.[20] Specifically, when surveyed by RT-PCR, the TNBC cell lines HCC1937, MDA-MB-231, SUM149PT, Hs 578T, MDA-MB-436, and MDA-MB-157 were found to have enhanced *XBP1* splicing compared to the luminal breast cancer cell lines MCF7, ZR-75-1, T-47D, and BT-474. We leveraged the clear distinction in *XBP1* splicing between the TNBC and non-TNBC cell lines by pairing this cellular model with direct, small molecule-mediated inhibition of IRE1 with 4μ8C.[41] We employed a pharmacological approach in favor of a genetic approach to avoid potential cytotoxicity associated with transfection or transduction, and for tighter temporal control and dosability associated with direct inhibition.[58] Furthermore, IRE1 inhibitors including 4μ8C have been successfully applied to elucidate novel biology, including demonstrating that XBP1s drives natural killer (NK) cell responses against infections and cancer cells.[27, 47]

We characterized three TNBC (HCC1937, MDA-MB-231, Hs 578T) and three non-TNBC (MCF7, ZR-75-1, T-47D) cell lines by immunoblotting nuclear lysates for XBP1s (**Figure 3.2*A***) and by performing qRT-PCR (**Figure 3.2 *B*** and ***C***). Consistent with prior RT-PCR results demonstrating that TNBC cell lines have enhanced *XBP1* splicing,[20] our survey of TNBC cell lines shows enhanced levels of XBP1s relative to total XBP1 at both the protein and RNA levels (**Figure 3.2**). We observed that by immunoblot, the ZR-75-1 non-TNBC cell line did feature XBP1s levels comparable to the TNBC cell lines (**Figure 3.2*A***, *Left*). At the RNA level, the relative amount of splicing (spliced *XBP1* divided by total *XBP1*) in ZR-75-1 was comparable to the other non-TNBC cell lines (**Figure 3.2*B***). It is possible that the high levels of unspliced XBP1 (XBP1u) in ZR-75-1 cells interact with XBP1s, keeping it in an inactive state (**Figure 3.2*A***, *Left*).[44, 59-60] Positive controls included upregulation of XBP1s upon treatment with the global ER stressor, thapsigargin (Tg; **Figure 3.1*C***) in HEK293 and MCF7 cells. With this cellular model of ER stress for breast cancer in hand, we next sought to block XBP1s formation with direct inhibition of IRE1.

Direct Inhibition of IRE1 Disrupts Formation of XBP1s

To determine the appropriate concentration of 4μ8C to use for inhibiting XBP1s formation, we performed a dose-response from 1–32 μM of 4μ8C in the MDA-MB-231 and Hs 578T cell lines (**Figure 3.3*A***). We had previously determined that a similar range of 4μ8C concentrations was sufficient to block XBP1s activation induced by thapsigargin treatment in the MCF7 cell line.[55] We used qRT-PCR to

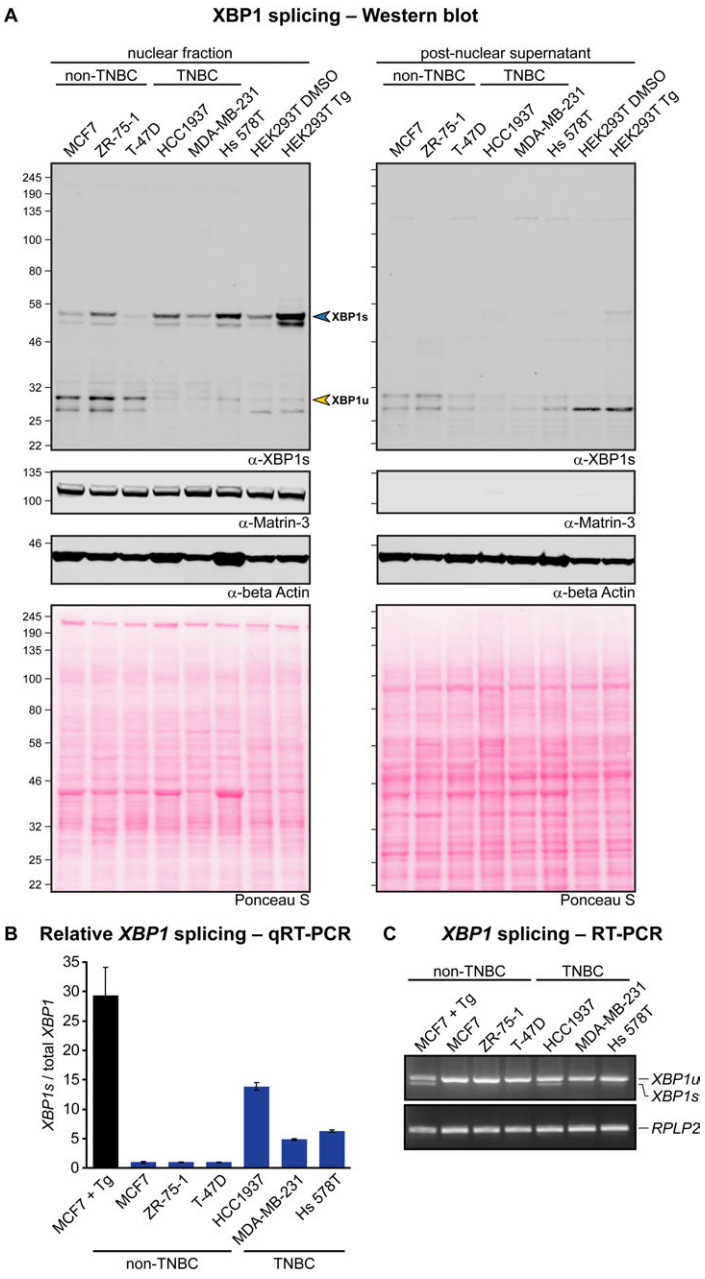

Figure 3.2: *XBP1* splicing is enhanced in TNBC cells compared to luminal (non-TNBC) cells. ***A***: XBP1s and XBP1u expression were profiled across six breast cancer cell lines by Western blot. Protein from thapsigargin-treated HEK293 cells (750 nM, 8 hours) was included as positive control for XBP1s activation. XBP1s was enriched in nuclear protein fractions and largely absent in the cytosolic fraction (post-nuclear supernatant, *Right*). XBP1u expression was markedly down in nuclear fractions from TNBC cell lines. Matrin-3 served as a nuclear protein marker. β-actin localization was high in both the cytosol and nucleus. Ponceau S staining was performed on nitrocellulose membranes prior to Western blotting to demonstrate even sample loading and protein transfer. 15 μg of protein was loaded for each sample. Similar results were obtained from Western blots repeated a total of three times, including two independent biological replicates. ***B***: *XBP1* splicing was profiled using quantitative real-time PCR (qRT-PCR) with primers designed to distinguish spliced *XBP1* from total *XBP1*. Data were normalized to the *RPLP2* housekeeping gene and reported as the average of three biological replicates (n = 3), with each reaction performed in technical triplicate. RNA from thapsigargin-treated MCF7 cells (5 μM, 3 hours) was included as positive control for *XBP1* splicing. Error bars: standard deviation of three biological replicates. 360 ng of input RNA was used for qRT-PCR. ***C***: After amplification of total *XBP1* from (*B*), qPCR products were separated on a 2% agarose gel to visualize *XBP1* splicing.

determine that 8 μM of 4μ8C reduced *XBP1* splicing in these two TNBC cell lines to levels comparable with MCF7 and T-47D without IRE1 inhibition. Furthermore, when we performed qRT-PCR to quantify mRNA expression of the XBP1s target ERdj4, we observed downregulation at all concentrations tested (**Figure 3.3*B***). In XBP1s immunoblots, 8 μM of 4μ8C was sufficient to block XBP1s formation in all the cell lines (**Figure 3.3*C***). We observed that, while 4μ8C effectively prevents *XBP1* splicing, it does not appear to lead to accumulation of unspliced XBP1 at these concentrations, likely due to rapid degradation of this unstable variant.[44, 59-60] Additionally, we observed that treatment with thapsigargin led to enhanced

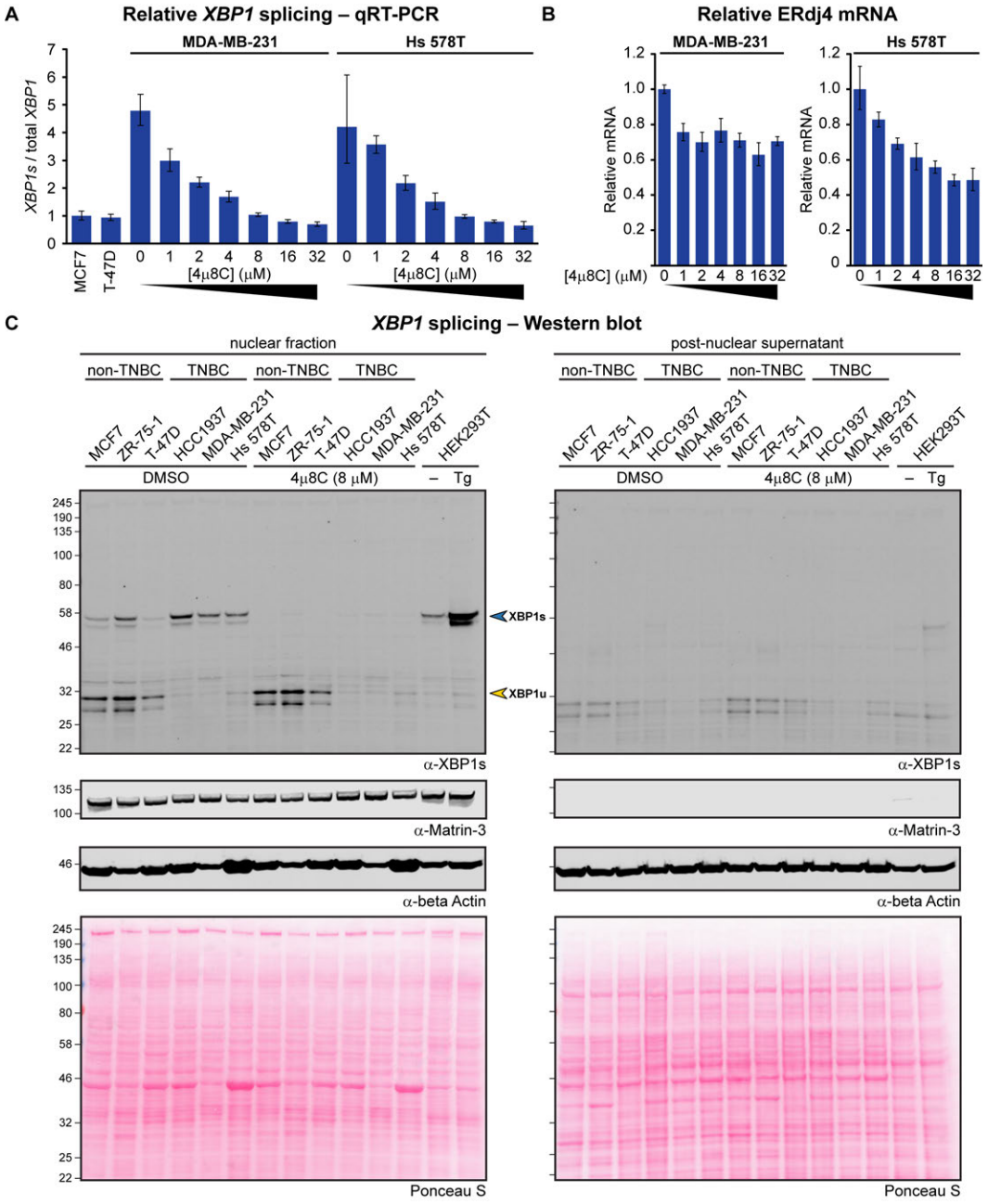

Figure 3.3: 4μ8C inhibits IRE1-mediated *XBP1* splicing in a dose-dependent manner. ***A***: Breast cancer cells were treated with 4μ8C over 2 days with daily compound renewal. A concentration of 8 μM was chosen to inhibit *XBP1* splicing in TNBC cells to levels comparable to MCF7 and T-47D cells under basal proteostasis conditions. ***B***: Relative mRNA expression of the XBP1s target ERdj4 was profiled in MDA-MB-231 and Hs 578T cells. Data were normalized to the *RPLP2* housekeeping gene and reported as the average of three technical replicates. Error bars: standard deviation of three technical replicates. 900 ng of input RNA was used for qRT-PCR. ***C***: Western blot for XBP1s shows that 4μ8C treatment (8 μM) over three days with daily compound renewal blocked XBP1s activation in breast cancer cells. Protein from thapsigargin-treated HEK293 cells (750 nM, 8 hours) was included for positive control. 15 μg of protein were loaded for each sample. Similar results were obtained when Western blots were repeated a total of three times.

XBP1 splicing in all cell lines tested, and that pre-treatment with 4μ8C reduced thapsigargin-induced splicing (**Figure 3.4*A***). Treatment with thapsigargin also led to induction of mRNA for UPR targets ERdj4, BiP, Grp94, and CHOP (**Figure 3.4 *B*–*E***). Notably, we observed that thapsigargin-induced expression of mRNA for ERdj4 was consistently reduced upon pre-treatment with 4μ8C in all cell lines, but mRNA for BiP, Grp94, and CHOP were not consistently reduced with 4μ8C, suggesting that the inhibitor is specific for the IRE1-XBP1s branch of the UPR. BiP, Grp94, and CHOP are targets of XBP1s/ATF6, ATF6, and PERK-ATF4, respectively.[39, 61-64] We did not observe induced expression of mRNA for the ER stress markers Grp94 and CHOP in cells treated with 4μ8C alone (**Figure 3.4 *D*** and ***E***), indicating that selective IRE1 inhibition with 4μ8C does not cause ER stress at the concentration used in this study.

GSEA of TNBC Cells Reveals Enrichment of EMT, Hypoxia, Angiogenesis, and UPR genes

To characterize the transcriptome of our cells, we performed RNA-seq and gene set enrichment analysis (GSEA) with samples in biological quadruplicate. We were able to recapitulate known TNBC signatures in our data set, including positive enrichment in genes involved in the epithelial–mesenchymal transition (EMT), hypoxia, and angiogenesis (**Figure 3.5**).[20, 65-68] We also observed negative enrichment in genes involved in the response to estrogen, consistent with the loss of the estrogen receptor in TNBC (**Figure 3.5*B***). Additionally, we found that the UPR gene set is positively enriched in our TNBC group, supporting the notion of ER stress as an emerging cancer hallmark.[7] When we analyzed gene sets involved in protein glycosylation, we did not observe statistically significant changes (i.e. FDR q-value < 0.10). For example, the *N*-glycan processing gene set was enriched in the positive direction, but without reaching the significance threshold (**Figure 3.5*B***). The lack of significant changes to entire gene sets relating to glycosylation is consistent with our previous finding that XBP1s activation does not globally alter transcripts involved in *N*-glycan maturation,[37] but rather XBP1s is likely to affect specific subsets of glycosylation genes.

GSEA of IRE1-Inhibited Cells Reveals Changes in Glycosylation, Proteostasis, and Translation Genes

We questioned whether the heterogeneity across cell lines could have contributed to the lack of a clear glycosylation signature in the GSEA comparing TNBC vs non-TNBC cells. To gain insight into how IRE1 inhibition affected glycosylation, and more generally what effects 4μ8C had on each cell line, we next performed GSEA comparing 4μ8C treatment vs DMSO treatment in individual cell lines. We observed that, among the positively enriched gene sets, those relating to the ribosome and protein translation were enriched (**Figure 3.6**). When we focused on the genes sets negatively enriched upon 4μ8C treatment, we observed that processes relating to sugar metabolism (glucose, monosaccharide, and hexose catabolism),

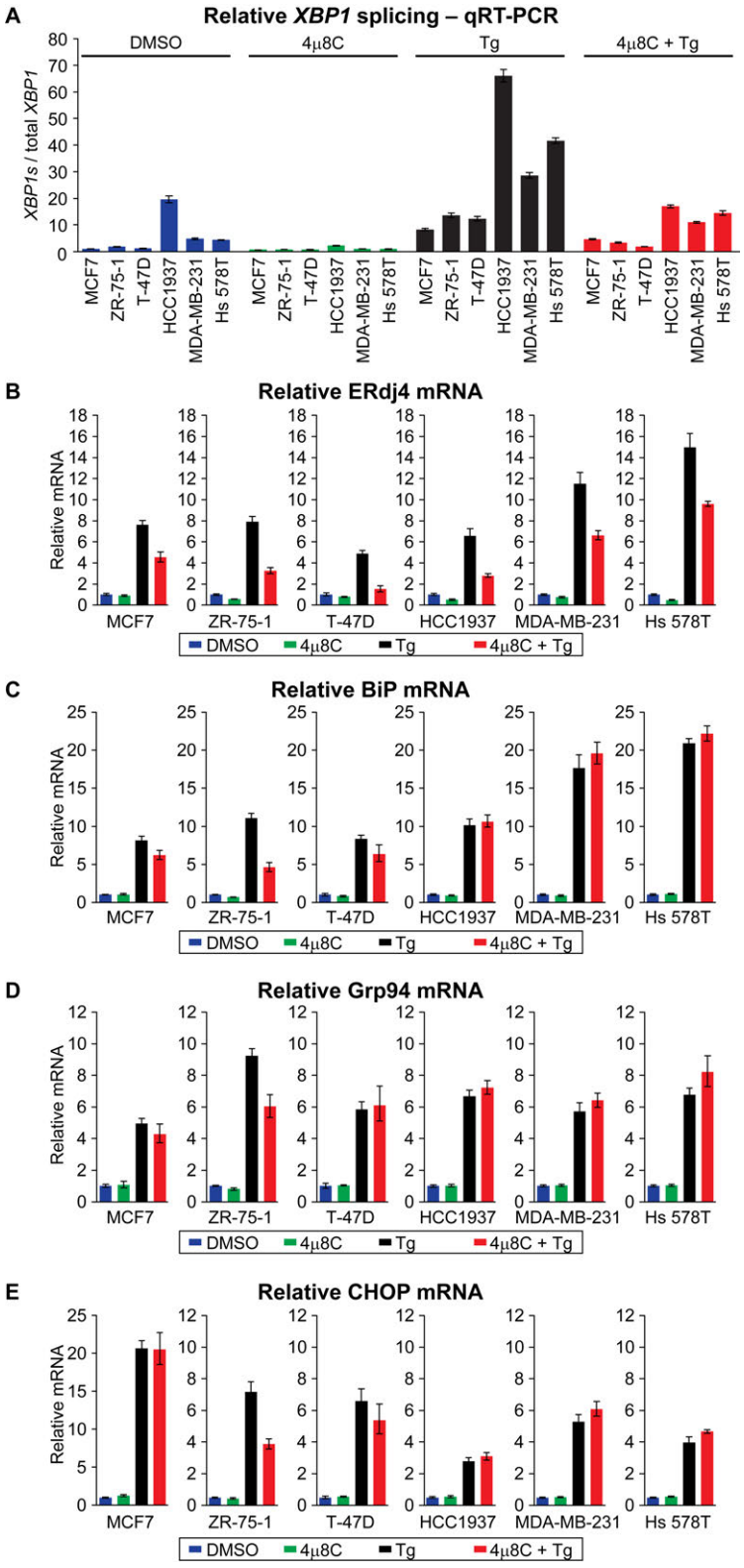

Figure 3.4: IRE1 inhibition with 4μ8C diminishes *XBP1* splicing across breast cancer cell lines, but does not induce ER stress. ***A***: *XBP1* splicing was assayed by qRT-PCR in breast cancer cell lines that were treated with DMSO, 4μ8C (8 μM, 3 days), thapsigargin (750 nM, 1 day), or pre-treated with 4μ8C (2 days) prior to co-treatment with thapsigargin for 1 day. ***B***–***E***: Expression of mRNA for UPR targets ERdj4, BiP, Grp94, and CHOP was assayed by qRT-PCR. Pre-treating cells with 4μ8C reduced thapsigargin-induced expression of mRNA for ERdj4 (a target of XBP1s), but thapsigargin-induced expression of mRNA for BiP (a target of XBP1s and ATF6), Grp94 (a target of ATF6), and CHOP (a target of PERK-ATF4) was not greatly impacted by 4μ8C pre-treatment. 4μ8C treatment alone does not induced ER stress, indicated by the lack of Grp94 or CHOP mRNA expression. Data were normalized to the *RPLP2* housekeeping gene and reported as the average of three biological replicates. Error bars: standard deviation of three biological replicates. 1000 ng of input RNA was used for qRT-PCR.

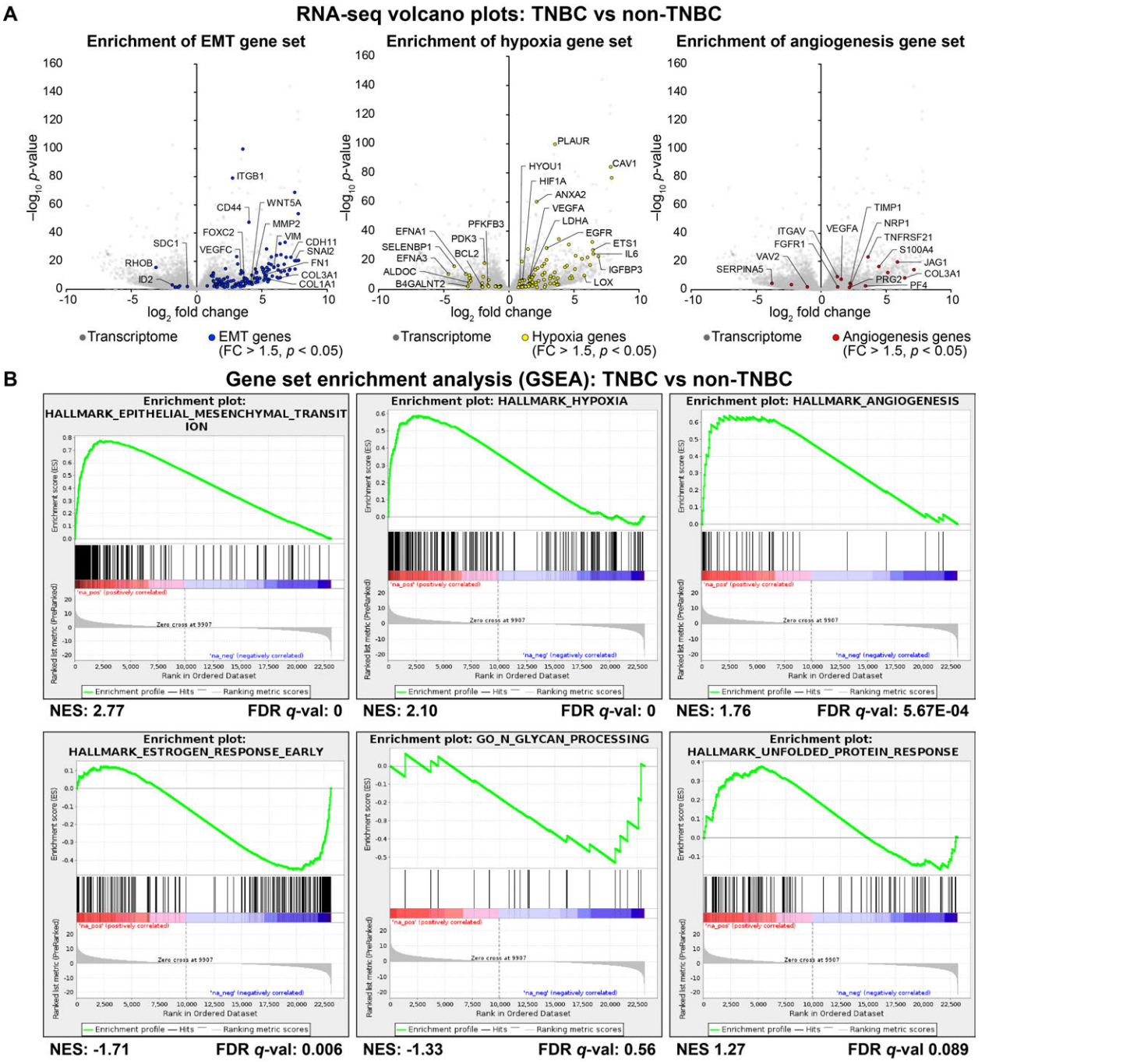

Figure 3.5: RNA-seq transcriptomics of the six breast cancer cell lines recapitulates known TNBC signatures. ***A***: Volcano plots showing the enrichment of genes involved in EMT, hypoxia, and angiogenesis in TNBC cells compared to luminal (non-TNBC) cells. Grey dots represent the transcriptome, and colored dots indicate differentially expressed genes (fold change > 1.5, *p*-value < 0.05). Select genes from each gene set are labeled. ***B***: Gene set enrichment analysis (GSEA) comparing TNBC vs non-TNBC cells. TNBC cells exhibited positive enrichment of genes involved in EMT, hypoxia, and angiogenesis, in addition to the UPR. Genes involved in the response to estrogen were negatively enriched, as were genes involved in *N*-glycan processing, although the latter did not reach statistical significance.

N-glycosylation, IRE1-mediated UPR, and endoplasmic reticulum–associated degradation (ERAD) were among those present. While the normalized enrichment scores (NES) did not reach statistical significance in all cases, the results suggested that IRE1 inhibition could negatively regulate *N*-glycosylation and sugar metabolism, which may affect the availability of glycan building blocks (**Figure 3.6**).

Of particular note, within the HCC1937 cell line, the most negatively enriched gene ontology terms were protein *N*-linked glycosylation (NES: -2.12; FDR *q*-val: 0.0042) and IRE1-mediated unfolded protein response (NES: -2.08; FDR *q*-val: 0.0047), suggesting that XBP1s may be important for regulating both

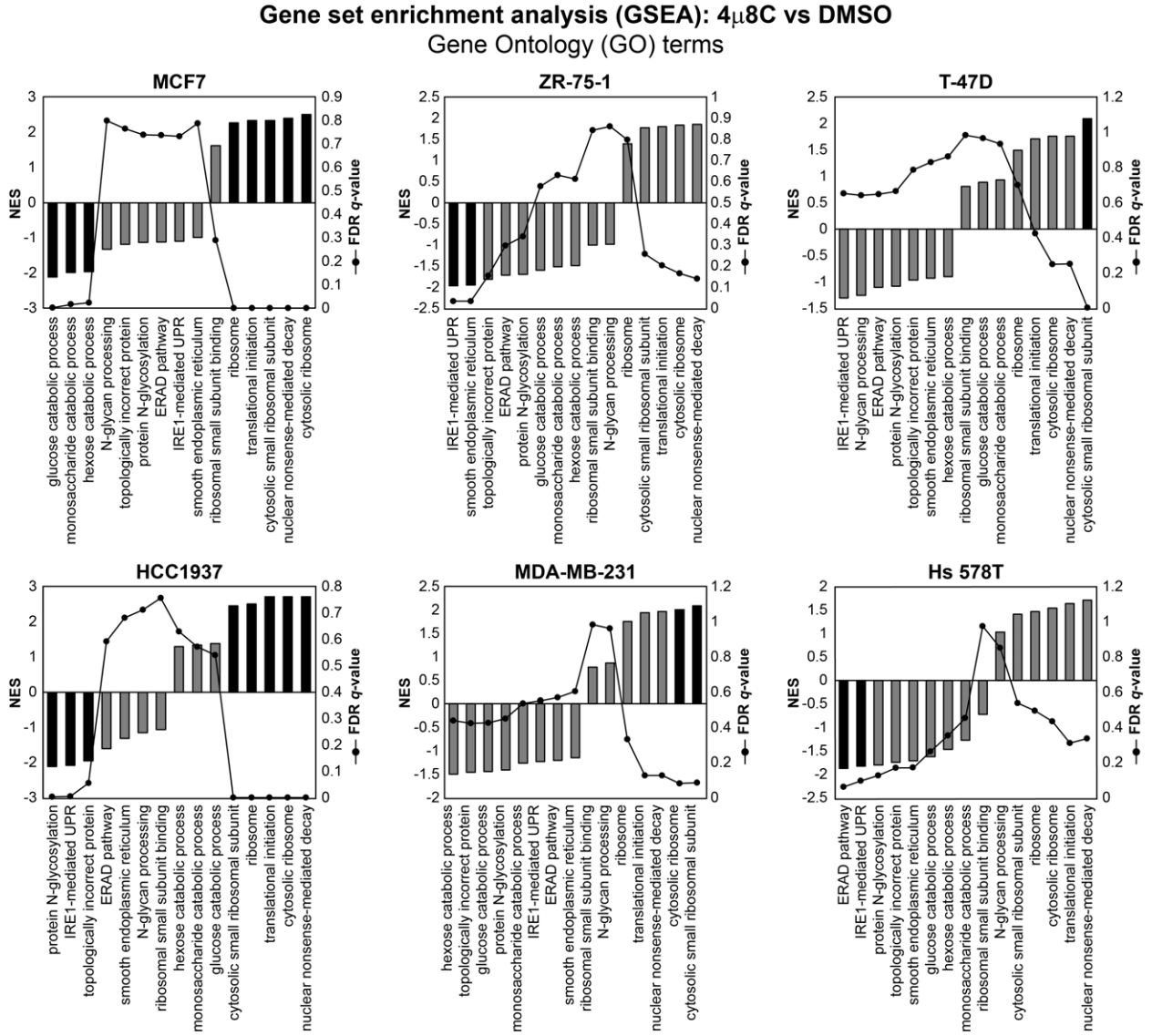

Figure 3.6: GSEA of individual breast cancer cell lines treated with 4μ8C vs DMSO. Select gene ontology (GO) terms were plotted with normalized enrichment score (NES) indicated by bars, and false discovery rate (FDR) *q*-values indicated by lines. NES scores with associated FDR *q*-values < 0.10 are shown as black bars. Among the GO terms positively enriched upon 4μ8C treatment were those associated with protein translation and the ribosome. Several cell lines showed negative enrichment of GO terms relating to sugar metabolism, the unfolded protein response, and *N*-glycosylation when treated with 4μ8C.

processes in this cell line, supporting our hypothesis that direct inhibition of IRE1 may lead to changes in glycogene expression.

Lectin Microarray Glycomics of Breast Cancer Cells Reveal Glycosylation Signatures

Motivated by these GSEA data, we next performed glycomics of our breast cancer cell lines with or without IRE1 inhibition to determine whether these changes in glycogene expression and sugar metabolism could lead to changes in the breast cancer glycome. We profiled the membrane proteins of the six breast cancer cell lines using lectin microarrays,[56] leveraging the carbohydrate-binding specificities of several dozen different lectins (**Figure 3.7**). A comparison between the TNBC and non-TNBC cell lines showed that TNBC membrane proteins were enriched in α2,3-sialic acid and bisecting GlcNAc, indicated by greater binding to the SLBR family of lectins and diCBM40 for the former, and to PHA-E lectins for the latter. Additionally, we observed that the membranes from TNBC cells displayed less binding to AAL, AOL, and TJA-II lectins, indicating less fucosylated glycans compared to non-TNBC samples. Prior studies have shown that breast cancer metastases are enriched in α2,3-sialic acid compared to their primary tumors, and in particular that the MDA-MB-231 cell line stained heavily for α2,3 sialic acid.[69] Additionally, triple-negative breast cancers were found to display high expression of *MGAT3,* a gene that encodes the GlcNAc transferase that attaches bisecting GlcNAc.[70] Although overexpression of fucosyltransferases has been shown to enhance breast cancer progression by modulating cell-surface proteins and signaling pathways,[71] we observed a decrease in general fucosylation in our TNBC cells. In melanoma, loss of α1,2 fucosylation promotes invasiveness,[72] but it is unknown if this would also be the case for triple-negative breast cancer.

IRE1 Inhibition in TNBC Cells Leads to Modest Changes in the Breast Cancer Glycome

Next, we sought to determine whether IRE1 inhibition was sufficient to alter the TNBC glycosylation signatures we observed. We analyzed the membrane proteome from each of the six cell lines with or without IRE1 inhibition after 3 days (**Figure 3.8**). Most of the changes to lectin binding were modest, with *p*-values > 0.05 in most cases. However, the shifts in lectin binding were generally consistent across binding preferences (i.e. multiple lectins binding to the same types of glycans moved together in the same direction), suggesting a consistent effect despite the small effect sizes.

One of the stronger signatures we observed was in the MDA-MB-231 cell line, where treatment with 4μ8C over 3 days led to a significant increase in binding to the AOL lectin, which binds to fucosylated glycans (fold change: 2.60; *p*-value: 0.040) (**Figure 3.8**). Additionally, although not reaching the *p*-value cut-off, binding to the AAL lectin, another fucose binder, was found to be increased upon 4μ8C treatment

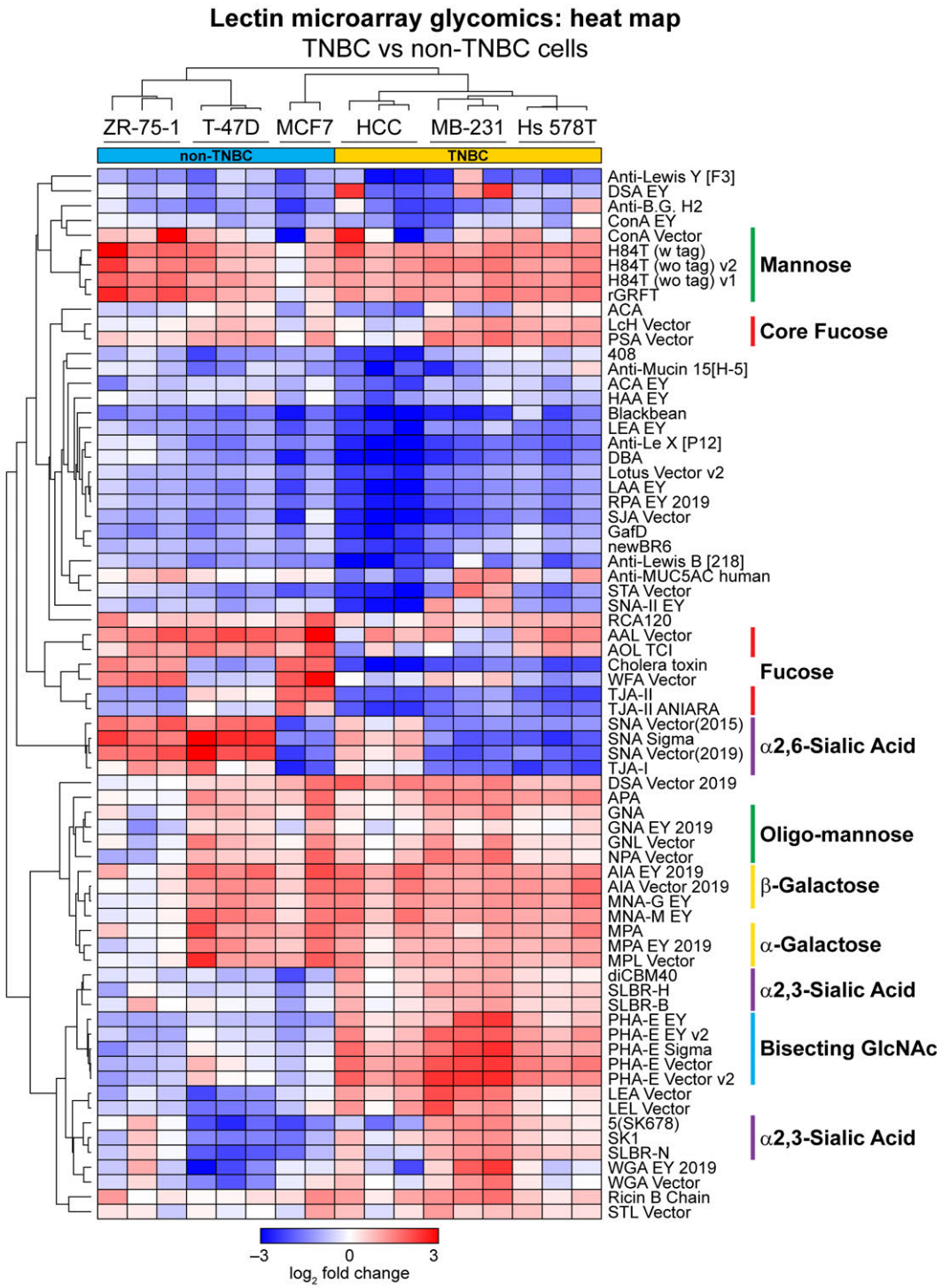

Figure 3.7: Lectin microarray analysis of TNBC cells vs luminal (non-TNBC) cells. ***A***: Heat map of data generated from lectin microarray analysis of membranes isolated from cells at basal proteostasis conditions. TNBC cell lines displayed less general fucose compared to non-TNBC cells lines (indicated by less binding to the lectins TJA-II, AAL, and AOL), more α2,3-sialic acid (indicated by binding to the lectins SLBR-N/H/B, SK1, 5(SK678), and diCBM40), and more bisected GlcNAc glycans (indicated by binding to several sources of the PHA-E lectin). Color intensity represents normalized $\log_2$ ratio data relative to a pooled sample reference. Each column represents one biological replicate of the indicated sample. Select lectin groups with shared binding specificities are annotated (*Right*).

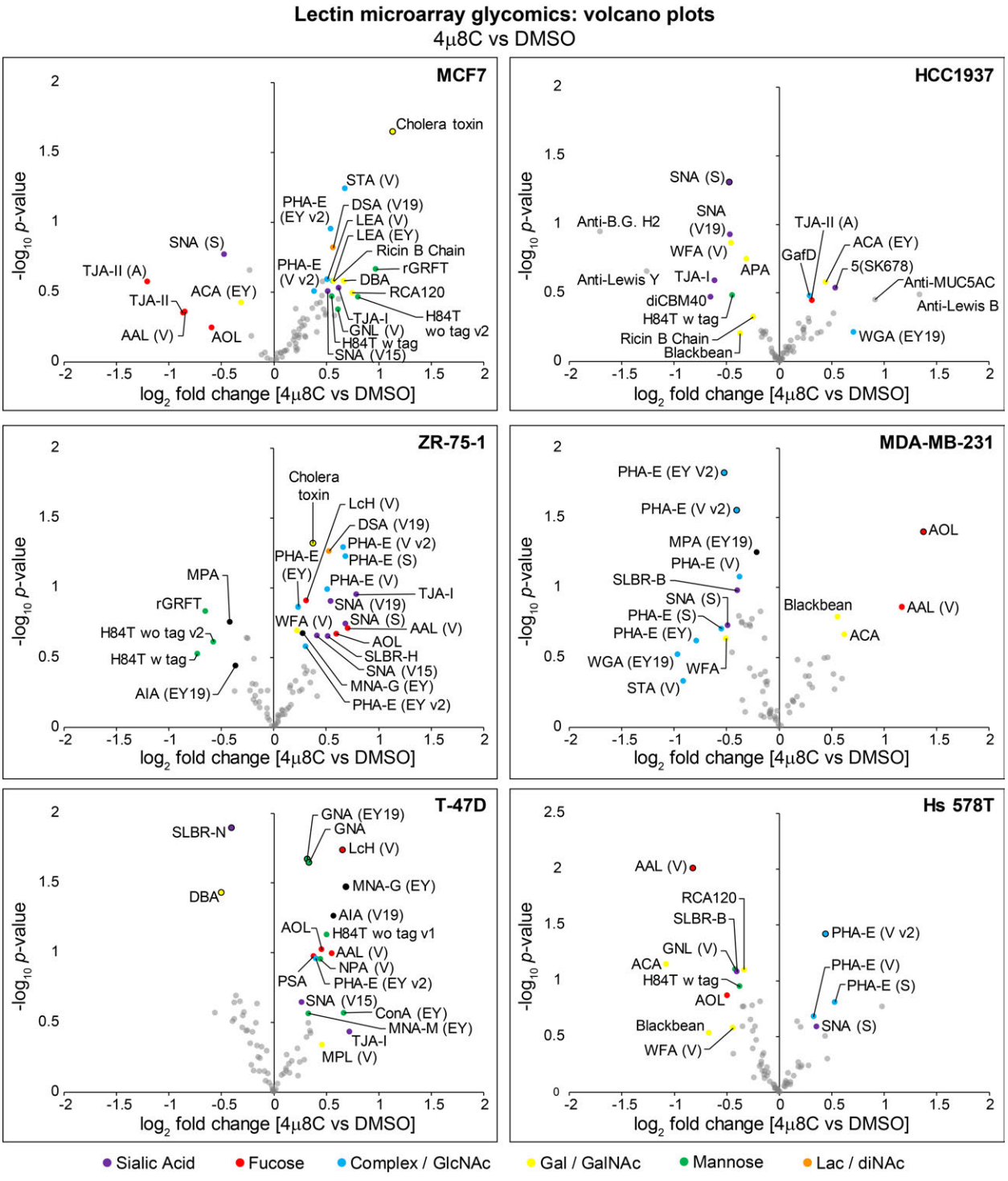

Figure 3.8: Lectin microarray analysis of breast cancer cell lines treated with 4μ8C vs DMSO over three days. Overall the effects of 4μ8C treatment (8 μM) after three days were modest, with most changes to the membrane glycome occurring without statistical significance (i.e. most changes had associated *p*-value > 0.05, or -$\log_{10}$ *p*-value < 1.3). Among the stronger effects observed were the increases in AOL and AAL (fucose binders) signals with 4μ8C treatment in MDA-MB-231 cells.

(fold change: 2.25; *p*-value: 0.14). These changes to the MDA-MB-231 membrane glycome led us to perform time-course glycomics with this cell line, treating cells with 4μ8C for 3, 7, or 10 days, and subsequently performing lectin microarray analysis[56] (**Figure 3.9**: Note that AOL is not present in this heat map; lectins not passing quality control are removed from analysis). We found that 4μ8C treatment over

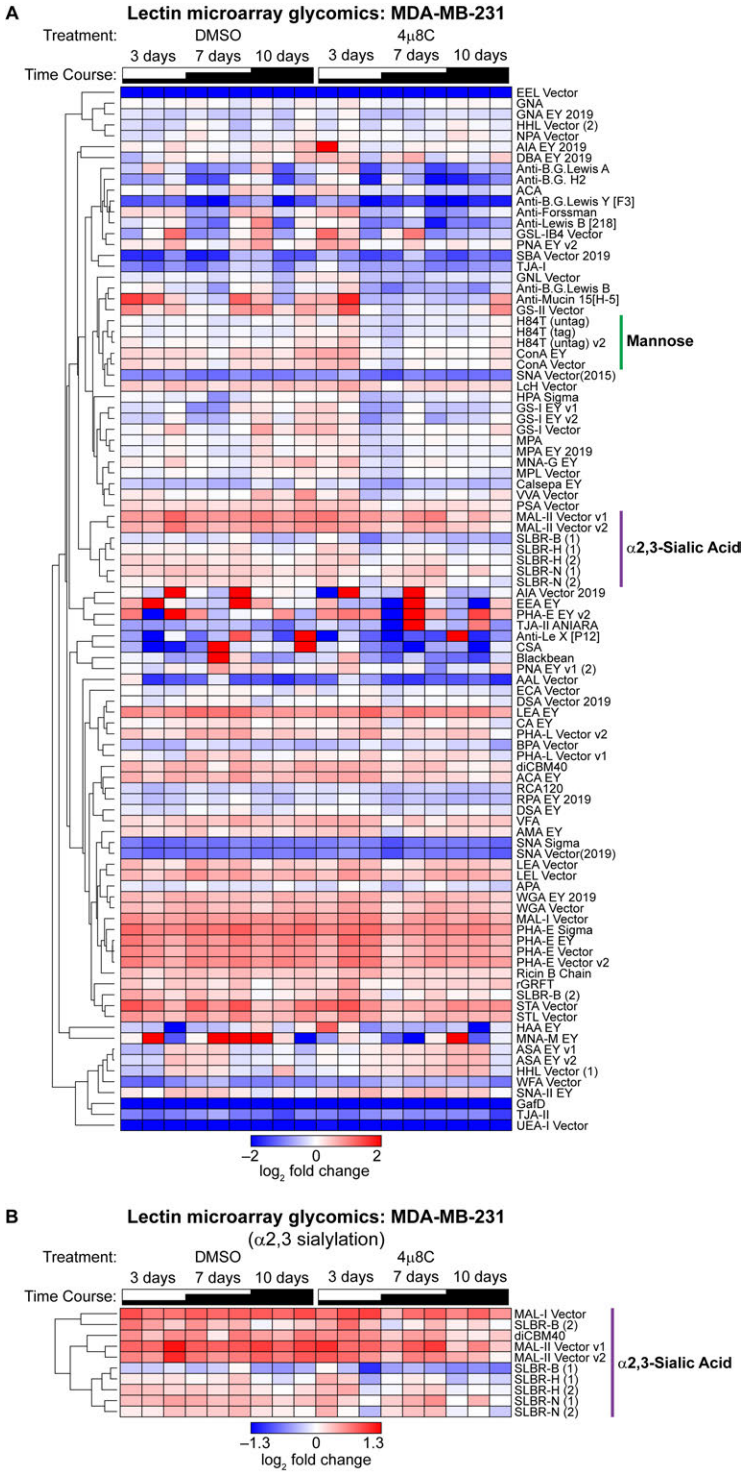

Figure 3.9: Lectin microarray analysis of the MDA-MB-231 cell line with DMSO or 4μ8C over the course of 3, 7, and 10 days. ***A***: Full heat map showing that most of the membrane glycome does not change with 4μ8C treatment (8 μM), but 4μ8C treatment does induce modest changes to α2,3-sialic acids. ***B***: Heat map with α2,3-sialic acid-binding lectins showing a modest decrease in α2,3-sialylation in MDA-MB-231 cells with 4μ8C over the time course. Color intensity represents normalized $\log_2$ ratio data relative to a pooled sample reference. Each column represents one biological replicate of the indicated sample. Select lectin groups with shared binding specificities are annotated (*Right*).

the course of 10 days did lead to changes in the MDA-MB-231 membrane glycome, but instead of a fucose signature at 7 or 10 days, we instead found a decrease in α2,3-sialic acids, becoming more apparent after 10 days (**Figure 3.9*B***). The discrepancy between the signatures observed at 3, 7, and 10 days may suggest a dynamic glycome with temporal control in direct response to physiological conditions, as previously reported during cell differentiation and development.[56,73] Perhaps the glycome composition also dynamically changes in response to proteostasis perturbations.

To structurally characterize the glycome of the MDA-MB-231 membrane proteome, we performed mass spectrometry-based glycomics of the released *N*- and *O*-glycans after 11 days with IRE1 inhibition (**Figure 3.10**). We were unable to discern differences between samples treated with either DMSO or 4μ8C

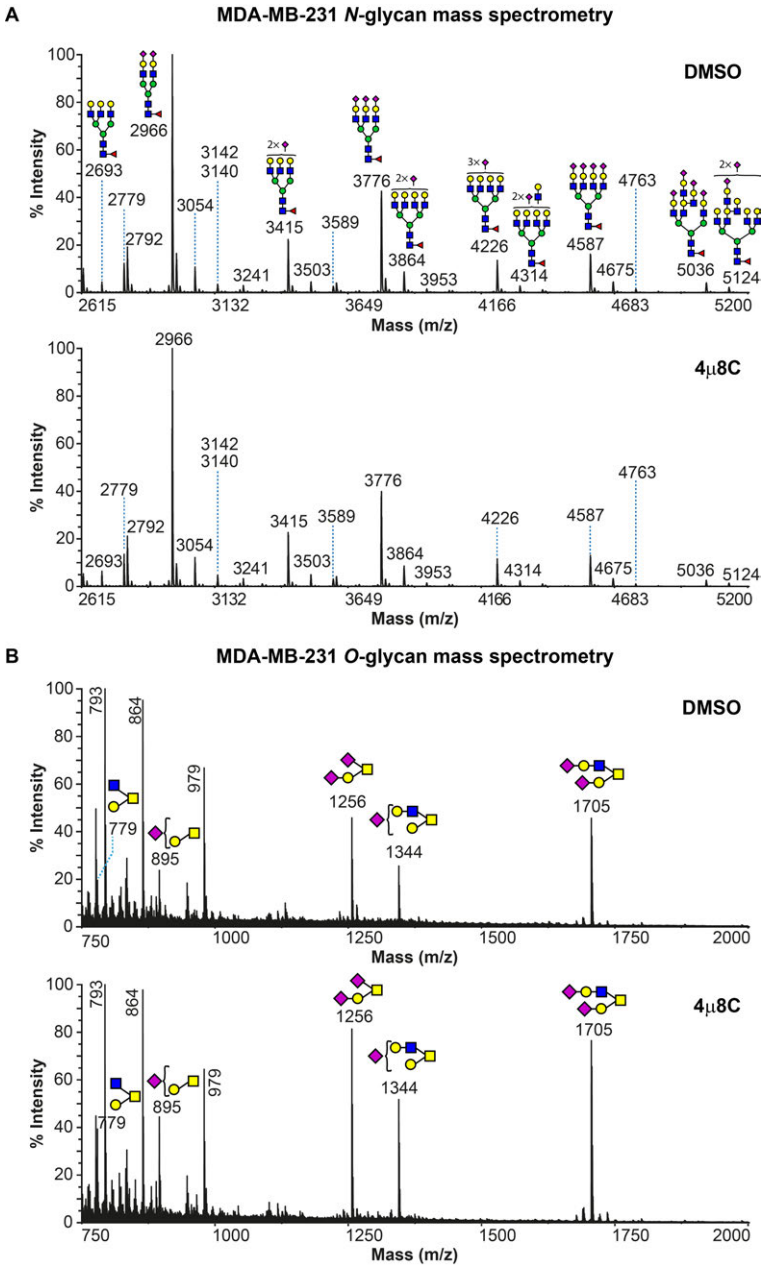

Figure 3.10: MALDI-TOF MS analysis of glycans released from membrane proteins from MDA-MB-231 cells treated with DMSO or 4μ8C (8 μM) after 11 days.
A: Partial MALDI-TOF MS spectra of *N*-glycans released from MDA-MB-231 membrane proteins by PNGase F. ***B***: MALDI-TOF MS spectra of *O*-glycans released from membrane proteins by reductive elimination. Putative structures are based on composition, tandem MS, and knowledge of biosynthetic pathways. All molecular ions are $[M+Na]^+$. Peaks not labeled with *m/z* value in the *O*-glycan mass spectra are not glycans and are either matrix or general chemical background peaks.

by mass spectrometry. It is possible that changes to the glycome observed by lectin microarray were not detected by mass spectrometry due to the complexity of sample preparation or the labile nature of glycosidic bonds, especially sialic acid linkages. However, our samples were permethylated to enhance glycan stability and predictability during fragmentation. It may be possible that there were no changes in this sample preparation. Also, the redundancy of lectins in the microarrays may be better suited to detect subtle changes.

Lectin microarray glycomics was also performed with the Hs 578T and HCC1937 TNBC cell lines after 7 days of IRE1 inhibition. Although we did not observe differences between DMSO and 4μ8C treatment in the Hs 578T samples (**Figure 3.11**), we did observe a modest increase in both α2,3- and α2,6-

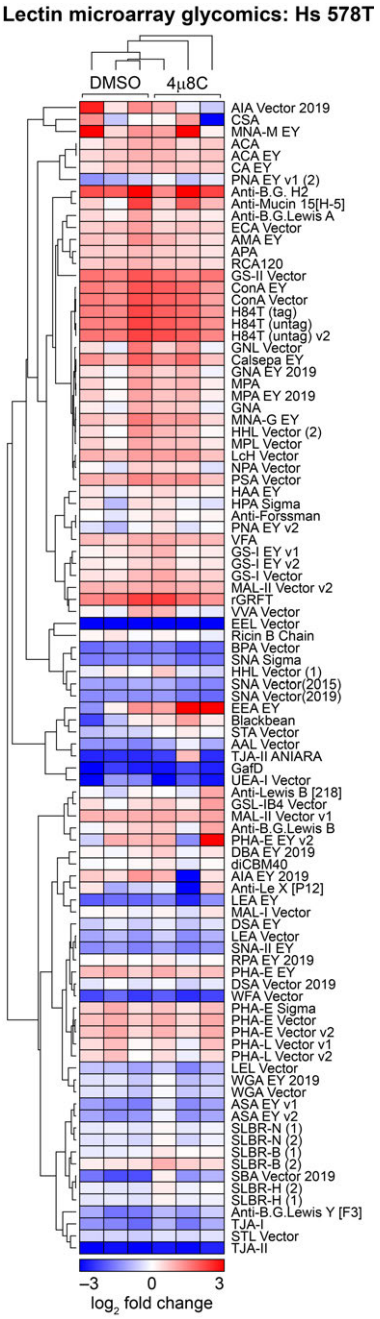

Figure 3.11: Lectin microarray analysis of the membrane proteome from Hs 578T cells with DMSO or 4μ8C (8 μM) for 7 days. The effects of IRE1 inhibition on the glycome for this cell line were not apparent. Color intensity represents normalized $\log_2$ ratio data relative to a pooled sample reference. Each column represents one biological replicate of the indicated sample.

sialic acids in the HCC1937 samples (**Figure 3.12**), contrasting the decrease in α2,3-sialic acid in the MDA-MB-231 samples with 4μ8C (**Figure 3.9*B***). When we profiled for sialyltransferase and neuraminidase gene expression across the breast cancer cell lines, we found that the expression of sialyltransferase genes were varied, and that neuraminidase gene expression in general did not appear to change (**Supporting Table 1**). While expression of α2,3 sialyltransferase genes (*ST3GAL1–6*) were generally increased in the grouped TNBC vs non-TNBC comparison (right-most column), supporting our observations by lectin microarray

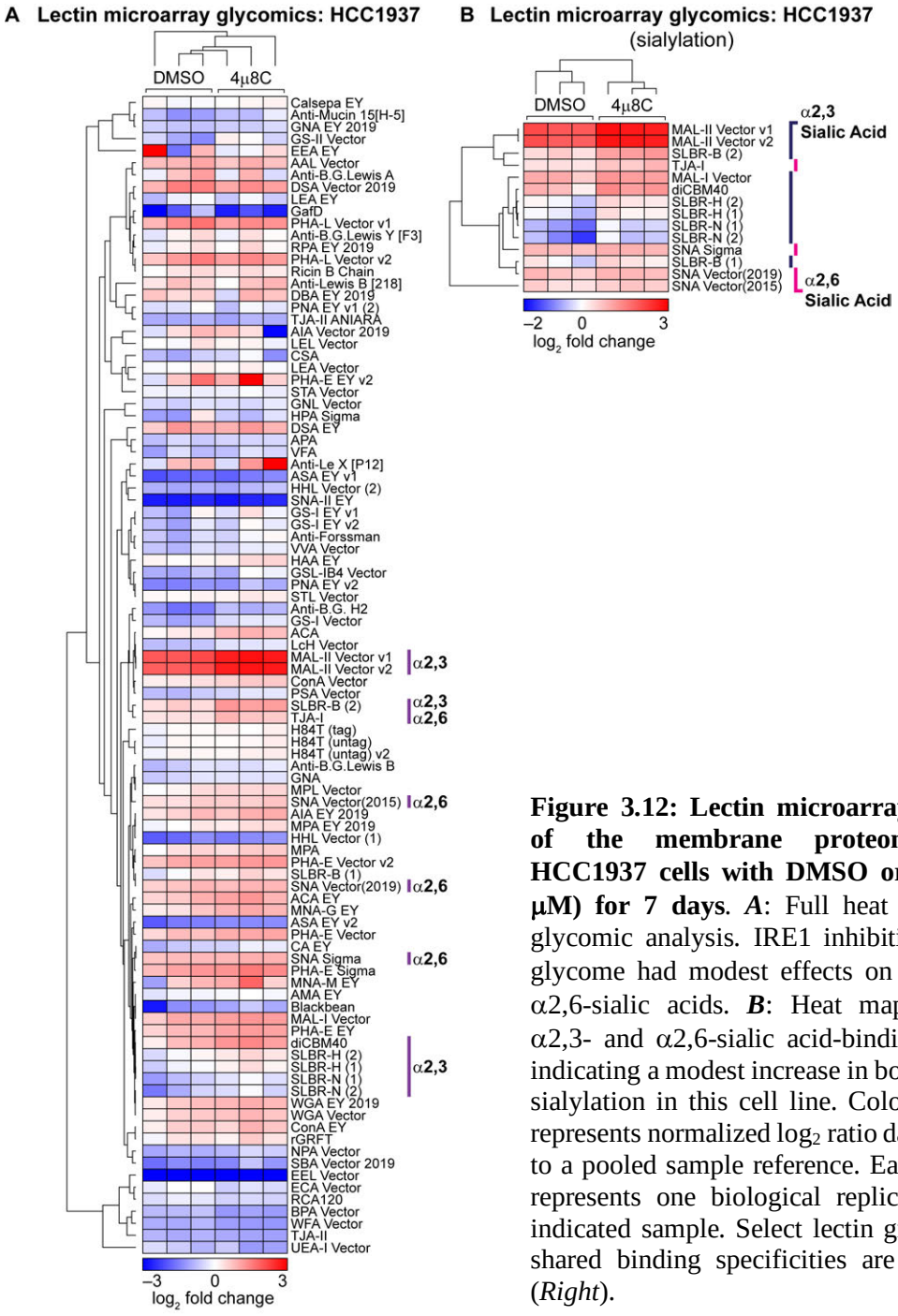

Figure 3.12: Lectin microarray analysis of the membrane proteome from HCC1937 cells with DMSO or 4μ8C (8 μM) for 7 days. ***A***: Full heat map from glycomic analysis. IRE1 inhibition on the glycome had modest effects on α2,3- and α2,6-sialic acids. ***B***: Heat map showing α2,3- and α2,6-sialic acid-binding lectins, indicating a modest increase in both types of sialylation in this cell line. Color intensity represents normalized $\log_2$ ratio data relative to a pooled sample reference. Each column represents one biological replicate of the indicated sample. Select lectin groups with shared binding specificities are annotated (*Right*).

glycomics, no clear signature was observed with 4μ8C treatment across the cell lines. Perhaps IRE1 inhibition affects select sialylation glycogenes rather than on the entire classes of glycogenes.

The lack of statistically significant correlations between sialyltransferase gene expression and glycosylation feature is not necessarily disconcerting, considering the potential for additional layers of glycogene regulation (e.g. via miRNA),[74] the low expression of many glycogenes,[75] and previous studies also demonstrating lack of a clear correlation between *N*-glycan features and mRNA expression levels.[76] In our prior work, we were also unable to identify correlative changes above significance thresholds for sialyltransferase and neuraminidase gene expression, despite observing a clear reduction in sialylation features upon XBP1s activation in HEK293 cells (**Chapter 2**).[37] The opposing effects of IRE1 inhibition between the HCC1937 and MDA-MB-231 cell lines suggest that the effects of IRE1 inhibition may be cell-line dependent, a phenomenon we have previously observed,[37] meriting follow-up experiments based on cell line.

Additional Cellular Models of ER Stress

Our breast cancer glycomics experiments suggest that IRE1 inhibition may remodel the breast cancer glycome, although the overall effect sizes may be modest. We wondered if perhaps the endogenous levels of XBP1s in TNBC cells were not sufficiently high enough to lead to changes upon IRE1 inhibition. In an alternative approach to model ER stress in cells, we induced the UPR with thapsigargin in HEK293 cells while blocking XBP1s formation by pre-treating with 4μ8C (**Figure 3.13**). We previously

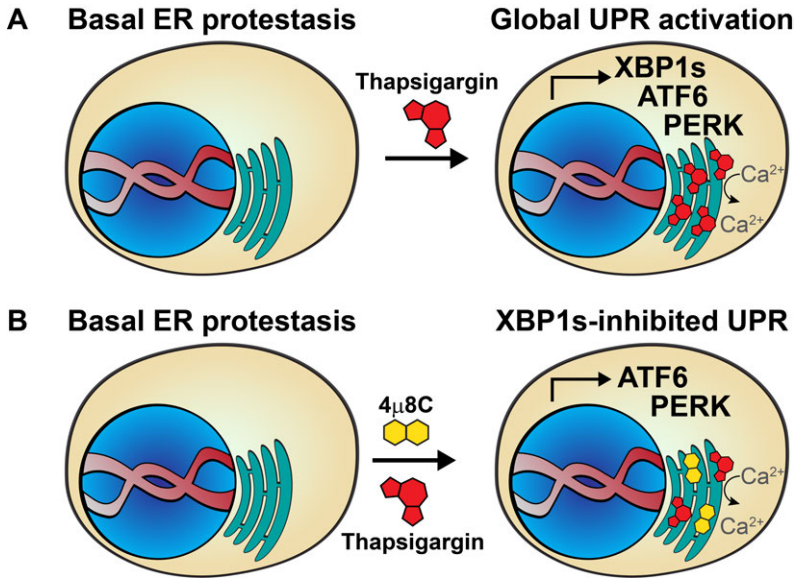

Figure 3.13: Modulating the UPR with small molecules. Pharmacological approach for global UPR activation (***A***) and for an IRE1-inhibited UPR condition (***B***). Thapsigargin induces activation of the three branches of the UPR (IRE1-XBP1s, ATF6, and PERK-ATF4), but pre-treatment with 4μ8C blunts activation of the IRE1-XBP1s branch.

demonstrated that thapsigargin treatment in HEK293 cells leads to remodeling of the glycome (**Chapter 2**).[37] In this current study we pre-treated cells with 4μ8C for one day and followed with thapsigargin co-treatment for another day to induce ER stress. We first demonstrated that 4μ8C pre-treatment in HEK293 cells blocks thapsigargin-induced XBP1s formation in a dose-dependent manner (**Figure 3.14*A***). Additionally, we observed accumulation of XBP1u upon increasing concentrations of 4μ8C. We further demonstrated that pre-treatment of HEK293 cells with 16 μM of 4μ8C prevents thapsigargin-induced formation of XBP1s in biological triplicate (**Figure 3.14*B***). We also verified that UPR signaling is intact

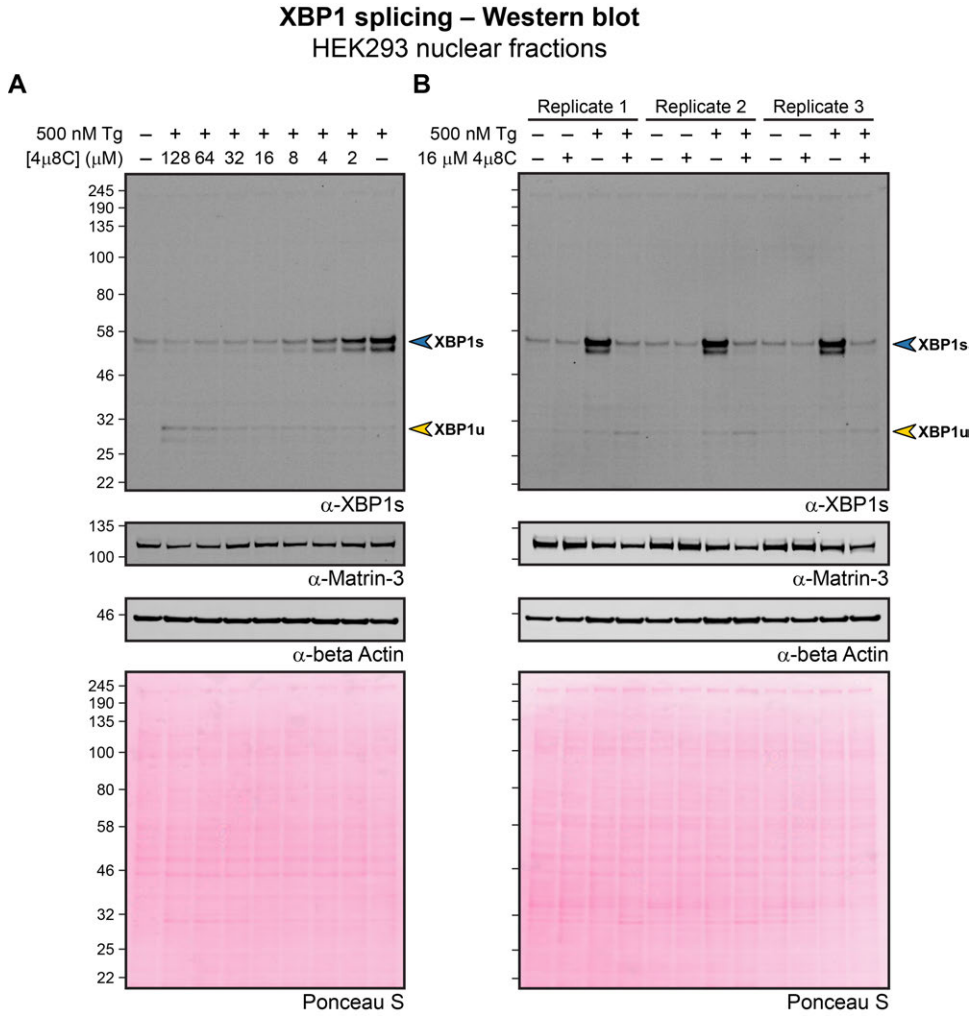

Figure 3.14: Thapsigargin-induced activation of XBP1s was blocked in HEK293 cells when pre-treated with 4μ8C for 1 day. ***A***: Dose-response was performed in HEK293 cells by pre-treating with 4μ8C at the indicated concentrations for 1 day followed by co-treatment with thapsigargin for an additional day. Nuclear fractions were isolated and blotted for XBP1s. XBP1u protein accumulated at higher concentrations of 4μ8C. ***B***: Western blot showing biological triplicates of HEK293 cells treated with DMSO, 4μ8c (2 days), Tg (1 day), or pre-treatment with 4μ8C for 1 day followed by co-treatment with Tg for an additional day. 10 μg of protein was loaded for each sample. Similar results were obtained when each Western blot was repeated for a total of two times.

with immunoblots for Grp78 (BiP), Grp94, and HYOU1 (**Figure 3.15*A***), which are in part regulated by ATF6. By qRT-PCR we also showed that PERK-ATF4 signaling is intact through upregulation of mRNA for CHOP (**Figure 3.15*B***). As was the case for 4μ8C treatment in breast cancer cells (**Figure 3.4**), treating HEK293 cells with 4μ8C does not induce ER stress at the concentrations used in this study.

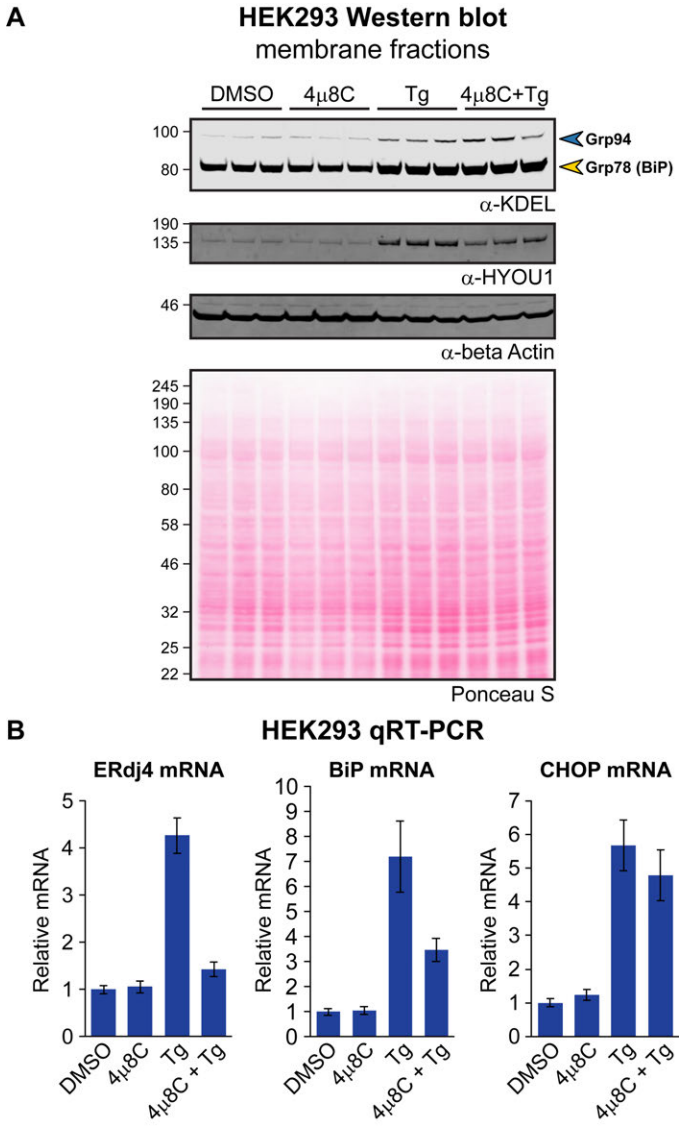

Figure 3.15: UPR stress markers with thapsigargin and IRE1 inhibition in HEK293 cells. ***A***: Western blots for Grp78 (BiP), Grp94, and HYOU1 from membrane proteomes isolated from HEK293 cells treated with DMSO, 4μ8C (16 μM, 2 days), Tg (500 nM, 1 day), or pre-treated with 4μ8C for 1 day followed by co-treatment with Tg for an additional day. Thapsigargin treatment induced expression of the three ER stress markers, while 4μ8C pre-treatment blunted HYOU1 (regulated by both XBP1s and ATF6) induction. 50 μg of protein was loaded for each sample. ***B***: Expression of mRNA for ERdj4, BiP, and CHOP were surveyed in HEK293 cells treated as described in (*A*). 4μ8C pre-treatment blunted thapsigargin-induced expression of mRNA for ERdj4 and BiP, without inducing ER stress (CHOP). Data were normalized to the *RPLP2* housekeeping gene and reported as the average of four biological replicates (n = 4), with each reaction performed in technical quadruplicate. Error bars: standard deviation of four biological replicates. 1000 ng of input RNA was used for qRT-PCR.

When we performed lectin microarray analysis of the membrane proteome isolated from HEK293 cells, we reproduced previously reported results[37] (**Chapter 2**). Namely, we observed a decrease in sialic acids and bisecting GlcNAc, and an increase in mannose glycans (**Figure 3.16)** upon treatment with thapsigargin alone. Treatment with 4μ8C alone did not induce significant changes to the glycome in this cell line, likely as a reflection of its low basal levels of UPR activity (**Figure 13.14** and **Figure 13.15**). In cells treated with both 4μ8C and thapsigargin, we observed that overall the glycome did not significantly change, but we did note that the increase in mannose glycans induced by thapsigargin was slightly attenuated when pre-treated with 4μ8C (**Figure 13.16*B***). These data suggest that other players in the UPR or pleiotropic consequences of ER stress may also be driving the glycosylation phenotype of thapsigargin-treated cells. These findings warrant additional studies of the UPR to determine what factors are required for remodeling the glycome as a result of ER stress, as these data indicate XBP1s inhibition alone is not sufficient to prevent the global glycosylation changes in HEK293 cells.

Discussion

While prior work had focused on the effects of ectopic XBP1s overexpression on the glycome (**Chapter 2**),[37, 40] this current study focused on inhibiting endogenous XBP1s activation in breast cancer models featuring upregulation of the transcription factor. Our work shows that blocking formation of XBP1s by inhibiting the IRE1 endoribonuclease can lead to changes to the breast cancer glycome at modest levels, reproducibly observed across several different lectins recognizing similar glycan epitopes. We report the first study to our knowledge demonstrating that IRE1 inhibition in breast cancer can lead to perturbations in the glycome. We find that, in different TNBC cell lines, sialylation is likely regulated by XBP1s, both positively in MDA-MB-231 cells (**Figure 3.9**) and negatively in HCC1937 cells (**Figure 3.12**). Given that sialic acid metabolism and sialylated glycan alterations have been found to affect breast cancer progression and metastasis,[77-78] dissecting the differential effects of IRE1 inhibition on sialylation would fundamentally advance our understanding of cancer glycobiology. The diverging effects of IRE1 inhibition likely results from heterogeneity within the group of cell lines. It may also reflect dynamic changes to the glycome. There are also additional levels of regulation; for example, epigenetics and miRNA are both important players in cancer and regulation of glycosylation.[70, 78-79 80-84] The modest effect sizes we observed in our glycomics experiments may reflect the effects of dominating miRNA or epigenetic regulation overshadowing the effects of IRE1 inhibition. XBP1s is known to regulate certain miRNA downstream,[85] but it is unclear what roles they might have on glycosylation in cancer.

We demonstrated that XBP1s activation is upregulated in TNBC cell lines both at the protein and RNA levels (**Figure 3.2** and **Figure 3.3**). By Western blotting, we observed that XBP1u is present at higher levels in non-TNBC nuclear fractions compared to the TNBC fractions. The unspliced variant of XBP1 is

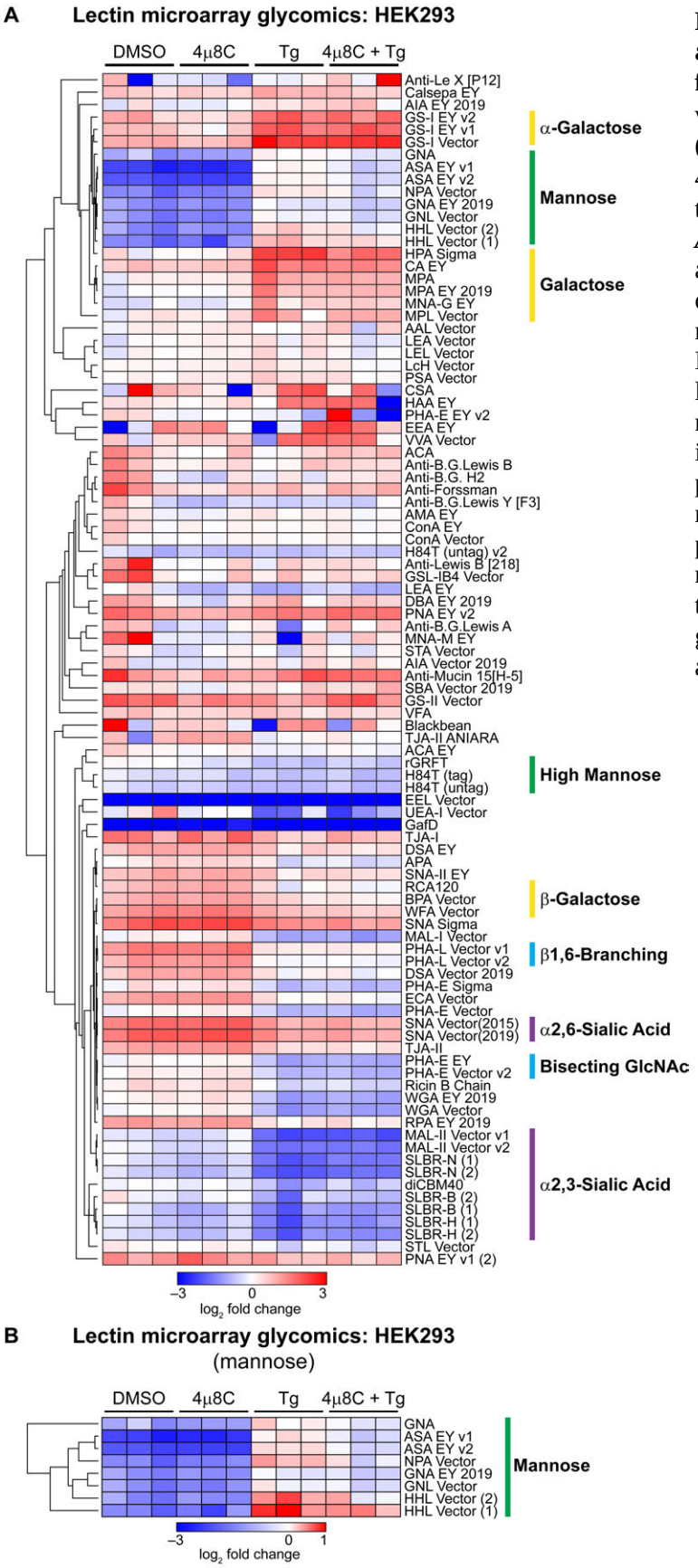

Figure 3.16: Lectin microarray analysis of the membrane proteome from HEK293 cells. Cells were treated with DMSO, 4μ8C (16 μM, 2 days), Tg (500 nM, 1 day), or pre-treated with 4μ8C for 1 day followed by co-treatment with Tg for an additional day. ***A***: Full heat map from glycomic analysis. The effects of IRE1 inhibition on the thapsigargin-induced glycome modestly affected mannose glycans. ***B***: Heat map focusing on mannose-binding lectins shows IRE1 inhibition leads to a modest decrease in the thapsigargin-induced hypermannosylation phenotype. Color intensity represents normalized $\log_2$ ratio data relative to a pooled sample reference. Each column represents one biological replicate of the indicated sample. Select lectin groups with shared binding specificities are annotated (*Right*).

known to act as a negative regulator of XBP1s, capable of shuttling between the cytoplasm and nucleus to interact with XBP1s and facilitating its degradation.[44, 59-60] Although we did not discern an accumulation of XBP1u in our breast cancer cells upon IRE1 inhibition (**Figure 3.3*C***), we were able to observe an increase in XBP1u upon increasing concentrations of 4μ8C in HEK293 cells (**Figure 3.14*A***).

Another possible explanation for the modest effect sizes we observed upon 4μ8C treatment in TNBC cells may be that endogenous levels of XBP1s in TNBC cells were not great enough to elicit a larger response with IRE1 inhibition, in contrast to our prior work with XBP1s overexpression (**Chapter 2**).[37, 40] It may be possible that the conditions used in this study were not sufficient to drive larger effects on the breast cancer glycome. Perhaps the cancer cell's response to IRE1 inhibition may be more dramatic in hypoxic conditions, a hypothesis supported by the role of XBP1s in regulating the hypoxic response in breast cancer cells.[20] Furthermore, hypoxia can induce changes to glycosylation, affecting proteins such as amino acid transporters and adhesion molecules, including integrins and EpCAM.[86-88] Mechanistically, hypoxia can enhance the expression of glycosyltransferases that mediate glycosylation, including fucosyltransferases, sialyltransferases, *O*-GlcNAc transferase, and *O*-GlcNAcase, as well as nucleotide sugar transporters.[89-90] Hypoxic conditions were shown to increase the amounts of β1,6-branched GlcNAc *N*-glycans and poly-LacNAc structures, and to reduce α2,6 sialylation in tumor-associated vessels.[91] Perhaps XBP1s plays a role in regulating the expression of such glycogenes and glycan structures induced by hypoxia.

Outstanding areas of investigation include identification of glycoproteins affected by alterations in glycosylation mediated by XBP1s perturbations. In our glycomics approaches, we lose information on the identity of proteins and instead gain information across the entire repertoire of glycans. While this information is helpful for understanding the wide-spread effects of XBP1s on glycosylation patterns, it tells us little about what proteins are being modified. The glycome-wide nature of our studies has the potential to mask protein-specific effects that are lost in the bulk glycoprotein analysis performed. For example, whether glycosylation patterns change for specific integrins or receptors remains unknown. Specific α2,6-sialylation of the Fas death receptor (CD95) by the ST6Gal I sialyltransferase in colon cancer was shown to prevent apoptosis stimulated by Fas ligand, demonstrating that resisting cell death can be attributed to a specific protein substrate–sialyltransferase pair.[92] Determining whether XBP1s affects the activity of death receptors by modulating their glycan structures would provide clues about novel mechanisms co-opted by cancer cells for survival. Glycoproteomics approaches may be applied to identify proteins of interest. Enrichment of glycoproteins by lectins, followed by mass spectrometry proteomics for example, may provide information on differentially glycosylated proteins and their abundance in XBP1s-perturbed systems. Specific proteins of interest may be enriched through immunoprecipitation experiments, then profiled by glycan mass spectrometry to identify shifts in glycan structures, as our lab had previously

performed.[40] Lastly, we acknowledge that XBP1s-induced remodeling of secreted proteins such as cytokines and growth factors may have important effects on cell signaling.[93]

An XBP1s-remodeled glycome has implications for interactions with the tumor microenvironment. The microenvironment consists of cancer stem cells, cancer-associated fibroblasts, and several types of immune cells. These cells can be co-opted by cancer to enhance tumorigenesis, and inflammation can promote angiogenesis and breast cancer.[94] XBP1s-mediated remodeling of glycans on the cell surface or on secreted proteins have the potential to alter interactions with the microenvironment and affect cancer immunotherapies and resistance mechanisms. Determining the extent to which XBP1s drives glycosylation changes could represent ways to enhance targeted therapies. For example, XBP1s may impact the glycans on the immune checkpoint proteins PD-1 and PD-L1, and such glycan alterations could affect detection and activity.[95-99] Engineering antibodies recognizing certain glycoforms of these proteins have the potential to enhance cancer immunotherapy.

In conclusion, we have demonstrated that treating TNBC cells with a small molecule inhibitor of IRE1 can effectively block XBP1s activation. IRE1 inhibition led to modest changes in the TNBC glycome. While the effect sizes were small, they were consistently observed across different lectins within the same sample, and affected principally the sialylation of glycans. Using a thapsigargin ER stress model in HEK293 cells, we also showed that the effects of 4μ8C treatment affects mannose glycans, but effects on sialylation were not observed in this model. These data demonstrate the dynamic nature of XBP1s on the glycome, and suggest that unattributed factors are likely regulating the glycome in addition to XBP1s.

Materials and Methods

Cell Lines and Reagents

All breast cancer cell lines were authenticated by short-tandem repeat profiling (ATCC) and were cultured as described by Neve, Chin et al.[100] The HEK293 (DAX) cell line was cultured as previously described.[40] Briefly, cells were grown in DMEM (Corning 15-017-CM) (for MCF7, MDA-MB-231, Hs578T, and HEK293) or RPMI 1640 (Gibco 27016-021) (for ZR-75-1, T-47D, and HCC1937) supplemented with 10% FBS (Corning 35-010-CV), L-glutamine (Corning 25-005-CI), and penicillin/streptomycin (Corning 30-002-CI) at 37 °C and 5% CO_2 in a humidified tissue culture incubator. Cells were regularly screened for mycoplasma using the MycoAlert PLUS Mycoplasma Detection Kit (Lonza LT07-710). To induce global ER stress, cells were treated with thapsigargin (Sigma-Aldrich T9033) at the indicated concentrations. To inhibit IRE1 activity and *XBP1* splicing, cells were treated with 4μ8C (Sigma-Aldrich SML0949) at the indicated concentrations, and replenished with fresh 4μ8C daily.

RNA Extraction and Quantitative Real-Time PCR

RNA was isolated from cells using the E.Z.N.A. Total RNA Kit I (Omega R6834-02) following the manufacturer's protocol, including the on-column DNase digestion (Omega E1091-02). RNA quantity and quality were assessed via $A_{260/280}$ readings on a Synergy H1 Hybrid plate reader with a Take3 micro-volume plate. RNA was frozen at –80 °C unless processed immediately for qRT-PCR. To generate cDNA from RNA, up to 1000 ng of RNA was reverse transcribed using the High-Capacity cDNA Reverse Transcription Kit (Applied Biosystems 4368813). cDNA was then diluted 5X in molecular biology grade water, and qPCR was performed using the Universal KAPA SYBR FAST qPCR Master Mix (Roche KK4618) on a LightCycler 480 II (Roche). Relative gene expression was normalized to the *RPLP2* housekeeping gene and analyzed by the ΔΔCt method.[101-102]

Primers used were as follows:

total XBP1 forward: AATGAAGTGAGGCCAGTGGC, rev: TGAAGAGTCAATACCGCCAGAA;
XBP1s forward: CTGAGTCCGCAGCAGGT, rev: TCCAGAATGCCCAACAGGAT;
RPLP2 forward: CCATTCAGCTCACTGATAACCTTG, rev: CGTCGCCTCCTACCTGCT;
ERDJ4 forward: CTGTATGCTGATTGGTAGAGTCAA, rev: AGTAGACAAAGGCATCATTTCCAA;
BIP forward: GCCTGTATTTCTAGACCTGCC, rev: TTCATCTTGCCAGCCAGTTG;
GRP94 forward: GGCCAGTTTGGTGTCGGTTT, rev: CGTTCCCCGTCCTAGAGTGTT;
CHOP forward: GGAGCTGGAAGCCTGGTATG, rev: GCCAGAGAAGCAGGGTCAAG.

To visualize *XBP1* splicing, qRT-PCR products using the total *XBP1* primer pair were separated on 2% agarose (Lonza 50090) TBE gels pre-mixed with GelGreen Nucleic Acid Gel Stain (Biotium 41005), and imaged on a 470 nm blue LED transilluminator (Maestrogen SLB-01W).

3' DGE RNA-seq

Breast cancer cells were plated at 4×10^4 cells per well in 12-well plates and allowed to adhere overnight. Cells were treated with 4μ8C over the course of three days with fresh compound renewal daily. RNA was isolated from cells using the E.Z.N.A. Total RNA Kit I following the manufacturer's protocol, including the on-column DNase digestion. RNA was frozen at –80 °C until processed for 3' digital gene expression (3' DGE) RNA-seq library preparation.[103]

3' DGE Library Preparation

RNA samples were quantified and quality assessed using an Advanced Analytical Fragment Analyzer. The initial steps were performed on a Tecan EVO150. 10 ng of total RNA was used for library preparation. 3' DGE-custom primers 3V6NEXT-bmc#1-12 were added to a final concentration of 1 μM. (5'-/5Biosg/ACACTCTTTCCCTACACGACGCTCTTCCGATCT[BC_6]$N_{10}T_{30}$VN-3' where 5Biosg = 5'

biotin, [BC6] = 6 bp barcode specific to each sample/well, N10 = Unique Molecular Identifiers, Integrated DNA technologies).

After addition of the oligonucleotides, Maxima H Minus RT was added per the manufacturer's recommendations with Template-Switching oligo5V6NEXT (10 μM, [5V6NEXT: 5'-iCiGiCACACTCTTTCCCTACACGACGCrGrGrG-3' where iC: iso-dC, iG: iso-dG, rG: RNA G]) followed by incubation at 42 °C for 90 minutes and inactivation at 80 °C for 10 minutes.

Following the template switching reaction, cDNA from 12 wells containing unique well identifiers were pooled together and cleaned using RNA Ampure beads at 1.0X. cDNA was eluted with 17 μl of water followed by digestion with Exonuclease I at 37 °C for 30 minutes and inactivation at 80 °C for 20 minutes.

Second strand synthesis and PCR amplification was done by adding the Advantage 2 Polymerase Mix (Clontech) and the SINGV6 primer (10 pmol, Integrated DNA Technologies 5'-/5Biosg/ACACTCTTTCCCTACACGACGC-3') directly to the exonuclease reaction. 15 cycles of PCR were performed followed by clean up using regular SPRI beads at 0.6X, and eluted with 20 μl of Buffer EB. Successful amplification of cDNA was confirmed using a Fragment Analyzer. Illumina libraries were then produced using standard Nextera tagmentation substituting P5NEXTPT5-bmc primer (25 μM, Integrated DNA Technologies, (5'-AATGATACGGCGACCACCGAGATCTACACTCTTTCCC-TACACGACGCTCTTCCG*A*T*C*T*-3' where * = phosphorothioate bonds) in place of the normal N500 primer.

Final libraries were cleaned using SPRI beads at 0.7X and quantified using a Fragment Analyzer and qPCR before being loaded for paired-end sequencing using the Illumina NextSeq500 in paired-end mode (20/50 nt reads).

Sequencing Data Analysis

Post-sequencing, quality-control on each of the libraries was performed to assess coverage depth, enrichment for messenger RNA (exon/intron and exon/intergenic density ratios), fraction of rRNA reads and number of detected genes using bespoke scripts.

3' DGE Quantification

Read pairs were combined into a single fastq with well/UMI information concatenated with the second read name, reads sharing sequence and UMI information were collapsed into single exemplars.

Sequences were aligned against the human genome GRCh38/hg38 ENSEMBL 89 using STAR,[104-105] with parameters --runThreadN 8 --runMode alignReads --outFilterType BySJout --outFilterMultimapNmax 20 --alignSJoverhangMin 8 --alignSJDBoverhangMin 1 --outFilterMismatchNmax 999 --alignIntronMin 10 --alignIntronMax 1000000 --alignMatesGapMax 1000000 --outSAMtype BAM SortedByCoordinate --quantMode TranscriptomeSAM, pointing to a Suffix Array assembly containing exon-exon junctions for 75 nucleotide reads. Gene expression was estimated based on reads mapping near the 3' end of transcripts using ESAT[106] with the following parameters -task score3p -alignments $sample_list -wLen 50 -wExt 5000 -wOlap 0 -sigTest 0.01 -multimap ignore, poiting to a refseq-based gene annotation (hg38, as downloaded from the UCSC Genome Browser) and gene-level data were used for downstream analyses.

Differential Expression Analysis

Briefly, differential expression was performed in the R statistical environment (R v. 3.4.0) using Bioconductor's DESeq 2 package on all annotated genes.[107] Data set parameters were estimated using the estimateSizeFactors(), and estimateDispersions() functions; read counts across conditions were modeled based on a negative binomial distribution and a Wald test was used to test for differential expression (nbinomWaldtest(), all packaged into the DESeq() function), using the treatment type as a contrast and the replicate of origin as a factor. Fold-changes, *p*-values and Benjamin-Hochberg-adjusted *p*-values (BH) were reported for each gene. Regularized fold-changes were calculated using the lfcShrink() function in "normal" mode.

GSEA Analysis

Differential expression results from DESeq2 were retrieved, and the "stat" column was used to pre-rank genes for GSEA analysis.[108] Briefly, this "stat" values reflects the Wald's test performed on read counts as modeled by DESeq2 using the negative binomial distribution. Genes that were not expressed were excluded from the analysis. Alternatively, gene loadings from PCA analysis were used as a ranking metrics. GSEA (desktop version, v3.0)[109-110] was run in the pre-ranked mode against MsigDB 6.1 Hallmark, C2 (signatures) and C5 (Gene Ontology) sets, using the official gene symbol as the key, with a weighted scoring scheme, normalizing by meandiv, with gene sets between 10 and 2000 genes (4329 gene sets retained for C2, 5780 for C5 and 50 for Hallmarks), and 5000 permutations were run for p-value estimation.

Nuclear Enrichment

For XBP1s immunoblotting, cells were lysed using a nuclear enrichment protocol as previously described.[39] Briefly, pelleted cells were resuspended in Buffer A (10 mM HEPES pH 7.5, 50 mM NaCl, 0.5 M sucrose, 0.1 mM EDTA, 0.5% Triton X-100, protease and phosphatase inhibitors (Pierce A32961))

and incubated on ice for 10 minutes. After incubation, lysates were pelleted at 1000 × g for 5 minutes. Pelleted nuclei were washed 1× with Buffer A, and 1× with Buffer B (10 mM HEPES pH 7.5, 10 mM KCl, 0.1 mM EDTA, 0.1 mM EGTA). The pelleted nuclei were then lysed in Buffer C (10 mM HEPES pH 7.5, 500 mM NaCl, 0.1 mM EDTA, 0.1 mM EGTA, 0.1% IGEPAL (NP-40), protease and phosphatase inhibitors (Pierce A32961)) with constant vortexing for 15 minutes at 4 °C, yielding nuclear extract. Lysates were cleared by centrifugation at 16,1000 × g for 15 minutes at 4 °C. Nuclear proteins and post-nuclear supernatants were stored at –80 °C until they were processed for Western blotting.

Western Blotting

Primary antibodies were obtained from Cell Signaling Technology (XBP1s: 12782S), Sigma-Aldrich (β-Actin: A1978), Bethyl Laboratories (Matrin-3: A300-591A), Enzo Life Sciences (KDEL: ADI-SPA-827), and GeneTex (HYOU1: GTX102255). All primary antibodies were diluted in 5% BSA with 0.02% sodium azide in TBS at manufacturer-recommended dilutions.

For gel electrophoresis, up to 50 μg of protein were separated on NuPAGE 4–12% Bis-Tris PAGE gels (Invitrogen NP0336BOX) ran with MOPS SDS running buffer (Invitrogen NP0050), and transferred to nitrocellulose membranes using the Trans-Blot Turbo Transfer System (Bio-Rad). Transferred membranes were stained with Ponceau S and imaged on an Epson Perfection V19 Scanner prior to blocking with 5% milk (Carnation) in TBS for 30 minutes at room temperature. After blocking, membranes were incubated with primary antibodies overnight, rocking in a 4 °C cold room. After overnight incubation, primary antibodies were removed, and membranes were washed 3× 10 minutes with TBS-T at room temperature. After the final wash, membranes were incubated with secondary antibodies (LI-COR) at 1:5,000 dilution, rocking at room temperature for 1 hour. After secondary antibody incubation, membranes were washed 3× 10 minutes with TBS-T at room temperature. Membranes were scanned using a LI-COR Odyssey Classic imager.

Membrane Proteome Enrichment

To enrich for membrane proteins for glycomic analysis, cells were grown on 150 mm tissue culture dishes to 80% confluency, washed with room temperature PBS, then scraped on ice with cold PBS containing protease and phosphatase inhibitors (Pierce A32961). Scraped cells were then pelleted at 200 × g, and were washed once in cold PBS. Cells were then resuspended in cold PBS containing protease and phosphatase inhibitors and sonicated at 4 °C three times at 5-second pulses separated by 10-second lapses (70% amplitude, Cole-Parmer) to disrupt cell membranes. Nuclei and intact cells were pellet at 200 × g, and the supernatant was centrifuged at 100,000 × g (Beckman Coulter SW 41 Ti rotor) for 1 hour at 4 °C to pellet membranes. Pelleted membranes were then resuspended in PBS containing protease and

phosphatase inhibitors, and passed through 21- and 27- gauge needles for homogenization. Protein concentrations were determined using a Pierce 660 nm Protein Assay (Pierce 22660) and aliquots were frozen at –80 °C until processed through glycomics workflows.

Lectin Microarray Glycomic Analyses

Lectin microarray print conditions and fluorescent labeling were performed as previously described.[37, 111] Briefly, they were manufactured in-house at New York University (Mahal Lab) with a Nano-plotter v2.0 piezoelectric non-contact array printer (GeS-iM) using a nano A-J tip. Arrays were printed on Nexterion Slide H (Schott Nexterion) under 50% relative humidity at a surface temperature of 12 °C. Commercial lectins and antibodies were purchased from Vector Labs, R&D Systems, Santa Cruz, TCI, AbCam, E.Y. Labs, or Sigma-Aldrich. The recombinant lectins rGRFT, rCVN, and rSVN were generous gifts from Dr. B. O'Keefe (NCI Frederick). Prior to sample hybridization, lectin microarray slides were blocked for 1 h with 50 mM ethanolamine in 50 mM sodium borate buffer (pH 8.8) followed by three washes with 0.005% PBS-T (pH 7.4). Sample protein concentration and the degree of fluorescent label incorporation was determined by measuring absorbances at 280, 555, and 650 nm per the manufacturer's instructions on a NanoDrop ND-2000c spectrophotometer (Thermo Scientific). Slides were loaded into a hybridization cassette (Arrayit) to isolate individual arrays (24 per slide). Samples were loaded onto individual arrays along with one array for the reference vs reference sample per slide. Samples were hybridized for 2 h at 25 °C with gentle agitation. After hybridization, samples were removed and arrays were washed 4× with 0.005% PBS-T (pH 7.4) for 10 min each. Slides were removed, submerged in ddH2O, and spun dry. Arrays were scanned using a GenePix 4300A array scanner (PMT 550 laser power 100% for both fluorescent channels). Background-subtracted median fluorescence intensities were extracted using GenePix Pro v7.2. Non-active lectins were defined as having an average of both channel SNRs < 3 in > 90% of the data and removed prior to further analysis.

Data were median-normalized in each fluorescent channel and the $\log_2$ of the sample/reference ratio was calculated for each technical replicate for each lectin. Technical replicates were then averaged for each lectin within each array. The ratios across individual biological triplicates per lectin were compared across treatments using a two-tailed Student's *t*-test. Heat maps were generated using Morpheus (https://software.broadinstitute.org/morpheus). Hierarchical clustering was performed using one minus Pearson correlation with the average linkage method.

Glycan Mass Spectrometry

Mass spectrometry profiling of glycans were performed as previously described.[37, 112] Briefly, each sample was subjected to sonication in the presence of detergent (CHAPS), reduction in 4 M guanidine-HCl

(Pierce, Cramlington, Northumberland, UK), carboxymethylation, and trypsin digestion. The digested glycoproteins were then purified by HLB plus C18-Sep-Pak (Waters Corp, Hertfordshire, UK; 186000132). *N*-Glycans were released by peptide *N*-glycosidase F (E.C. 3.5.1.52; Roche Applied Science, Burgess Hill, UK) digestion. Released *N*-glycans were permethylated using the sodium hydroxide procedure and purified by classic C18-Sep-Pak (Waters, WAT051910). Permethylated *N*-glycans were eluted at the 50% acetonitrile fraction. *O*-glycans were released from membrane proteins by reductive elimination with KBH_4/KOH, followed by Dowex columns. Released *O*-glycans were permethylated using the sodium hydroxide procedure and purified by a classic short C18-Sep-Pak (Waters Corp.). MS and MS/MS data were acquired using a 4800 MALDI-TOF/TOF (Applied Biosystems, Darmstadt, Germany) mass spectrometer. Permethylated samples were dissolved in 10 μL of methanol and 1 μL of dissolved sample was premixed with 1 μL of matrix (10 mg/mL 3,4-diaminobenzophenone in 75% (v/v) aqueous acetonitrile), spotted onto a target plate and dried under vacuum. For the MS/MS studies the collision energy was set to 1 kV, and Ar was used as the collision gas. The 4700 Calibration standard kit, calmix (Applied Bio-systems), was used as the external calibrant for the MS mode and [Glu1] fibrinopeptide B human (Sigma-Aldrich) was used as an external calibrant for the MS/MS mode. MS and MS/MS data were processed using Data Explorer 4.9 Software (Applied Biosystems). The processed spectra were subjected to manual assignment and annotation with the aid of a glycobioinformatics tool, GlycoWorkBench.[113] The proposed assignments for the selected peaks were based on 12C isotopic composition together with knowledge of the biosynthetic pathways.

Acknowledgements

We thank our collaborators Shuhui Chen (NYU), Lara K. Mahal (UAlberta), Aristotelis Antonopoulos, Anne Dell, Stuart Haslam (all at Imperial College London), and Vincent Butty (MIT).

This work was supported by an MIT George H. Büchi Fellowship sponsored by Ping S. Chu, PhD ’80 (to K.C.); the 56th Edward Mallinckrodt Jr. Foundation Faculty Scholar Award, a Mizutani Foundation for Glycoscience Innovation Grant, an American Cancer Society–Ellison Foundation Research Scholar Award, and MIT (to M.D.S.); NIH/NIAID Grant U01AI111598 (to L.K.M.); and BBSRC Grant BB/K016164/1 (to S.M.H. and A.D.). This work was also supported in part by the NIH/NIEHS (Grant P30-ES002109) and Koch Institute Support (Core) Grant P30-CA14051 from the National Cancer Institute.

Supporting Tables

Supporting Table 3.1: Gene expression fold changes for sialyltransferase and neuraminidase genes in breast cancer cell lines comparing 4μ8C vs DMSO treatment, and TNBC vs non-TNBC cell lines. Fold changes > 1.5 are bolded in red text. Fold-changes < 0.667 are bolded in blue text. *p*-values < 0.05 are bolded in black text.

Supporting Table 3.1

	MCF7 4μ8C vs DMSO		ZR-75-1 4μ8C vs DMSO		T-47D 4μ8C vs DMSO		HCC1937 4μ8C vs DMSO		MDA-MB-231 4μ8C vs DMSO		Hs 578T 4μ8C vs DMSO		TNBC vs non-TNBC	
Gene	fold change	*p*-val	fold change	*p*-val	fold change	*p*-val	fold change	*p*-val	fold change	*p*-val	fold change	*p*-val	fold change	*p*-val
ST3GAL1	1.41	**0.00**	1.24	**0.01**	1.30	**0.01**	0.91	0.25	0.78	**0.01**	0.91	0.26	**1.64**	**0.03**
ST3GAL2	1.36	0.40	**0.66**	0.15	1.00	0.99	**0.61**	0.09	1.09	0.75	1.22	0.45	**1.66**	**0.03**
ST3GAL3	0.88	0.84	**2.20**	0.19	**1.99**	0.24	0.67	0.46	0.75	0.49	0.96	0.89	**8.28**	**0.00**
ST3GAL4	1.06	0.81	1.29	0.23	0.89	0.58	0.92	0.66	1.23	0.30	0.86	0.46	**1.99**	**0.00**
ST3GAL5	1.28	0.53	1.34	0.34	1.25	0.74	1.03	0.95	**0.66**	0.30	**1.98**	0.08	**0.45**	0.09
ST3GAL6	0.72	0.58	**0.62**	0.27	1.30	0.61	0.81	0.65	0.67	0.25	0.93	0.82	**5.29**	**0.00**
ST6GAL1	**0.66**	0.35	0.76	0.08	1.24	0.23	0.86	0.70	**0.62**	0.34	**0.26**	**0.01**	**0.03**	**0.00**
ST6GAL2	0.98	0.97	1.00	0.99	0.99	0.98	1.03	0.96	1.00	1.00	0.69	0.77	**1.53**	0.70
ST6GALNAC1	0.94	0.89	1.06	0.91	0.99	0.98	1.03	0.96	0.86	0.78	1.06	0.91	1.04	0.96
ST6GALNAC2	0.91	0.64	0.99	0.97	0.83	0.55	**0.58**	0.21	1.06	0.88	1.35	0.58	**0.04**	**0.00**
ST6GALNAC3	1.00	0.97	1.00	0.99	1.00	0.97	1.00	0.95	1.00	1.00	1.03	0.99	**2.01**	0.47
ST6GALNAC4	0.84	0.49	0.88	0.39	1.41	0.33	**0.60**	**0.03**	0.68	**0.05**	1.41	0.10	**0.59**	0.15
ST6GALNAC5	0.69	0.55	1.04	0.96	0.90	0.88	1.12	0.56	**2.06**	0.21	1.23	0.38	**40.67**	**0.00**
ST6GALNAC6	1.07	0.80	0.98	0.97	0.78	0.43	**1.51**	0.16	0.83	0.48	0.91	0.76	1.44	**0.05**
ST8SIA1	0.89	0.87	**2.10**	0.20	1.08	0.80	1.20	0.80	0.68	0.51	**0.30**	0.06	**0.09**	**0.00**
ST8SIA2	0.98	0.97	1.00	0.99	0.99	0.98	1.03	0.96	1.00	1.00	0.87	0.80	1.09	0.92
ST8SIA3	0.98	0.97	1.06	0.91	0.99	0.98	1.03	0.96	1.00	1.00	1.00	0.99	0.94	0.94
ST8SIA4	0.82	0.52	**0.53**	0.35	**0.63**	0.53	0.68	0.22	0.68	0.42	1.04	0.96	0.89	0.90
ST8SIA5	0.98	0.97	1.00	0.99	0.99	0.98	1.03	0.96	1.05	0.93	0.91	0.86	1.09	0.92
ST8SIA6	0.89	0.86	1.03	0.97	0.67	0.63	1.17	0.84	0.99	0.99	1.40	0.67	**0.10**	**0.01**
NEU1	1.35	**0.04**	1.04	0.80	0.87	0.28	**1.57**	**0.00**	1.10	0.45	0.89	0.36	1.25	0.25
NEU2	0.98	0.97	1.06	0.91	0.99	0.98	1.08	0.88	1.00	1.00	1.00	0.99	0.94	0.94
NEU3	0.77	0.45	1.19	0.68	**0.53**	0.10	0.97	0.94	0.74	0.40	0.72	0.36	1.05	0.82
NEU4	1.42	0.82	**0.58**	0.57	0.82	0.81	1.08	0.92	0.99	0.99	1.01	0.98	**0.31**	0.16

References

[1] Hoadley, K. A.; Yau, C.; Hinoue, T.; Wolf, D. M.; Lazar, A. J.; Drill, E.; Shen, R.; Taylor, A. M.; Cherniack, A. D.; Thorsson, V.; Akbani, R.; Bowlby, R.; Wong, C. K.; Wiznerowicz, M.; Sanchez-Vega, F.; Robertson, A. G.; Schneider, B. G.; Lawrence, M. S.; Noushmehr, H.; Malta, T. M.; Stuart, J. M.; Benz, C. C.; Laird, P. W., Cell-of-Origin Patterns Dominate the Molecular Classification of 10,000 Tumors from 33 Types of Cancer. *Cell* **2018,** *173* (2), 291-304.e6.

[2] Consortium, I. T. P.-C. A. o. W. G., Pan-cancer analysis of whole genomes. *Nature* **2020,** *578* (7793), 82-93.

[3] Alexandrov, L. B.; Kim, J.; Haradhvala, N. J.; Huang, M. N.; Tian Ng, A. W.; Wu, Y.; Boot, A.; Covington, K. R.; Gordenin, D. A.; Bergstrom, E. N.; Islam, S. M. A.; Lopez-Bigas, N.; Klimczak, L. J.; McPherson, J. R.; Morganella, S.; Sabarinathan, R.; Wheeler, D. A.; Mustonen, V.; Getz, G.; Rozen, S. G.; Stratton, M. R., The repertoire of mutational signatures in human cancer. *Nature* **2020,** *578* (7793), 94-101.

[4] Campbell, B. B.; Light, N.; Fabrizio, D.; Zatzman, M.; Fuligni, F.; de Borja, R.; Davidson, S.; Edwards, M.; Elvin, J. A.; Hodel, K. P.; Zahurancik, W. J.; Suo, Z.; Lipman, T.; Wimmer, K.; Kratz, C. P.; Bowers, D. C.; Laetsch, T. W.; Dunn, G. P.; Johanns, T. M.; Grimmer, M. R.; Smirnov, I. V.; Larouche, V.; Samuel, D.; Bronsema, A.; Osborn, M.; Stearns, D.; Raman, P.; Cole, K. A.; Storm, P. B.; Yalon, M.; Opocher, E.; Mason, G.; Thomas, G. A.; Sabel, M.; George, B.; Ziegler, D. S.; Lindhorst, S.; Issai, V. M.; Constantini, S.; Toledano, H.; Elhasid, R.; Farah, R.; Dvir, R.; Dirks, P.; Huang, A.; Galati, M. A.; Chung, J.; Ramaswamy, V.; Irwin, M. S.; Aronson, M.; Durno, C.; Taylor, M. D.; Rechavi, G.; Maris, J. M.; Bouffet, E.; Hawkins, C.; Costello, J. F.; Meyn, M. S.; Pursell, Z. F.; Malkin, D.; Tabori, U.; Shlien, A., Comprehensive Analysis of Hypermutation in Human Cancer. *Cell* **2017,** *171* (5), 1042-1056.e10.

[5] Hanahan, D.; Weinberg, R. A., The hallmarks of cancer. *Cell* **2000,** *100* (1), 57-70.

[6] Hanahan, D.; Weinberg, R. A., Hallmarks of cancer: the next generation. *Cell* **2011,** *144* (5), 646-74.

[7] Urra, H.; Dufey, E.; Avril, T.; Chevet, E.; Hetz, C., Endoplasmic Reticulum Stress and the Hallmarks of Cancer. *Trends Cancer* **2016,** *2* (5), 252-262.

[8] Macheret, M.; Halazonetis, T. D., DNA replication stress as a hallmark of cancer. *Annu Rev Pathol* **2015,** *10*, 425-48.

[9] Munkley, J.; Elliott, D. J., Hallmarks of glycosylation in cancer. *Oncotarget* **2016,** *7* (23), 35478-89.

[10] Peixoto, A.; Relvas-Santos, M.; Azevedo, R.; Santos, L. L.; Ferreira, J. A., Protein Glycosylation and Tumor Microenvironment Alterations Driving Cancer Hallmarks. *Front Oncol* **2019,** *9*, 380.

[11] Vajaria, B. N.; Patel, P. S., Glycosylation: a hallmark of cancer? *Glycoconj J* **2017,** *34* (2), 147-156.

[12] El-Athman, R.; Relogio, A., Escaping Circadian Regulation: An Emerging Hallmark of Cancer? *Cell Syst* **2018,** *6* (3), 266-267.

[13] Siegel, R. L.; Miller, K. D.; Jemal, A., Cancer statistics, 2020. *CA Cancer J Clin* **2020,** *70* (1), 7-30.

[14] DeSantis, C. E.; Ma, J.; Gaudet, M. M.; Newman, L. A.; Miller, K. D.; Goding Sauer, A.; Jemal, A.; Siegel, R. L., Breast cancer statistics, 2019. *CA Cancer J Clin* **2019,** *69* (6), 438-451.

[15] Waks, A. G.; Winer, E. P., Breast Cancer Treatment: A Review. *Jama* **2019,** *321* (3), 288-300.

[16] Narayan, P.; Wahby, S.; Gao, J. J.; Amiri-Kordestani, L.; Ibrahim, A.; Bloomquist, E.; Tang, S.; Xu, Y.; Liu, J.; Fu, W.; Song, P.; King-Kallimanis, B. L.; Hou, S.; Gong, Y.; Kalavar, S.; Ghosh, S.;

Philip, R.; Goldberg, K. B.; Theoret, M. R.; Blumenthal, G. M.; Kluetz, P. G.; Sridhara, R.; Pazdur, R.; Beaver, J. A., FDA Approval Summary: Atezolizumab Plus Paclitaxel Protein-bound for the Treatment of Patients with Advanced or Metastatic TNBC Whose Tumors Express PD-L1. *Clin Cancer Res* **2020**.

[17] Schmid, P.; Adams, S.; Rugo, H. S.; Schneeweiss, A.; Barrios, C. H.; Iwata, H.; Dieras, V.; Hegg, R.; Im, S. A.; Shaw Wright, G.; Henschel, V.; Molinero, L.; Chui, S. Y.; Funke, R.; Husain, A.; Winer, E. P.; Loi, S.; Emens, L. A., Atezolizumab and Nab-Paclitaxel in Advanced Triple-Negative Breast Cancer. *N Engl J Med* **2018,** *379* (22), 2108-2121.

[18] Fachal, L.; Aschard, H.; Beesley, J.; Barnes, D. R.; Allen, J.; Kar, S.; Pooley, K. A.; Dennis, J.; Michailidou, K.; Turman, C.; Soucy, P.; Lemacon, A.; Lush, M.; Tyrer, J. P.; Ghoussaini, M.; Moradi Marjaneh, M.; Jiang, X.; Agata, S.; Aittomaki, K.; Alonso, M. R.; Andrulis, I. L.; Anton-Culver, H.; Antonenkova, N. N.; Arason, A.; Arndt, V.; Aronson, K. J.; Arun, B. K.; Auber, B.; Auer, P. L.; Azzollini, J.; Balmana, J.; Barkardottir, R. B.; Barrowdale, D.; Beeghly-Fadiel, A.; Benitez, J.; Bermisheva, M.; Bialkowska, K.; Blanco, A. M.; Blomqvist, C.; Blot, W.; Bogdanova, N. V.; Bojesen, S. E.; Bolla, M. K.; Bonanni, B.; Borg, A.; Bosse, K.; Brauch, H.; Brenner, H.; Briceno, I.; Brock, I. W.; Brooks-Wilson, A.; Bruning, T.; Burwinkel, B.; Buys, S. S.; Cai, Q.; Caldes, T.; Caligo, M. A.; Camp, N. J.; Campbell, I.; Canzian, F.; Carroll, J. S.; Carter, B. D.; Castelao, J. E.; Chiquette, J.; Christiansen, H.; Chung, W. K.; Claes, K. B. M.; Clarke, C. L.; Collee, J. M.; Cornelissen, S.; Couch, F. J.; Cox, A.; Cross, S. S.; Cybulski, C.; Czene, K.; Daly, M. B.; de la Hoya, M.; Devilee, P.; Diez, O.; Ding, Y. C.; Dite, G. S.; Domchek, S. M.; Dork, T.; Dos-Santos-Silva, I.; Droit, A.; Dubois, S.; Dumont, M.; Duran, M.; Durcan, L.; Dwek, M.; Eccles, D. M.; Engel, C.; Eriksson, M.; Evans, D. G.; Fasching, P. A.; Fletcher, O.; Floris, G.; Flyger, H.; Foretova, L.; Foulkes, W. D.; Friedman, E.; Fritschi, L.; Frost, D.; Gabrielson, M.; Gago-Dominguez, M.; Gambino, G.; Ganz, P. A.; Gapstur, S. M.; Garber, J.; Garcia-Saenz, J. A.; Gaudet, M. M.; Georgoulias, V.; Giles, G. G.; Glendon, G.; Godwin, A. K.; Goldberg, M. S.; Goldgar, D. E.; Gonzalez-Neira, A.; Tibiletti, M. G.; Greene, M. H.; Grip, M.; Gronwald, J.; Grundy, A.; Guenel, P.; Hahnen, E.; Haiman, C. A.; Hakansson, N.; Hall, P.; Hamann, U.; Harrington, P. A.; Hartikainen, J. M.; Hartman, M.; He, W.; Healey, C. S.; Heemskerk-Gerritsen, B. A. M.; Heyworth, J.; Hillemanns, P.; Hogervorst, F. B. L.; Hollestelle, A.; Hooning, M. J.; Hopper, J. L.; Howell, A.; Huang, G.; Hulick, P. J.; Imyanitov, E. N.; Isaacs, C.; Iwasaki, M.; Jager, A.; Jakimovska, M.; Jakubowska, A.; James, P. A.; Janavicius, R.; Jankowitz, R. C.; John, E. M.; Johnson, N.; Jones, M. E.; Jukkola-Vuorinen, A.; Jung, A.; Kaaks, R.; Kang, D.; Kapoor, P. M.; Karlan, B. Y.; Keeman, R.; Kerin, M. J.; Khusnutdinova, E.; Kiiski, J. I.; Kirk, J.; Kitahara, C. M.; Ko, Y. D.; Konstantopoulou, I.; Kosma, V. M.; Koutros, S.; Kubelka-Sabit, K.; Kwong, A.; Kyriacou, K.; Laitman, Y.; Lambrechts, D.; Lee, E.; Leslie, G.; Lester, J.; Lesueur, F.; Lindblom, A.; Lo, W. Y.; Long, J.; Lophatananon, A.; Loud, J. T.; Lubinski, J.; MacInnis, R. J.; Maishman, T.; Makalic, E.; Mannermaa, A.; Manoochehri, M.; Manoukian, S.; Margolin, S.; Martinez, M. E.; Matsuo, K.; Maurer, T.; Mavroudis, D.; Mayes, R.; McGuffog, L.; McLean, C.; Mebirouk, N.; Meindl, A.; Miller, A.; Miller, N.; Montagna, M.; Moreno, F.; Muir, K.; Mulligan, A. M.; Munoz-Garzon, V. M.; Muranen, T. A.; Narod, S. A.; Nassir, R.; Nathanson, K. L.; Neuhausen, S. L.; Nevanlinna, H.; Neven, P.; Nielsen, F. C.; Nikitina-Zake, L.; Norman, A.; Offit, K.; Olah, E.; Olopade, O. I.; Olsson, H.; Orr, N.; Osorio, A.; Pankratz, V. S.; Papp, J.; Park, S. K.; Park-Simon, T. W.; Parsons, M. T.; Paul, J.; Pedersen, I. S.; Peissel, B.; Peshkin, B.; Peterlongo, P.; Peto, J.; Plaseska-Karanfilska, D.; Prajzendanc, K.; Prentice, R.; Presneau, N.; Prokofyeva, D.; Pujana, M. A.; Pylkas, K.; Radice, P.; Ramus, S. J.; Rantala, J.; Rau-Murthy, R.; Rennert, G.; Risch, H. A.; Robson, M.; Romero, A.; Rossing, M.; Saloustros, E.; Sanchez-Herrero, E.; Sandler, D. P.; Santamarina, M.; Saunders, C.; Sawyer, E. J.; Scheuner, M. T.; Schmidt, D. F.; Schmutzler, R. K.; Schneeweiss, A.; Schoemaker, M. J.; Schottker, B.; Schurmann, P.; Scott, C.; Scott, R. J.; Senter, L.; Seynaeve, C. M.; Shah, M.; Sharma, P.; Shen, C. Y.; Shu, X. O.; Singer, C. F.; Slavin, T. P.; Smichkoska, S.; Southey, M. C.; Spinelli, J. J.; Spurdle, A. B.; Stone, J.; Stoppa-Lyonnet, D.; Sutter, C.; Swerdlow,

A. J.; Tamimi, R. M.; Tan, Y. Y.; Tapper, W. J.; Taylor, J. A.; Teixeira, M. R.; Tengstrom, M.; Teo, S. H.; Terry, M. B.; Teule, A.; Thomassen, M.; Thull, D. L.; Tischkowitz, M.; Toland, A. E.; Tollenaar, R.; Tomlinson, I.; Torres, D.; Torres-Mejia, G.; Troester, M. A.; Truong, T.; Tung, N.; Tzardi, M.; Ulmer, H. U.; Vachon, C. M.; van Asperen, C. J.; van der Kolk, L. E.; van Rensburg, E. J.; Vega, A.; Viel, A.; Vijai, J.; Vogel, M. J.; Wang, Q.; Wappenschmidt, B.; Weinberg, C. R.; Weitzel, J. N.; Wendt, C.; Wildiers, H.; Winqvist, R.; Wolk, A.; Wu, A. H.; Yannoukakos, D.; Zhang, Y.; Zheng, W.; Hunter, D.; Pharoah, P. D. P.; Chang-Claude, J.; Garcia-Closas, M.; Schmidt, M. K.; Milne, R. L.; Kristensen, V. N.; French, J. D.; Edwards, S. L.; Antoniou, A. C.; Chenevix-Trench, G.; Simard, J.; Easton, D. F.; Kraft, P.; Dunning, A. M., Fine-mapping of 150 breast cancer risk regions identifies 191 likely target genes. *Nat Genet* **2020,** *52* (1), 56-73.

[19] The Cancer Genome Atlas Network, Comprehensive molecular portraits of human breast tumours. *Nature* **2012,** *490* (7418), 61-70.

[20] Chen, X.; Iliopoulos, D.; Zhang, Q.; Tang, Q.; Greenblatt, M. B.; Hatziapostolou, M.; Lim, E.; Tam, W. L.; Ni, M.; Chen, Y.; Mai, J.; Shen, H.; Hu, D. Z.; Adoro, S.; Hu, B.; Song, M.; Tan, C.; Landis, M. D.; Ferrari, M.; Shin, S. J.; Brown, M.; Chang, J. C.; Liu, X. S.; Glimcher, L. H., XBP1 promotes triple-negative breast cancer by controlling the HIF1alpha pathway. *Nature* **2014,** *508* (7494), 103-107.

[21] Zhao, N.; Cao, J.; Xu, L.; Tang, Q.; Dobrolecki, L. E.; Lv, X.; Talukdar, M.; Lu, Y.; Wang, X.; Hu, D. Z.; Shi, Q.; Xiang, Y.; Wang, Y.; Liu, X.; Bu, W.; Jiang, Y.; Li, M.; Gong, Y.; Sun, Z.; Ying, H.; Yuan, B.; Lin, X.; Feng, X. H.; Hartig, S. M.; Li, F.; Shen, H.; Chen, Y.; Han, L.; Zeng, Q.; Patterson, J. B.; Kaipparettu, B. A.; Putluri, N.; Sicheri, F.; Rosen, J. M.; Lewis, M. T.; Chen, X., Pharmacological targeting of MYC-regulated IRE1/XBP1 pathway suppresses MYC-driven breast cancer. *J Clin Invest* **2018,** *128* (4), 1283-1299.

[22] Harnoss, J. M.; Le Thomas, A.; Reichelt, M.; Guttman, O.; Wu, T. D.; Marsters, S. A.; Shemorry, A.; Lawrence, D. A.; Kan, D.; Segal, E.; Merchant, M.; Totpal, K.; Crocker, L. M.; Mesh, K.; Dohse, M.; Solon, M.; Modrusan, Z.; Rudolph, J.; Koeppen, H.; Walter, P.; Ashkenazi, A., IRE1alpha disruption in triple-negative breast cancer cooperates with anti-angiogenic therapy by reversing ER stress adaptation and remodeling the tumor microenvironment. *Cancer Res* **2020**.

[23] Harnoss, J. M.; Le Thomas, A.; Shemorry, A.; Marsters, S. A.; Lawrence, D. A.; Lu, M.; Chen, Y. A.; Qing, J.; Totpal, K.; Kan, D.; Segal, E.; Merchant, M.; Reichelt, M.; Ackerly Wallweber, H.; Wang, W.; Clark, K.; Kaufman, S.; Beresini, M. H.; Laing, S. T.; Sandoval, W.; Lorenzo, M.; Wu, J.; Ly, J.; De Bruyn, T.; Heidersbach, A.; Haley, B.; Gogineni, A.; Weimer, R. M.; Lee, D.; Braun, M. G.; Rudolph, J.; VanWyngarden, M. J.; Sherbenou, D. W.; Gomez-Bougie, P.; Amiot, M.; Acosta-Alvear, D.; Walter, P.; Ashkenazi, A., Disruption of IRE1alpha through its kinase domain attenuates multiple myeloma. *Proc Natl Acad Sci U S A* **2019,** *116* (33), 16420-16429.

[24] Sheng, X.; Nenseth, H. Z.; Qu, S.; Kuzu, O. F.; Frahnow, T.; Simon, L.; Greene, S.; Zeng, Q.; Fazli, L.; Rennie, P. S.; Mills, I. G.; Danielsen, H.; Theis, F.; Patterson, J. B.; Jin, Y.; Saatcioglu, F., IRE1alpha-XBP1s pathway promotes prostate cancer by activating c-MYC signaling. *Nat Commun* **2019,** *10* (1), 323.

[25] Ji, H.; Huang, C.; Wu, S.; Kasim, V., XBP1-s promotes colorectal cancer cell proliferation by inhibiting TAp73 transcriptional activity. *Biochem Biophys Res Commun* **2019,** *508* (1), 203-209.

[26] Wong, M. Y.; DiChiara, A. S.; Suen, P. H.; Chen, K.; Doan, N. D.; Shoulders, M. D., Adapting Secretory Proteostasis and Function Through the Unfolded Protein Response. *Curr Top Microbiol Immunol* **2018,** *414*, 1-25.

[27] Dong, H.; Adams, N. M.; Xu, Y.; Cao, J.; Allan, D. S. J.; Carlyle, J. R.; Chen, X.; Sun, J. C.; Glimcher, L. H., The IRE1 endoplasmic reticulum stress sensor activates natural killer cell immunity in part by regulating c-Myc. *Nat Immunol* **2019,** *20* (7), 865-878.

[28] Song, M.; Sandoval, T. A.; Chae, C. S.; Chopra, S.; Tan, C.; Rutkowski, M. R.; Raundhal, M.; Chaurio, R. A.; Payne, K. K.; Konrad, C.; Bettigole, S. E.; Shin, H. R.; Crowley, M. J. P.; Cerliani, J. P.; Kossenkov, A. V.; Motorykin, I.; Zhang, S.; Manfredi, G.; Zamarin, D.; Holcomb, K.; Rodriguez, P. C.; Rabinovich, G. A.; Conejo-Garcia, J. R.; Glimcher, L. H.; Cubillos-Ruiz, J. R., IRE1alpha-XBP1 controls T cell function in ovarian cancer by regulating mitochondrial activity. *Nature* **2018,** *562* (7727), 423-428.

[29] Chopra, S.; Giovanelli, P.; Alvarado-Vazquez, P. A.; Alonso, S.; Song, M.; Sandoval, T. A.; Chae, C. S.; Tan, C.; Fonseca, M. M.; Gutierrez, S.; Jimenez, L.; Subbaramaiah, K.; Iwawaki, T.; Kingsley, P. J.; Marnett, L. J.; Kossenkov, A. V.; Crespo, M. S.; Dannenberg, A. J.; Glimcher, L. H.; Romero-Sandoval, E. A.; Cubillos-Ruiz, J. R., IRE1alpha-XBP1 signaling in leukocytes controls prostaglandin biosynthesis and pain. *Science* **2019,** *365* (6450).

[30] Martinez, G.; Vidal, R. L.; Mardones, P.; Serrano, F. G.; Ardiles, A. O.; Wirth, C.; Valdes, P.; Thielen, P.; Schneider, B. L.; Kerr, B.; Valdes, J. L.; Palacios, A. G.; Inestrosa, N. C.; Glimcher, L. H.; Hetz, C., Regulation of Memory Formation by the Transcription Factor XBP1. *Cell Rep* **2016,** *14* (6), 1382-1394.

[31] Cisse, M.; Duplan, E.; Lorivel, T.; Dunys, J.; Bauer, C.; Meckler, X.; Gerakis, Y.; Lauritzen, I.; Checler, F., The transcription factor XBP1s restores hippocampal synaptic plasticity and memory by control of the Kalirin-7 pathway in Alzheimer model. *Mol Psychiatry* **2017,** *22* (11), 1562-1575.

[32] Pan, Y.; Ballance, H.; Meng, H.; Gonzalez, N.; Kim, S. M.; Abdurehman, L.; York, B.; Chen, X.; Schnytzer, Y.; Levy, O.; Dacso, C. C.; McClung, C. A.; O'Malley, B. W.; Liu, S.; Zhu, B., 12-h clock regulation of genetic information flow by XBP1s. *PLoS Biol* **2020,** *18* (1), e3000580.

[33] Pluquet, O.; Dejeans, N.; Bouchecareilh, M.; Lhomond, S.; Pineau, R.; Higa, A.; Delugin, M.; Combe, C.; Loriot, S.; Cubel, G.; Dugot-Senant, N.; Vital, A.; Loiseau, H.; Gosline, S. J.; Taouji, S.; Hallett, M.; Sarkaria, J. N.; Anderson, K.; Wu, W.; Rodriguez, F. J.; Rosenbaum, J.; Saltel, F.; Fernandez-Zapico, M. E.; Chevet, E., Posttranscriptional regulation of PER1 underlies the oncogenic function of IREalpha. *Cancer Res* **2013,** *73* (15), 4732-43.

[34] Cretenet, G.; Le Clech, M.; Gachon, F., Circadian clock-coordinated 12 Hr period rhythmic activation of the IRE1alpha pathway controls lipid metabolism in mouse liver. *Cell Metab* **2010,** *11* (1), 47-57.

[35] Brandt, C.; Nolte, H.; Henschke, S.; Engstrom Ruud, L.; Awazawa, M.; Morgan, D. A.; Gabel, P.; Sprenger, H. G.; Hess, M. E.; Gunther, S.; Langer, T.; Rahmouni, K.; Fenselau, H.; Kruger, M.; Bruning, J. C., Food Perception Primes Hepatic ER Homeostasis via Melanocortin-Dependent Control of mTOR Activation. *Cell* **2018,** *175* (5), 1321-1335.e20.

[36] Madden, E.; Logue, S. E.; Healy, S. J.; Manie, S.; Samali, A., The role of the unfolded protein response in cancer progression: From oncogenesis to chemoresistance. *Biol Cell* **2019,** *111* (1), 1-17.

[37] Wong, M. Y.; Chen, K.; Antonopoulos, A.; Kasper, B. T.; Dewal, M. B.; Taylor, R. J.; Whittaker, C. A.; Hein, P. P.; Dell, A.; Genereux, J. C.; Haslam, S. M.; Mahal, L. K.; Shoulders, M. D., XBP1s activation can globally remodel N-glycan structure distribution patterns. *Proc Natl Acad Sci U S A* **2018,** *115* (43), E10089-E10098.

[38] Reily, C.; Stewart, T. J.; Renfrow, M. B.; Novak, J., Glycosylation in health and disease. *Nat Rev Nephrol* **2019,** *15* (6), 346-366.

[39] Shoulders, M. D.; Ryno, L. M.; Genereux, J. C.; Moresco, J. J.; Tu, P. G.; Wu, C.; Yates, J. R., 3rd; Su, A. I.; Kelly, J. W.; Wiseman, R. L., Stress-independent activation of XBP1s and/or ATF6 reveals three functionally diverse ER proteostasis environments. *Cell Rep* **2013,** *3* (4), 1279-92.

[40] Dewal, M. B.; DiChiara, A. S.; Antonopoulos, A.; Taylor, R. J.; Harmon, C. J.; Haslam, S. M.; Dell, A.; Shoulders, M. D., XBP1s Links the Unfolded Protein Response to the Molecular Architecture of Mature N-Glycans. *Chem Biol* **2015,** *22* (10), 1301-12.

[41] Cross, B. C.; Bond, P. J.; Sadowski, P. G.; Jha, B. K.; Zak, J.; Goodman, J. M.; Silverman, R. H.; Neubert, T. A.; Baxendale, I. R.; Ron, D.; Harding, H. P., The molecular basis for selective inhibition of unconventional mRNA splicing by an IRE1-binding small molecule. *Proc Natl Acad Sci U S A* **2012,** *109* (15), E869-78.

[42] Yoshida, H.; Matsui, T.; Yamamoto, A.; Okada, T.; Mori, K., XBP1 mRNA is induced by ATF6 and spliced by IRE1 in response to ER stress to produce a highly active transcription factor. *Cell* **2001,** *107* (7), 881-91.

[43] Lee, K.; Tirasophon, W.; Shen, X.; Michalak, M.; Prywes, R.; Okada, T.; Yoshida, H.; Mori, K.; Kaufman, R. J., IRE1-mediated unconventional mRNA splicing and S2P-mediated ATF6 cleavage merge to regulate XBP1 in signaling the unfolded protein response. *Genes Dev* **2002,** *16* (4), 452-66.

[44] Calfon, M.; Zeng, H.; Urano, F.; Till, J. H.; Hubbard, S. R.; Harding, H. P.; Clark, S. G.; Ron, D., IRE1 couples endoplasmic reticulum load to secretory capacity by processing the XBP-1 mRNA. *Nature* **2002,** *415* (6867), 92-6.

[45] Ghosh, R.; Wang, L.; Wang, E. S.; Perera, B. G.; Igbaria, A.; Morita, S.; Prado, K.; Thamsen, M.; Caswell, D.; Macias, H.; Weiberth, K. F.; Gliedt, M. J.; Alavi, M. V.; Hari, S. B.; Mitra, A. K.; Bhhatarai, B.; Schurer, S. C.; Snapp, E. L.; Gould, D. B.; German, M. S.; Backes, B. J.; Maly, D. J.; Oakes, S. A.; Papa, F. R., Allosteric inhibition of the IRE1alpha RNase preserves cell viability and function during endoplasmic reticulum stress. *Cell* **2014,** *158* (3), 534-48.

[46] Mahameed, M.; Wilhelm, T.; Darawshi, O.; Obiedat, A.; Tommy, W. S.; Chintha, C.; Schubert, T.; Samali, A.; Chevet, E.; Eriksson, L. A.; Huber, M.; Tirosh, B., The unfolded protein response modulators GSK2606414 and KIRA6 are potent KIT inhibitors. *Cell Death Dis* **2019,** *10* (4), 300.

[47] Wang, Y.; Zhang, Y.; Yi, P.; Dong, W.; Nalin, A. P.; Zhang, J.; Zhu, Z.; Chen, L.; Benson, D. M.; Mundy-Bosse, B. L.; Freud, A. G.; Caligiuri, M. A.; Yu, J., The IL-15-AKT-XBP1s signaling pathway contributes to effector functions and survival in human NK cells. *Nat Immunol* **2019,** *20* (1), 10-17.

[48] Grandjean, J. M. D.; Madhavan, A.; Cech, L.; Seguinot, B. O.; Paxman, R. J.; Smith, E.; Scampavia, L.; Powers, E. T.; Cooley, C. B.; Plate, L.; Spicer, T. P.; Kelly, J. W.; Wiseman, R. L., Pharmacologic IRE1/XBP1s Activation Confers Targeted Endoplasmic Reticulum Proteostasis Reprogramming. *Nature Chemical Biology* **2020,** *in press*.

[49] Prasad, V.; Suomalainen, M.; Jasiqi, Y.; Hemmi, S.; Hearing, P.; Hosie, L.; Burgert, H. G.; Greber, U. F., The UPR sensor IRE1alpha and the adenovirus E3-19K glycoprotein sustain persistent and lytic infections. *Nat Commun* **2020,** *11* (1), 1997.

[50] Sun, S.; Kelekar, S.; Kliewer, S. A.; Mangelsdorf, D. J., The orphan nuclear receptor SHP regulates ER stress response by inhibiting XBP1s degradation. *Genes Dev* **2019,** *33* (15-16), 1083-1094.

[51] Amin-Wetzel, N.; Neidhardt, L.; Yan, Y.; Mayer, M. P.; Ron, D., Unstructured regions in IRE1alpha specify BiP-mediated destabilisation of the luminal domain dimer and repression of the UPR. *Elife* **2019,** *8*.

[52] Rosen, D. A.; Seki, S. M.; Fernandez-Castaneda, A.; Beiter, R. M.; Eccles, J. D.; Woodfolk, J. A.; Gaultier, A., Modulation of the sigma-1 receptor-IRE1 pathway is beneficial in preclinical models of inflammation and sepsis. *Sci Transl Med* **2019,** *11* (478).

[53] Poe, C.; Youngblood, C.; Hodge, K.; Kemp, K., Treatment of established TH2 cells with 4mu8c, an inhibitor of IRE1alpha, blocks IL-5 but not IL-4 secretion. *BMC Immunol* **2019,** *20* (1), 3.

[54] Urano, Y.; Ho Vo, D. K.; Hirofumi, A.; Noguchi, N., 24(S)-Hydroxycholesterol induces ER dysfunction-mediated unconventional cell death. *Cell Death Discov* **2019,** *5*, 113.

[55] Cole, K. S.; Grandjean, J. M. D.; Chen, K.; Witt, C. H.; O'Day, J.; Shoulders, M. D.; Wiseman, R. L.; Weerapana, E., Characterization of an A-Site Selective Protein Disulfide Isomerase A1 Inhibitor. *Biochemistry* **2018,** *57* (13), 2035-2043.

[56] Pilobello, K. T.; Slawek, D. E.; Mahal, L. K., A ratiometric lectin microarray approach to analysis of the dynamic mammalian glycome. *Proc Natl Acad Sci U S A* **2007,** *104* (28), 11534-9.

[57] Haslam, S. M.; North, S. J.; Dell, A., Mass spectrometric analysis of N- and O-glycosylation of tissues and cells. *Curr Opin Struct Biol* **2006,** *16* (5), 584-91.

[58] Sebastian, R. M.; Shoulders, M. D., Chemical Biology Framework to Illuminate Proteostasis. *Annu Rev Biochem* **2020**.

[59] Yoshida, H.; Oku, M.; Suzuki, M.; Mori, K., pXBP1(U) encoded in XBP1 pre-mRNA negatively regulates unfolded protein response activator pXBP1(S) in mammalian ER stress response. *J Cell Biol* **2006,** *172* (4), 565-75.

[60] Tirosh, B.; Iwakoshi, N. N.; Glimcher, L. H.; Ploegh, H. L., Rapid turnover of unspliced Xbp-1 as a factor that modulates the unfolded protein response. *J Biol Chem* **2006,** *281* (9), 5852-60.

[61] Adachi, Y.; Yamamoto, K.; Okada, T.; Yoshida, H.; Harada, A.; Mori, K., ATF6 is a transcription factor specializing in the regulation of quality control proteins in the endoplasmic reticulum. *Cell Struct Funct* **2008,** *33* (1), 75-89.

[62] Lee, A. H.; Iwakoshi, N. N.; Glimcher, L. H., XBP-1 regulates a subset of endoplasmic reticulum resident chaperone genes in the unfolded protein response. *Mol Cell Biol* **2003,** *23* (21), 7448-59.

[63] Scheuner, D.; Song, B.; McEwen, E.; Liu, C.; Laybutt, R.; Gillespie, P.; Saunders, T.; Bonner-Weir, S.; Kaufman, R. J., Translational control is required for the unfolded protein response and in vivo glucose homeostasis. *Mol Cell* **2001,** *7* (6), 1165-76.

[64] Harding, H. P.; Novoa, I.; Zhang, Y.; Zeng, H.; Wek, R.; Schapira, M.; Ron, D., Regulated translation initiation controls stress-induced gene expression in mammalian cells. *Mol Cell* **2000,** *6* (5), 1099-108.

[65] Shapiro, I. M.; Cheng, A. W.; Flytzanis, N. C.; Balsamo, M.; Condeelis, J. S.; Oktay, M. H.; Burge, C. B.; Gertler, F. B., An EMT-driven alternative splicing program occurs in human breast cancer and modulates cellular phenotype. *PLoS Genet* **2011,** *7* (8), e1002218.

[66] Ye, I. C.; Fertig, E. J.; DiGiacomo, J. W.; Considine, M.; Godet, I.; Gilkes, D. M., Molecular Portrait of Hypoxia in Breast Cancer: A Prognostic Signature and Novel HIF-Regulated Genes. *Mol Cancer Res* **2018,** *16* (12), 1889-1901.

[67] Hu, Z.; Fan, C.; Livasy, C.; He, X.; Oh, D. S.; Ewend, M. G.; Carey, L. A.; Subramanian, S.; West, R.; Ikpatt, F.; Olopade, O. I.; van de Rijn, M.; Perou, C. M., A compact VEGF signature associated with distant metastases and poor outcomes. *BMC Med* **2009,** *7*, 9.

[68] Bender, R. J.; Mac Gabhann, F., Expression of VEGF and semaphorin genes define subgroups of triple negative breast cancer. *PLoS One* **2013,** *8* (5), e61788.

[69] Cui, H.; Lin, Y.; Yue, L.; Zhao, X.; Liu, J., Differential expression of the alpha2,3-sialic acid residues in breast cancer is associated with metastatic potential. *Oncol Rep* **2011,** *25* (5), 1365-71.

[70] Kohler, R. S.; Anugraham, M.; Lopez, M. N.; Xiao, C.; Schoetzau, A.; Hettich, T.; Schlotterbeck, G.; Fedier, A.; Jacob, F.; Heinzelmann-Schwarz, V., Epigenetic activation of MGAT3 and corresponding bisecting GlcNAc shortens the survival of cancer patients. *Oncotarget* **2016,** *7* (32), 51674-51686.

[71] Keeley, T. S.; Yang, S.; Lau, E., The Diverse Contributions of Fucose Linkages in Cancer. *Cancers (Basel)* **2019,** *11* (9).

[72] Lau, E.; Feng, Y.; Claps, G.; Fukuda, M. N.; Perlina, A.; Donn, D.; Jilaveanu, L.; Kluger, H.; Freeze, H. H.; Ronai, Z. A., The transcription factor ATF2 promotes melanoma metastasis by suppressing protein fucosylation. *Sci Signal* **2015,** *8* (406), ra124.

[73] Laughlin, S. T.; Bertozzi, C. R., Imaging the glycome. *Proc Natl Acad Sci U S A* **2009,** *106* (1), 12-7.

[74] Thu, C. T.; Mahal, L. K., Sweet Control: MicroRNA Regulation of the Glycome. *Biochemistry* **2019**.

[75] Nairn, A. V.; York, W. S.; Harris, K.; Hall, E. M.; Pierce, J. M.; Moremen, K. W., Regulation of glycan structures in animal tissues: transcript profiling of glycan-related genes. *J Biol Chem* **2008,** *283* (25), 17298-313.

[76] Holst, S.; Deuss, A. J.; van Pelt, G. W.; van Vliet, S. J.; Garcia-Vallejo, J. J.; Koeleman, C. A.; Deelder, A. M.; Mesker, W. E.; Tollenaar, R. A.; Rombouts, Y.; Wuhrer, M., N-glycosylation Profiling of Colorectal Cancer Cell Lines Reveals Association of Fucosylation with Differentiation and Caudal Type Homebox 1 (CDX1)/Villin mRNA Expression. *Mol Cell Proteomics* **2016,** *15* (1), 124-40.

[77] Kohnz, R. A.; Roberts, L. S.; DeTomaso, D.; Bideyan, L.; Yan, P.; Bandyopadhyay, S.; Goga, A.; Yosef, N.; Nomura, D. K., Protein Sialylation Regulates a Gene Expression Signature that Promotes Breast Cancer Cell Pathogenicity. *ACS Chem Biol* **2016,** *11* (8), 2131-9.

[78] Ma, X.; Dong, W.; Su, Z.; Zhao, L.; Miao, Y.; Li, N.; Zhou, H.; Jia, L., Functional roles of sialylation in breast cancer progression through miR-26a/26b targeting ST8SIA4. *Cell Death Dis* **2016,** *7* (12), e2561.

[79] Vaiana, C. A.; Kurcon, T.; Mahal, L. K., MicroRNA-424 Predicts a Role for beta-1,4 Branched Glycosylation in Cell Cycle Progression. *J Biol Chem* **2016,** *291* (3), 1529-37.

[80] Chen, F.; Luo, N.; Hu, Y.; Li, X.; Zhang, K., MiR-137 Suppresses Triple-Negative Breast Cancer Stemness and Tumorigenesis by Perturbing BCL11A-DNMT1 Interaction. *Cell Physiol Biochem* **2018,** *47* (5), 2147-2158.

[81] Flavahan, W. A.; Gaskell, E.; Bernstein, B. E., Epigenetic plasticity and the hallmarks of cancer. *Science* **2017,** *357* (6348).

[82] Aprelikova, O.; Chen, K.; El Touny, L. H.; Brignatz-Guittard, C.; Han, J.; Qiu, T.; Yang, H. H.; Lee, M. P.; Zhu, M.; Green, J. E., The epigenetic modifier JMJD6 is amplified in mammary tumors and cooperates with c-Myc to enhance cellular transformation, tumor progression, and metastasis. *Clin Epigenetics* **2016,** *8*, 38.

[83] Liu, Y.; Long, Y. H.; Wang, S. Q.; Zhang, Y. Y.; Li, Y. F.; Mi, J. S.; Yu, C. H.; Li, D. Y.; Zhang, J. H.; Zhang, X. J., JMJD6 regulates histone H2A.X phosphorylation and promotes autophagy in

triple-negative breast cancer cells via a novel tyrosine kinase activity. *Oncogene* **2019,** *38* (7), 980-997.

[84] Gao, W. W.; Xiao, R. Q.; Zhang, W. J.; Hu, Y. R.; Peng, B. L.; Li, W. J.; He, Y. H.; Shen, H. F.; Ding, J. C.; Huang, Q. X.; Ye, T. Y.; Li, Y.; Liu, Z. Y.; Ding, R.; Rosenfeld, M. G.; Liu, W., JMJD6 Licenses ERalpha-Dependent Enhancer and Coding Gene Activation by Modulating the Recruitment of the CARM1/MED12 Co-activator Complex. *Mol Cell* **2018,** *70* (2), 340-357.e8.

[85] Cho, Y. M.; Kim, T. M.; Hun Kim, D.; Hee Kim, D.; Jeong, S. W.; Kwon, O. J., miR-148a is a downstream effector of X-box-binding protein 1 that silences Wnt10b during adipogenesis of 3T3-L1 cells. *Exp Mol Med* **2016,** *48*, e226.

[86] Morotti, M.; Bridges, E.; Valli, A.; Choudhry, H.; Sheldon, H.; Wigfield, S.; Gray, N.; Zois, C. E.; Grimm, F.; Jones, D.; Teoh, E. J.; Cheng, W. C.; Lord, S.; Anastasiou, D.; Haider, S.; McIntyre, A.; Goberdhan, D. C. I.; Buffa, F.; Harris, A. L., Hypoxia-induced switch in SNAT2/SLC38A2 regulation generates endocrine resistance in breast cancer. *Proc Natl Acad Sci U S A* **2019,** *116* (25), 12452-12461.

[87] Ren, Y.; Hao, P.; Law, S. K.; Sze, S. K., Hypoxia-induced changes to integrin alpha 3 glycosylation facilitate invasion in epidermoid carcinoma cell line A431. *Mol Cell Proteomics* **2014,** *13* (11), 3126-37.

[88] Zhang, D.; Yang, L.; Liu, X.; Gao, J.; Liu, T.; Yan, Q.; Yang, X., Hypoxia modulates stem cell properties and induces EMT through N-glycosylation of EpCAM in breast cancer cells. *J Cell Physiol* **2020,** *235* (4), 3626-3633.

[89] Guillaumond, F.; Leca, J.; Olivares, O.; Lavaut, M. N.; Vidal, N.; Berthezene, P.; Dusetti, N. J.; Loncle, C.; Calvo, E.; Turrini, O.; Iovanna, J. L.; Tomasini, R.; Vasseur, S., Strengthened glycolysis under hypoxia supports tumor symbiosis and hexosamine biosynthesis in pancreatic adenocarcinoma. *Proc Natl Acad Sci U S A* **2013,** *110* (10), 3919-24.

[90] Koike, T.; Kimura, N.; Miyazaki, K.; Yabuta, T.; Kumamoto, K.; Takenoshita, S.; Chen, J.; Kobayashi, M.; Hosokawa, M.; Taniguchi, A.; Kojima, T.; Ishida, N.; Kawakita, M.; Yamamoto, H.; Takematsu, H.; Suzuki, A.; Kozutsumi, Y.; Kannagi, R., Hypoxia induces adhesion molecules on cancer cells: A missing link between Warburg effect and induction of selectin-ligand carbohydrates. *Proc Natl Acad Sci U S A* **2004,** *101* (21), 8132-7.

[91] Croci, D. O.; Cerliani, J. P.; Dalotto-Moreno, T.; Mendez-Huergo, S. P.; Mascanfroni, I. D.; Dergan-Dylon, S.; Toscano, M. A.; Caramelo, J. J.; Garcia-Vallejo, J. J.; Ouyang, J.; Mesri, E. A.; Junttila, M. R.; Bais, C.; Shipp, M. A.; Salatino, M.; Rabinovich, G. A., Glycosylation-dependent lectin-receptor interactions preserve angiogenesis in anti-VEGF refractory tumors. *Cell* **2014,** *156* (4), 744-58.

[92] Swindall, A. F.; Bellis, S. L., Sialylation of the Fas death receptor by ST6Gal-I provides protection against Fas-mediated apoptosis in colon carcinoma cells. *J Biol Chem* **2011,** *286* (26), 22982-90.

[93] Logue, S. E.; McGrath, E. P.; Cleary, P.; Greene, S.; Mnich, K.; Almanza, A.; Chevet, E.; Dwyer, R. M.; Oommen, A.; Legembre, P.; Godey, F.; Madden, E. C.; Leuzzi, B.; Obacz, J.; Zeng, Q.; Patterson, J. B.; Jager, R.; Gorman, A. M.; Samali, A., Inhibition of IRE1 RNase activity modulates the tumor cell secretome and enhances response to chemotherapy. *Nat Commun* **2018,** *9* (1), 3267.

[94] Kolb, R.; Kluz, P.; Tan, Z. W.; Borcherding, N.; Bormann, N.; Vishwakarma, A.; Balcziak, L.; Zhu, P.; Davies, B. S.; Gourronc, F.; Liu, L. Z.; Ge, X.; Jiang, B. H.; Gibson-Corley, K.; Klingelhutz, A.; Tan, N. S.; Zhu, Y.; Sutterwala, F. S.; Shen, X.; Zhang, W., Obesity-associated inflammation promotes angiogenesis and breast cancer via angiopoietin-like 4. *Oncogene* **2019,** *38* (13), 2351-2363.

[95] Lee, H. H.; Wang, Y. N.; Xia, W.; Chen, C. H.; Rau, K. M.; Ye, L.; Wei, Y.; Chou, C. K.; Wang, S. C.; Yan, M.; Tu, C. Y.; Hsia, T. C.; Chiang, S. F.; Chao, K. S. C.; Wistuba, II; Hsu, J. L.; Hortobagyi, G. N.; Hung, M. C., Removal of N-Linked Glycosylation Enhances PD-L1 Detection and Predicts Anti-PD-1/PD-L1 Therapeutic Efficacy. *Cancer Cell* **2019,** *36* (2), 168-178.e4.

[96] Li, C. W.; Lim, S. O.; Chung, E. M.; Kim, Y. S.; Park, A. H.; Yao, J.; Cha, J. H.; Xia, W.; Chan, L. C.; Kim, T.; Chang, S. S.; Lee, H. H.; Chou, C. K.; Liu, Y. L.; Yeh, H. C.; Perillo, E. P.; Dunn, A. K.; Kuo, C. W.; Khoo, K. H.; Hsu, J. L.; Wu, Y.; Hsu, J. M.; Yamaguchi, H.; Huang, T. H.; Sahin, A. A.; Hortobagyi, G. N.; Yoo, S. S.; Hung, M. C., Eradication of Triple-Negative Breast Cancer Cells by Targeting Glycosylated PD-L1. *Cancer Cell* **2018,** *33* (2), 187-201.e10.

[97] Wang, M.; Wang, J.; Wang, R.; Jiao, S.; Wang, S.; Zhang, J.; Zhang, M., Identification of a monoclonal antibody that targets PD-1 in a manner requiring PD-1 Asn58 glycosylation. *Commun Biol* **2019,** *2*, 392.

[98] Hsu, J. M.; Xia, W.; Hsu, Y. H.; Chan, L. C.; Yu, W. H.; Cha, J. H.; Chen, C. T.; Liao, H. W.; Kuo, C. W.; Khoo, K. H.; Hsu, J. L.; Li, C. W.; Lim, S. O.; Chang, S. S.; Chen, Y. C.; Ren, G. X.; Hung, M. C., STT3-dependent PD-L1 accumulation on cancer stem cells promotes immune evasion. *Nat Commun* **2018,** *9* (1), 1908.

[99] Li, C. W.; Lim, S. O.; Xia, W.; Lee, H. H.; Chan, L. C.; Kuo, C. W.; Khoo, K. H.; Chang, S. S.; Cha, J. H.; Kim, T.; Hsu, J. L.; Wu, Y.; Hsu, J. M.; Yamaguchi, H.; Ding, Q.; Wang, Y.; Yao, J.; Lee, C. C.; Wu, H. J.; Sahin, A. A.; Allison, J. P.; Yu, D.; Hortobagyi, G. N.; Hung, M. C., Glycosylation and stabilization of programmed death ligand-1 suppresses T-cell activity. *Nat Commun* **2016,** *7*, 12632.

[100] Neve, R. M.; Chin, K.; Fridlyand, J.; Yeh, J.; Baehner, F. L.; Fevr, T.; Clark, L.; Bayani, N.; Coppe, J. P.; Tong, F.; Speed, T.; Spellman, P. T.; DeVries, S.; Lapuk, A.; Wang, N. J.; Kuo, W. L.; Stilwell, J. L.; Pinkel, D.; Albertson, D. G.; Waldman, F. M.; McCormick, F.; Dickson, R. B.; Johnson, M. D.; Lippman, M.; Ethier, S.; Gazdar, A.; Gray, J. W., A collection of breast cancer cell lines for the study of functionally distinct cancer subtypes. *Cancer Cell* **2006,** *10* (6), 515-27.

[101] Schmittgen, T. D.; Livak, K. J., Analyzing real-time PCR data by the comparative C(T) method. *Nat Protoc* **2008,** *3* (6), 1101-8.

[102] Livak, K. J.; Schmittgen, T. D., Analysis of relative gene expression data using real-time quantitative PCR and the 2(-Delta Delta C(T)) Method. *Methods* **2001,** *25* (4), 402-8.

[103] Soumillon, M.; Cacchiarelli, D.; Semrau, S.; van Oudenaarden, A.; Mikkelsen, T. S., Characterization of directed differentiation by high-throughput single-cell RNA-Seq. *bioRxiv* **2014**, 003236.

[104] Dobin, A.; Davis, C. A.; Schlesinger, F.; Drenkow, J.; Zaleski, C.; Jha, S.; Batut, P.; Chaisson, M.; Gingeras, T. R., STAR: ultrafast universal RNA-seq aligner. *Bioinformatics* **2013,** *29* (1), 15-21.

[105] Li, H.; Handsaker, B.; Wysoker, A.; Fennell, T.; Ruan, J.; Homer, N.; Marth, G.; Abecasis, G.; Durbin, R., The Sequence Alignment/Map format and SAMtools. *Bioinformatics* **2009,** *25* (16), 2078-9.

[106] Derr, A.; Yang, C.; Zilionis, R.; Sergushichev, A.; Blodgett, D. M.; Redick, S.; Bortell, R.; Luban, J.; Harlan, D. M.; Kadener, S.; Greiner, D. L.; Klein, A.; Artyomov, M. N.; Garber, M., End Sequence Analysis Toolkit (ESAT) expands the extractable information from single-cell RNA-seq data. *Genome Res* **2016,** *26* (10), 1397-1410.

[107] Love, M. I.; Huber, W.; Anders, S., Moderated estimation of fold change and dispersion for RNA-seq data with DESeq2. *Genome Biol* **2014,** *15* (12), 550.

[108] Mootha, V. K.; Lindgren, C. M.; Eriksson, K. F.; Subramanian, A.; Sihag, S.; Lehar, J.; Puigserver, P.; Carlsson, E.; Ridderstrale, M.; Laurila, E.; Houstis, N.; Daly, M. J.; Patterson, N.; Mesirov, J. P.; Golub, T. R.; Tamayo, P.; Spiegelman, B.; Lander, E. S.; Hirschhorn, J. N.; Altshuler, D.; Groop, L. C., PGC-1alpha-responsive genes involved in oxidative phosphorylation are coordinately downregulated in human diabetes. *Nat Genet* **2003,** *34* (3), 267-73.

[109] Subramanian, A.; Tamayo, P.; Mootha, V. K.; Mukherjee, S.; Ebert, B. L.; Gillette, M. A.; Paulovich, A.; Pomeroy, S. L.; Golub, T. R.; Lander, E. S.; Mesirov, J. P., Gene set enrichment analysis: a knowledge-based approach for interpreting genome-wide expression profiles. *Proc Natl Acad Sci U S A* **2005,** *102* (43), 15545-50.

[110] Quinlan, A. R.; Hall, I. M., BEDTools: a flexible suite of utilities for comparing genomic features. *Bioinformatics* **2010,** *26* (6), 841-2.

[111] Pilobello, K. T.; Agrawal, P.; Rouse, R.; Mahal, L. K., Advances in lectin microarray technology: optimized protocols for piezoelectric print conditions. *Curr Protoc Chem Biol* **2013,** *5* (1), 1-23.

[112] Jang-Lee, J.; North, S. J.; Sutton-Smith, M.; Goldberg, D.; Panico, M.; Morris, H.; Haslam, S.; Dell, A., Glycomic profiling of cells and tissues by mass spectrometry: fingerprinting and sequencing methodologies. *Methods Enzymol* **2006,** *415*, 59-86.

[113] Ceroni, A.; Maass, K.; Geyer, H.; Geyer, R.; Dell, A.; Haslam, S. M., GlycoWorkbench: a tool for the computer-assisted annotation of mass spectra of glycans. *J Proteome Res* **2008,** *7* (4), 1650-9.

Chapter 4

Mechanistic Exploration of the IRE1 Negative Feedback Loop

Summary

The unfolded protein response (UPR) mitigates endoplasmic reticulum (ER) stress by enhancing the secretory pathway's protein folding capacity, upregulating the expression of chaperone proteins and quality control factors. The UPR can also transiently arrest protein translation to reduce the new protein load in the ER. The three stress sensors of the UPR—IRE1, PERK, and ATF6—are responsible for transmitting signals through their respective downstream transcription factors. Unresolved ER stress commits cells to apoptosis through PERK signaling. Mechanisms of regulating the stress sensors, in particular IRE1, are often debated. Hypotheses include activation via unfolded proteins binding directly to the stress sensors, as well as a more widely accepted model of chaperone-mediated repression, whereby binding to the BiP chaperone represses signaling. While small molecules have been developed to target and activate IRE1 signaling, the compounds are often cytotoxic or lead to transient activation that lasts just a few hours. Two ER co-chaperones, ERdj4 and Sec63 (also known as ERdj2), have been shown to recruit BiP to form repressive complexes with IRE1. Thus, as downstream targets of IRE1 activation, ERdj4 and BiP function in a negative feedback loop to restrict IRE1 activation. We hypothesized that ERdj4 and Sec63 are responsible for limiting pharmacological activation of IRE1, and that activation could be sustained with loss of ERdj4 or Sec63. Here, we employed CRISPR-Cas9 technology to knockout ERdj4 in HEK293 cells, and tested whether pharmacological IRE1 activation could be sustained. Additionally, we tested our hypothesis in Sec63 knockout HEK293 cells. We determined that neither loss of ERdj4 nor Sec63 was sufficient to sustain pharmacological IRE1 activation, suggesting that other repressive elements are likely regulating the UPR.

Introduction

The unfolded protein response (UPR) safeguards cells against toxic protein-misfolding stress. Accumulation of misfolded proteins in the endoplasmic reticulum (ER) activates the transmembrane sensor proteins IRE1, PERK, and ATF6 (**Figure 4.1*A***). Dimerization and autophosphorylation of IRE1 and PERK, or trafficking and proteolytic processing of ATF6, result in the production of three UPR transcription factors. The dual-function enzyme IRE1 is capable of *trans*-autophosphorylation via its kinase domain, leading to a conformational change activating its RNase domain, which is responsible for splicing *XBP1* mRNA to yield the active transcription factor, spliced XBP1 (XBP1s).[1-3] PERK autophosphorylation leads to conformation shifts in the kinase domain and enhances its affinity for the non-phosphorylated eIF2 eukaryotic translation initiation complex.[4] Phosphorylation of eIF2α ultimately leads to a transient arrest in global protein translation while selectively enhancing translation of the ATF4 transcription factor.[5-6] Trafficking of ATF6 to the Golgi and proteolytic processing by S1P and S2P proteases releases ATF6f from the Golgi membrane, allowing the transcription factor to traffic to the nucleus.[7-8] The activities of XBP1s, ATF4, and ATF6f collectively remodel the ER proteostasis environment by upregulating chaperones, quality control factors, and other UPR target genes to maintain or recover secretory proteostasis.[9] Unresolved ER stress and chronic activation of the PERK arm can lead to apoptosis, threatening tissue homeostasis.[10] ER stress is linked to the development of diabetes, obesity, atherosclerosis, and other metabolic diseases. There is active interest in developing small molecules to target specific branches of the UPR to mitigate ER stress or to improve protein folding capacity, while avoiding its destructive outputs.

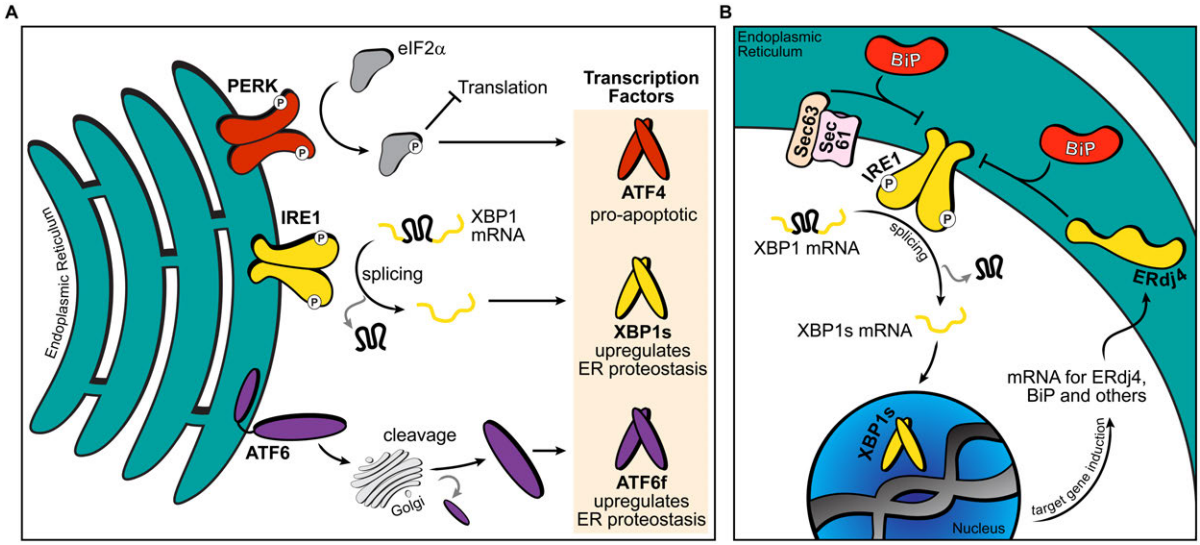

Figure 4.1: The three branches of the unfolded protein response. ***A***: PERK, IRE1, and ATF6 signal to their downstream transcription factors ATF4, XBP1s, and ATF6f, respectively, in response to ER stress. ***B***: Negative feedback loops regulate IRE1 signaling. Activation of the IRE1-XBP1s pathway upregulates the expression of proteostasis network components, including ERdj4 and BiP. ERdj4 and the Sec63 translocon complex protein can recruit BiP to repress IRE1 activity.

The IRE1-XBP1s arm of the UPR displays cytoprotective functions against acute stress, injury, and apoptosis induced by viral infections, and is also capable of prolonging cell and organism survival.[11-24] Well-characterized IRE1 activators with desired potency profiles have the potential to be harnessed for treating diseases such as amyloid-associated neurotoxicity or diabetes. For example, control of IRE1 can positively regulate insulin biosynthesis and secretion.[25-27] However, chronic hyperactivation of IRE1 can suppress insulin gene expression.[26] Thus, tight control of IRE1 activation and temporal regulation are important factors for clinical development of such modulators.

Various IRE1 inhibitors such as STF-083010 and 4μ8C (**Figure 4.2**) have been applied to elucidate novel functions of the IRE1-XBP1s pathway in biology, including its roles in inflammation, atherosclerosis progression, and natural killer cell function in the immune system.[28-31] However, compounds that can stimulate IRE1 activity exhibit less than ideal properties, including off-target cytotoxicity[32-33] and mild activation lasting only a few hours,[34] limiting their efficacy as potential long-term therapies. Kinase inhibitors such as APY29 and the FDA-approved sunitinib for cancer[35-38] (**Figure 4.2**) were also shown to activate the IRE1 RNase domain. As type I kinase inhibitors, APY29 and sunitinib act as IRE1 RNase agonists, inducing dimerization and RNase activity, by engaging the ATP-binding pocket and inducing a conformational change to mimic the active conformation.[39] However, animal studies and preclinical models with these compounds are currently lacking, and the compounds are not sufficiently selective.[40] Compounds targeting new potential drug-binding sites on IRE1 include the flavanol quercetin (**Figure 4.2**), which was identified as a yeast IRE1 activator via an *in vitro* fluorescence quenching-based screening approach.[41] Quercetin promoted IRE1 dimerization and RNase activation as a result of binding to the so-called Q-site at the dimer interface of the kinase-RNase domain. However, quercetin is a promiscuous compound that hits multiple targets, and is a well-known aggregator and pan-assay interference compound (PAIN), and thus not suitable as a lead compound.[42-44] A second-generation IRE1 activator, termed IPA (**Figure 4.2**), was designed from the APY29 scaffold and was shown to induce IRE1 oligomerization and RNase activity, but at the expense of strong cytotoxicity and PERK activity induction specifically at paradoxically low concentrations.[32] In our hands (unpublished results), it was very difficult to uncouple PERK activation and cytotoxicity from IRE1 activation. The opposing effects of IPA emphasize the importance of tightly controlled UPR activation profiles by small molecules to avoid unintended effects.

Recently, a luciferase-based high-throughput screening approach performed in conjunction with transcriptomic and phosphokinase profiling identified a novel, selective IRE1 activator that targets IRE1 independent of the nucleotide-binding pocket.[45] The small molecule, termed Compound **474 (Figure 4.2)**, was shown to reduce secretion of toxic amyloid precursor protein (APP) and reduced APP-associated mitochondrial toxicity in cellular models. Although the exact mechanism of activation remains unknown,

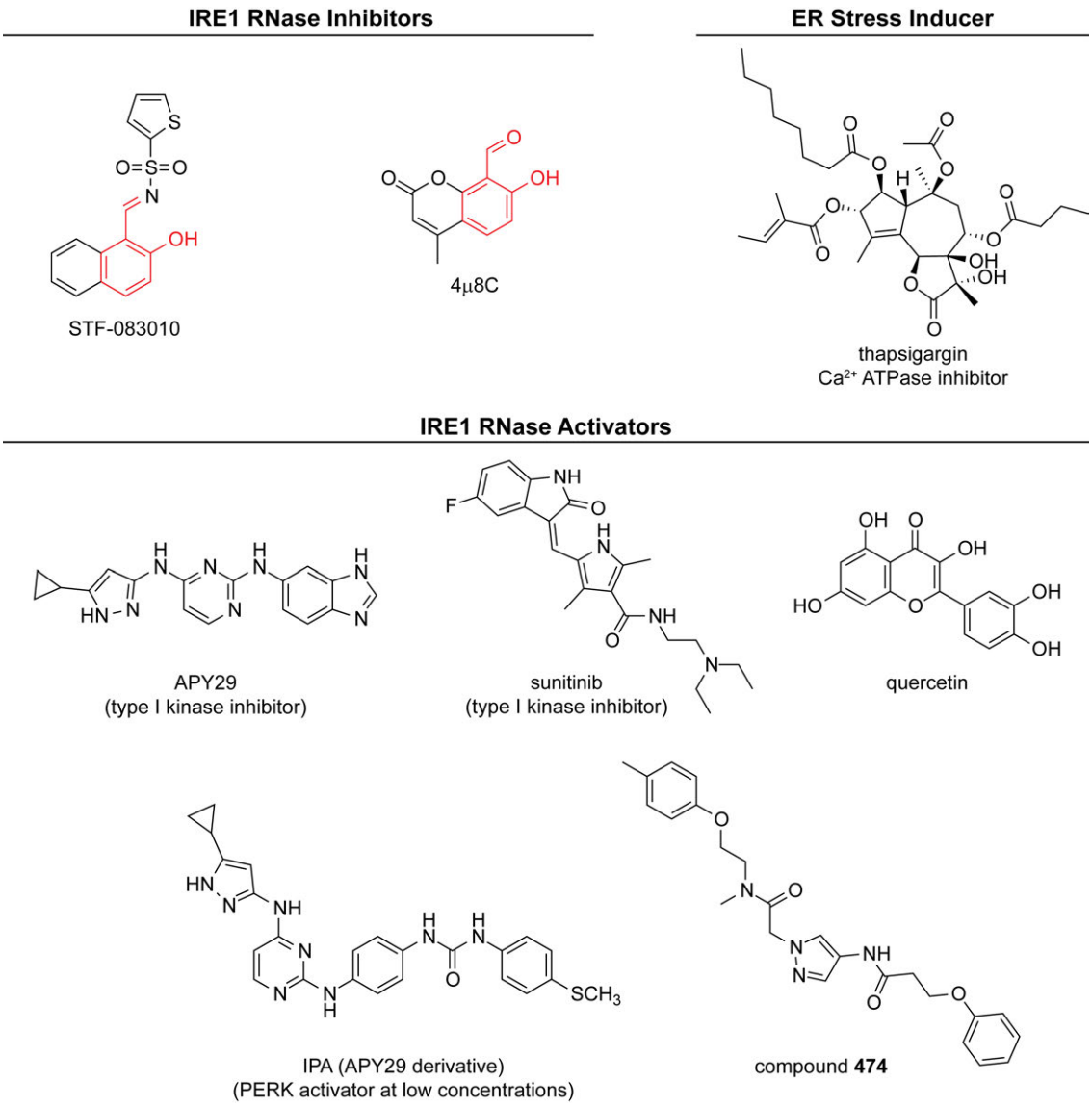

Figure 4.2: Chemical structures of IRE1 modulators and the ER stressor thapsigargin. IRE1 RNase inhibitors including STF-083010 and 4μ8C commonly feature the salicylaldehyde pharmacophore (red) that inhibits RNase activity by forming a Schiff base with the active site. Global UPR activity can be induced by an ER stressor such as the Ca^{2+} ATPase inhibitor thapsigargin. IRE1 RNase activators include APY29 and its derivative IPA, sunitinib, and quercetin, but these compounds display off-target cytoxicity and promiscuous binding. The novel compound **474** selectively activates IRE1 without binding to the kinase active site, but its mechanism of action is currently unknown.

474 does not rely on binding to the IRE1 kinase active site, in contrast to other IRE1 activators, suggesting that off-target cytotoxicity associated with other activators may not be an issue with **474**. Novel compounds such as **474** are distinct from previously reported IRE1 activators, and have the potential to modulate IRE1 signaling without off-pathway activity, thus representing a first-in-class IRE1 activator with potential to alleviate proteostasis pathologies such as Alzheimer's and diabetes. However, the long-term effects of **474** treatment on cells have not been not reported.

The existence of a negative feedback loop counteracting IRE1 activation could explain the lack of sustained IRE1 activation by small molecules (see Figure 4.3 below).[34] ERdj4, an Hsp40 co-chaperone, was demonstrated to recruit BiP, an Hsp70 chaperone, to IRE1 to form a repressive BiP-IRE1 complex (**Figure 4.1*B***).[46] ERdj4-directed BiP-mediated repression was capable of disrupting IRE1 dimers and reducing XBP1s activation when measured using a fluorescent reporter system. Furthermore, it was shown that BiP client proteins competed for the repressive machinery to restore IRE1 to its default, dimeric active state. ERdj4 and BiP are transcriptional targets of XBP1s,[47-48] thus they act in a negative feedback loop to attenuate IRE1 activity. The work described above involved genetically inactivated ERdj4 in Chinese Hamster Ovary (CHO) cell lines and measured IRE1 activity with an XBP1s–turquoise fluorescent reporter for *XBP1* splicing.[46] However, the reporter construct lacked the DNA-binding domain of XBP1s, rendering the reporter incapable of activating downstream targets, and with uncertain biological relevance to endogenous IRE1-XBP1s signaling. Furthermore, recombinant ERdj4, BiP, and IRE1 proteins were purified and reconstituted *in vitro* for mechanistic work, also leaving uncertainty whether the findings extended to endogenous systems. This initial study supported a hypothesis for a reversible chaperone repression model,[46] and could explain the inverse correlation between IRE1 activity and ER-localized BiP expression reported elsewhere.[49-51] In follow-up work, it was shown that loading endogenous BiP onto endogenous IRE1 also repressed IRE1 signaling in CHO cells.[52] An ERdj4-directed BiP-mediated model of repression (**Figure 4.1*B***) could explain why small molecules targeting IRE1 for activation fail to sustain activity past a few hours.

Another model for IRE1 repression involves recruitment of BiP to IRE1 by the Sec63 (also known as ERdj2) co-chaperone. The translocon complex, comprised namely of the Sec61 channel and the Sec62 and Sec63 proteins, mediates transfer of secretory proteins into the ER. Sec61 and Sec63 were previously demonstrated to limit IRE1 signaling.[53-58] Specifically, Sec63 recruits BiP to bind to IRE1 in complex with Sec61 (but not Sec62) in cells and in biochemical reconstitution assays *in vitro*, suppressing IRE1 oligomerization and attenuating its RNase activity (**Figure 4.1*B***).[53] Thus, the Sec63-directed BiP-mediated model of repression is analogous to the ERdj4-directed model. Moreover, as Sec63 comprises part of the Sec61 translocon complex, it is hypothesized that Sec63 couples IRE1-mediated protein folding capacity with the flux of proteins into the ER to maintain ER proteostasis.[53, 57] We further hypothesized that inactivation of Sec63 may be another method to sustain IRE1 activation by small molecules.

Here, motivated by the chaperone-mediated repression model for regulating IRE1 activity, whereby either ERdj4 or Sec63 recruits BiP to form repressive complexes with IRE1, we assessed whether pharmacological IRE1 activation with the small molecule **474** can be sustained in HEK293 cells with genetic inactivation of either ERdj4 or Sec63.

Results

Pharmacological Activation of IRE1 Is Short-Lived

We first assessed IRE1 activation by the small molecule **474** in HEK293T cells at 10 μM, a concentration previously demonstrated to activate IRE1 and reprogram ER proteostasis in this cell line (**Figure 4.3**).[45] HEK293T cells were treated with **474** at 2-, 4-, 6-, and 24-hour time points, and RNA was extracted for quantitative real-time PCR (qRT-PCR) of *XBP1* splicing and UPR target gene induction. Consistent with previous findings,[45] treatment with **474** induced *XBP1* splicing and upregulation of transcripts for Sec24D and ERdj4, two XBP1s targets (**Figure 4.3 *A* – *C***). However, IRE1 activation could not be sustained past 6 hours when downstream *XBP1* splicing and target gene induction were profiled. Peak *XBP1* splicing was observed at the 2-hour time point (3.7-fold increase relative to DMSO), and peak ERdj4 mRNA upregulation was observed at the 4-hour time point (2.9-fold increase relative to DMSO). Thapsigargin-treated cells were included as positive controls for IRE1, ATF6, and PERK activity. Upregulation of Sec24D mRNA was not as robust (even under thapsigargin treatment) with a maximal increase of 1.9-fold at the 6-hour time point. BiP and HYOU1 are UPR targets regulated by both IRE1-XBP1s and ATF6 signaling. Treatment with **474** led to modest (at most 2-fold) increases in BiP and HYOU1 mRNA (**Figure 4.3 *D*** and ***E***), but not for the PERK target CHOP (**Figure 4.3*F***) indicating that **474** treatment did not lead to off-target UPR activity. We hypothesized that negative regulation of IRE1 activity directed by ERdj4 or Sec63 could be repressing *XBP1* splicing and ERdj4 mRNA induction at the later time points.

Employing CRISPR-Cas9 to Inactivate ERdj4 in Human Cells

To test our hypothesis whether loss of ERdj4 is sufficient to sustain pharmacological activation of IRE1, we applied CRISPR-Cas9 technology[59-60] to inactivate ERdj4 (encoded by the *DNAJB9* gene) via insertions or deletions (indels) in the HEK293T human cell line (**Figure 4.4*A***). We cloned five single guide RNAs (sgRNAs) targeting ERdj4, in addition to non-targeting controls, into Cas9 plasmids.[59] Cloned plasmids were then transfected into HEK293T cells, and cells were grown in culture for two days before antibiotic selection with puromycin at 2.5 μg/mL for three days. Genomic DNA was extracted from cells and the *DNAJB9* amplicon was amplified by PCR. Initial PCR conditions did not yield an amplification product (**Figure 4.4*B***), but optimizing PCR conditions (reducing amount of template DNA, increasing extension time, testing a temperature gradient and addition of High GC Enhancer) led to amplification from parental cells and edited cells (**Figure 4.4 *C*** and ***D***). Single colonies were generated by limiting dilution, evaluated with the Surveyor Nuclease assay for DNA mismatches (**Figure 4.4*E***), and genotyped by Sanger sequencing (**Figure 4.4*F***). Five homogenous clones were identified and termed Clones 1B, 1C, 3A, 7C, and 9B.

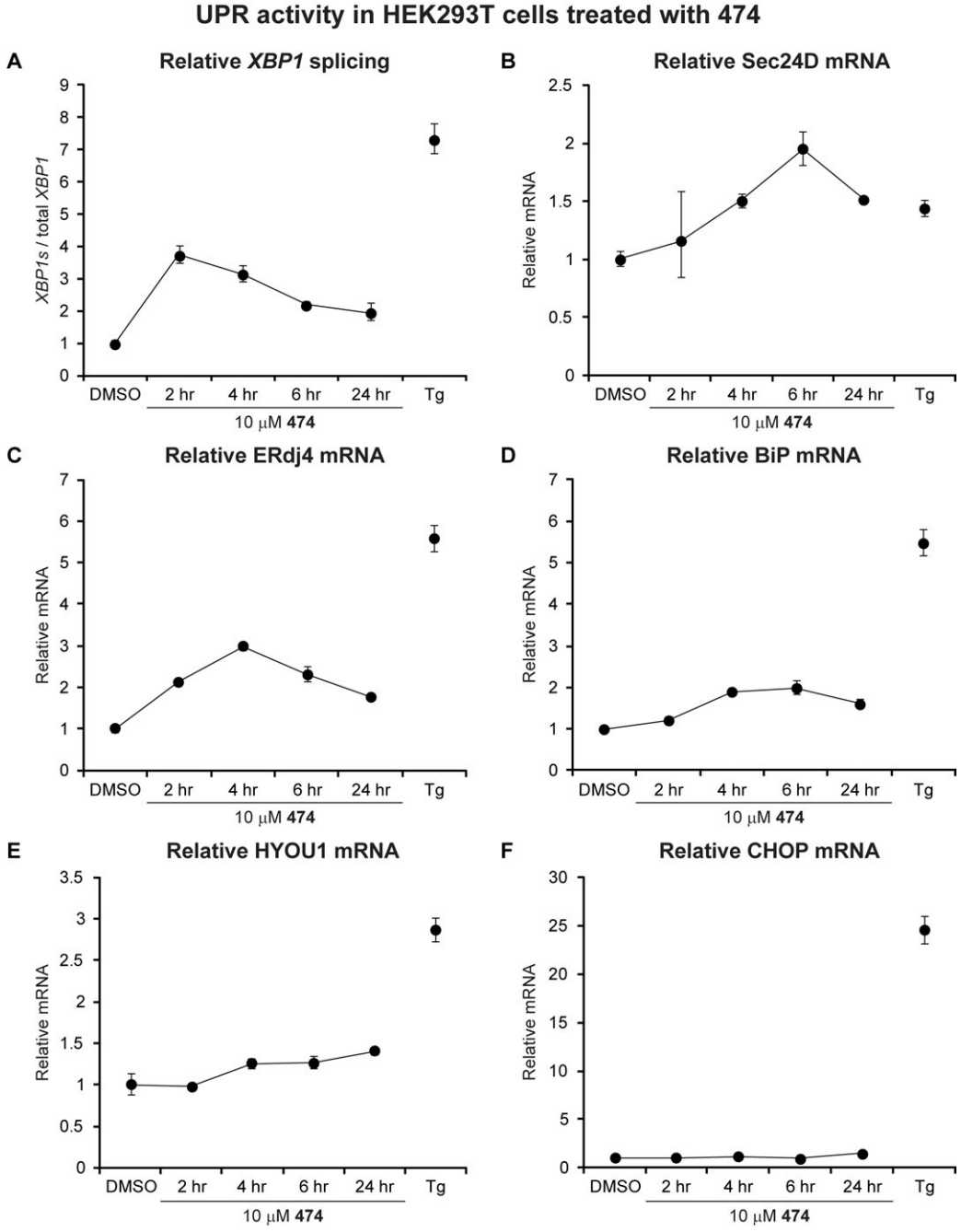

Figure 4.3: UPR activity in HEK293T cells treated with the small molecule 474 (10 μM) at 2-, 4-, 6-, and 24-hour time points. *XBP1* splicing (***A***) and induction mRNA for the IRE1-XBP1s targets Sec24D and ERdj4 (***B*** and ***C***, respectively) were measured by qRT-PCR. Expression of mRNA for the IRE1-XBP1s and ATF6 targets BiP and HYOU1 were also measured (***D*** and ***E***, respectively). **474** treatment did not lead to an increase in mRNA for the PERK target CHOP (***F***) demonstrating that off-target UPR activity was not present. Cells treated with thapsigargin (Tg; 5 μM, 2 hours) served as positive control for global UPR induction. Data were normalized to the *RPLP2* housekeeping gene and reported as the average of reactions performed in quadruplicate. Error bars: standard deviation of four technical replicates.

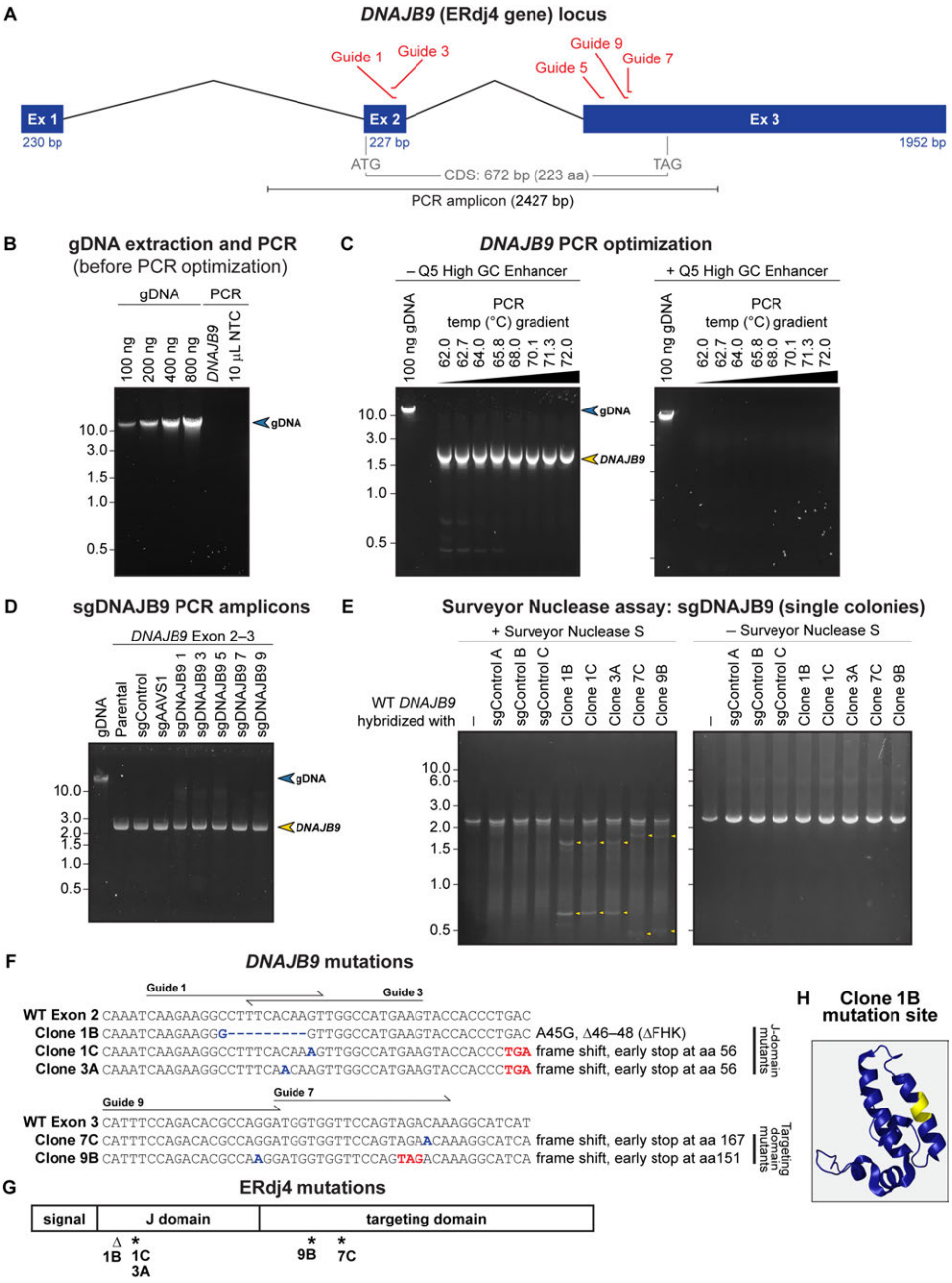

Figure 4.4: CRISPR-Cas9 approach to disrupt ERdj4 in HEK293T cells. ***A***: Diagram of the *DNAJB9* locus with locations of sgRNA targets on Exon 2 or Exon 3. The coding region of *DNAJB9* is contained within Exons 2 and 3, and primers were designed to amplify the entire coding region. ***B***: Genomic DNA (gDNA) extracted from HEK293T cells and initial attempt to amplify *DNAJB9*. ***C***: PCR optimization included reducing the amount of template, increasing extension time, a temperature gradient, and addition of High GC Enhancer. The *DNAJB9* amplicon consisted of 32% GC, and High GC Enhancer was detrimental to amplification. ***D***: After optimization, amplicons were generated from WT and edited cells. ***E***: Single colonies were generated, and DNA mismatches were detected using the Surveyor Nuclease assay (cleavage products indicated by yellow arrows, L*eft*). No mismatches were detected without addition of nuclease (*Right*). ***F***: Edits included J domain mutations and insertions leading to premature termination codons. ***G***: Deletion (Δ) and premature termination codons (*) mapped onto ERdj4. ***H***: Solution NMR structure of the J domain of human ERdj4 (PDB 2CTR) with the Clone 1B mutated region shown in yellow.

Clones with non-sense mutations introduced by CRISPR-Cas9[61-62] feature premature termination codons that can result in truncated loss-of-function products. Clones 1C and 3A had premature termination codons in the J domain responsible for recruiting BiP, while Clones 7C and 9B contained premature termination codons in the targeting domain responsible for targeting to substrates such as IRE1 (**Figure 4.4*G***). Clone 1B harbored a point mutation and deletion of nine nucleotides from Exon 2, resulting in a mutation in the J domain responsible for recruiting BiP, but maintaining the reading frame (**Figure 4.4 *G*** and ***H***). Because the premature termination codons occurred less than 55 nucleotides upstream of an exon-exon junction (Clones 1C and 3A), or occurred on the last exon (Clones 7C and 9B), they were not likely subject to non-sense mediated decay,[63] meaning that ERdj4 transcript induction could still be detected by qRT-PCR. To further characterize the clones, immunoblots for ERdj4 were performed with two commercial antibodies. However, due to the low expression of endogenous ERdj4, as had been previously reported by others,[64-67] and non-specific antibody staining, we could not detect ERdj4 at the protein level with or without ER stress (**Figure 4.5**) despite seeing increases in XBP1s protein expression with thapsigargin treatment (**Figure 4.5*B***). Furthermore, ERdj4 expression is often only be detectable following enrichment by immunoprecipitation,[68-69] but we were still unable to detect ERdj4 following enrichment.

Mutations in the J domain of ERdj4 were shown to be sufficient to ablate repression of IRE1.[46, 52] Specifically, mutations in the highly conserved HPD motif (amino acids 54–56) of ERdj4 were introduced to compromise its ability to stimulate the ATPase activity of BiP. Clones 1C and 3A disrupted this motif with frameshifts leading to premature termination codons at amino acid 56. Clone 1B contained a point mutation and deletion of three amino acids upstream of the HPD motif. Clones 7C and 9B did not disrupt the J domain, but instead disrupted the C-terminal targeting domain. ERdj4 mutants lacking the entire targeting domain were previously shown to be deficient in attenuating IRE1 activity. Thus, integrity of both domains is important for ERdj4 to attenuate IRE1 activity, and our clones featured mutations in both, including disruption of the HPD motif. We tested the effects of **474** on IRE1 activation in all five clones.

Pharmacological IRE1 Activation Is Not Sustained in WT ERdj4 or Edited Cells

We sought to determine whether our ERdj4-edited cells could sustain IRE1 activation past the short-lived (i.e. 2–4 hour) activation that we observed in HEK293T cells with WT ERdj4 (**Figure 4.3**). We treated WT ERdj4 and edited cells with **474** in a time course experiment with time points at 2, 4, 6, and 24 hours. After treatment with **474**, RNA was extracted and qRT-PCR was performed to quantify relative *XBP1* splicing and UPR target gene induction (**Figure 4.6**). We observed that across all clones tested, *XBP1* splicing peaked at 2 hours with **474** treatment, and had decreased at later time points (**Figure 4.6*A***). Expression of mRNA for XBP1s targets Sec24D and ERdj4 similarly peaked at earlier time points, then decreased by 24 hours (**Figure 4.6 *B*** and ***C***). Expression of mRNA for XBP1s- and ATF6- regulated targets

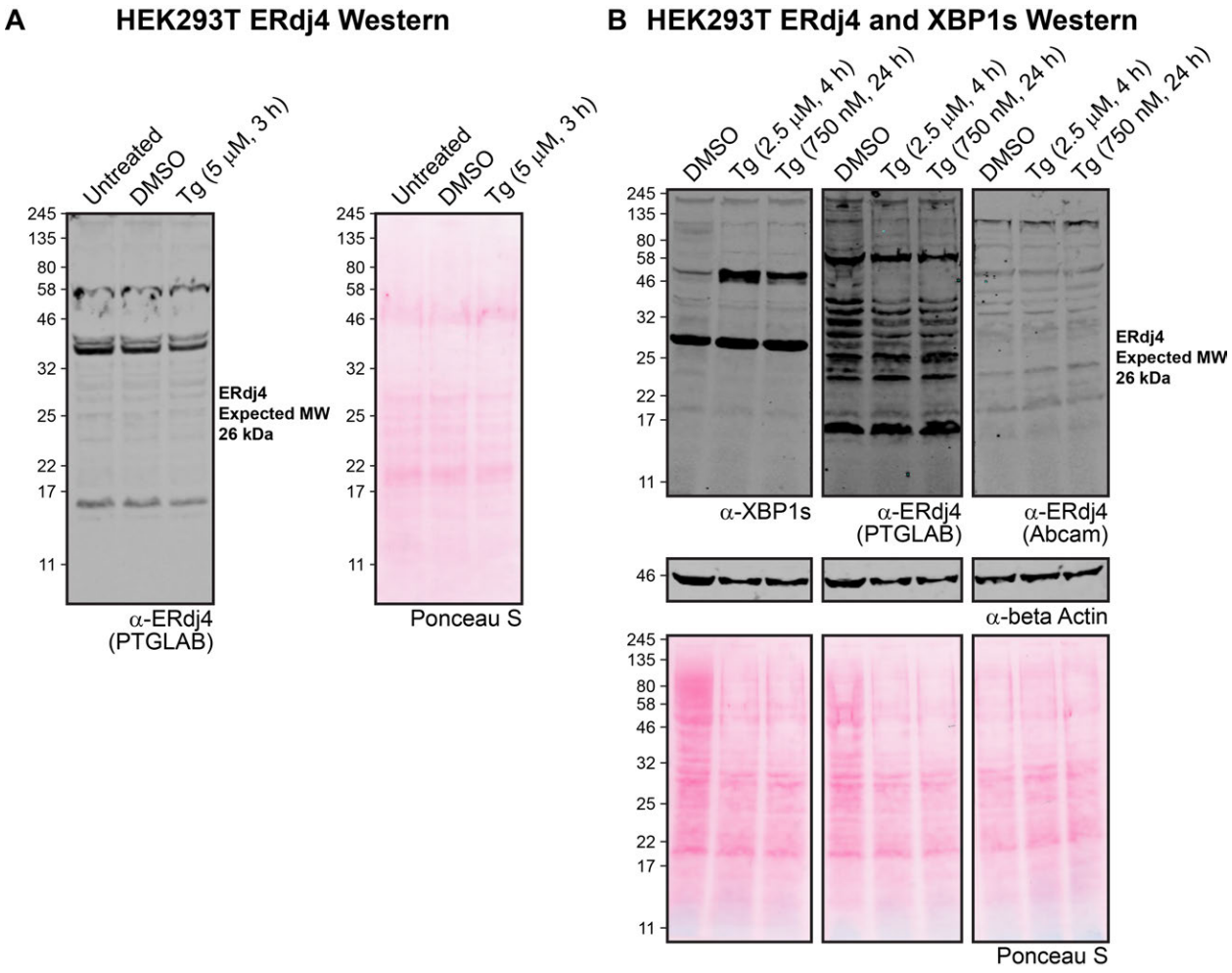

Figure 4.5: Difficulty in detecting ERdj4 in Western blots. ***A***: Western blot for ERdj4 using a commercial antibody from Proteintech (PTGLAB) on cell lysates (Triton X-100 lysis). ***B***: XBP1s and ERdj4 expression were probed using an XBP1s antibody and two ERdj4 antibodies (PTGLAB and Abcam) on cell lysates (RIPA lysis). An increase in XBP1s expression (54 kDa) was observed with thapsigargin treatment (*Left*), but ERdj4 expression was not detected under the same conditions (*Middle* and *Right*). 100 μg of protein was loaded for each sample. β-actin was used as a loading control, and Ponceau S staining was performed on nitrocellulose membranes prior to Western blotting to visualize sample loading and protein transfer.

BiP and HYOU1 showed relatively little induction (**Figure 4.6** ***D*** and ***E***). mRNA expression for the ATF6 target Grp94 and the PERK target CHOP was not substantially affected, demonstrating that **474** treatment did not induce off-target UPR activity (**Figure 4.6** ***F*** and ***G***). *XBP1* splicing was also visualized by separating total *XBP1* from qRT-PCR reactions on a 2% agarose gel (**Figure 4.7**). Overall, we did not observe a difference between WT and ERdj4-edited cells in response to IRE1 activation by **474**. Induction of *XBP1* splicing peaked at 2 hours and decreased at later time points, indicating that disruption of ERdj4 was not sufficient to sustain pharmacological IRE1 activation, and that another mechanism (or a combination of mechanisms) negatively regulates IRE1 activity in response to small molecules.

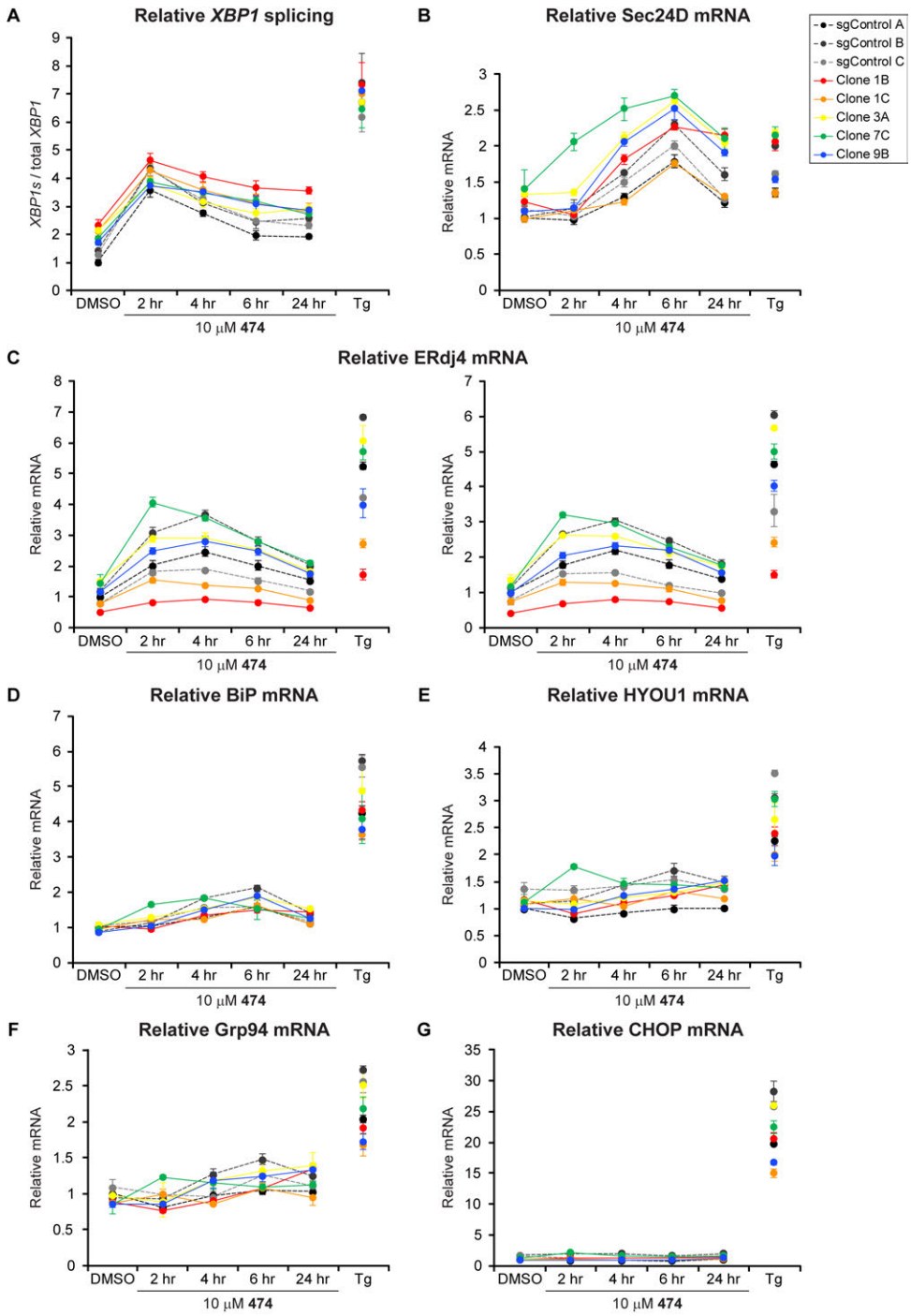

Figure 4.6: Time course with 474 treatment (10 μM) in HEK293T clones with WT or edited ERdj4. *XBP1* splicing (***A***) was profiled using qRT-PCR. Expression of mRNA for UPR targets were also profiled, including the XBP1s targets Sec24D and ERdj4 (***B*** and ***C***, respectively), the XBP1s/ATF6 targets BiP and HYOU1 (***D*** and ***E***, respectively), the ATF6 target Grp94 (***F***), and the PERK target CHOP (***G***). Splicing and expression profiles were similar among cells with WT or edited ERdj4, with peak *XBP1* splicing at 2 hours, and decreasing at later time points. Cells treated with thapsigargin (Tg; 5 μM, 2 hours) served as positive control for global UPR induction. Data were normalized to the *RPLP2* housekeeping gene and reported as the average of reactions performed in quadruplicate (*XBP1* splicing) or duplicate (others). ERdj4 mRNA expression was profiled by qRT-PCR twice. Error bars: standard deviation of four technical replicates.

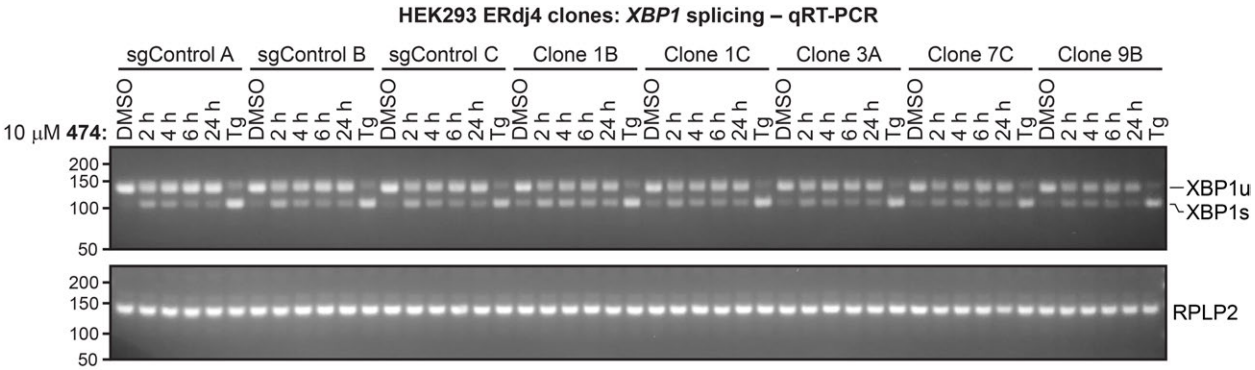

Figure 4.7: *XBP1* splicing was visualized by separating total *XBP1* qRT-PCR products on a 2% agarose gel. The intensity of *XBP1s* (bottom band) increased as early as 2 hours with **474**, but had decreased at later time points for all clones tested (see also Figure 4.6 for qPCR plots).

Inactivation of Sec63 Is Also Not Sufficient to Sustain Pharmacological IRE1 Activation

In addition to an ERdj4-directed model of BiP-mediated IRE1 repression, we hypothesized that Sec63 may be directing BiP to repress IRE1 when activated by small molecules. We next sought to assess whether inactivation of Sec63 may be sufficient to sustain pharmacological IRE1 activation. We obtained HEK293 Sec63 knockout cells[53] from the Mariappan group at the Yale School of Medicine and tested whether **474** can sustain IRE1 activation in these cells. We treated the Sec63 knockout cells with **474** for 2, 4, 6, or 24 hours and profiled *XBP1* splicing and expression of ERdj4 and BiP mRNA by qRT-PCR (**Figure 4.8**). Knockout of Sec63 led to increased basal levels of *XBP1* splicing and upregulation of ERdj4 and BiP mRNA (**Figure 4.8**, *DMSO*), consistent with the role of Sec63 in repressing IRE1 activity.[53] We observed that *XBP1* splicing and mRNA expression for ERdj4 and BiP had increased at the earlier time points with **474** treatment, reaching maximal levels by 4–6 hours, but had decreased by 24 hours. These results with Sec63 disruption, along with the results for ERdj4 disruption (**Figure 4.6**) mimic the transient activation of IRE1 induced by **474** in WT cells (**Figure 4.3**). These data suggest that neither Sec63 inactivation nor ERdj4 inactivation alone is sufficient to sustain pharmacological IRE1 activation. Again, another mechanism (or combination of mechanisms) is likely repressing IRE1 signaling induced by small molecules.

Discussion

We hypothesized that ERdj4 and Sec63, two proteins reported to recruit BiP to suppress IRE1 activity, may be limiting pharmacological activation of IRE1 to shorter time points. In our work with ERdj4- or Sec63-disrupted cells, we were unable to sustain IRE1 activation beyond a few hours (i.e. 4–6 hours) by **474** when we profiled *XBP1* splicing and XBP1s target gene induction by qRT-PCR. Thus, the exact mechanisms by which cells attenuate IRE1 activity induced by small molecules remain elusive. Our studies suggest that another factor (or a combination of factors) suppressing IRE1 signaling limits

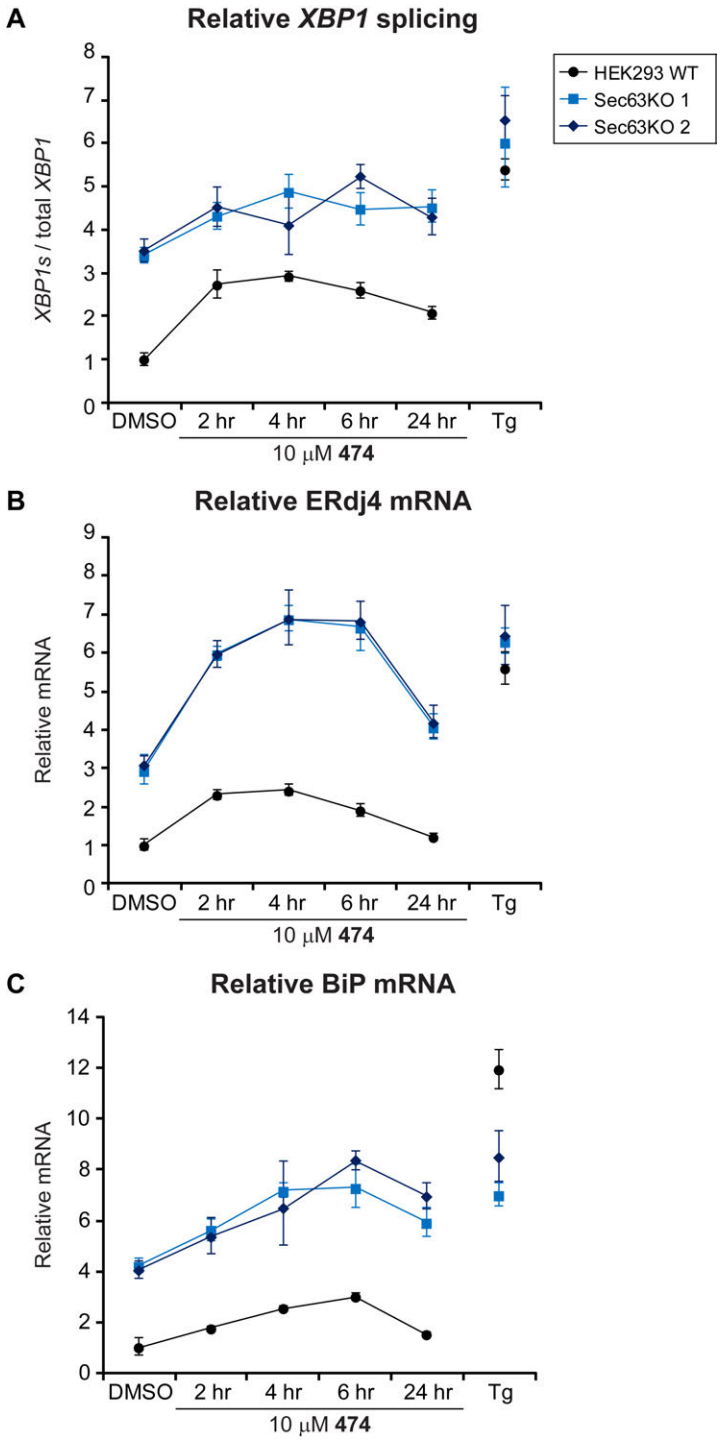

Figure 4.8: Time course with 474 treatment (10 μM) in HEK293 cells with WT or edited Sec63. *XBP1* splicing (***A***) was profiled using qRT-PCR. Expression of mRNA for the XBP1s target ERdj4 and the XBP1s/ATF6 target BiP was also profiled (***B*** and ***C***, respectively). *XBP1* splicing and mRNA expression for ERdj4 and BiP were enhanced at basal conditions (DMSO) in the Sec63 knockout cells. Splicing and target gene induction by **474** peaked at earlier timepoints in both WT and edited cells, decreasing at later timepoints. Cells treated with thapsigargin (Tg; 5 μM, 2 hours) served as positive control. Data were normalized to the *RPLP2* housekeeping gene and reported as the average of reactions performed in quadruplicate. Error bars: standard deviation of four technical replicates.

pharmacological activation. It may be possible that simultaneous inactivation of both ERdj4 and Sec63 in cells is required to bypass the suppressive machineries. Of note, **474** activates IRE1 independent of the kinase binding site, but it remains unknown how **474** carries out IRE1 activation,[45] raising the possibility of novel binding sites or undiscovered mechanisms to regulate the UPR.

We disrupted motifs known to be critical for IRE1 repression, but due to technical challenges we were unable to detect ERdj4 in immunoblots, consistent with previous reports of undetectable or low ERdj4 expression levels,[64-67] despite attempts to enrich the protein via immunoprecipitation. Alternatively, ERdj4 protein levels may be quantified by mass spectrometry-based proteomics approaches, but they would also likely require enrichment, for example via immunoprecipitation or microsome fractionation.[68-69]

In conclusion, we were unable to find evidence that ERdj4 or Sec63 disruption can facilitate sustained pharmacological IRE1 activation. Rather, our findings suggest that our understanding of UPR regulation may yet be incomplete. ERdj4 and Sec63 (ERdj2) are just two of seven co-chaperones in the ERdj family of proteins reported to interact with BiP.[64] IRE1 repression is perhaps mediated by additional ERdj proteins in a redundant manner. Furthermore, ERdj4 deletion was reported to only partially deregulate IRE1,[46] and Sec63 was also reported to influence PERK[46] and ATF6 activity[53] in addition to IRE1, highlighting potential promiscuity and redundancy in regulation of the UPR. Additionally, a minority of IRE1 molecules can be attenuated in Sec63-disrupted cells,[53] suggesting that repression via mechanisms other than Sec63 may be regulating IRE1. Elucidating the mechanism by which pharmacological activation of IRE1 is suppressed would provide fundamental knowledge regarding regulation of UPR signaling. Such knowledge could provide additional clues to improve our understanding of drug resistance mechanisms and potential therapeutic uses for UPR-targeted therapies should they progress into the clinic.

Materials and Methods

Cell Lines and Reagents

HEK293T cells were authenticated by short-tandem repeat profiling (ATCC) prior to genetic engineering, and were grown in DMEM (Corning 15-017-CM) supplemented with 10% FBS (Corning 35-010-CV), L-glutamine (Corning 25-005-CI), and penicillin/streptomycin (Corning 30-002-CI) at 37 °C and 5% CO_2 in a humidified tissue culture incubator. A puromycin dihydrochloride (Gibco A1113803) antibiotic kill curve was performed to select cells at 2.5 μg/mL for three days. Sec63 knockout cells were a kind gift from the Mariappan group (Yale School of Medicine). Cells were regularly screened for mycoplasma using the MycoAlert PLUS Mycoplasma Detection Kit (Lonza LT07-710) prior to experimentation. To induce global ER stress, cells were treated with thapsigargin (Sigma-Aldrich T9033) at 5 μM for 2 hours.

sgRNA Guides and Cloning

sgRNA Sequences and Cloning Oligos

sgDNAJB9_1 guide sequence: CAAGAAGGCCTTTCACAAGT

sgDNAJB9_1 cloning oligo: CACCGCAAGAAGGCCTTTCACAAGT (sense)

sgDNAJB9_1 cloning oligo: AAACACTTGTGAAAGGCCTTCTTGC (antisense)

sgDNAJB9_3 guide sequence: CTTCATGGCCAACTTGTGAA (negative strand)

sgDNAJB9_3 cloning oligo: CACCGCTTCATGGCCAACTTGTGAA (sense)

sgDNAJB9_3 cloning oligo: AAACTTCACAAGTTGGCCATGAAGC (antisense)

sgDNAJB9_5 guide sequence: GGTAAAGGACAAAGAGGTAG

sgDNAJB9_5 cloning oligo: CACCGGGTAAAGGACAAAGAGGTAG (sense)

sgDNAJB9_5 cloning oligo: AAACCTACCTCTTTGTCCTTTACCC (antisense)

sgDNAJB9_7

sgDNAJB9_7 guide sequence: ATGGTGGTTCCAGTAGACAA

sgDNAJB9_7 cloning oligo: CACCGATGGTGGTTCCAGTAGACAA (sense)

sgDNAJB9_7 cloning oligo: AAACTTGTCTACTGGAACCACCATC (antisense)

sgDNAJB9_9 guide sequence: CATTTCCAGACACGCCAGGA

sgDNAJB9_9 cloning oligo: CACCGCATTTCCAGACACGCCAGGA (sense)

sgDNAJB9_9 cloning oligo: AAACTCCTGGCGTGTCTGGAAATGC (antisense)

non-targeting control guide sequence: GGATACTTCTTCGAACGTTT

non-targeting control cloning oligo: CACCGGGATACTTCTTCGAACGTTT (sense)

non-targeting control cloning oligo: AAACAAACGTTCGAAGAAGTATCCC (antisense)

AAVS1-targeting control guide sequence: GGGGCCACTAGGGACAGGAT

AAVS1-targeting control cloning oligo: CACCGGGGGCCACTAGGGACAGGAT (sense)

AAVS1-targeting control cloning oligo: AAACATCCTGTCCCTAGTGGCCCCC (antisense)

Target Sequence Cloning

The CRISPR target sequence cloning protocol was adapted from Cong *et al.*[60] Briefly, oligo annealing was performed in T4 DNA Ligase Reaction Buffer (New England Biolabs B0202S) with T4

Polynucleotide Kinase (New England Biolabs M0201S). Digestion and ligation to the backbone vector pSpCas9(BB)-2A-Puro (PX459) V2.0[70] was performed in T4 DNA Ligase Reaction Buffer with FastDigest BpiI (ThermoFisher FD1014) and T7 DNA Ligase (New England Biolab M0318S). Ligated products were transformed into 10-beta Competent *E. coli* (High Efficiency) cells (New England Biolabs C3019I), and colonies were picked and sequence-verified after miniprep.

Transfection and Single-Colony Generation

HEK293T cells were grown to 80% confluency on 6-well plates and transfected with 2.5 μg of DNA using Lipofectamine 3000 Transfection Reagent (Invitrogen L3000015) following manufacturer's protocol with Opti-MEM Reduced Serum Medium (Gibco 31985070). Two days post-transfection, cells were selected with 2.5 μg/mL of puromycin for three days. Single colonies were generated by limiting dilution in 96-well plates, and homogenous colonies were verified by Sanger sequencing.

Genomic DNA Extraction, DNAJB9 PCR, and Surveyor Assay

Genomic DNA was extracted from cells using the Quick-DNA Miniprep kit following manufacturer's protocols (Zymo Research D3024). The *DNAJB9* amplicon spanning the entire coding region was amplified using the Q5 High-Fidelity DNA Polymerase (New England Biolabs M0491L) with 100 ng of template DNA, a 120 second extension time, a 68 °C annealing temperature, and 35 cycles of amplification. Amplicons were column purification using the E.Z.N.A. Cycle Pure Kit (Omega Bio-tek D6492-02). Primers used to amplify *DNAJB9* were as follows:

DNAJB9 Exon 2 forward: TGGCTCACCTGCTGAAATGA

DNAKB9 Exon 3 reverse: TGAGCCCAAGGGCAGGTAGA

To detect DNA mismatches in edited cells, Surveyor Nuclease assays were performed using the Surveyor Mutation Detection Kit following the manufacturer's protocols (Integrated DNA Technologies 706020). Briefly, *DNAJB9* PCR amplicons were generated from genomic DNA, and DNA from edited cells was hybridized with WT DNA from the parental HEK293T cell line in a 1:1 ratio (200 ng each) in Q5 Reaction Buffer. After hybridization, duplexes were digested at 42 °C for 60 minutes, with or without Nuclease S (for negative control). Stop solution was added, and reactions were mixed with Purple Gel Loading Dye (New England Biolabs B7024S) prior to separation on 0.8% agarose TBE gels pre-mixed with GelGreen Nucleic Acid Gel Stain (Biotium 41005), and imaged on a 470 nm blue LED transilluminator (Maestrogen SLB-01W). Samples were run alongside a 1 kb DNA Ladder (New England Biolabs N3232S).

RNA Extraction and Quantitative Real-Time PCR

RNA was isolated from cells using the E.Z.N.A. Total RNA Kit I (Omega R6834-02) following the manufacturer's protocol, including the on-column DNase digestion (Omega E1091-02). RNA quantity and quality were assessed via $A_{260/280}$ readings on a Synergy H1 Hybrid plate reader with a Take3 micro-volume plate. RNA was frozen at –80 °C unless processed immediately for qRT-PCR. To generate cDNA from RNA, 1000 ng of RNA was reverse transcribed using the High-Capacity cDNA Reverse Transcription Kit (Applied Biosystems 4368813). cDNA was then diluted 5X in molecular biology grade water, and qPCR was performed using the Universal KAPA SYBR FAST qPCR Master Mix (Roche KK4618) on a LightCycler 480 II (Roche). Relative gene expression was normalized to the *RPLP2* housekeeping gene and analyzed by the ΔΔCt method.[71-72]

Primers used are as follows:

total XBP1 forward: AATGAAGTGAGGCCAGTGGC, rev: TGAAGAGTCAATACCGCCAGAA;
XBP1s forward: CTGAGTCCGCAGCAGGT, rev: TCCAGAATGCCCAACAGGAT;
RPLP2 forward: CCATTCAGCTCACTGATAACCTTG, rev: CGTCGCCTCCTACCTGCT;
ERDJ4 forward: CTGTATGCTGATTGGTAGAGTCAA, rev: AGTAGACAAAGGCATCATTTCCAA;
SEC24D forward: AGCAGACTGTCCTGGGAAGC, rev: TTTGTTTGGGGCTGGAAAAG;
BIP forward: GCCTGTATTTCTAGACCTGCC, rev: TTCATCTTGCCAGCCAGTTG;
HYOU1 forward: GCAGACCTGTTGGCACTGAG, rev: TCACGATCACCGGTGTTTTC;
GRP94 forward: GGCCAGTTTGGTGTCGGTTT, rev: CGTTCCCCGTCCTAGAGTGTT;
CHOP forward: GGAGCTGGAAGCCTGGTATG, rev: GCCAGAGAAGCAGGGTCAAG.

To visualize *XBP1* splicing, qRT-PCR products using the total *XBP1* primer pair were separated on 2% agarose (Lonza 50090) TBE gels pre-mixed with GelGreen Nucleic Acid Gel Stain (Biotium 41005), and imaged on a 470 nm blue LED transilluminator (Maestrogen SLB-01W). Samples were run alongside 50 bp DNA Ladder (New England Biolabs N3236S).

Western Blot and Immunoprecipitation

Cell lysates were generated by incubating cells in Triton-X100 Lysis Buffer (50 mM Tris pH 7.5, 1% Triton X-100, 200 mM NaCl, 1 mM EDTA, 1.5 mM $MgCl_2$, protease and phosphatase inhibitors (Pierce A32961)) or RIPA Lysis Buffer (10 mM Tris pH 7.4, 150 mM NaCl, 10 mM KCl, 1 mM EDTA, 0.5% deoxycholic acid, 0.5% Tween 20, 0.5% NP-40, 0.1% SDS, protease and phosphatase inhibitors (Pierce A32961)) on ice for 20 minutes with intermittent vortexing. Insoluble debris were pelleted by centrifugation at maximum speed for 15 minutes. Protein concentrations were determined using a Pierce 660 nm Protein Assay (Pierce 22660). Immunoprecipitations (IP) were performed by incubating 1 mg of denatured protein (0.5% SDS, 40 mM DTT) with 2 μg of primary antibody in PBS for 1 hour at 4 °C. Protein A/G PLUS-

Agarose beads (SantaCruz sc-2003) were then added at 40 μL of resuspended slurry per 1 mL IP volume. Beads were then incubated at 4 °C rocking end-over-end overnight. After overnight incubation, beads were washed 4× with RIPA buffer, then resuspended in 40 μL of 2X electrophoresis buffer and heated to 95 °C for 10 minutes prior to analysis by SDS-PAGE.

Primary antibodies were obtained from Cell Signaling Technology (XBP1s: 12782S), Sigma-Aldrich (β-Actin: A1978), Proteintech (ERdj4: PTGLAB 13157-1-AP) and Abcam (ERdj4: ab118282). All primary antibodies were diluted in 5% BSA with 0.02% sodium azide in TBS at manufacturer-recommended dilutions.

For gel electrophoresis, up to 100 μg of protein were separated on NuPAGE 12% Bis-Tris PAGE gels (Invitrogen NP0341BOX) ran with MES SDS running buffer (Invitrogen NP0060), and transferred to nitrocellulose membranes using the Trans-Blot Turbo Transfer System (Bio-Rad). Transferred membranes were stained with Ponceau S and imaged on an Epson Perfection V19 Scanner prior to blocking with 5% milk (Carnation) in TBS for 30 minutes at room temperature. After blocking, membranes were incubated with primary antibodies overnight, rocking in a 4 °C cold room. After overnight incubation, primary antibodies were removed, and membranes were washed 3× 10 minutes with TBS-T at room temperature. After the final wash, membranes were incubated with secondary antibodies (LI-COR) at 1:5,000 dilution in 5% milk in TBS, rocking at room temperature for 1 hour. After secondary antibody incubation, membranes were washed 3× 10 minutes with TBS-T at room temperature. Membranes were scanned using a LI-COR Odyssey Classic imager.

Acknowledgements

We acknowledge the Wiseman group at The Scripps Research Institute for providing Compound **474**, and the Mariappan group at the Yale School of Medicine for providing Sec63 knockout HEK293 cells.

This work was supported by an MIT George H. Büchi Fellowship sponsored by Ping S. Chu, PhD ’80 (to K.C.); and an American Cancer Society–Ellison Foundation Research Scholar Award (to M.D.S.). This work was also supported in part by the NIH/NIEHS (Grant P30-ES002109) and Koch Institute Support (Core) Grant P30-CA14051 from the National Cancer Institute.

References

[1] Yoshida, H.; Matsui, T.; Yamamoto, A.; Okada, T.; Mori, K., XBP1 mRNA is induced by ATF6 and spliced by IRE1 in response to ER stress to produce a highly active transcription factor. *Cell* **2001,** *107* (7), 881-91.

[2] Lee, K.; Tirasophon, W.; Shen, X.; Michalak, M.; Prywes, R.; Okada, T.; Yoshida, H.; Mori, K.; Kaufman, R. J., IRE1-mediated unconventional mRNA splicing and S2P-mediated ATF6 cleavage merge to regulate XBP1 in signaling the unfolded protein response. *Genes Dev* **2002,** *16* (4), 452-66.

[3] Calfon, M.; Zeng, H.; Urano, F.; Till, J. H.; Hubbard, S. R.; Harding, H. P.; Clark, S. G.; Ron, D., IRE1 couples endoplasmic reticulum load to secretory capacity by processing the XBP-1 mRNA. *Nature* **2002,** *415* (6867), 92-6.

[4] Marciniak, S. J.; Garcia-Bonilla, L.; Hu, J.; Harding, H. P.; Ron, D., Activation-dependent substrate recruitment by the eukaryotic translation initiation factor 2 kinase PERK. *J Cell Biol* **2006,** *172* (2), 201-9.

[5] Harding, H. P.; Novoa, I.; Zhang, Y.; Zeng, H.; Wek, R.; Schapira, M.; Ron, D., Regulated translation initiation controls stress-induced gene expression in mammalian cells. *Mol Cell* **2000,** *6* (5), 1099-108.

[6] Vattem, K. M.; Wek, R. C., Reinitiation involving upstream ORFs regulates ATF4 mRNA translation in mammalian cells. *Proc Natl Acad Sci U S A* **2004,** *101* (31), 11269-74.

[7] Ye, J.; Rawson, R. B.; Komuro, R.; Chen, X.; Dave, U. P.; Prywes, R.; Brown, M. S.; Goldstein, J. L., ER stress induces cleavage of membrane-bound ATF6 by the same proteases that process SREBPs. *Mol Cell* **2000,** *6* (6), 1355-64.

[8] Shen, J.; Prywes, R., Dependence of site-2 protease cleavage of ATF6 on prior site-1 protease digestion is determined by the size of the luminal domain of ATF6. *J Biol Chem* **2004,** *279* (41), 43046-51.

[9] Wong, M. Y.; DiChiara, A. S.; Suen, P. H.; Chen, K.; Doan, N. D.; Shoulders, M. D., Adapting Secretory Proteostasis and Function Through the Unfolded Protein Response. *Curr Top Microbiol Immunol* **2018,** *414*, 1-25.

[10] Chang, T. K.; Lawrence, D. A.; Lu, M.; Tan, J.; Harnoss, J. M.; Marsters, S. A.; Liu, P.; Sandoval, W.; Martin, S. E.; Ashkenazi, A., Coordination between Two Branches of the Unfolded Protein Response Determines Apoptotic Cell Fate. *Mol Cell* **2018,** *71* (4), 629-636.e5.

[11] Valdes, P.; Mercado, G.; Vidal, R. L.; Molina, C.; Parsons, G.; Court, F. A.; Martinez, A.; Galleguillos, D.; Armentano, D.; Schneider, B. L.; Hetz, C., Control of dopaminergic neuron survival by the unfolded protein response transcription factor XBP1. *Proc Natl Acad Sci U S A* **2014,** *111* (18), 6804-9.

[12] Casas-Tinto, S.; Zhang, Y.; Sanchez-Garcia, J.; Gomez-Velazquez, M.; Rincon-Limas, D. E.; Fernandez-Funez, P., The ER stress factor XBP1s prevents amyloid-beta neurotoxicity. *Hum Mol Genet* **2011,** *20* (11), 2144-60.

[13] Fung, T. S.; Liao, Y.; Liu, D. X., The endoplasmic reticulum stress sensor IRE1alpha protects cells from apoptosis induced by the coronavirus infectious bronchitis virus. *J Virol* **2014,** *88* (21), 12752-64.

[14] Wang, Z. V.; Deng, Y.; Gao, N.; Pedrozo, Z.; Li, D. L.; Morales, C. R.; Criollo, A.; Luo, X.; Tan, W.; Jiang, N.; Lehrman, M. A.; Rothermel, B. A.; Lee, A. H.; Lavandero, S.; Mammen, P. P. A.;

Ferdous, A.; Gillette, T. G.; Scherer, P. E.; Hill, J. A., Spliced X-box binding protein 1 couples the unfolded protein response to hexosamine biosynthetic pathway. *Cell* **2014,** *156* (6), 1179-1192.

[15] Taylor, R. C.; Dillin, A., XBP-1 is a cell-nonautonomous regulator of stress resistance and longevity. *Cell* **2013,** *153* (7), 1435-47.

[16] Xia, Z.; Wu, S.; Wei, X.; Liao, Y.; Yi, P.; Liu, Y.; Liu, J.; Liu, J., Hypoxic ER stress suppresses beta-catenin expression and promotes cooperation between the transcription factors XBP1 and HIF1alpha for cell survival. *J Biol Chem* **2019,** *294* (37), 13811-13821.

[17] Xie, H.; Tang, C. H.; Song, J. H.; Mancuso, A.; Del Valle, J. R.; Cao, J.; Xiang, Y.; Dang, C. V.; Lan, R.; Sanchez, D. J.; Keith, B.; Hu, C. C.; Simon, M. C., IRE1alpha RNase-dependent lipid homeostasis promotes survival in Myc-transformed cancers. *J Clin Invest* **2018,** *128* (4), 1300-1316.

[18] Liu, D.; Liu, X.; Zhou, T.; Yao, W.; Zhao, J.; Zheng, Z.; Jiang, W.; Wang, F.; Aikhionbare, F. O.; Hill, D. L.; Emmett, N.; Guo, Z.; Wang, D.; Yao, X.; Chen, Y., IRE1-RACK1 axis orchestrates ER stress preconditioning-elicited cytoprotection from ischemia/reperfusion injury in liver. *J Mol Cell Biol* **2016,** *8* (2), 144-56.

[19] Valenzuela, V.; Collyer, E.; Armentano, D.; Parsons, G. B.; Court, F. A.; Hetz, C., Activation of the unfolded protein response enhances motor recovery after spinal cord injury. *Cell Death Dis* **2012,** *3*, e272.

[20] Vidal, R. L.; Figueroa, A.; Court, F. A.; Thielen, P.; Molina, C.; Wirth, C.; Caballero, B.; Kiffin, R.; Segura-Aguilar, J.; Cuervo, A. M.; Glimcher, L. H.; Hetz, C., Targeting the UPR transcription factor XBP1 protects against Huntington's disease through the regulation of FoxO1 and autophagy. *Hum Mol Genet* **2012,** *21* (10), 2245-62.

[21] Gupta, S.; Deepti, A.; Deegan, S.; Lisbona, F.; Hetz, C.; Samali, A., HSP72 protects cells from ER stress-induced apoptosis via enhancement of IRE1alpha-XBP1 signaling through a physical interaction. *PLoS Biol* **2010,** *8* (7), e1000410.

[22] Lin, J. H.; Li, H.; Zhang, Y.; Ron, D.; Walter, P., Divergent effects of PERK and IRE1 signaling on cell viability. *PLoS One* **2009,** *4* (1), e4170.

[23] Iwakoshi, N. N.; Pypaert, M.; Glimcher, L. H., The transcription factor XBP-1 is essential for the development and survival of dendritic cells. *J Exp Med* **2007,** *204* (10), 2267-75.

[24] Romero-Ramirez, L.; Cao, H.; Nelson, D.; Hammond, E.; Lee, A. H.; Yoshida, H.; Mori, K.; Glimcher, L. H.; Denko, N. C.; Giaccia, A. J.; Le, Q. T.; Koong, A. C., XBP1 is essential for survival under hypoxic conditions and is required for tumor growth. *Cancer Res* **2004,** *64* (17), 5943-7.

[25] Tsuchiya, Y.; Saito, M.; Kadokura, H.; Miyazaki, J. I.; Tashiro, F.; Imagawa, Y.; Iwawaki, T.; Kohno, K., IRE1-XBP1 pathway regulates oxidative proinsulin folding in pancreatic beta cells. *J Cell Biol* **2018,** *217* (4), 1287-1301.

[26] Lipson, K. L.; Fonseca, S. G.; Ishigaki, S.; Nguyen, L. X.; Foss, E.; Bortell, R.; Rossini, A. A.; Urano, F., Regulation of insulin biosynthesis in pancreatic beta cells by an endoplasmic reticulum-resident protein kinase IRE1. *Cell Metab* **2006,** *4* (3), 245-54.

[27] Engin, F.; Yermalovich, A.; Nguyen, T.; Hummasti, S.; Fu, W.; Eizirik, D. L.; Mathis, D.; Hotamisligil, G. S., Restoration of the unfolded protein response in pancreatic beta cells protects mice against type 1 diabetes. *Sci Transl Med* **2013,** *5* (211), 211ra156.

[28] Tufanli, O.; Telkoparan Akillilar, P.; Acosta-Alvear, D.; Kocaturk, B.; Onat, U. I.; Hamid, S. M.; Cimen, I.; Walter, P.; Weber, C.; Erbay, E., Targeting IRE1 with small molecules counteracts progression of atherosclerosis. *Proc Natl Acad Sci U S A* **2017,** *114* (8), E1395-e1404.

[29] Qiu, Q.; Zheng, Z.; Chang, L.; Zhao, Y. S.; Tan, C.; Dandekar, A.; Zhang, Z.; Lin, Z.; Gui, M.; Li, X.; Zhang, T.; Kong, Q.; Li, H.; Chen, S.; Chen, A.; Kaufman, R. J.; Yang, W. L.; Lin, H. K.; Zhang, D.; Perlman, H.; Thorp, E.; Zhang, K.; Fang, D., Toll-like receptor-mediated IRE1alpha activation as a therapeutic target for inflammatory arthritis. *Embo j* **2013,** *32* (18), 2477-90.

[30] Dong, H.; Adams, N. M.; Xu, Y.; Cao, J.; Allan, D. S. J.; Carlyle, J. R.; Chen, X.; Sun, J. C.; Glimcher, L. H., The IRE1 endoplasmic reticulum stress sensor activates natural killer cell immunity in part by regulating c-Myc. *Nat Immunol* **2019,** *20* (7), 865-878.

[31] Wang, Y.; Zhang, Y.; Yi, P.; Dong, W.; Nalin, A. P.; Zhang, J.; Zhu, Z.; Chen, L.; Benson, D. M.; Mundy-Bosse, B. L.; Freud, A. G.; Caligiuri, M. A.; Yu, J., The IL-15-AKT-XBP1s signaling pathway contributes to effector functions and survival in human NK cells. *Nat Immunol* **2019,** *20* (1), 10-17.

[32] Mendez, A. S.; Alfaro, J.; Morales-Soto, M. A.; Dar, A. C.; McCullagh, E.; Gotthardt, K.; Li, H.; Acosta-Alvear, D.; Sidrauski, C.; Korennykh, A. V.; Bernales, S.; Shokat, K. M.; Walter, P., Endoplasmic reticulum stress-independent activation of unfolded protein response kinases by a small molecule ATP-mimic. *Elife* **2015,** *4*.

[33] Ghosh, R.; Wang, L.; Wang, E. S.; Perera, B. G.; Igbaria, A.; Morita, S.; Prado, K.; Thamsen, M.; Caswell, D.; Macias, H.; Weiberth, K. F.; Gliedt, M. J.; Alavi, M. V.; Hari, S. B.; Mitra, A. K.; Bhhatarai, B.; Schurer, S. C.; Snapp, E. L.; Gould, D. B.; German, M. S.; Backes, B. J.; Maly, D. J.; Oakes, S. A.; Papa, F. R., Allosteric inhibition of the IRE1alpha RNase preserves cell viability and function during endoplasmic reticulum stress. *Cell* **2014,** *158* (3), 534-48.

[34] Cole, K. S.; Grandjean, J. M. D.; Chen, K.; Witt, C. H.; O'Day, J.; Shoulders, M. D.; Wiseman, R. L.; Weerapana, E., Characterization of an A-Site Selective Protein Disulfide Isomerase A1 Inhibitor. *Biochemistry* **2018,** *57* (13), 2035-2043.

[35] Wang, L.; Perera, B. G.; Hari, S. B.; Bhhatarai, B.; Backes, B. J.; Seeliger, M. A.; Schurer, S. C.; Oakes, S. A.; Papa, F. R.; Maly, D. J., Divergent allosteric control of the IRE1alpha endoribonuclease using kinase inhibitors. *Nat Chem Biol* **2012,** *8* (12), 982-9.

[36] Korennykh, A. V.; Egea, P. F.; Korostelev, A. A.; Finer-Moore, J.; Zhang, C.; Shokat, K. M.; Stroud, R. M.; Walter, P., The unfolded protein response signals through high-order assembly of Ire1. *Nature* **2009,** *457* (7230), 687-93.

[37] Han, D.; Lerner, A. G.; Vande Walle, L.; Upton, J. P.; Xu, W.; Hagen, A.; Backes, B. J.; Oakes, S. A.; Papa, F. R., IRE1alpha kinase activation modes control alternate endoribonuclease outputs to determine divergent cell fates. *Cell* **2009,** *138* (3), 562-75.

[38] Korennykh, A. V.; Egea, P. F.; Korostelev, A. A.; Finer-Moore, J.; Stroud, R. M.; Zhang, C.; Shokat, K. M.; Walter, P., Cofactor-mediated conformational control in the bifunctional kinase/RNase Ire1. *BMC Biol* **2011,** *9*, 48.

[39] Gonzalez-Teuber, V.; Albert-Gasco, H.; Auyeung, V. C.; Papa, F. R.; Mallucci, G. R.; Hetz, C., Small Molecules to Improve ER Proteostasis in Disease. *Trends Pharmacol Sci* **2019,** *40* (9), 684-695.

[40] Hetz, C.; Axten, J. M.; Patterson, J. B., Pharmacological targeting of the unfolded protein response for disease intervention. *Nat Chem Biol* **2019,** *15* (8), 764-775.

[41] Wiseman, R. L.; Zhang, Y.; Lee, K. P.; Harding, H. P.; Haynes, C. M.; Price, J.; Sicheri, F.; Ron, D., Flavonol activation defines an unanticipated ligand-binding site in the kinase-RNase domain of IRE1. *Mol Cell* **2010,** *38* (2), 291-304.

[42] Bisson, J.; McAlpine, J. B.; Friesen, J. B.; Chen, S. N.; Graham, J.; Pauli, G. F., Can Invalid Bioactives Undermine Natural Product-Based Drug Discovery? *J Med Chem* **2016,** *59* (5), 1671-90.

[43] Russo, G. L.; Russo, M.; Spagnuolo, C.; Tedesco, I.; Bilotto, S.; Iannitti, R.; Palumbo, R., Quercetin: a pleiotropic kinase inhibitor against cancer. *Cancer Treat Res* **2014,** *159*, 185-205.

[44] Pohjala, L.; Tammela, P., Aggregating behavior of phenolic compounds--a source of false bioassay results? *Molecules* **2012,** *17* (9), 10774-90.

[45] Grandjean, J. M. D.; Madhavan, A.; Cech, L.; Seguinot, B. O.; Paxman, R. J.; Smith, E.; Scampavia, L.; Powers, E. T.; Cooley, C. B.; Plate, L.; Spicer, T. P.; Kelly, J. W.; Wiseman, R. L., Pharmacologic IRE1/XBP1s Activation Confers Targeted Endoplasmic Reticulum Proteostasis Reprogramming. *Nature Chemical Biology* **2020,** *in press*.

[46] Amin-Wetzel, N.; Saunders, R. A.; Kamphuis, M. J.; Rato, C.; Preissler, S.; Harding, H. P.; Ron, D., A J-Protein Co-chaperone Recruits BiP to Monomerize IRE1 and Repress the Unfolded Protein Response. *Cell* **2017,** *171* (7), 1625-1637.e13.

[47] Lee, A. H.; Iwakoshi, N. N.; Glimcher, L. H., XBP-1 regulates a subset of endoplasmic reticulum resident chaperone genes in the unfolded protein response. *Mol Cell Biol* **2003,** *23* (21), 7448-59.

[48] Shoulders, M. D.; Ryno, L. M.; Genereux, J. C.; Moresco, J. J.; Tu, P. G.; Wu, C.; Yates, J. R., 3rd; Su, A. I.; Kelly, J. W.; Wiseman, R. L., Stress-independent activation of XBP1s and/or ATF6 reveals three functionally diverse ER proteostasis environments. *Cell Rep* **2013,** *3* (4), 1279-92.

[49] Bertolotti, A.; Zhang, Y.; Hendershot, L. M.; Harding, H. P.; Ron, D., Dynamic interaction of BiP and ER stress transducers in the unfolded-protein response. *Nat Cell Biol* **2000,** *2* (6), 326-32.

[50] Oikawa, D.; Kimata, Y.; Kohno, K.; Iwawaki, T., Activation of mammalian IRE1alpha upon ER stress depends on dissociation of BiP rather than on direct interaction with unfolded proteins. *Exp Cell Res* **2009,** *315* (15), 2496-504.

[51] Okamura, K.; Kimata, Y.; Higashio, H.; Tsuru, A.; Kohno, K., Dissociation of Kar2p/BiP from an ER sensory molecule, Ire1p, triggers the unfolded protein response in yeast. *Biochem Biophys Res Commun* **2000,** *279* (2), 445-50.

[52] Amin-Wetzel, N.; Neidhardt, L.; Yan, Y.; Mayer, M. P.; Ron, D., Unstructured regions in IRE1alpha specify BiP-mediated destabilisation of the luminal domain dimer and repression of the UPR. *Elife* **2019,** *8*.

[53] Li, X.; Sun, S.; Appathurai, S.; Sundaram, A.; Plumb, R.; Mariappan, M., The Sec63/BiP complex suppresses higher-order oligomerization and RNase activity of IRE1α during ER stress. *bioRxiv* **2020**, 2020.04.03.024356.

[54] Fedeles, S. V.; So, J. S.; Shrikhande, A.; Lee, S. H.; Gallagher, A. R.; Barkauskas, C. E.; Somlo, S.; Lee, A. H., Sec63 and Xbp1 regulate IRE1alpha activity and polycystic disease severity. *J Clin Invest* **2015,** *125* (5), 1955-67.

[55] Ishikawa, Y.; Fedeles, S.; Marlier, A.; Zhang, C.; Gallagher, A. R.; Lee, A. H.; Somlo, S., Spliced XBP1 Rescues Renal Interstitial Inflammation Due to Loss of Sec63 in Collecting Ducts. *J Am Soc Nephrol* **2019**.

[56] Hassan, H.; Tian, X.; Inoue, K.; Chai, N.; Liu, C.; Soda, K.; Moeckel, G.; Tufro, A.; Lee, A. H.; Somlo, S.; Fedeles, S.; Ishibe, S., Essential Role of X-Box Binding Protein-1 during Endoplasmic Reticulum Stress in Podocytes. *J Am Soc Nephrol* **2016,** *27* (4), 1055-65.

[57] Sundaram, A.; Plumb, R.; Appathurai, S.; Mariappan, M., The Sec61 translocon limits IRE1alpha signaling during the unfolded protein response. *Elife* **2017,** *6*.

[58] Plumb, R.; Zhang, Z. R.; Appathurai, S.; Mariappan, M., A functional link between the co-translational protein translocation pathway and the UPR. *Elife* **2015,** *4*.

[59] Wang, T.; Birsoy, K.; Hughes, N. W.; Krupczak, K. M.; Post, Y.; Wei, J. J.; Lander, E. S.; Sabatini, D. M., Identification and characterization of essential genes in the human genome. *Science* **2015,** *350* (6264), 1096-101.

[60] Cong, L.; Ran, F. A.; Cox, D.; Lin, S.; Barretto, R.; Habib, N.; Hsu, P. D.; Wu, X.; Jiang, W.; Marraffini, L. A.; Zhang, F., Multiplex genome engineering using CRISPR/Cas systems. *Science* **2013,** *339* (6121), 819-23.

[61] Shalem, O.; Sanjana, N. E.; Hartenian, E.; Shi, X.; Scott, D. A.; Mikkelson, T.; Heckl, D.; Ebert, B. L.; Root, D. E.; Doench, J. G.; Zhang, F., Genome-scale CRISPR-Cas9 knockout screening in human cells. *Science* **2014,** *343* (6166), 84-87.

[62] Hsu, P. D.; Lander, E. S.; Zhang, F., Development and applications of CRISPR-Cas9 for genome engineering. *Cell* **2014,** *157* (6), 1262-78.

[63] Kurosaki, T.; Popp, M. W.; Maquat, L. E., Quality and quantity control of gene expression by nonsense-mediated mRNA decay. *Nat Rev Mol Cell Biol* **2019,** *20* (7), 406-420.

[64] Pobre, K. F. R.; Poet, G. J.; Hendershot, L. M., The endoplasmic reticulum (ER) chaperone BiP is a master regulator of ER functions: Getting by with a little help from ERdj friends. *J Biol Chem* **2019,** *294* (6), 2098-2108.

[65] Kurisu, J.; Honma, A.; Miyajima, H.; Kondo, S.; Okumura, M.; Imaizumi, K., MDG1/ERdj4, an ER-resident DnaJ family member, suppresses cell death induced by ER stress. *Genes Cells* **2003,** *8* (2), 189-202.

[66] Dong, M.; Bridges, J. P.; Apsley, K.; Xu, Y.; Weaver, T. E., ERdj4 and ERdj5 are required for endoplasmic reticulum-associated protein degradation of misfolded surfactant protein C. *Mol Biol Cell* **2008,** *19* (6), 2620-30.

[67] van Galen, P.; Kreso, A.; Mbong, N.; Kent, D. G.; Fitzmaurice, T.; Chambers, J. E.; Xie, S.; Laurenti, E.; Hermans, K.; Eppert, K.; Marciniak, S. J.; Goodall, J. C.; Green, A. R.; Wouters, B. G.; Wienholds, E.; Dick, J. E., The unfolded protein response governs integrity of the haematopoietic stem-cell pool during stress. *Nature* **2014,** *510* (7504), 268-72.

[68] Lai, C. W.; Otero, J. H.; Hendershot, L. M.; Snapp, E., ERdj4 protein is a soluble endoplasmic reticulum (ER) DnaJ family protein that interacts with ER-associated degradation machinery. *J Biol Chem* **2012,** *287* (11), 7969-78.

[69] Shen, Y.; Meunier, L.; Hendershot, L. M., Identification and characterization of a novel endoplasmic reticulum (ER) DnaJ homologue, which stimulates ATPase activity of BiP in vitro and is induced by ER stress. *J Biol Chem* **2002,** *277* (18), 15947-56.

[70] Ran, F. A.; Hsu, P. D.; Wright, J.; Agarwala, V.; Scott, D. A.; Zhang, F., Genome engineering using the CRISPR-Cas9 system. *Nat Protoc* **2013,** *8* (11), 2281-2308.

[71] Schmittgen, T. D.; Livak, K. J., Analyzing real-time PCR data by the comparative C(T) method. *Nat Protoc* **2008,** *3* (6), 1101-8.

[72] Livak, K. J.; Schmittgen, T. D., Analysis of relative gene expression data using real-time quantitative PCR and the 2(-Delta Delta C(T)) Method. *Methods* **2001,** *25* (4), 402-8.

Chapter 5

Perspectives on the Field

Significant work has shown the paradigmatic roles of IRE1 and XBP1s in the unfolded protein response.[1-9] Research in the 90s and early 2000s helped to delineate the mechanisms by which IRE1 and XBP1s (in addition to ATF6 and PERK-ATF4) contribute to the ER stress response.[10] Since identifying IRE1 and XBP1s as key regulators of proteostasis, researchers have examined their roles in biology and diseases, leading to discoveries demonstrating their roles in memory formation, neurodegeneration, lipogenesis, atherosclerosis, diabetes, immunity, and cancer.[11-25] Our findings that XBP1s can also drive glycosylation changes bridges ER stress with a post-translational modification that can modulate virtually every aspect of biology.[26-27] It would be intriguing to determine whether XBP1s can, at least in part, drive biology by remodeling the glycans on proteins that influence biology and disease progression. For example, in our work, we sought to determine whether blocking XBP1s expression in triple-negative breast cancers with constitutively high levels of XBP1s can influence glycosylation phenotypes associated with breast cancer malignancy (**Chapter 3**). While our results with IRE1 inhibition in triple-negative breast cancer cells were modest, they suggest a role, however modest, for endogenous XBP1s in regulating the glycome.

Looking forward, understanding which proteins these glycosylation changes are occurring on will identify potential therapeutic targets. Leveraging a systems biology approach including lectin microarray glycomic analysis, researchers discovered that the FUT8 core fucosyltransferase was responsible for initiating core fucosylation of *N*-glycans on the L1CAM adhesion molecule to drive melanoma metastasis.[28] In a different study, XBP1s induced *Fut8* expression in mouse B cells stimulated with lipopolysaccharide.[9] Although these studies did not report whether XBP1s-driven *FUT8* expression can drive metastasis, they lay the groundwork for such studies. In our own work, we determined that XBP1s activation increases the proportion of core fucosylated *N*-glycans in HeLa membrane proteins (**Chapter 2**),[27] but we did not observe a significant change in *FUT8* expression. Future work examining the biological consequences of XBP1s activation can provide insight into whether the increase in core fucosylated *N*-glycans in HeLa cells influences cell migration and invasion. Due to the affinity of lectins to certain carbohydrates, lectins can be leveraged to perform enrichment assays followed by mass spectrometry to identify proteins with specific *N*-glycan epitopes, as had previously been performed for core fucosylated L1CAM.[28] This method can be used in conjunction with XBP1s perturbation to identify glycoproteins differentially enriched by lectins. Understanding whether XBP1s alters the glycans on for example, integrins, growth factor receptors, or receptor tyrosine kinases would prompt studies to investigate the upstream signals regulating the glycosylation and function of such proteins.

The chaperone-mediated repression model of regulating the UPR has led to informative studies demonstrating the roles of the ERdj4 and Sec63 co-chaperones in facilitating the repressive function of BiP on the ER stress sensor IRE1.[29-31] We hypothesized that ERdj4 and Sec63 may be responsible for repressing IRE1 activation following pharmacological activation with small molecules. We were unable to find evidence that knockout of either co-chaperone was sufficient to sustain pharmacological IRE1 activation (**Chapter 4**), leading to the possibility that both co-chaperones must be disrupted to sustain IRE1 activation induced by small molecules. It would perhaps be challenging to disrupt both co-chaperones since it may induce significant proteotoxic stress due to impaired protein folding. On the other hand, disrupting both co-chaperones may induce a compensatory ER stress response via ATF6 signaling to alleviate the induced protein misfolding stress.[8]

Given the growing list of proteins reported to interact with IRE1,[32] it is likely that additional, uncharacterized interactions repress IRE1, potentially forming negative feedback loops suppressing pharmacological IRE1 activation as an adaptive response of the UPR. Indeed, a proposed model in osteogenic differentiation suggests that the granulin-epithelin precursor (GEP) stimulates IRE1 activity via the JunB transcription factor, but IRE1 itself inhibits GEP and bone morphogenetic protein 2 (BMP2) upstream of GEP.[33] The GEP–JunB–IRE1 feedback loop, or other mechanisms functioning in a similar manner, may be responsible for repressing IRE1 activation induced by small molecule activators, possibly explaining the lack of sustained pharmacological IRE1 activation. Careful mapping and exploration of IRE1 feedback loops will help to identify promising targets for sustained pharmacological IRE1 activation. Sustained IRE1 activation by small molecules can be leveraged as a therapeutic approach for treating diseases with pathways regulated by IRE1 signaling, such as the response to glucose and insulin production in diabetes.[34-35]

We have shown that XBP1s influences the post-translational modifications of other proteins, including *N*-glycosylation of membrane-associated and secreted proteins,[27] suggesting that XBP1s can impact the function of proteins in addition to merely upregulating gene expression. The number of studies investigating the post-translational modifications of XBP1s itself are growing, with evidence showing that XBP1s can be phosphorylated, SUMOylated, and acetylated. Phosphorylation of XBP1s was shown to take place on Thr48 and/or Ser61 by the p38 MAP kinase or the CDK5 kinase.[36-37] XBP1s phosphorylation enhances its nuclear translocation. Modification of XBP1s with SUMO represses its transcriptional activity.[38] The p300 acetyltransferase and Sirt1/6 deacetylase enzymes mediate the addition and removal, respectively, of acetyl groups on XBP1s.[39-40] XBP1s acetylation enhances protein stability and transcriptional activity, while deacetylation promotes its degradation through the ubiquitin-proteasome system. The diversity of post-translational modifications opens profound possibilities to modulate XBP1s stability, localization, and activity, which in turn will have consequences for disease.

Roles for XBP1s beyond proteostasis maintenance continue to be discovered, [41] and we have only touched the surface of understanding the breadth of functions that XBP1s adopts, and the mechanisms for its regulation. Continued studies are needed to elucidate the underlying mechanisms by which XBP1s mediates alterations in *N*-glycosylation. For example, ChIP-seq experiments suggest that XBP1s is unlikely to regulate global glycogene expression via direct binding to promoters upstream of glycogenes.[24] A more likely hypothesis is that XBP1s directly binds to the ER stress response element (ERSE) of another transcription factor, and regulation of glycogenes is perhaps a secondary effect of XBP1s activity. Continued work contributing to a thorough understanding of XBP1s function and regulation will help to inform programs targeting these areas for disease intervention.

References

[1] Cox, J. S.; Shamu, C. E.; Walter, P., Transcriptional induction of genes encoding endoplasmic reticulum resident proteins requires a transmembrane protein kinase. *Cell* **1993,** *73* (6), 1197-206.

[2] Mori, K.; Ma, W.; Gething, M. J.; Sambrook, J., A transmembrane protein with a cdc2+/CDC28-related kinase activity is required for signaling from the ER to the nucleus. *Cell* **1993,** *74* (4), 743-56.

[3] Shamu, C. E.; Walter, P., Oligomerization and phosphorylation of the Ire1p kinase during intracellular signaling from the endoplasmic reticulum to the nucleus. *Embo j* **1996,** *15* (12), 3028-39.

[4] Sidrauski, C.; Walter, P., The transmembrane kinase Ire1p is a site-specific endonuclease that initiates mRNA splicing in the unfolded protein response. *Cell* **1997,** *90* (6), 1031-9.

[5] Wang, X. Z.; Harding, H. P.; Zhang, Y.; Jolicoeur, E. M.; Kuroda, M.; Ron, D., Cloning of mammalian Ire1 reveals diversity in the ER stress responses. *Embo j* **1998,** *17* (19), 5708-17.

[6] Yoshida, H.; Matsui, T.; Yamamoto, A.; Okada, T.; Mori, K., XBP1 mRNA is induced by ATF6 and spliced by IRE1 in response to ER stress to produce a highly active transcription factor. *Cell* **2001,** *107* (7), 881-91.

[7] Lee, K.; Tirasophon, W.; Shen, X.; Michalak, M.; Prywes, R.; Okada, T.; Yoshida, H.; Mori, K.; Kaufman, R. J., IRE1-mediated unconventional mRNA splicing and S2P-mediated ATF6 cleavage merge to regulate XBP1 in signaling the unfolded protein response. *Genes Dev* **2002,** *16* (4), 452-66.

[8] Lee, A. H.; Iwakoshi, N. N.; Glimcher, L. H., XBP-1 regulates a subset of endoplasmic reticulum resident chaperone genes in the unfolded protein response. *Mol Cell Biol* **2003,** *23* (21), 7448-59.

[9] Shaffer, A. L.; Shapiro-Shelef, M.; Iwakoshi, N. N.; Lee, A. H.; Qian, S. B.; Zhao, H.; Yu, X.; Yang, L.; Tan, B. K.; Rosenwald, A.; Hurt, E. M.; Petroulakis, E.; Sonenberg, N.; Yewdell, J. W.; Calame, K.; Glimcher, L. H.; Staudt, L. M., XBP1, downstream of Blimp-1, expands the secretory apparatus and other organelles, and increases protein synthesis in plasma cell differentiation. *Immunity* **2004,** *21* (1), 81-93.

[10] Mori, K., The unfolded protein response: the dawn of a new field. *Proc Jpn Acad Ser B Phys Biol Sci* **2015,** *91* (9), 469-80.

[11] Martinez, G.; Vidal, R. L.; Mardones, P.; Serrano, F. G.; Ardiles, A. O.; Wirth, C.; Valdes, P.; Thielen, P.; Schneider, B. L.; Kerr, B.; Valdes, J. L.; Palacios, A. G.; Inestrosa, N. C.; Glimcher, L. H.; Hetz, C., Regulation of Memory Formation by the Transcription Factor XBP1. *Cell Rep* **2016,** *14* (6), 1382-1394.

[12] Valdes, P.; Mercado, G.; Vidal, R. L.; Molina, C.; Parsons, G.; Court, F. A.; Martinez, A.; Galleguillos, D.; Armentano, D.; Schneider, B. L.; Hetz, C., Control of dopaminergic neuron survival by the unfolded protein response transcription factor XBP1. *Proc Natl Acad Sci U S A* **2014,** *111* (18), 6804-9.

[13] Cisse, M.; Duplan, E.; Lorivel, T.; Dunys, J.; Bauer, C.; Meckler, X.; Gerakis, Y.; Lauritzen, I.; Checler, F., The transcription factor XBP1s restores hippocampal synaptic plasticity and memory by control of the Kalirin-7 pathway in Alzheimer model. *Mol Psychiatry* **2017,** *22* (11), 1562-1575.

[14] Acosta-Alvear, D.; Zhou, Y.; Blais, A.; Tsikitis, M.; Lents, N. H.; Arias, C.; Lennon, C. J.; Kluger, Y.; Dynlacht, B. D., XBP1 controls diverse cell type- and condition-specific transcriptional regulatory networks. *Mol Cell* **2007,** *27* (1), 53-66.

[15] Lee, A. H.; Scapa, E. F.; Cohen, D. E.; Glimcher, L. H., Regulation of hepatic lipogenesis by the transcription factor XBP1. *Science* **2008,** *320* (5882), 1492-6.

[16] Zeng, L.; Zampetaki, A.; Margariti, A.; Pepe, A. E.; Alam, S.; Martin, D.; Xiao, Q.; Wang, W.; Jin, Z. G.; Cockerill, G.; Mori, K.; Li, Y. S.; Hu, Y.; Chien, S.; Xu, Q., Sustained activation of XBP1 splicing leads to endothelial apoptosis and atherosclerosis development in response to disturbed flow. *Proc Natl Acad Sci U S A* **2009,** *106* (20), 8326-31.

[17] Lee, A. H.; Heidtman, K.; Hotamisligil, G. S.; Glimcher, L. H., Dual and opposing roles of the unfolded protein response regulated by IRE1alpha and XBP1 in proinsulin processing and insulin secretion. *Proc Natl Acad Sci U S A* **2011,** *108* (21), 8885-90.

[18] Laybutt, D. R.; Preston, A. M.; Akerfeldt, M. C.; Kench, J. G.; Busch, A. K.; Biankin, A. V.; Biden, T. J., Endoplasmic reticulum stress contributes to beta cell apoptosis in type 2 diabetes. *Diabetologia* **2007,** *50* (4), 752-63.

[19] Brandt, C.; Nolte, H.; Henschke, S.; Engstrom Ruud, L.; Awazawa, M.; Morgan, D. A.; Gabel, P.; Sprenger, H. G.; Hess, M. E.; Gunther, S.; Langer, T.; Rahmouni, K.; Fenselau, H.; Kruger, M.; Bruning, J. C., Food Perception Primes Hepatic ER Homeostasis via Melanocortin-Dependent Control of mTOR Activation. *Cell* **2018,** *175* (5), 1321-1335.e20.

[20] Cubillos-Ruiz, J. R.; Silberman, P. C.; Rutkowski, M. R.; Chopra, S.; Perales-Puchalt, A.; Song, M.; Zhang, S.; Bettigole, S. E.; Gupta, D.; Holcomb, K.; Ellenson, L. H.; Caputo, T.; Lee, A. H.; Conejo-Garcia, J. R.; Glimcher, L. H., ER Stress Sensor XBP1 Controls Anti-tumor Immunity by Disrupting Dendritic Cell Homeostasis. *Cell* **2015,** *161* (7), 1527-38.

[21] Martinon, F.; Chen, X.; Lee, A. H.; Glimcher, L. H., TLR activation of the transcription factor XBP1 regulates innate immune responses in macrophages. *Nat Immunol* **2010,** *11* (5), 411-8.

[22] Song, M.; Sandoval, T. A.; Chae, C. S.; Chopra, S.; Tan, C.; Rutkowski, M. R.; Raundhal, M.; Chaurio, R. A.; Payne, K. K.; Konrad, C.; Bettigole, S. E.; Shin, H. R.; Crowley, M. J. P.; Cerliani, J. P.; Kossenkov, A. V.; Motorykin, I.; Zhang, S.; Manfredi, G.; Zamarin, D.; Holcomb, K.; Rodriguez, P. C.; Rabinovich, G. A.; Conejo-Garcia, J. R.; Glimcher, L. H.; Cubillos-Ruiz, J. R., IRE1alpha-XBP1 controls T cell function in ovarian cancer by regulating mitochondrial activity. *Nature* **2018,** *562* (7727), 423-428.

[23] Romero-Ramirez, L.; Cao, H.; Nelson, D.; Hammond, E.; Lee, A. H.; Yoshida, H.; Mori, K.; Glimcher, L. H.; Denko, N. C.; Giaccia, A. J.; Le, Q. T.; Koong, A. C., XBP1 is essential for survival under hypoxic conditions and is required for tumor growth. *Cancer Res* **2004,** *64* (17), 5943-7.

[24] Chen, X.; Iliopoulos, D.; Zhang, Q.; Tang, Q.; Greenblatt, M. B.; Hatziapostolou, M.; Lim, E.; Tam, W. L.; Ni, M.; Chen, Y.; Mai, J.; Shen, H.; Hu, D. Z.; Adoro, S.; Hu, B.; Song, M.; Tan, C.; Landis, M. D.; Ferrari, M.; Shin, S. J.; Brown, M.; Chang, J. C.; Liu, X. S.; Glimcher, L. H., XBP1 promotes triple-negative breast cancer by controlling the HIF1alpha pathway. *Nature* **2014,** *508* (7494), 103-107.

[25] Mimura, N.; Fulciniti, M.; Gorgun, G.; Tai, Y. T.; Cirstea, D.; Santo, L.; Hu, Y.; Fabre, C.; Minami, J.; Ohguchi, H.; Kiziltepe, T.; Ikeda, H.; Kawano, Y.; French, M.; Blumenthal, M.; Tam, V.; Kertesz, N. L.; Malyankar, U. M.; Hokenson, M.; Pham, T.; Zeng, Q.; Patterson, J. B.; Richardson, P. G.; Munshi, N. C.; Anderson, K. C., Blockade of XBP1 splicing by inhibition of IRE1alpha is a promising therapeutic option in multiple myeloma. *Blood* **2012,** *119* (24), 5772-81.

[26] Dewal, M. B.; DiChiara, A. S.; Antonopoulos, A.; Taylor, R. J.; Harmon, C. J.; Haslam, S. M.; Dell, A.; Shoulders, M. D., XBP1s Links the Unfolded Protein Response to the Molecular Architecture of Mature N-Glycans. *Chem Biol* **2015,** *22* (10), 1301-12.

[27] Wong, M. Y.; Chen, K.; Antonopoulos, A.; Kasper, B. T.; Dewal, M. B.; Taylor, R. J.; Whittaker, C. A.; Hein, P. P.; Dell, A.; Genereux, J. C.; Haslam, S. M.; Mahal, L. K.; Shoulders, M. D., XBP1s activation can globally remodel N-glycan structure distribution patterns. *Proc Natl Acad Sci U S A* **2018,** *115* (43), E10089-E10098.

[28] Agrawal, P.; Fontanals-Cirera, B.; Sokolova, E.; Jacob, S.; Vaiana, C. A.; Argibay, D.; Davalos, V.; McDermott, M.; Nayak, S.; Darvishian, F.; Castillo, M.; Ueberheide, B.; Osman, I.; Fenyo, D.; Mahal, L. K.; Hernando, E., A Systems Biology Approach Identifies FUT8 as a Driver of Melanoma Metastasis. *Cancer Cell* **2017,** *31* (6), 804-819.e7.

[29] Amin-Wetzel, N.; Saunders, R. A.; Kamphuis, M. J.; Rato, C.; Preissler, S.; Harding, H. P.; Ron, D., A J-Protein Co-chaperone Recruits BiP to Monomerize IRE1 and Repress the Unfolded Protein Response. *Cell* **2017,** *171* (7), 1625-1637.e13.

[30] Amin-Wetzel, N.; Neidhardt, L.; Yan, Y.; Mayer, M. P.; Ron, D., Unstructured regions in IRE1alpha specify BiP-mediated destabilisation of the luminal domain dimer and repression of the UPR. *Elife* **2019,** *8*.

[31] Li, X.; Sun, S.; Appathurai, S.; Sundaram, A.; Plumb, R.; Mariappan, M., The Sec63/BiP complex suppresses higher-order oligomerization and RNase activity of IRE1α during ER stress. *bioRxiv* **2020**, 2020.04.03.024356.

[32] Woehlbier, U.; Hetz, C., Modulating stress responses by the UPRosome: a matter of life and death. *Trends Biochem Sci* **2011,** *36* (6), 329-37.

[33] Guo, F. J.; Jiang, R.; Xiong, Z.; Xia, F.; Li, M.; Chen, L.; Liu, C. J., IRE1a constitutes a negative feedback loop with BMP2 and acts as a novel mediator in modulating osteogenic differentiation. *Cell Death Dis* **2014,** *5*, e1239.

[34] Lipson, K. L.; Fonseca, S. G.; Ishigaki, S.; Nguyen, L. X.; Foss, E.; Bortell, R.; Rossini, A. A.; Urano, F., Regulation of insulin biosynthesis in pancreatic beta cells by an endoplasmic reticulum-resident protein kinase IRE1. *Cell Metab* **2006,** *4* (3), 245-54.

[35] Akiyama, M.; Liew, C. W.; Lu, S.; Hu, J.; Martinez, R.; Hambro, B.; Kennedy, R. T.; Kulkarni, R. N., X-box binding protein 1 is essential for insulin regulation of pancreatic alpha-cell function. *Diabetes* **2013,** *62* (7), 2439-49.

[36] Jiao, F. J.; Wang, Q. Z.; Zhang, P.; Yan, J. G.; Zhang, Z.; He, F.; Zhang, Q.; Lv, Z. X.; Peng, X.; Cai, H. W.; Tian, B., CDK5-mediated phosphorylation of XBP1s contributes to its nuclear translocation and activation in MPP(+)-induced Parkinson's disease model. *Sci Rep* **2017,** *7* (1), 5622.

[37] Lee, J.; Sun, C.; Zhou, Y.; Lee, J.; Gokalp, D.; Herrema, H.; Park, S. W.; Davis, R. J.; Ozcan, U., p38 MAPK-mediated regulation of Xbp1s is crucial for glucose homeostasis. *Nat Med* **2011,** *17* (10), 1251-60.

[38] Chen, H.; Qi, L., SUMO modification regulates the transcriptional activity of XBP1. *Biochem J* **2010,** *429* (1), 95-102.

[39] Wang, F. M.; Chen, Y. J.; Ouyang, H. J., Regulation of unfolded protein response modulator XBP1s by acetylation and deacetylation. *Biochem J* **2011,** *433* (1), 245-52.

[40] Bang, I. H.; Kwon, O. K.; Hao, L.; Park, D.; Chung, M. J.; Oh, B. C.; Lee, S.; Bae, E. J.; Park, B. H., Deacetylation of XBP1s by sirtuin 6 confers resistance to ER stress-induced hepatic steatosis. *Exp Mol Med* **2019,** *51* (9), 1-11.

[41] He, Y.; Sun, S.; Sha, H.; Liu, Z.; Yang, L.; Xue, Z.; Chen, H.; Qi, L., Emerging roles for XBP1, a sUPeR transcription factor. *Gene Expr* **2010,** *15* (1), 13-25.

Appendix 1

Supporting Information for Chapter 2

Supporting Datasets

Published online at www.pnas.org/lookup/suppl/doi:10.1073/pnas.1805425115/-/DCSupplemental.

Dataset S.1: GSEA results and gene sets (online Excel Spreadsheet).

Dataset S.1*A* (Sheet 1). GSEA results for Tg treatment using c5bp (MSigDB), shown in Figure S.1*D*.

Dataset S.1*B* (Sheet 2). GSEA results for Tg treatment using c5mf (MSigDB), shown in Figure S.1*D*.

Dataset S.1*C* (Sheet 3). GSEA results for XBP1s activation using c5bp (MSigDB), shown in Figure S.1*D*.

Dataset S.1*D* (Sheet 4). GSEA results for XBP1s activation using c5mf (MSigDB), shown in Figure S.1*D*.

Dataset S.1*E* (Sheet 5). Full list of glycogenes in custom "lipid-linked oligosaccharide biosynthesis" and "trimming and elaboration" gene sets used for generating enrichment plots shown in Figure S.8 *A* and *B*.

Dataset S.2. List of lectins used on the microarrays (online Excel Spreadsheet).

Dataset S.2*A* (Sheet 1). List of lectins used for HEK293^{XBP1s} microarray experiments. Lectin print concentration, print sugar, and glycan epitope are indicated. Duplicate lectins obtained from different sources are noted in the last column.

Dataset S.2*B* (Sheet 2). List of lectins used for HeLa^{XBP1s} microarray experiments. Lectin print concentration, print sugar, and glycan epitope are indicated. Duplicate lectins obtained from different sources are noted in the last column.

Dataset S.3. Processed lectin microarray data (online Excel Spreadsheet). Data represent median normalized $\log_2$ values of sample to pooled-sample reference ratios.

Dataset S.3*A* (Sheet 1). HEK^{XBP1s} membrane data.

Dataset S.3*B* (Sheet 2). HeLa^{XBP1s} membrane data.

Dataset S.3*C* (Sheet 3). HEK^{XBP1s} media data.

Dataset S.4. MS analysis of the HEK^{XBP1s} secretome with XBP1s activation (online Excel Spreadsheet). Spectral counts, *m/z* ratios, and normalized intensities for all proteins detected by TMT-MS with or without XBP1s activation in Replicates 1–3 (*A*–*C*, respectively). Processed data are presented in Dataset S.4*D*.

Dataset S.4*A* (Sheet 1). Full TMT-MS data for the 6 h secretome of HEK^{XBP1s} cells (Replicate 1).

Dataset S.4*B* (Sheet 2). Full TMT-MS data for the 6 h secretome of HEK^{XBP1s} cells (Replicate 2).

Dataset S.4*C* (Sheet 3). Full TMT-MS data for the 6 h secretome of HEK^{XBP1s} cells (Replicate 3).
Dataset S.4*D* (Sheet 4). Fold-change and significance values for all proteins in the XBP1s secretome. Proteins that met fold-change and significance cut-offs are highlighted; significance and fold-change cut-offs were as follows: *p*-value ≤ 0.05, fold-change ≥ 1.5-fold. Proteins annotated as *N*-glycosylated (UniProtKB) are indicated along with the reported number of *N*-glycan sequons.

Dataset S.5: HEK^{XBP1s} and $HeLa^{XBP1s}$ glycogene data (online Excel Spreadsheet).
Dataset S.5*A* (Sheet 1). Gene sets related to *N*-glycosylation (including glycosyltransferases, glucosidases, and sugar transporters) selected from MSigDB and used to generate Figure 2.5.
Dataset S.5*B* (Sheet 2). Full list of unique genes contained in the selected gene sets listed in Dataset S.5*A*.
Dataset S.5*C* (Sheet 3). Fold-change and significance values for glycogenes in HEK^{XBP1s} cells with XBP1s activation used to generate Figure 2.5*A*. Glycosylation-related genes listed in Dataset S.5*B* were extracted from the HEK^{XBP1s} microarray data and were integrated with glycosylation PCR array data; bold-faced genes have fold-change and significance values obtained from the qPCR arrays. Significance and fold-change cut-offs were as follows: FDR or *p*-value ≤ 0.05, fold-changes ≥ 1.5-fold (XBP1s versus vehicle).
Dataset S.5*D* (Sheet 4). Fold-change and significance values for glycogenes in $HeLa^{XBP1s}$ cells with XBP1s activation used to generate Figure 2.5*C*. Glycosylation-related genes listed in Dataset S.5*B* were extracted from the $HeLa^{XBP1s}$ RNA-Seq data and integrated with glycosylation PCR array data; bold-faced genes have fold-change and significance values obtained from the qPCR arrays. Significance and fold-change cut-offs were as follows: FDR or *p*-value ≤ 0.05, fold-changes ≥ 1.5-fold (XBP1s versus vehicle).

Biographical Note

A native of Los Angeles, Kenny Chen attended the University of California, Los Angeles (UCLA) and graduated in 2014 with a B.S. in Chemistry with Departmental Highest Honors. During his undergraduate studies, Kenny performed research in the laboratory of Prof. Albert J. Courey, focusing on transcriptional regulation using *Drosophila* as a model organism. Kenny went on to work at the National Institutes of Health in Bethesda, MD after graduating from UCLA to work in the laboratory of Dr. Jeffrey E. Green. There, he performed research in cancer biology and genetics, focusing on the role of the JMJD6 epigenetic modifier in breast cancer. Kenny began his graduate studies at MIT in 2015, joining the laboratory of Prof. Matthew D. Shoulders. At MIT, Kenny led projects on protein homeostasis, focusing on the role of the XBP1s transcription factor in *N*-glycosylation. While at MIT, Kenny also worked collaboratively on projects studying the thermostability of proteins from Influenza A. He was also an active member of the MIT community, notably serving as a member of the Department of Chemistry EHS Committee, and as a Resident Assistant at the Warehouse Graduate Residence.

Research Experience

Massachusetts Institute of Technology, Cambridge, MA — 2015 – 2020 (expected)
Doctoral Candidate

Vertex Pharmaceuticals, Boston, MA — Summer 2018
Graduate Student Intern

National Institutes of Health, Bethesda, MD — 2014 – 2015
Postbaccalaureate Research Fellow

University of California, Los Angeles, Los Angeles, CA — 2012 – 2014
Undergraduate Research Assistant

California Institute of Technology, Pasadena, CA — Summer 2013
Amgen Scholar

UCLA David Geffen School of Medicine, Los Angeles, CA — 2011
Undergraduate Research Assistant

Publications

[#] Denotes equal contribution

Aprelikova, O.; Chen, K.; El Touny, L. H.; Brignatz-Guittard, C.; Han, J.; Qiu, T.; Yang, H. H.; Lee, M. P.; Zhu, M.; Green, J. E., The epigenetic modifier JMJD6 is amplified in mammary tumors and cooperates with c-Myc to enhance cellular transformation, tumor progression, and metastasis. *Clin Epigenetics* **2016,** *8*, 38.

Chambers, M.; Turki-Judeh, W.; Kim, M. W.; Chen, K.; Gallaher, S. D.; Courey, A. J., Mechanisms of Groucho-mediated repression revealed by genome-wide analysis of Groucho binding and activity. *BMC Genomics* **2017,** *18*, 215.

Wong, M. Y.; DiChiara, A. S.; Suen, P. H.; Chen, K.; Doan, N. D.; Shoulders, M. D., Adapting secretory proteostasis and function through the unfolded protein response. *Curr Top Microbiol Immunol* **2018,** *414*, 1-25.

Cole, K. S.; Grandjean, J. M. D.; Chen, K.; Witt, C. H.; O'Day, J.; Shoulders, M. D.; Wiseman, R. L.; Weerapana, E., Characterization of an A-site selective protein disulfide isomerase A1 inhibitor. *Biochemistry* **2018,** *57* (13), 2035-2043.

[#]Phillips, A. M.; [#]Ponomarenko, A. I.; Chen, K.; Ashenberg, O.; Miao, J.; McHugh, S. M.; Butty, V. L.; Whittaker, C. A.; Moore, C. L.; Bloom, J. D.; Lin, Y. S.; Shoulders, M. D., Destabilized adaptive influenza variants critical for innate immune system escape are potentiated by host chaperones. *PLoS Biol* **2018,** *16* (9), e3000008.

[#]Wong, M. Y.; [#]Chen, K.; [#]Antonopoulos, A.; [#]Kasper, B. T.; Dewal, M. B.; Taylor, R. J.; Whittaker, C. A.; Hein, P. P.; Dell, A.; Genereux, J. C.; Haslam, S. M.; Mahal, L. K.; Shoulders, M. D., XBP1s activation can globally remodel *N*-glycan structure distribution patterns. *Proc Natl Acad Sci U S A* **2018,** *115* (43), E10089-E10098.